# THE IMMUNITY–RELATED GTPASE (IRG) RESISTANCE SYSTEM AGAINST INTRACELLULAR PARASITES

INAUGURAL-DISSERTATION

ZUR

ERLANGUNG DES DOKTORGRADES

DER MATHEMATISCH-NATURWISSENSCHAFTLICHEN FAKULTÄT

DER UNIVERSITÄT ZU KÖLN

VORGELEGT VON

**HELEN MARIA SPRINGER-FRAUENHOFF**

AUS HAAN

2014

Berichterstatter: Prof. Dr. Jonathan Howard
Prof. Dr. Jürgen Dohmen

Tag der mündlichen Prüfung: 26.6.2014

**Das Studium und allgemein das Streben nach Wahrheit und Schönheit ist ein Gebiet,
auf dem wir das ganze Leben lang Kinder bleiben dürfen.
Albert Einstein**

# Table of content

# List of abbreviations

| | |
|---|---|
| aa | amino acid |
| APS | ammonium persulfate |
| ATP | adenosine triphosphate |
| BCG | Bacillus Calmette Guérin |
| BL/6 | mouse strain C57BL/6 |
| BLAST | basic local alignment search tool |
| BMM | bone marrow-derived macrophages |
| bp | base pair |
| BSA | bovine serum albumin |
| DAMP | danger-associated molecular patterns |
| DAPI | 4',6-Diamidino-2-phenylindol |
| DMEM | Dulbecco's modified Eagle's medium |
| DNA | desoxyribonucleic acid |
| *E. coli* | *Escherichia coli* |
| EDTA | ethylenediaminetetraacetic acid |
| ER | endoplasmatic reticulum |
| EST | expressed sequence tags |
| FCS | fetal calf serum |
| GAF | gamma-activation factor |
| GAP | GTPase-activating protein |
| GAS | IFNγ-activated sequence |
| GBP | guanylate-binding protein |
| GDI | guanine nucleotide dissociation inhibitor |
| G-domain | GTPase domain |
| GEF | guanine nucleotide exchange factor |
| GM130 | cis-Golgi matrix protein |
| GMP/GDP/GTP | Guanosin-mono/di/tri-phosphate |
| GRA | dense granule protein |
| h | hour |
| HEK | human embryonic kidney |
| HKLM | heat-killed *Listeria monocytogenes* |
| HRP | horseradish peroxidase |
| IB | immunoblot |
| IF | immunofluorescence |
| IDO | indoleamine 2,3-dioxygenase |
| IFN, IFNγ | interferon, interferon-gamma |
| IL | interleukin |
| IRG | Immunity-related GTPase |
| IRF9 | IFN Regulatory Factor 9 |
| ISG | IFN-Stimulated Gene |
| ISGF3 | IFN-Stimulated Gene Factor 3 |
| ISRE | IFN-Stimulated response element |
| IP/Co-IP | immunoprecipitation/ co-immunoprecipitation |
| JAK | Janus kinase |
| k | kilo or 1000 |
| kDa | kilodalton |

| | |
|---|---|
| LAMP1 | lysosomes-associated membrane protein |
| LC ESI-MS/MS | Nano-liquid chromatography-coupled electrospray ionization mass spectrometry/mass spectrometry |
| LLO | listeriolysin O |
| *L. m.* | *Listeria monocytogenes* |
| LPS | lipopolysaccharide |
| LRR | leucine-rich repeat |
| MAMP | microbial-associated molecular pattern |
| MEFs | mouse embryonic fibroblasts |
| min | minute |
| MOI | multiplicity of infection |
| NF-κB | nuclear factor-κ B |
| NK cells | natural killer cells |
| NLR | nucleotide-binding domain and leucine rich repeat containing gene family |
| NO | nitric oxide |
| PAMP | pathogen-associated molecular pattern |
| PBS | phosphate buffered saline solution |
| PCR | polymerase chain reaction |
| p. i. | post infection |
| PRR | pattern recognition receptor |
| PV | parasitophorous vacuole |
| PVM | parasitophorous vacuolar membrane |
| RON | rhoptry neck protein |
| ROP | rhoptry bulb protein |
| ROS | reactive oxygen species |
| RLR | RIG-like helicases receptor |
| RNA | ribonucleic acid |
| SD | standard deviation |
| SDS-PAGE | sodiumdodecyl sulphate - polyacrylamide gel electrophoresis |
| TEMED | N, N, N', N' – tetramethylethylene |
| TLR | Toll-like receptor |
| TNF | tumour necrosis factor |
| Tris | tris(hydroxymethyl-) aminoethan |
| TRITC | Tetramethylrhodamine isothiocyanate |
| Triton X-100 | polyethylene glycol p-(1,1,3,3-tetramethylbuthyl)-phenylether |
| Tween 20 | polyoxyethylene (20) sorbitan monolaurate |
| U | unit |
| v/v | volume/volume |
| WB | Western Blot |
| w/v | weight per volume |
| wt | wildtype |
| x | fold |

# Introduction

## 1.1 Pathogens and immunity

All organisms on earth have evolved and adapted in response to their environment, which harbours not only abiotic factors such as climate, but also an immense ecological network of other species. From the beginning on, organisms of different kinds started persistently to interact with each other, a relationship termed symbiosis (Greek *syn bios* "living together"). Symbiosis has been classified into three main categories according to the consequences for the individual species with fluent transitions. The most common and probably evolutionary oldest type of relationship is parasitism: one member, the parasite, benefits at the expense of the other, the host. Furthermore, there is commensalism: only one species benefits without affecting the other; as well as mutualism: both species benefit from the relationship (Paracer et al. 2000). Parasites causing disease are also called pathogens (Greek *pathos* "suffering/emotion" *genus* "to give birth to"). Pathogens comprise subcellular organisms (viruses), bacteria, as well as uni- and multicellular eukaryotes (protozoa, fungi, worms). They can infect a broad range of organisms, which are usually at a higher taxonomic level than themselves. The host organisms, in contrast, combat the constant attacks by the pathogens with resistance molecules and mechanisms that together constitute the host immune system. The constant battle of pathogens and hosts can provoke co-evolution resulting in a pathogen that could either manage to evade the host immune system or adapt to a non-harmful symbiont (Roy et al. 2007).

The immune system (Latin *immunis*, in a biological sense "exemption from foreign agents") is a multilayered system with increasing specificity. Ancient forms of immune systems can be found even in bacteria which protect themselves with invariant restriction endonucleases or with the recently discovered adaptive CRIPR/CAS system against foreign nucleic acids of bacteriophages (Barrangou et al. 2007; Samson et al. 2013).

The first lines of defence in eukaryotes are represented by surface barriers that simply prevent pathogens from entering the host. They can be mechanical (cuticle, exoskeleton, shell, skin, mucus), chemical (antimicrobial peptides, defensins, gastric acid) or biological (commensal flora). However, when pathogens succeed in breaching these first surface barriers, they are met by non-specific but immediate defence reactions of the innate immune system. This second layer of immunity is the dominant defence strategy in plants, insects and primitive multicellular organisms and sufficient against attacks by the majority of pathogens (Murphy 2012).

In vertebrates, the innate mechanisms can be further distinguished in cell-mediated and humoral immunity. Specialised immune cells, termed innate leukocytes (neutrophil granulocytes, macrophages, dendritic cells or natural killer cells), drive cell-mediated immunity by various defence mechanisms. They circulate in the blood or reside in specific tissues and sample their environment for foreign particles. Further, they are recruited to the site of infection (also to sites of tissue damage or inflammation), where they phagocytose and eliminate microbes or cellular debris. Finally, they secrete signalling molecules termed cytokines to recruit or activate other immune cells. These cytokines together with the complement system drive the humoral immunity. The complement system is characterised by an activation cascade of several proteins (mostly zymogens), mediating opsonisation of bacteria to enable phagocytosis, attraction of immune cells, formation of pores in the membrane of foreign cells and clumping of antigen-bearing agents (Murphy 2012).

In addition, an even more sophisticated adaptive immune system has evolved in vertebrates (Cooper et al. 2006) as an additional third layer. This adaptive immunity is, in contrast to the innate layer, highly specific for each particular pathogen and provides long-lasting protection after a lag-phase of activation. The two major cell types of the adaptive immune system are B- and T-lymphocytes. One of their main features is to express a diverse array of receptors generated through complex somatic DNA rearrangements, which allow them to specifically recognise a great diversity of antigens and secrete specific antigen-targeting molecules called antibodies (Murphy 2012).

It is critical for the host to discriminate not only self from non-self to defend against potential pathogens (Janeway 1992; Medzhitov 2009), but also to discriminate harmful pathogens from essential commensals. To this end, the innate immune system in mammals can recognise potential pathogens via invariant compounds that are only produced by microbes, so-called microbial-associated molecular patterns (MAMPs), in combination with endogenous signals produced upon cell stress or infection, so called danger-associated molecular patterns (DAMPs) (Matzinger 1994; Matzinger 2002). The recognition is mainly mediated by a variety of germ line-encoded pattern recognition receptors (PRRs), which are mainly expressed on sentinel cells but can also be found in non-immune cells. PRRs comprise several receptor families: transmembrane Toll-like receptors (TLR) (Trinchieri et al. 2007; Kawai et al. 2010), intracellular retinoid acid-inducible gene-1 (RIG-1)–like receptors (RLR) (Eisenacher et al. 2012), intracellular nucleotide-binding domain and leucine-rich repeat containing protein family (NLR), which can also form large protein complexes (inflammasomes) to recognise a variety of MAMPs or DAMPs (Chen et al. 2009), as well as

C-type lectins and Scavenger receptors (Canton et al. 2013). Non-self recognition also plays an important role for NK-cells or in the adaptive immune system, e.g.in terms of elimination of self-antigen receptor, which is essential for self-tolerance (Murphy 2012).

Another crucial aspect of the immune system is the crosstalk between innate and adaptive components. This involves both cell-cell interactions and signalling through messenger molecules, the cytokines. Cytokines are a large group of small proteins, which are produced in response to microbes, antigenic or inflammatory stimuli. They often act pleiotropically and redundantly and they can have synergistic or antagonistic effects (Abbas et al. 2007). Cytokines can be classified according to their different functions: chemo-attraction between cells (chemokines), communication between leukocytes and other immune cells (interleukins), differentiation of haematopoietic cells (hematopoietins, formally colony-stimulating factors), mediation of acute inflammation (tumour necrosis factor) as well as the ”virus interfering” interferons (Murphy 2012). Thus, cytokines are not only involved in regulating the specialised immune cells, but can also induce resistance mechanisms intrinsic to almost every somatic cell. These so called cell-autonomous mechanisms are independent of other immune cells or molecules, apart from its first external activation stimulus. Cell-autonomous immunity enables individual cells to cope with microbial challenge and stress and can be interpreted as an additional facet of the innate immune system (Howard 2007; MacMicking 2012).

## 1.2 Interferon-stimulated genes and their role in immunity

Interferons (IFN) were first cytokines discovered and described as a substance that “interfered with viral replication” (Isaacs et al. 1957; Isaacs et al. 1957). Interferons are pro-inflammatory cytokines secreted by immune and non-immune cells in a brief and self-limiting manner (Murphy 2012). According to their sequence homology and receptor specificity, the glycosylated IFNs can be classified into three groups: Type I, including IFNα (14-20 members depending on species), IFNβ, IFNω, IFNκ, IFNε, IFNδ (pigs), IFNτ (ruminants); Type II with IFNγ as the only member; and Type III with 3 members of IFNλ. Type I IFNs are secreted by almost every cell type, whereas IFNα and IFNω are mainly produced by hematopoietic cells and IFNβ mainly by fibroblasts (Borden et al. 2007). In contrast, IFNγ is mainly produced by T-lymphocytes (Mosmann et al. 1989) and NK-cells (Handa et al. 1983; Bancroft et al. 1987; Chan et al. 1991). However, there is increasing evidence that macrophages (Munder et al. 1998), professional antigen-presenting cells (Ohteki et al. 1999)

as well as neutophils (Sturge et al. 2013) can also secrete limited amounts of IFNγ [reviewed in (Farrar et al. 1993; Frucht et al. 2001; Schroder et al. 2004; Bogdan et al. 2006)].

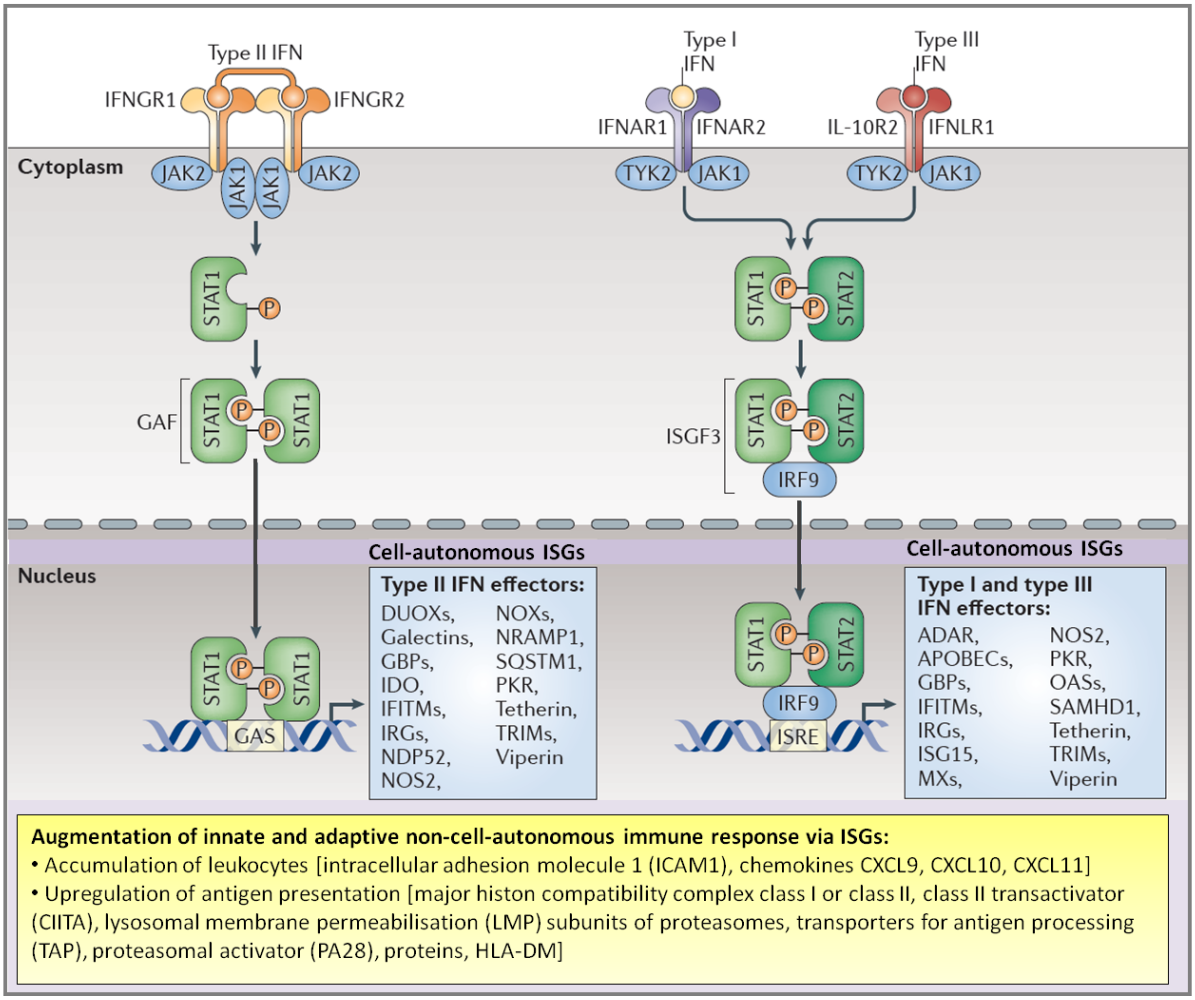


**Figure 1.1: Interferon induces IFN-stimulated genes (ISGs) via the JAK/STAT pathway.**
Interferon binds to its specific receptor in an autocrine or paracrine manner (e.g. IFNγ binds to a tetramer of two interferon-gamma receptor IFNGR1 and two IFNGR2) which triggers the activation of the receptor-associated Janus kinases (JAK) and tyrosinkinase 2 (TYK2). The kinases autophosphorylate themselves and tyrosine phosphorylate the interferon receptors enabling the recruitment of the signal transducer and activator of transcription 1 (STAT1) and STAT2. Phosphorylated homodimers of STAT1 (now termed gamma activation factor, GAF) or heterodimers of STAT1 and STAT2 in complex with IRF9 (now termed interferon-stimulated gene factor 3, ISGF3) translocate to the nucleus to bind the promoter elements IFNγ-activated site (GAS) or IFN-stimulates response element (ISRE), respectively. The activation of this JAK/STAT signalling pathway results in the transcription of a huge number of ISGs, which can have overlapping promotes elements or require transactivation of additional cofactors (e.g. IRF1 or IRF8). ISGs can act cell-autonomously (listed in blue box) or non-cell-autonomously (listed in yellow box) [modified from (MacMicking 2012)].

The production of IFN is induced via TLR- or RLR-dependent recognition of viruses, microbial products or chemicals and the main transcription factors acting downstream are interferon regulatory factor 3 (IRF3), IRF7 and nuclear factor κB (NF-κB). Upon secretion, IFNs engage specific high affinity receptors on cell surfaces, and signal via the JAK/STAT (Janus kinase/ signal transducer and activator of transcription 1) pathway to induce the

expression of interferon stimulated genes (ISGs) (Figure 1.1; see Figure legend for detailed description of JAK/STAT pathway).

Nearly 2000 human and mouse ISGs have been identified (Rusinova et al. 2013) corroborating the important role of interferons in multiple processes of innate and adaptive immunity. IFNs are responsible for (1) activation and accumulation of immune cells, (2) up-regulation of antigen presentation to T-lymphocytes, (3) isotype switching in B-cells to produce opsonising and complement-fixing antibodies, and (4) triggering of defence mechanisms in uninfected cells to resist new infections. The resistance mechanisms can act systemically (Figure 1.1, yellow box) or cell-autonomously (Figure 1.1, blue boxes) (Borden et al. 2007). The names and functions of cell-autonomous ISGs, which are listed in the blue boxes of Figure 1.1, will shortly be explained in the following paragraph.

Since interference with viral replication was discovered first, many different ISGs mediating viral restrictions on a cell-autonomous level are now known. Some prominent examples are: (a) blockage of viral entry and uncoating [IFN-inducible transmembrane (IFITMs), tripartite motif (TRIMs), or orthomyxovirus resistance gene (Mxs) proteins]; (b) interference with transcriptional and translational control [2′,5′-oligoadenylate synthetases (OASs), dsRNA-activated protein kinase (PKR), ribunuclease L (RNASEL), or ubiquitin-like ISGylation (ISG15)], or (c) prevention of viral assembly, budding and release [tetherin and viperin] (MacMicking 2012).

Moreover, ISGs mediate cell-autonomous defence against microbes via various mechanisms. Firstly, these mechanisms may rely on reactive oxygen species (ROS) and reactive nitrogen species (RNS). These cytotoxic gases are generated by the ISGs: NADPH oxidases (NOXs for $O_2^-$), dual oxidases (DUOXs for $H_2O_2$), and nitric oxidase synthases (NOS2 for NO). Because ROS and RNS can damage DNA, lipids and proteins rather unspecifically (Nathan et al. 2013), their production has to be tightly controlled and is often compartmentalised to phagolysosomes containing microbes (MacMicking 2012). Besides bacterial killing, ROS and NOS function in signal transduction, transcriptional activation, inflammation and carcinogenesis (Nathan et al. 2013). Secondly, ISGs can hinder microbes from acquiring essential nutrients from the host cell by deprivation, for example restriction of intracellular cations by the $Mn^{2+}$ $Fe^{2+}$ efflux pump natural resistance-associated macrophage protein1 (NRAMP1) or amino acids by the tryptophan degrading enzyme indoleamine-2,3-dioxygenase (IDO) and tryptophan-2,3-dioxygenase (TDO). Thirdly, ISGs can also target free bacteria via their exposed glycan patterns with galectins or, since they are ubiquitinated in the cytosol, with ubiquitin receptors [sequestosome 1 (SQSTM1), NDP52, optineurin], leading to

recruitment of the autophagic machinery (Chang et al. 2011; Deretic et al. 2013). Lastly, ISGs can directly target and destroy pathogen-containing vacuoles (e.g. *Toxoplasma gondii)* [immunity-related GTPases (IRG), guanylate-binding protein (GBP)] (see 1.4), and it has been proposed that they may target vacuolar or cytosolic bacteria (MacMicking 2012).

## 1.3 Interferon-inducible GTPases

Four GTPase families were found to be strongly upregulated by IFNs: (1) immunity-related GTPases (IRG, 47 kDa, former p47 GTPases) (Boehm et al. 1998; Bekpen et al. 2005); (2) the antiviral Mx proteins (72-82 kDa) (Staeheli et al. 1986; Haller et al. 2007); (3) guanylate-binding proteins (GBP, 65-67 kDa, former p65 GTPases) (Degrandi et al. 2007; Kim et al. 2012); and (4) Very Large Inducible GTPases (VLIG, 200-285 kDa) (Klamp et al. 2003). With the exception of Mx proteins, which are not induced by type II IFNs (Hug et al. 1988; von Wussow et al. 1990), all families can be induced by type I, II and III IFNs (Martens et al. 2006). In fact, in a pioneer mRNA screen of IFNγ-induced mouse cells, IRG and GBP transcripts were the most abundant (35%) induced target genes (Boehm et al. 1998).

All GTPases cycle between two alternative conformations: the GDP-bound form, which is considered inactive, and the GTP-bound form, which represents the active state mediating effector functions. The transition between these two states can be regulated by other proteins. According to their function these factors are called: guanine dissociation inhibitors (GDI) preventing dissociation of GDP; guanine exchange factors (GEF) releasing bound GDP; or GTPase –activating proteins (GAP) accelerating GTP hydrolysis. The GTPase domain (G-domain) of almost all GTPases comprises five nucleotide binding motifs termed (G1-G5) and two flexible regions called switch 1 and switch 2 (Leipe et al. 2002; Martens et al. 2006). IRG and Mx proteins contain the universally conserved G1 (GxxxGKS), G3 (DxxG) and G4 (N/TKXD) (Bourne et al. 1991), in contrast to GBP and VLIG proteins, which have a functionally different G4 motif (Cheng et al. 1991; Praefcke et al. 1999; Klamp et al. 2003). The interferon-inducible GTPases share several biochemical features with the conserved dynamins (see also 1.3.3). Dynamins are able to deform and tubulate cellular membranes, a process required for the scission of clathrin-coated endosomes, and are further implicated in vesicular processes, organelle and cell division [reviewed in (Praefcke et al. 2004; Pucadyil et al. 2009)]. Interestingly, interferon-inducible GTPases occur sporadically during evolution in deuterostomia since they have experienced gene gain and loss in different chordate (see Figure 1.2).

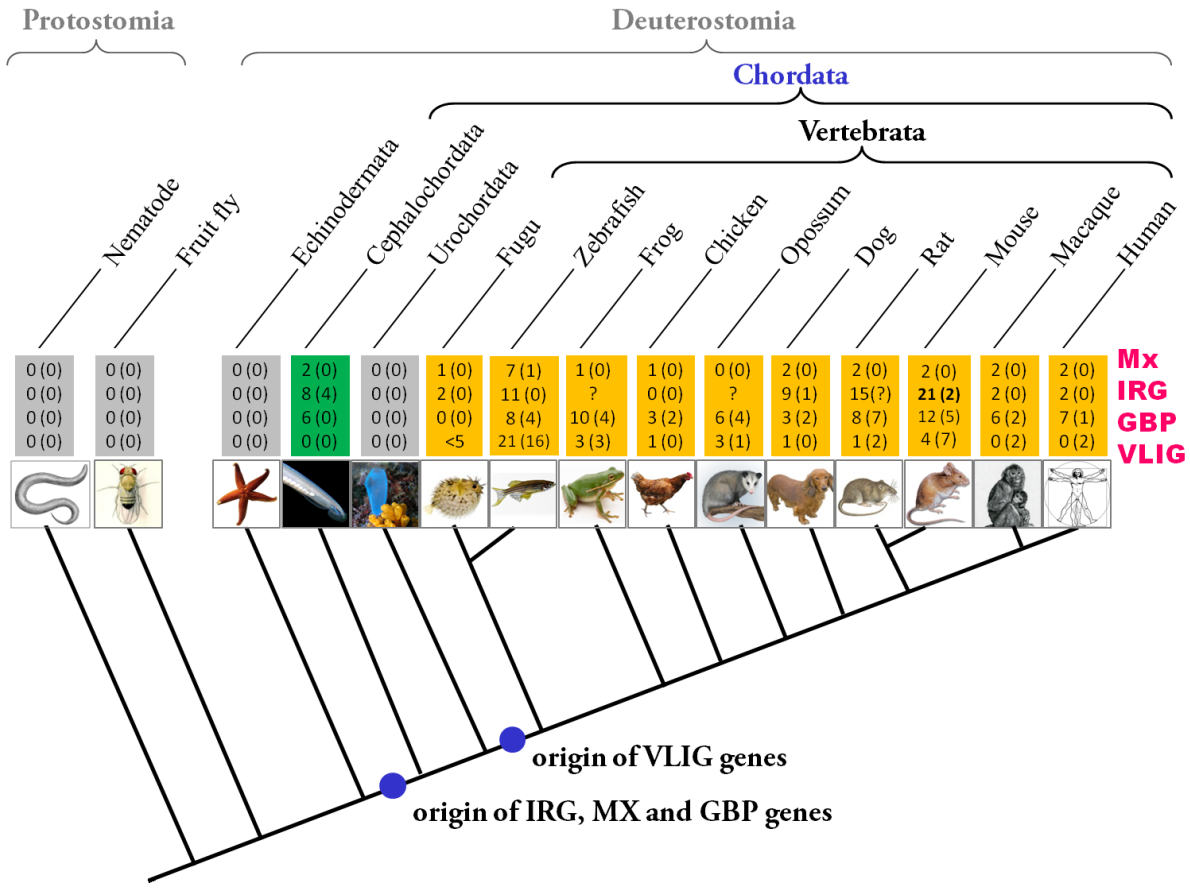


**Figure 1.2: Sporadic occurrence of interferon-inducible GTPases during evolution of chordata.**
Number of putatively functional genes and number of pseudogenes in brackets are listed. So far, no interferon-inducible GTPases have been found in protostomia, which include the model organisms *Drosophila melangaster* and *Caenorhabditis elegans*. For vertebrate genes, ISRE elements could be identified in the promoter elements (yellow background). The blue spheres indicate the diverging positions (modified from (Li et al. 2009)).

For example, Mx and GBP genes are lost in opossum and chicken, respectively. IRG genes are present in several chordates such as Branchiostoma (lancelet fish, subphylum cephalochordate/acrania), teleost fish, dogs, rat and primates. However, IRG genes are apparently absent in bird, cat and horse but largely expanded in rodents. (Bekpen et al. 2005; Hunn 2007; Li et al. 2009; Gazzinelli et al. 2014).

### 1.3.1 Immunity-related GTPase (IRG) gene family

The first six *IRG* genes were identified and sequenced in the 1990s, namely *IRG-47* (now *Irgd*) (Gilly et al. 1992), *LRG-47* (now *Irgm1*) (Sorace et al. 1995), *TGTP/Mg21* (now *Irgb6*) (Carlow et al. 1995; Lafuse et al. 1995), *IGTP* (now *Irgm3*) (Taylor et al. 1996) as well as *IIGP* (now *Irga6*) and *GTPI* (now *Irgm2*) (Boehm et al. 1998). The corresponding proteins together with Irgb10 still constitute the best studied IRG protein family members.

In 2005, genomic investigations in the C57BL/6 laboratory mouse genome identified a group of about 23 IRG genes and pseudogenes and a uniform nomenclature according to their phylogeny was introduced (Bekpen et al. 2005). Three genes (*Irgm1, Irgm2, Irgm3*) encode proteins with the non-canonical sequence $GX_4G\mathbf{M}S$ in the G1 motif of the GTP binding site and are therefore informally called the GMS or IRGM subfamily. The second subfamily (IRGA, IRGB, Irgc and Irgd) possesses the universally conserved G1 sequence ($GX_4G\mathbf{K}S$) and are informally called GKS proteins (Boehm et al. 1998; Bekpen et al. 2005). From there on, rodent IRGs were written with capital I followed by small letters (in italics for genes, regular for proteins) and for other mammals as well as for the gene/protein family in general (e.g. Irgm1-3) only capital letters (IRGM) were used (Martens et al. 2006).

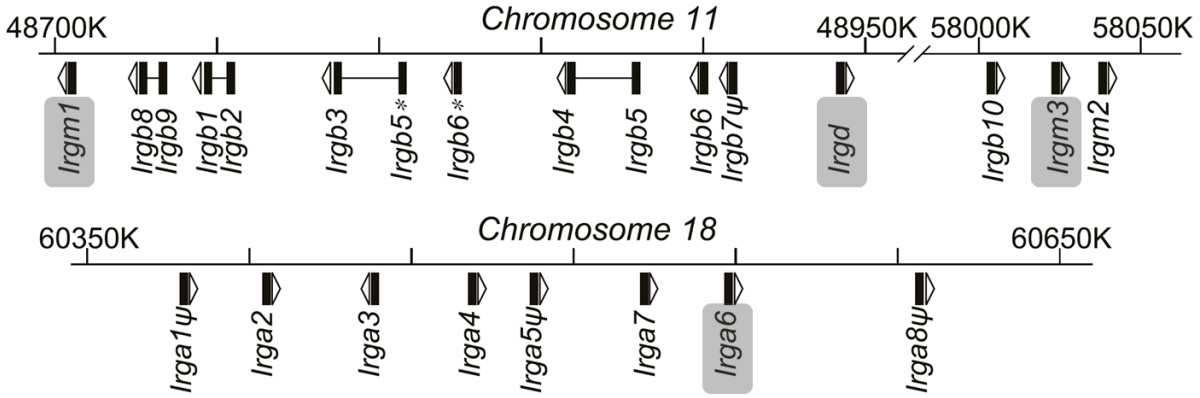


**Figure 1.3: Linear order of IRG gene clusters on Chr. 11 and Chr. 18 of C57BL/6 mouse strain.**
The black blocks mark the position of the IRG coding unit and the arrowhead the direction of transcription. Some genes are transcribed as tandem, connected with a line. Numbers give the position on the chromosome. For the four genes in gray boxes, single knock-out mice, as well as an IRG double knock-out mouse strain *(Irgm1/Irgm3)* were generated so far. ψ indicates pseudogenes, * marks the second copy of the gene [modified from (Lilue et al. 2013)].

The mouse *IRG* genes are distributed on chromosome 11 in two clusters separated by 10 Mb (*Irgm1*/*Irgb1-Irgb9/Irgd* and *Irgb10*/*Irgm3*/ *Irgm2*), on chromosome 18 in one cluster (*Irga1-Irga8*) (Figure 1.3) as well as a single member on chromosome 7 (*Irgc*, also known as *CINEMA*). The open reading frame of *IRG* genes is typically encoded on one long 3´ exon following one or more 5´untranslated exons. However, *Irgm1-3* genes are encoded on two coding exons allowing two possible isoforms for *Irgm1* and *Irgm2* due to alternative splicing (see also Figure 1.3). Another exception are four pairs of tandem genes, namely *Irgb2-Irgb1*, *Irgb5-Irgb3, Irgb5-Irgb4, Irgb9-Irgb8,* which are transcribed across two chromosomally adjacent *IRG* coding units, resulting in the expression of 94 kDa proteins (Bekpen et al. 2005; Lilue et al. 2013). Sequencing analysis of different laboratory and wild mouse strains revealed

that some members of the IRG family are remarkably polymorphic (e.g. *Irgb2-b1, Irgb6*) whereas others are rather conserved (e.g. *Irgm1*, *Irga6*) (Lilue et al. 2013).

Humans have only two transcribed *IRG* genes. *IRGC* is an orthologue of mouse *Irgc* that matches 90 % on the amino acid level, and is localised on chromosome 19 in a region syntenic to mouse chromosome 7. *IRGM* on human chromosome 5 encodes an amino- and carboxyterminally truncated G-domain homologue of mouse Irgm1/2/3 (Bekpen et al. 2005). Five mRNA transcripts for 3´-splicing isoforms (IRGM a-e) could be detected so far (Bekpen et al. 2010) and were individually examinated (Singh et al. 2010). Interestingly, the mammalian IRGM gene family contracted to a single-copy gene that became pseudogenised in the ancestral lineage of apes and monkeys due to an $AluS_c$ retrotransposition event leading to the disruption of the open reading frame. In great apes and human, however, integration of an endogenous retroviral EVR9 element serving as a functional promoter along with a mutation generating a new ATG codon could revive IRGM gene. Thus, the human IRGM can be considered as a "resurrected gene" that is homologous to all three mouse IRGM genes but clearly differs in size, promoter region and splicing (Bekpen et al. 2009).

Lastly, an *IRG* homologous gene family, so-called *quasi-IRG*, could be identified in the zebrafish (*irgq1-irgq3*), mouse (*Irgq, Fksg27*) and human (*IRGQ,* also *FKSG27*) genome (Bekpen et al. 2005; Martens et al. 2006) and other chordates (Hunn 2007). It differs from the canonical family members by a radically modified GTP-binding site that shows a clear disruption of the universally conserved G1 motif. Mammalian *IRGQ* is closely linked to IRGC in human and mouse, but despite its phylogenetic relationship, it is not a functional GTPase (Bekpen et al. 2005; Martens et al. 2006). In the following, only mouse *IRG* or human *IRG* (hIRG) genes and proteins will be discussed.

### 1.3.2 Induction and Expression of IRG proteins

Almost all mouse *IRG* gens have ISRE and GAS sequences in their promotor region and can therefore be induced with Type I and Type II IFNs (Lafuse et al. 1995; Sorace et al. 1995; Gilly et al. 1996; Taylor et al. 1996; Boehm et al. 1998; Carlow et al. 1998; Collazo et al. 2001; Zerrahn et al. 2002; MacMicking et al. 2003; Bekpen et al. 2005). Upon IFN stimulation IRG proteins can be detected in any IFN-responsive mouse cell. *Irga6* has an additional liver-specific promoter that allows expression of an alternative isoform in the liver, which however has the same amino acid sequence (Zeng et al. 2009). Some studies reported *IRG* transcription upon other stimuli (e.g. LPS or TNFα) (Taylor et al. 1996; Zerrahn et al. 2002; Lapaque et al. 2006; Bafica et al. 2007; Yamada et al. 2009), but since no NF-κB

binding sites were identified in their promoter region (Bekpen et al. 2005), this may reflect secondary induction of interferons. As an exception, the *Irgc* promoter carries weak Sox elements but no ISRE or GAS sequences and is therefore not induced by IFN stimulation or *Listeria* infection (Bekpen et al. 2005). Instead, Irgc can be detected in tissue of adult testis and is expressed constitutively and exclusively in haploid spermatids suggesting a role in reproduction or development (Bekpen et al. 2005; Rohde 2006).

None of the human *IRG* genes are IFN-inducible, because *hIRGM* has an altered promoter region and *hIRGC* is homologous to the exceptional mouse IRG without GAS or ISRE elements (see 1.3.1). Endogenous hIRGM as well as mRNA for *hIRGMa/b/c/d* isoforms could be detected in human cell lines and overexpression of isoform-specific fusion proteins is possible (Bekpen et al. 2005; Singh et al. 2006; Singh et al. 2010). In contrast, hIRGC is strongly expressed only in testis but not in brain or liver, similar to observations in mice (Bekpen et al. 2005; Rohde 2006). Thus, human IRG proteins are not considered to exert an interferon-dependent immunity-related function.

### 1.3.3 Structural and biochemical properties of IRG proteins

Initial biochemical studies on GTPase activity were performed for immunoprecipitated Irgm3 and recombinant GST-Irgm3 (Taylor et al. 1996; Taylor et al. 1997) as well as for recombinant GST-Irgb6 (Carlow et al. 1998). Using GTP hydrolysis assays with radiolabelled nucleotides followed by thin layer chromatography, it was demonstrated that these IRG proteins are able to hydrolyse GTP to GDP, even though it was only a minor percentage for Irgm3 (Taylor et al. 1996; Taylor et al. 1997). Soon after, recombinant Irga6 was biochemically and enzymatically characterised in detail (Uthaiah et al. 2003). Irga6 binds GTP and GDP with a dissociation constant in the micromolar range, with a 10-15 fold higher affinity for GDP (1 µM) than GTP (15 µM). Because intracellular concentrations of GTP and GDP are approximately 330 µM and 120 µM respectively (Kleineke et al. 1979), it is very likely that Irga6 resides in the cytosol predominantly in the GDP-bound form. In uninfected cells, endogenous Irga6 can indeed hardly be detected microscopically with the 10D7 monoclonal antibody specific for GTP-bound Irga6 (Papic et al. 2008). Upon GTP-binding, Irga6 homo-oligomerises *in vitro* without external GEF (Uthaiah et al. 2003). Furthermore, it is suggested that Irga6 activation by binding of GTP is accompanied by a conformational change of the protein, probably in the flexible switch I region (Papic et al. 2008; Pawlowski et al. 2011). The oligomers can resolve upon GTP hydrolysis and the correlation of increased

protein concentration with increased GTP hydrolysis demonstrates that there is a cooperative mechanism between Irga6 molecules (Uthaiah et al. 2003).

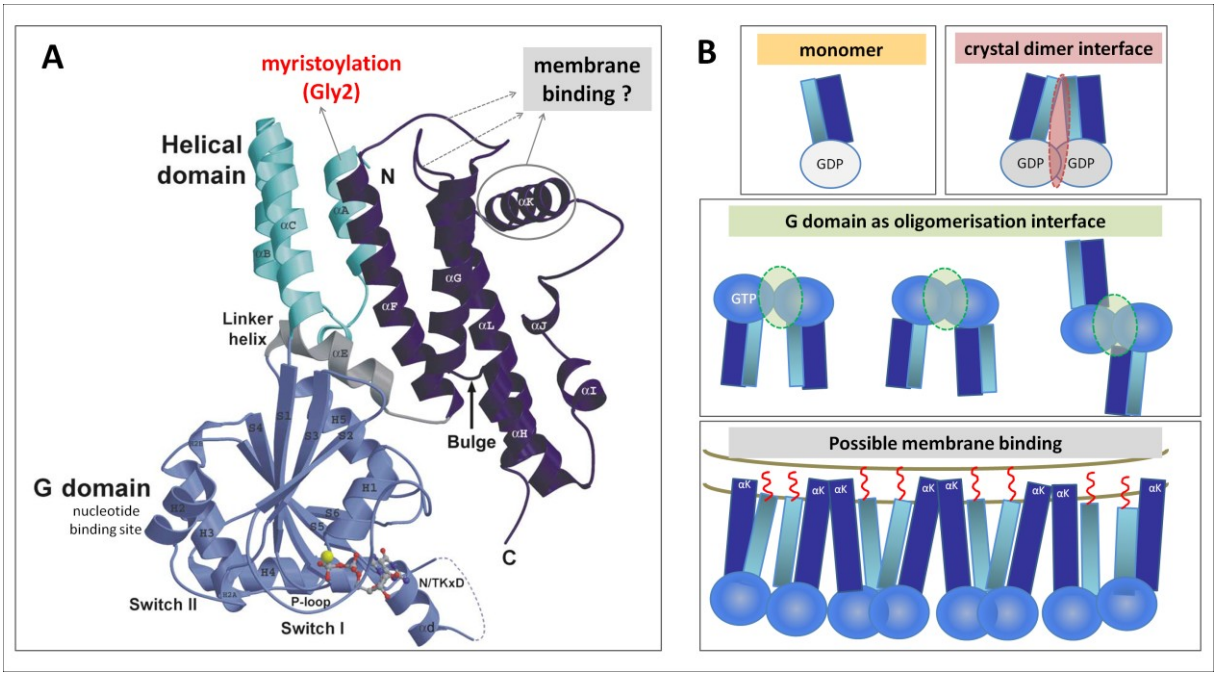


**Figure 1.4: Crystal structure of Irga6.**
**(A)** Ribbon presentation of the GDP/$Mg^{2+}$-bound Irga6 crystal consisting of an N-terminal helical region (cyan), a Ras-like G-domain (blue), a linker helix (grey) and a C-terminal region formed by helices and loops. The N-terminus of Irga6 is myristoylated, and together with the αK helix and two loops opposing the G-domain they may mediate membrane-binding (modified from (Ghosh et al. 2004)). **(B)** Schematic models for Irga6 interactions showing the GDP-bound monomers and the GDP-bound crystal dimer with an interface of parts of the G-domain and the N-terminal helical domain. A second catalytic interface essential for GTP hydrolysis for has been identified on the G-domain which is also necessary for Irga6 oligomerisation. The αK-helices and the myristoylation may directly bind membranes [prepared according to (Pawlowski et al. 2011)].

The Irga6 crystal was resolved in 2004 as dimer in a nucleotide-free, GDP-bound or GppNHp-bound state (Ghosh et al. 2004). Since it is the only IRG protein for which the crystal structure has been resolved so far and IRG proteins have a high sequence homology, Irga6 serves as a model for other IRG family members. It reveals a Ras-like G-domain consisting of six β-strands (S1-S6) and six helices (H1-H5 and αD) connected by a linker helix (αE) to a helical domain that is formed by three helices (αA, αB, αC) of the N-terminal domain and seven helices (αF-αL) and loops of the C-terminus (Figure 1.4 and (Ghosh et al. 2004)). Because the first 13 amino acids could not be resolved in the crystal structure (Ghosh et al. 2004), there is little information concerning the N-terminus of the Irga6. Irga6, as well as other IRG proteins (IRGA, Irgb2/5/9/10), carry an N-terminal myristoylation motif at Glycine 2 (Bekpen et al. 2005). Indeed, endogenous Irga6 is myristoylated and this lipid

modification has been shown to play a role in membrane-binding (Martens et al. 2004) as well as in GTP-dependent Irga6 homo-oligomerisation (Papic et al. 2008).

In 2011, the catalytic interface of Irga6 essential for GTP hydrolysis was defined by an extensive mutagenesis screen of surface-exposed residues (Pawlowski et al. 2011). The catalytic interface is localised in the G-domain including the nucleotide-binding site and the switch regions. In addition, the bound nucleotide itself could be demonstrated to be part of the catalytic interface, which interacts reciprocally in a dimer via the 3´hydroxyls and the γ-phosphates of the opposed nucleotides in *trans*. This conserved catalytic interface is furthermore responsible for GTP-dependent interaction with Irgb6 and GDP-dependent interaction with Irgm3 (Pawlowski et al. 2011).

Some of the biochemical features of Irga6, namely GTP-dependent oligomerisation, micromolar affinities for guanine nucleotides, as well as cooperative hydrolysis of GTP, are shared with other interferon-inducible GTPases and the conserved dynamins (also see 1.3.) (Praefcke et al. 2004). However, the observed higher affinity for GDP than GTP and the low GTPase activity are unique to Irga6 (and probably other IRG proteins). In contrast, GBP proteins bind GTP, GDP and GMP with the same affinity (Cheng et al. 1991) and hydrolyse GTP in two consecutive cleavage reactions to GDP and GMP (Schwemmle et al. 1994; Neun et al. 1996; Praefcke et al. 1999; Ghosh et al. 2006). Moreover, the crystal structure of hGBP1 reveals an N-terminal G-domain and C-terminal helical domain (Prakash et al. 2000).

### 1.3.4 Membrane-binding of IRG proteins and other interferon-inducible GTPases

IRG proteins seem to have an intrinsic ability to interact with lipids, because recombinant Irga6 co-sediments with phosphatidylserine vesicles (Martens et al. 2004) and bacterially expressed GKS proteins can co-sediment with Folch liposomes (Nikolaus Pawlowski, unpublished data). Moreover, GST-tagged Irgm1 was shown to interact with the following immobilised lipids on nitrocellulose filters: PtdIns(3,4)$P_2$, PtdIns(3,4,5)$P_3$, cardiolipin and weakly with phosphatic acid (Tiwari et al. 2009).

It is not entirely understood how IRG proteins mediate membrane-binding. For GMS proteins, it has been shown that a C-terminal sequence, which corresponds to the αK helix of Irga6 (Figure 1.4), is essential for membrane targeting to their respective subcellular compartment (see also 1.3.5) (Martens 2004; Martens et al. 2004; Martens et al. 2006; Zhao et al. 2010). In case of Irgm1, the responsible amino acids 350 – 374 are predicted to constitute an amphipathic helix. Disruption of the amphipathic character by mutation of more than one hydrophilic residue or insertion of glutamate completely abolishes membrane-binding

(Martens et al. 2004; Zhao et al. 2010). However, this protein region including the αK helix is highly divergent among IRG proteins. Therefore, it remains elusive whether the mechanism of membrane targeting via an amphipathic helix applies also to other IRG proteins (Martens 2004). Based on these results, a role for Irga6 in membrane attachment has been proposed not only for the helix αK, but also for the αK-αL and αF-αG loops, which are also exposed on the surface of Irga6 distal to the G-domain (see Figure 1.4) (Ghosh et al. 2004). Furthermore, the N-terminal myristoylation of Irga6 has been shown to partially mediate or enhance binding to the endoplasmatic reticulum (ER) (Martens et al. 2004). However, the non-myristoylated Irga6 (G2A mutant) is still associated with membranes (Martens et al. 2004), but is strongly impaired in relocalising to the parasitophorous vacuolar membrane (PVM) upon infection with *Toxoplasma gondii (T. gondii)* (Papic 2007).

A mutagenesis attempt to define the interface on Irga6 responsible for binding to the PVM of *T. gondii* provided only an unstructured region on the crystal structure of the GDP/GppNHp-bound Irga6 protein (Fleckenstein 2012). Because predominantly active GTP-bound Irga6 accumulates on the PVM (Papic et al. 2008) and since a GTP-bound dimer is likely to undergo conformational change, it remains unclear which part of Irga6 actually mediates binding to the PVM (Fleckenstein 2012).

There is increasing knowledge on how other interferon-inducible GTPases mediate membrane-binding via lipid modifications or via membrane-binding domains. Some GBP proteins possess a C-terminal CaaX box enabling either farnesylation (hGBP1 and mGBP5) or geranylgeranyliation (hGBP2, hGBP5, mGBP1, mGBP2) (Vestal et al. 2011). Indeed, protein prenylation has been confirmed for hGBP1 (Nantais et al. 1996; Modiano et al. 2005), mGBP2 (Vestal et al. 2000) and weakly for mGBP1 (Stickney et al. 2000). Human GBP1 requires farnesylation, GTP-binding and an interferon-inducible cofactor for Golgi targeting (Modiano et al. 2005). In contrast, Irgm1 targeting of the Golgi is GTP-independent and myristoylation of Irga6 only facilitates ER membrane-binding (Martens 2004). Mx proteins carry neither a lipid modification motif nor a pleckstrin-homology (PH) domain, which is a typical membrane-binding domain in dynamins (Haller et al. 2007). However, MxA has recently been shown to bind negatively charged membranes and tubulate liposomes via an unstructured L4 loop of the oligomer-forming Stalk domain (von der Malsburg et al. 2011).

### 1.3.5 Subcellular localisation of IRG proteins

IRG proteins associate with membranes to different degrees and distribute among distinct subcellular compartments. GMS proteins are almost exclusively membrane bound, whereas GKS proteins are mainly cytosolic (Martens 2004). Irgm1 localises to Golgi, endosomes, and lysosomes (Martens et al. 2004; Butcher et al. 2005; Tiwari et al. 2009; Zhao et al. 2010). Irgm1 requires functional integrity of the nucleotide binding site for targeting to the endolysosomal system but not to Golgi (Zhao et al. 2010). C- or N-terminal EGFP-tagging of Irgm1 shift the protein to the endolysosomal system, and mutations in the nucleotide binding site revert the tagged Irgm1 back to Golgi. Thus, artificial tagging can result in anomalous subcellular distributions of IRG proteins and may influence the nucleotide-bound state (Martens 2004; Zhao et al. 2010). Furthermore, studies reported that Irgm1 could be detected at mitochondria (Tiwari et al. 2009; Chang et al. 2011). Irgm2 localises to the Golgi (Martens et al. 2006; Hunn et al. 2008) but has also the largest cytosolic pool among the GMS proteins (Martens 2004). Irgm3 localises to the ER (Taylor et al. 1997; Martens 2004; Hunn et al. 2008). Moreover, a large proportion of Irgm3 and a part of Irgm1 have been detected at lipid droplets, a storage compartment for neutral lipids (Bougneres et al. 2009; Haldar et al. 2013). Except for the plasma membrane, all endomembranes seem to be covered by endogenous GMS proteins. In artificial overexpression systems, the GFP-tagged G-domain of Irgm1 localised also to the plasma membrane (Martens et al. 2004).

Irga6 partitions roughly 60:40 between ER and cytosol (Zerrahn et al. 2002; Martens et al. 2004), whereas native Irgb6, Irgb10 and Irgd are predominantly cytosolic (Martens 2004; Coers et al. 2008). IRG protein localisation in uninfected cells is largely independent of GTPase activity, because ectopically expressed nucleotide-binding mutants show similar subcellular localisation as the endogenous proteins (Taylor et al. 1997; Martens 2004; Zhao et al. 2010). Ectopic expression of GKS protein (Irga6, Irgb6, Irgb10, Irgd) in IFNγ-unstimulated cells results in the formation of aggregates (Martens et al. 2004; Hunn et al. 2008) (and Jelena Maric, unpublished data). For Irga6, these aggregates were found to be GTP-bound oligomers (Papic et al. 2008) that can be resolved by the co-expression of GMS proteins or induction of GMS proteins with interferon (Hunn et al. 2008). Since loss of GMS proteins causes premature activation of GKS proteins and unregulated oligomerisation, it can be concluded that GMS proteins are essential regulators to keep GKS proteins in an inactive GDP-bound state, suggestion a function as GDI (Hunn et al. 2008; Papic et al. 2008; Henry et al. 2009; Traver et al. 2011) (and Jelena Maric, unpublished data).

## 1.4 Role of IRG proteins in (cell-autonomous) immunity

### 1.4.1 IRG resistance system to certain pathogens

The analysis of *IRG*-deficient mice suggested that IRG proteins play an pivotal role in resistance against intracellular protozoa and bacteria [reviewed in (MacMicking 2004; Taylor et al. 2007; Hunn et al. 2011)].

**Table 1.1: IRG mediated resistance against intracellular pathogens**

| Pathogen | *in vivo* (knock-out mice) | | | | | | | Ref. *in vivo* data | *in vitro* | Ref. *in vitro* data |
|---|---|---|---|---|---|---|---|---|---|---|
| | **wt** | ***IFNγ*$^{-/-}$** | ***Irgm1*$^{-/-}$** | ***Irgm3*$^{-/-}$** | ***Irgm1*$^{-/-}$ *Irgm3*$^{-/-}$** | ***Irga6*$^{-/-}$** | ***Irgd*$^{-/-}$** | | →Impaired IFNγ-mediated growth inhibition? (subcellular localization) | |
| ***Toxoplasma gondii*** | R | S | S | S | S | S | S | (Scharton-Kersten et al. 1996; Taylor et al. 2000; Collazo et al. 2001; Butcher et al. 2005; Ling et al. 2006; Henry et al. 2009; Zhao et al. 2009; Liesenfeld 2011) | → in all *IRG* KO cells<br>(Irgm2, Irgm3, Irga6, Irgb2-b1, Irgb6, Irgb10and Irgd relocalise to the PVM) | s. a. + (Halonen et al. 2001; Butcher et al. 2005; Martens et al. 2005; Zhao et al. 2009; Khaminets et al. 2010; Fleckenstein et al. 2012; Lubitz et al. 2013) |
| ***Neospora caninum*** | R | S | | | | | | (Nishikawa et al. 2001) | (Irga6, Irgb6 and Irgd relocalise to the PVM) | (Reid et al. 2012; Spekker et al. 2013) |
| ***Leishmania major*** <br> ***L. mexicana*** | R | S | S | S | | R | | (Swihart et al. 1995; Taylor et al. 2004; Liesenfeld 2011) | | |
| ***Trypanosoma cruzi*** | R | S | S | R | | | | (Michailowsky et al. 2001; de Souza et al. 2003; Santiago et al. 2005) | → in Irgm1KO cells<br>→ upon siRNA-KD of Irgd | s. a. + (Koga et al. 2006) |
| ***Plasmodium berghei ANKA*** | S | R | | | | R | | (Amani et al. 2000; Liesenfeld 2011; Inoue et al. 2013) | NO relocalisation of IRG proteins to the PVM | s. a. |
| ***Chlamydia trachomatis*** | R | S | S | S | S* | R | | (Cotter et al. 1997; Nelson et al. 2005; Coers et al. 2008; Coers et al. 2011) | → upon siRNA-KD of Irgb10<br>→in Irgm3KO and Irga6KO cells (Irgb6, Irgb10 and Irgd relocalise to the PVM, conflicting data for Irgm3 and Irga6) | s. a. + (Bernstein-Hanley et al. 2006; Al-Zeer et al. 2009; Haldar et al. 2013) |
| ***Chlamydia psittaci*** | R | | | S | | | | (Miyairi et al. 2007) | → upon siRNA-KD of Irgm2 | s. a. |
| ***Chlamydia muridaum*** | R | R | | | | | | (Nelson et al. 2005) | → No IFNγ-mediated growth inhibition in MEFs | (Coers et al. 2008; Al-Zeer et al. 2009) |

| | | | | | | | | | | |
|---|---|---|---|---|---|---|---|---|---|---|
| ***Listeria mono-cytogenes*** | R | S | S | R | | R | | (Collazo et al. 2001; Liesenfeld 2011) | (conflicting data about Irgm1 localisation at the phagosome) | (Shenoy et al. 2007) and this study |
| ***Legionella pneumophila*** | R | S | | | | | | | → in Irgm3KO cells but not Irgm1KO or Irgm1/Irgm1KO | unpublished data in (Henry et al. 2009) |
| ***Myco-bacterium avium*** | R | S chronic | S | | | | | also R in *Irgm1*$^{-/-}$*IFNγR*$^{-/-}$ mice (Doherty et al. 1997; Feng et al. 2004; Feng et al. 2008) | | |
| ***M. tuberculosis*** <br> ***M. bovis*** **BCG** | R | S | S | R | R | R | R | (Cooper et al. 1993; Dalton et al. 1993; Flynn et al. 1993; MacMicking et al. 2003; Feng et al. 2004; Henry et al. 2009; Liesenfeld 2011) | (conflicting data about Irgm1 localisation at the phagosome) | this study and (Gutierrez et al. 2004; Singh et al. 2006; Deghmane et al. 2007; Shenoy et al. 2007; Saban et al. 2008; Tiwari et al. 2009; Tischler et al. 2013) |
| ***Salmonella typhimurium*** | R | S | S | R | R | | R | (Henry et al. 2007; Henry et al. 2009) | → in Irgm1KO cells but not Irgm3KO or Irgm1/Irgm3KO | s. a. |
| ***Rhodococcus equi*** <br> ***R.aurantiacus*** | R | S | | | | | | (Yimin et al. 2001) for R. aurantiacus | → No growth inhibition in Irgm1KO BMM | (von Bargen et al. 2011) for R. equi |
| ***Anaplasma phagocyto-philum*** | R | | | | | R | | (Liesenfeld 2011) | | |
| ***Brucella abortus 2308*** | | | | | | | | | → enhanced bacterial killing upon IFNγ-stimulation in *Irgm1KO* BMM compared to in wt | (Ritchie et al. 2012) |
| ***Schistosoma mansoni*** | R | R | R | | | | | (Feng et al. 2008) | | |
| ***Schistosoma japonicum*** | R | S* | S* | n. e. | | | S* | (Chen et al. 2010; Du et al. 2011) | | |
| ***Murine cytomegalo-virus*** | R | S | R | R | | | R | (Pomeroy et al. 1998; Taylor et al. 2000; Collazo et al. 2001) | | |
| ***Ebola virus*** | R | S* | | R | | | | (Taylor et al. 2000; Gupta et al. 2005) | | |
| ***Vesicular stomatitus virus*** | | | Overexpression of Irgb6 in fibroblasts inhibits VSV but not HSV plaque formation (Carlow et al. 1998) | | | | | | | |
| ***Coxsackievirus B3 (CVB3)*** | | | Overexpression of Irgm3 in HeLa cells inhibits CVB3 replication (Zhang et al. 2003; Liu et al. 2008) | | | | | | | |
| R resistant; S susceptible; *w*t wildtype; KO knock-out; KD knock-down; n. e. no effect; s. a. see above (in references for *in vivo* data), S* weak susceptibility; an empty field means not determined | | | | | | | | | | |

Table 1.1 provides a detailed list of susceptibility or resistance of different *IRG* knock-out mice (*Irgm1*$^{-/-}$, *Irgm3*$^{-/-}$, *Irgm1/Irgm3*$^{-/-}$, *Irga6*$^{-/-}$, *Irgd*$^{-/-}$) to all intracellular pathogens tested so

far in comparison to *IFNγ*-deficient mice or wildtype C57BL/6 mice. Information obtained from *in vitro* studies about impaired IFNγ-mediated growth inhibition in *IRG*-deficient cells or subcellular relocalisation of IRG proteins is also included in the table 1.1.

All *IRG*-knock-out mice show enhanced susceptibility to the protozoan *Toxoplasma gondii,* underscoring the outstanding role of the IRG resistance system to this pathogen, which will be further introduced in chapter 1.4.2.

A close phylogenetic relative of *T. gondii, Neospora caninum*, which is not a mouse pathogen, is proposed to be restricted by the IRG resistance system as well. Though *in vivo* data for infection of *IRG*-deficient mice is still missing, *in vitro* observations imply that IFNγ-mediated cell-autonomous immunity correlates with GKS proteins relocalisation to the intracellular parasitophorous vacuolar membrane (PVM). Irga6, Irgb6 and Irgd have been observed to accumulate on the PVM of *N. canium* in infected murine mesenchymal stromal cells and fibroblasts. However, in contrast to virulent *T. gondii* strains (see 1.4.2) phosphorylation of IRG proteins seem not to be an immune evasion strategy of the parasite, since no phosphorylated Irga6 could be detected at the PVM of *N. caninum*.

For all other pathogens, the picture is more complicated and still incomplete. In general, *IRG*-deficient mice are resistant to most other protozoa and intracellular bacteria. For mice deficient in *Irgm1*$^{-/-}$ or *Irgm3*$^{-/-}$, enhanced susceptibility to *Leishmania major, Chlamydia trachomastis* and *Chlamydia psittaci* has been reported, whereas *Irgm1*$^{-/-}$*/Irgm3*$^{-/-}$ deficient mice show a delayed clearance of *Chlamydia trachomatis*. However, both GKS-deficient mice, *Irga6*$^{-/-}$ and *Irgd*$^{-/-}$*,* are resistant to all pathogens tested so far, except for *T. gondii*. A remarkable exception is Irgm1, which will be introduced in chapter 1.4.4. *Irgm1*-deficient mice showed increased susceptibility to all intracellular bacteria and protozoa tested so far. In contrast, mice with a second knock-out in addition to *Irgm1* can show resistance to infection with *Salmonella typhimurium (Irgm1*$^{-/-}$*/Irgm3*$^{-/-}$) or *Mycobacteria avium* (*Irgm1*$^{-/-}$ */IFNγ*$^{-/-}$).

Parasites that do not induce IFNγ-response in the host are controlled independent of the IRG resistance system. For example, initial infection studies with the extracellular parasitic flatworm *Schistosoma* showed no or only little restriction in *IRG*-deficient mice.

Even tough, an antiviral function for Irgm3 and Irgb6 was suggested by two *in vitro* studies, *Irgm1*$^{-/-}$*, Irgm3*$^{-/-}$ and *Irgd*$^{-/-}$ showed normal resistance to murine cytomegalo-virus and Ebola virus infection. Therefore, there is currently no data supporting an antiviral role of the IRG resistance system *in vivo*.

In summary, only the protozoa *Toxoplasma* and *Neospora* as well as two strains of the bacteria *Chlamydia* have been shown to be controlled by the IRG system, while many other

organisms, including *Salmonella*, *Listeria*, *Mycobacteria*, *Trypanosoma* or *Plasmodium* are not engaged by the IRG resistance system. *Irgm1*-deficient mice show a general susceptibility to all pathogens that stimulate an IFNγ-mediated immune response. (see table 1.1 for all references).

### 1.4.2 *Toxoplasma gondii* as a model to study IRG protein function

The consistent susceptibility of all *IRG*-deficient mice to the protozoan *T. gondii* implies that this parasite is a good model to study IRG protein function. Upon infection, *T. gondii*-derived MAMPs like profilin are recognised by TLRs triggering IL-12 and subsequent IFNγ secretion mainly by NK-cells and T-cells. IFNγ is crucial in controlling replication and dissemination of *T. gondii* in both the haemopoietic and non-haemopoietic compartment [(Suzuki et al. 1988; Gazzinelli et al. 1994; Scharton-Kersten et al. 1996; Scharton-Kersten et al. 1998; Yap et al. 1999) reviewed in (Yarovinsky 2014)]. *In vitro* studies with mobile unicellular *T. gondii* infecting cell monolayers revealed a profound IFNγ-mediated cell-autonomous resistance mechanism in myeloid cells such as macrophages as well as in non-myeloid cells such as fibroblasts. Experiments with *IRG*-deficient mouse cells confirmed that this IFNγ-mediated resistance is conducted by IRG proteins [(Halonen et al. 2001; Butcher et al. 2005; Martens et al. 2005) reviewed in (Howard et al. 2011)].

*T. gondii* actively invades host cells and resides in a parasitophorous vacuole (PV) ((Morisaki et al. 1995), see chapter 1.6 for PV). Immediately after parasite entry, effector GKS proteins relocalise from their cytosolic phase to the parasitophorous vacuolar membrane (PVM) [(Martens et al. 2005; Melzer et al. 2008; Zhao et al. 2009; Khaminets et al. 2010); and later confirmed by (Lubitz et al. 2013)] in a nucleotide-dependent manner (Hunn et al. 2008; Papic et al. 2008) (Figure 1.5 A). IRG proteins accumulate in a cooperative and hierarchical manner, probably by formation of mixed GTP-dependent heterooligomers (Khaminets et al. 2010; Pawlowski et al. 2011). GMS proteins however do not target the PVM at all (Irgm1) or only to a limited extent (Irgm2, Irgm3) (Butcher et al. 2005; Martens et al. 2005; Khaminets et al. 2010; Haldar et al. 2013).

In mouse cells infected with an avirulent *T. gondii* strain, it appears that IRG proteins reduce the effective surface area of the PVM by vesiculating or ruffling it as observed by electronmicroscopy (Martens et al. 2005; Ling et al. 2006; Zhao et al. 2008), putting the membrane under tension and leading ultimately to its rupture (Howard et al. 2011) (Figure 1.5 B-D). Once exposed to the cytosol, the parasite dies for unclear reasons followed by death of the infected host cell (Martens et al. 2005; Ling et al. 2006; Melzer et al. 2008; Zhao et al.

2009). While several markers for apoptosis and other cell death types are absent (AnnexinV staining at the plasma membrane, cytochrom C release from mitochondria, cleavage of Caspase 1, Caspase 3 or IL-1β, LC3-co-localisation), this host cell death is

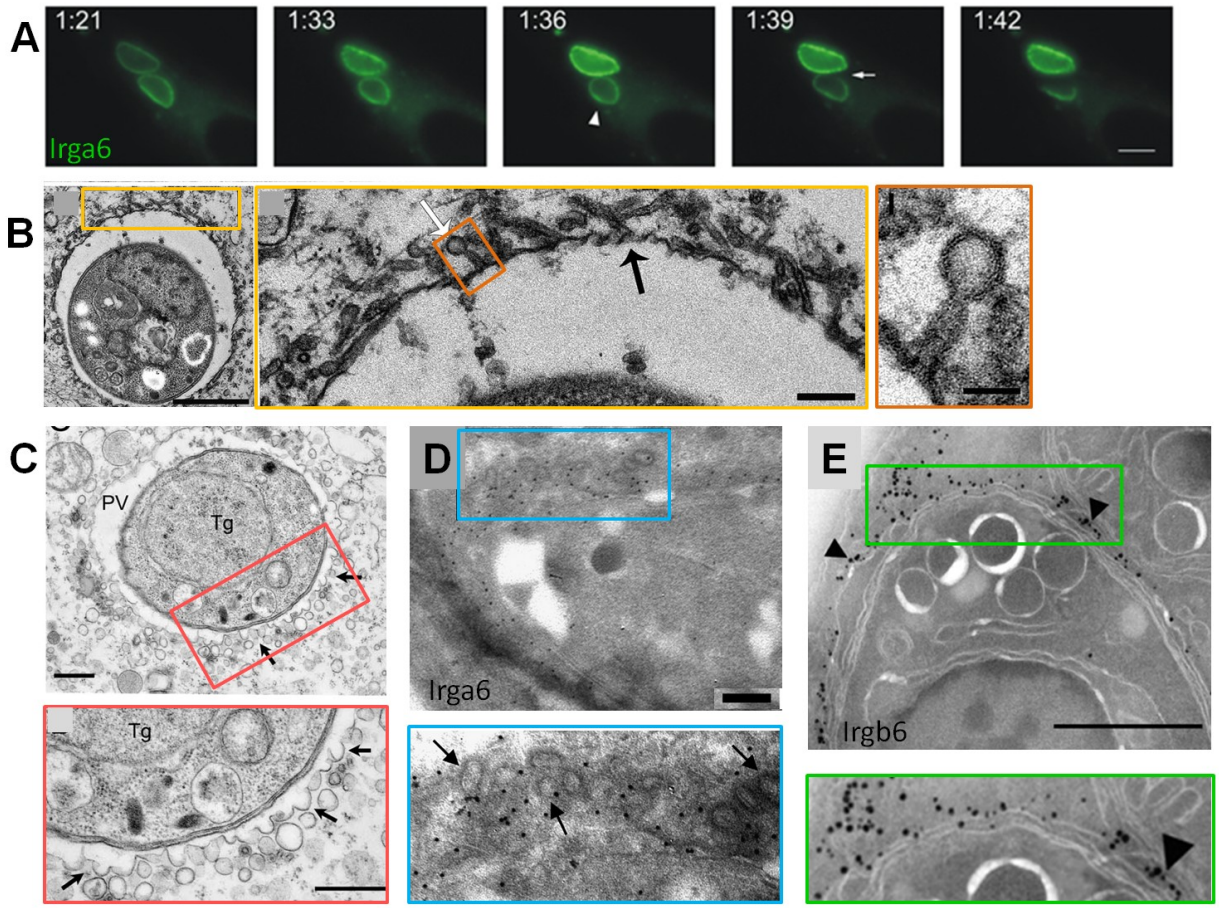


**Figure 1.5: Vesiculation and disruption parasitophorous vacuolar membrane (PVM) of avirulent *Toxoplasma gondii* strains in IFNγ-stimulated cells.**
Coloured inset boxes indicate magnified area shown next to it. **(A)** Picture series of time-lapse microscopy video showing IFNγ-induced mouse fibroblasts overexpressing Irga6-GFP and infected with *T. gondii* (ME49) for the indicated time points. Irga6-GFP intensely loads the PVM and seems to extract surface area from the PVM, thereby creating tension. Vacuoles and the included parasites round up (white arrows) just before the PVM ruptures (white arrow) and the disrupted vacuole springs back to a more banana-like form. Scale bar: 5 µm, from (Zhao et al. 2009; Howard et al. 2011) **(B)** Transmission electron microscopy (TEM) images of IFNγ-induced mouse asterocytes infected with *T. gondii* (ME49) for 2 h. The white arrow marks the "stemmed" vesicular and tubular structures and the black arrow PVM indentations. Scale bars: from left to right 1 µm, 0.1 µm, and 50 nm; from (Melzer et al. 2008). **(C)** TEM images of IFNγ-/LPS-activated primary macrophages infected with *T. gondii* (PTG) for 5 h. Arrows indicate vesiculation and membrane blebbing "protruding from" the PVM. Scale bars: 0.5 µm; from (Zhao et al. 2008). **(D)** Cryo-EM images of IFNγ-induced mouse asterocytes infected with *T. gondii* (ME49) for 6 h. Immunogold particles indicating the presence of Irga6 are located on the outside of the PVM and on vesicles next to the PVM (black arrows). Scale bar: 250 nm; from (Martens et al. 2005; Howard 2008). **(E)** Cryo-EM images of IFNγ-induced mouse macrophages infected with *T. gondii* (CTG). Irgb6 is detected by FluoreNanogold on the outside of the PVM (black arrow heads). Scale bar: 500 nm; from (Fentress et al. 2010).

characterised by plasma membrane permeabilisation and release of the inflammatory high-mobility group protein 1 (HMGB1) and is therefore currently considered as necrosis-like cell death (Zhao et al. 2009).

In contrast, during the infection with virulent strains of *T. gondii* only a low number of vacuoles are loaded with IRG proteins (Zhao et al. 2009; Zhao et al. 2009; Khaminets et al. 2010; Spekker et al. 2013). Virulent *T. gondii* strains can secrete kinases that act as virulence factors to counteract IRG protein function [reviewed in (Hunter et al. 2012)]. The secreted polymorphic kinase ROP18 together with the pseudokinase ROP5 trap Irga6 in a GDP-bound conformation. The threonines in the switch 1 loop of the target IRG protein are phosphorylated by ROP18 resulting in a permanent biochemical inactivation, partial inhibition of IRG protein loading and further action at the PVM and ultimately allowing unrestricted replication of the parasite (Fentress et al. 2010; Steinfeldt et al. 2010; Behnke et al. 2012; Fleckenstein et al. 2012; Niedelman et al. 2012). The virulent outcome of *T. gondii* infection (killing of the mouse as intermediate host by an exaggerated inflammatory immune response) is not beneficial for the parasite, because this ends the life cycle before the parasite can get into its definitive host, the cat. However, *T. gondii* must trigger a certain level of the immune response in order to form semidormant cysts in brain and muscle. In order to fight infection with virulent *T. gondii* strains, polymorphic IRG genes of wild mice counteract the *T. gondii* virulence factors. In wild-derived CIM mice the Irgb2-Irgb1 tandem protein prevents ROP18-mediated phosphorylation of Irga6, probably acting as decoy (Lilue et al. 2013).

### 1.4.3 *Chlamydia* as a model to study IRG protein function

Another pathogen, the gram-negative bacterium *Chlamydia,* has been shown to be mainly controlled by the IRG resistance system. As in case of *T. gondii,* the same IRG proteins Irga6, Irgb6, Irgb10 and Irgd accumulate on parasitophorous vacuoles termed inclusions of *C. trachomatis* (Coers et al. 2008; Al-Zeer et al. 2009), whereas GMS proteins are largely absent (Coers et al. 2008; Haldar et al. 2013). GMS–deficient mice but not *Irga6*-deficient mice are susceptible to *C. trachomatis* infection (Coers et al. 2008; Coers et al. 2011). *In vitro* studies with *IRG*-deficient cells (single siRNA knock-down or cells from knock-out mice) confirmed an essential role of GMS proteins and Irgb10 in bacterial growth restriction of the human pathogenic strain *C. trachomatis* and well as the avain (parrot) pathogenic strain *C. psittaci* (Nelson et al. 2005; Bernstein-Hanley et al. 2006; Miyairi et al. 2007; Coers et al. 2008). However, IRG proteins do not accumulate on inclusions of the

mouse pathogenic strain *C. muridarum* which is not restricted by IFNγ in mice (Nelson et al. 2005; Coers et al. 2008; Al-Zeer et al. 2009). The differences in IRG restriction to *Chlamydia* strains are likely to be due to *C. muridarum* being the only natural pathogen of mice. This may cause a selective pressure to develop strategies to counteract the IRG attack. *C. muridarum* secretes a cysteine protease, YopT, that was proposed to bind Irga6 since it has been shown to cleave and inactivate other host cell GTPases (Nelson et al. 2005), but this idea has not been substantiated up till now.

The entry mechanism of *Chlamydia* is less well understood. It comprises some features of clathrin-mediated endocytosis but not those of usual phagocytosis, caveola-mediated endocytosis, or macropinocytosis (Hybiske et al. 2007). Upon electrostatic-mediated cell association, the elementary body (EB), the *Chlamydia* metabolically inert "spore-like" form, and the host cell undergo an irreversible secondary binding. Host cell actin is recruited to the attachment site and the cytoskeleton undergoes rearrangements (Dautry-Varsat et al. 2004; Dautry-Varsat et al. 2005). After internalisation by the host cell, *Chlamydia* differentiates into the replicative form, the reticulate body (RB), which resides in an inclusion (Valdivia 2008; Betts et al. 2009) and 1.6).

In summary, GKS proteins have been shown to accumulate on four different vacuolar parasites: *T. gondii*, *N. caninum* and *C. trachomatis* and *C. psittaci*.

### 1.4.4 Proposed functions of Irgm1

Irgm1 seems to be a special IRG family member and several different aspects have been explored in *Irgm1*$^{-/-}$ mice or in *in vitro* experiments. In addition to the susceptibility to a large number of intracellular bacteria and protozoa (see 1.4.1), *Irgm1*$^{-/-}$ mice are also highly susceptible to endotoxin-induced shock (Bafica et al. 2007) and show increased clinical symptoms for acute colitis after dextran sodium sulphate exposure (Liu et al. 2013). In parallel, studies demonstrated that *Irgm1*-deficient macrophages are less motile and impaired in actin-remodelling (Henry et al. 2007; Henry et al. 2009). Moreover, a recent series of publications suggested firstly Irgm1 being implicated in experimental autoimmune encephalomyelitis (Xu et al. 2010; Wang et al. 2012), secondly upregulated upon permanent middle cerebral artery occlusion in the ischemic side of the brain (mouse model of stroke) (He et al. 2012), and thirdly regulating oxLDL uptake by macrophages during atherosclerosis (Xia et al. 2013). However, all of these studies should await further experimental validation.

Remarkably, several studies noted that *Irgm1*-deficient mice infected with a number of different organisms such as *M. avium*, *T. cruzi* and *S. typhimurium* are not only susceptible to

these pathogens, but also suffered a striking collapse of their lymphomyeloid systems (Feng et al. 2004; Santiago et al. 2005; Henry et al. 2007). This effect of Irgm1 deficiency on the lymphomyeloid system is critically dependent on IFNγ expression, because in trematodes , which excite exclusively Th2 immunity without IFNγ expression, no collapse of the lymphomyeloid system in *Irgm1*-deficient mice could be observed (Feng et al. 2008). A reduced proliferative potential in the lymphoid system as well as in hematopoietic stem cells has been described *in vitro*. Mature CD4+ T-lymphocytes from *Irgm1*-deficient mice undergo IFNγ-induced cell death and this effect disappears if the responding cells are also deficient in IFNγ expression (Feng et al. 2008; Xu et al. 2010). IFNγ-mediated self-renewal of hematopoietic stem cells after exposure to pathogens is also impaired in *Irgm1*-deficient mice, but this is abrogated in *Irgm1*$^{-/-}$*IFNγR1*$^{-/-}$, and *Irgm1*$^{-/-}$*Stat1*$^{-/-}$ double knock-out animals (Feng et al. 2008; Baldridge et al. 2010; King et al. 2011).

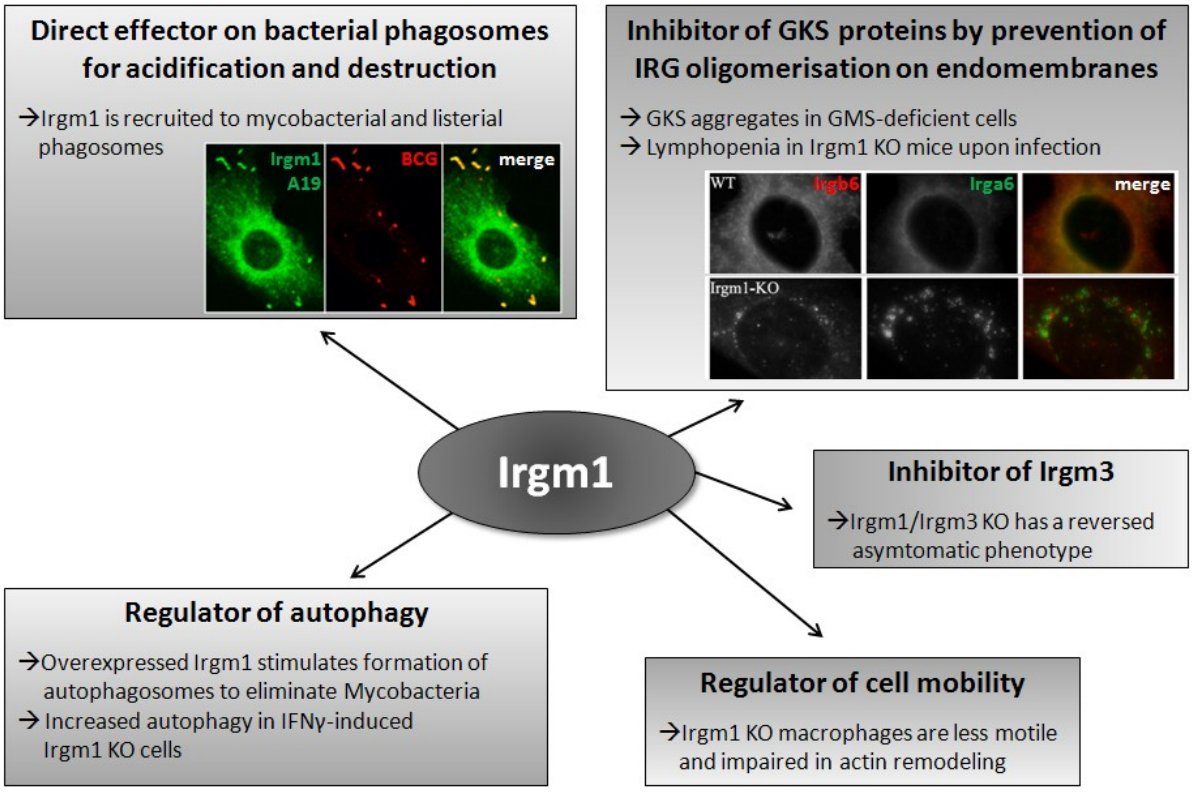


**Figure 1.6: Proposed models of Irgm1.**
Microscopic images in the left hand panel show IFNγ-induced mouse macrophages infected with *Mycobacterium bovis* BCG and stained for Irgm1 with A19 pAB; modified from (Shenoy et al. 2007). Microscopic images in the right hand panel show IFNγ-induced mouse embryonic fibroblasts from wt or *Irgm1*-deficient mice stained for Irgb6 or Irga6; modified from (Traver et al. 2011). See text 1.4.4 for other references.

Different models try to explain these Irgm1-associated phenotypes describing either cell-autonomous or systemic effects (Figure 1.6) (Taylor et al. 2007; Feng et al. 2009; Hunn et al. 2010; Deretic 2011; MacMicking 2012). The earliest model, which is still widely accepted, proposes a cell-autonomous role for Irgm1 in facilitating destruction of phagocytosed bacteria. Irgm1 was suggested to be recruited to the mycobacterial phagosome by recognition of specific host phosphoinositide lipids ($PtdInsP_2$ and $PtdInsP_3$) and then regulate the SNARE adaptor protein snapin enabling fusion with lysosomes (MacMicking et al. 2003; Shenoy et al. 2007; Tiwari et al. 2009). This model gained some support from the initial finding that Irgm1 could be found at the phagocytic cup and phagolysosomes of phagocytosed latex beads (Martens et al. 2004).

The second model discusses Irgm1 as regulator of autophagy. On the one hand it was suggested that Irgm1 can stimulate the formation of autophagosomes and thereby participate in IFNγ-dependent control of *Mycobacteria* (Gutierrez et al. 2004; Singh et al. 2006); in case of human IRGM by affecting mitochondrial fission (Singh et al. 2010). Deregulated autophagy and mitophagy was also observed in IFNγ-stimulated or untreated cells from *Irgm1*$^{-/-}$ mice (Traver et al. 2011; He et al. 2012; Liu et al. 2013). On the other hand Irgm1 was suggested to protect from autophagic cell death (Feng et al. 2008; King et al. 2011).

Lastly, the lymphopenia in infected *Irgm1*$^{-/-}$ mice suggested an alternative explanation for the systemic failure of immunity, based on the role of Irgm1 as an essential regulator of the IRG protein-based resistance mechanism. As noted in chapter 1.3.5, failure of GMS-mediated regulation causes accumulation of the GKS proteins into aggregates (Hunn et al. 2008). These aggregates may have cytopathic effects in dividing lymphomyeloid cells (Feng et al. 2009; Hunn et al. 2010) and also hematopoietic stem cells (King et al. 2011). In IFNγ-induced *Irgm1*/*Irgm3*$^{-/-}$-double-deficient cells, the concentrations of GKS proteins are greatly reduced, plausibly reducing the hypothetical cytopathic effects and reversing the susceptible Irgm1 phenotype (Henry et al. 2009). In fact, the bone marrow stem cell defect in *Irgm1/Irgm*3$^{-/-}$-, *Irgm1/IFNγR1*$^{-/-}$- and *Irgm1*/*Stat1*$^{-/-}$-double deficient mice as well as the immunological defect in *Irgm1/IFNγR1*$^{-/-}$-double-deficient mice are reversed (Feng et al. 2008; King et al. 2011). An alternative interpretation is that Irgm1, acting as promoter of cell survival, antagonizes possible cytopathic effects of Irgm3, which acts as inducer of cell death, thus fine-tuning T-cell homeostasis (Henry et al. 2009; Coers et al. 2011).

### 1.4.5 Human IRGM

Since the mouse Irgm1 protein has been implicated in many immunity-related processes, more than 100 studies have been published in the last 10 years attempting to link human IRGM to immunity, even though hIRGM is truncated, not conserved and not interferon-inducible (see 1.3.1, 1.3.2). The first studies adapted experiments from of mIrgm1 for hIRGM, proposing that hIRGM induces autophagy to eliminate phagosomal *Mycobacteria* via mitochondria (Singh et al. 2006; Singh et al. 2010). Polymorphisms in the *hIRGM* gene have been proposed to increase the risk to clinical tuberculosis in diverse human populations against different mycobacterial species [reviewed in (Kim et al. 2012)]. Moreover, genome-wide association analysis has also recently shown that IRGM acts as a major predisposing locus for Crohn's disease but not ulcerative colitis [meta-analysis (Lu et al. 2014)]. Deletion polymorphisms upstream of the hIRGM gene regulate different expression levels of hIRGM associated with the disease phenotype suggesting hIRGM as regulator of autophagy may dysregulate homeostasis with the microbial gut flora resulting in enhanced susceptibility to Crohn´s disease (McCarroll et al. 2008).

## 1.5 *Encephalitozoon cuniculi*

*E. cuniculi* belong to the abundant and diverse group of microsporidia, recently re-classified as fungi (Corradi et al. 2009) that are obligate intracellular eukaryotic parasites of many animal groups including mammals. There are approximately 1200 microsporidian species, but just 14 have been documented to infect humans including *E. cuniculi*, *E. hellem* and *E. intestinalis. Encephalitozoon* species can cause the mainly gasteroenteric disease microsporidiosis, primarily in immunocompromised patients, such as HIV-infected patients or organ transplant recipients (Didier et al. 2011). Three genotypes of *E. cuniculi* have been identified so far named I (rabbit and mouse), II (mouse and dog), and III (dog and fox) strain, according to their natural host. The genotypes differ in the number of 5´-GTTT-3´repeats present in the internal spacer region of the rRNA (Didier et al. 1995). *E. cuniculi* serves as a convenient model organism for microsporidia, since it is possible to maintain *E. cuniculi* by *in vitro* culture and its genome is fully sequenced (Katinka et al. 2001). Genome research revealed that *E. cuniculi* has one of the most compact genomes of all eukaryotic organisms (2.9 Mbp) with low intraindividual genetic variation (Selman et al. 2013). Consistent with such an extreme genome reduction, small mitosomes carrying mitochondrial HSP70 protein instead of mitochondria were recently identified in microsporidia [(Williams et al. 2002),

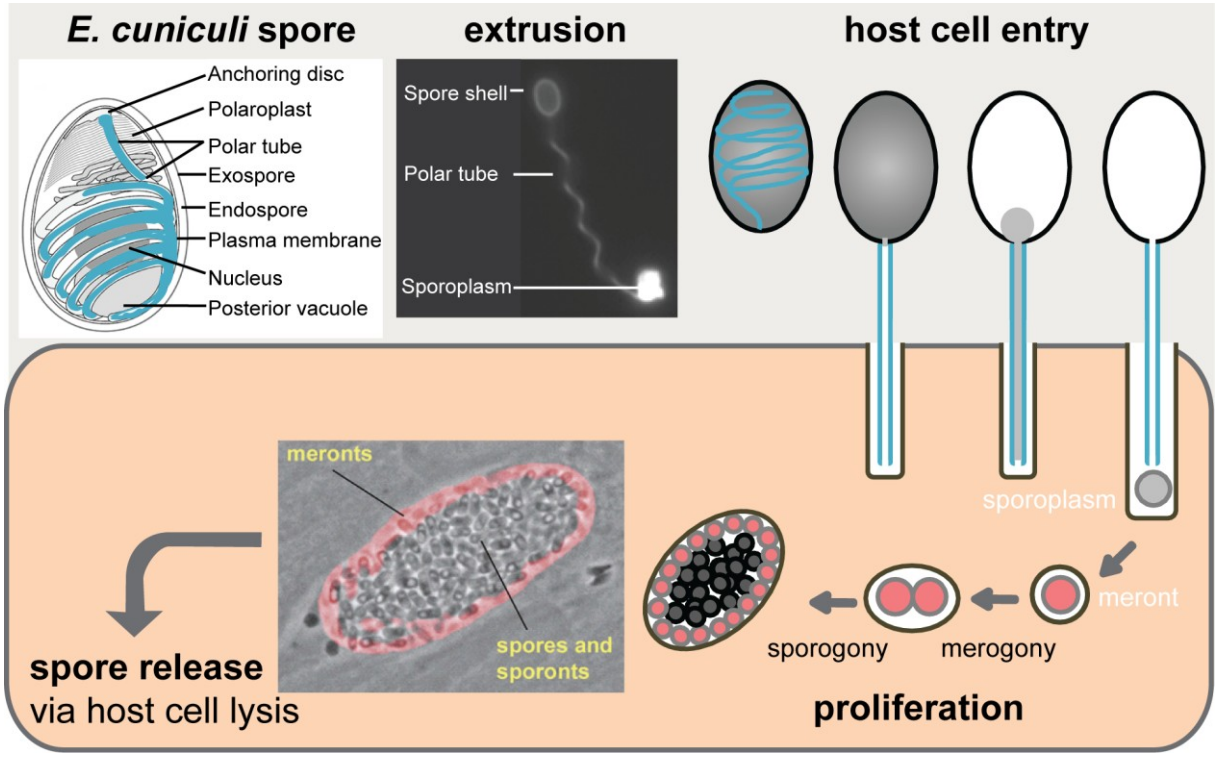


**Figure 1.7: *Encephalitozoon cuniculi* host cell invasion.**
The *E. cuniculi* spore is composed of an exo- and endospore layer and the plasma membrane enclosing the cytosol, nucleus, posterior vacuole, polaroplast and anchoring disc. The polar tube (cyan) is extruded and invaginates the host plasma membrane within seconds. The sporoplasm is transferred trough the polar tube and develops within a parasitophorous vacuole in the host cytosol, now termed meront. The meronts grow and divide by binary fission (merogony) and differentiate into sporonts and spores (sporogony) which are finally released by host cell lysis. Spore Figure (top left) modified from (Franzen et al. 2005) and large intracellular PV containing spores (bottom) from (Bohne et al. 2011).

reviewed in (Makiuchi et al. 2013)]. With regard to this project it is noteworthy that several studies have now established IFNγ as strong inducer of cell-autonomous immunity against *Encephalitozoon ssp*. [see results 3.3.1 and reviewed in (Mathews et al. 2009)].

In order to gain entry into the host cell, microsporidia have evolved a peculiar injection-based entry mechanism (Figure 1.7). The thick-walled spore of *E. cuniculi* carries a polar filament, which is expelled probably under osmotic pressure and invaginates the host cell plasma membrane. Thereafter, the sporoplasm, which is the cytosol and organelles of the organism, is transferred trough the polar tube and placed into the host cell cytoplasm. It is then termed meront and develops inside a parasitophorous vacuole (Ronnebaumer et al. 2008). The meront acquires nutrients and resources from the host cell, grows and divide by binary fission (merogony) and differentiates into sporonts and spores (sporogony), finally lysing the host cell to release the mature, environmentally-resistant spores (Bigliardi et al. 2001). Phagocytosis of spores by macrophages is also observed and was suggested as major entry route (Couzinet et al. 2000; Franzen et al. 2005). However, phagocytosis inhibition does

not affect the intracellular meront population (Orlik et al. 2010); therefore phagocytosis does not seem to be the natural entry mechanism of *E. cuniculi* or *E. intestinalis* (Leitch et al. 2005) into host cells.

## 1.6 Parasitophorous and inclusion vacuoles as intracellular niche

Different intracellular parasites evolved the strategy to replicate inside a parasitophorous or inclusion vacuole, which provides an intracellular niche that shields the invader from several endogenous host defence mechanisms [reviewed in (Sibley 2011)]. To enter the host cell, *T. gondii* establishes a protein complex called the moving junction at the parasite host cell interface, through which the parasite gains traction to pull itself with its own actin-myosin based motor system actively into the host cell [(Morisaki et al. 1995), reviewed in (Sibley 2004; Carruthers et al. 2007)].

The PVM is formed from the invaginated host cell plasma membrane (Suss-Toby et al. 1996) and is permissive for molecules under 1300 Da (Schwab et al. 1994). Apart from a transient activation of host actin, the host cortical cytoskeleton does not seem to be associated with the nascent vacuole (Gonzalez et al. 2009; Delorme-Walker et al. 2012). The PV does not fuse with endolysosomal compartments in macrophages or non-phagocytic cells, and is also devoid of several other host cell markers (Jones et al. 1972; Mordue et al. 1997; Mordue et al. 1999). Thereby, *T. gondii* blocks vacuole acidification (Sibley et al. 1985). In 1999, a detailed study revealed that during the invasion process, certain host cell surface proteins like the glycosylphosphatidylinositol (GPI)-anchored Sca-1 and CD55 are incorporated into the PVM, but transmembrane proteins including CD44, Na+/K+ ATPase and β1-integrin are excluded from the PVM (Mordue et al. 1999). It was suggested that the parasite-derived RON protein complex at the moving junction might act as a molecular sieve to selectively exclude host plasma membrane proteins (Tyler et al. 2011). This highly complex and not fully understood process is independent of lipid microdomains as both raft and non-raft-associated lipids and cytosolic leaflet proteins pass through the moving junction and are included into the PVM (Charron et al. 2004).

From the earliest studies it was noted that host cell mitochondria congregate around the PV (Gustafson et al. 1954) as well as strands of the rough ER (Jones et al. 1972; Endo et al. 1981; de Melo et al. 1992; Sinai et al. 1997) (reviewed in (Dubremetz et al. 2009)). Functional interactions of the PV and host cell organelles in terms of antigen delivery via the ER for MHC class I presentation (Goldszmid et al. 2009) or nutrient acquisition (Mordue et al. 1999; Coppens et al. 2006; Crawford et al. 2006; Romano et al. 2012; Romano et al. 2013)

are under debate. The invasion is accompanied by discharge of specialised secretory organelles filled with rhoptry (ROP, RON), microneme (MIC), and dense granule (GRA) proteins that fulfil various functions, e.g. composing the moving junction complex or interfering with host cell signalling [reviewed in (Hunter et al. 2012)]. Moreover, some of these virulence factors (ROP5, ROP18, and GRA7) decorate the PVM to counteract the IRG attack (see 1.4.2).

The *Chlamydia* inclusion is a membrane-bound vacuole also derived from the plasma membrane, but again segregated from the endolysosomal system (Scidmore et al. 2003). However, it can selectively orchestrate vesicles from several host cell organelles such as the exocytic pathway to acquire nutrients and host lipids [reviewed in (Saka et al. 2010; Scidmore 2011)]. Moreover, lipid scavenging is facilitated by either host Golgi fragmentation, whose mini stacks can be observed in close proximity to *Chlamydia* inclusions (Heuer et al. 2009), or direct transport of ceramide from the host ER to the inclusion (Subtil 2011). The inclusion membrane is extensively modified by insertion of diverse *Chlamydia* type III secreted effectors, termed inclusion membrane (Inc) proteins (Dehoux et al. 2011).

The polar tube of *E. cuniculi* invaginates the host cell plasma membrane extremely fast, suggesting that this invasion is independent of cytoskeletal rearrangements since those processes are slower than the observed >1.3 s (Ronnebaumer et al. 2008). The bulk lipids of this PVM were shown to be host cell derived, since both raft and non-raft microdomains of the host plasma membrane are incorporated. Moreover, the PVM possesses pores with an exclusion size of <10 kDa to allow nutrient uptake (Ronnebaumer et al. 2008). The PVM of *E. cuniculi* does not acquire host endolysosomal or ER markers (Weidner 1975; Fasshauer et al. 2005; Ronnebaumer et al. 2008) and the vacuole does not acidify (Weidner et al. 1985).

In summary, the specialised vacuoles of *Toxoplasma, Chlamydia* and *Encephalitozoon* are mainly or entirely derived from the host plasma membrane and non-fusogenic with the host endolysosomal system providing a safe niche for intracellular replication

## 1.7 Aim of Study

IRG proteins constitute a powerful resistance system against the protozoan *T. gondii* and its close relative *N. caninum* as well as against two strains of the bacteria *Chlamydia* in mice. However, it remains a great mystery why all other organisms tested so far are not restricted by the IRG system. Even though *T. gondii* and *Chlamydia* are so dissimilar, they have some features in common: (I) an unusual route of host cell entry, neither of which resembles conventional phagocytosis, and (II) replication within non-fusogenic intracellular vacuoles that are formed by invaginated host plasma membrane. To explain why the IRG system only targets these organisms, one can hypothesise that critical modulations during host cell entry, e.g. specific exclusion host plasma membrane proteins as shown for *T. gondii*, results in the formation of parasitophorous vacuoles, that clearly differ from host cell endomembranes. Such a protein-depleted PVM can thus be recognised as "non-self" by the IRG proteins and targeted for destruction.

The aim of this PhD thesis was to clarify the subcellular localisation of Irgm1 in order to understand its role in cell-autonomous immunity and moreover, to elaborate on which artificial membrane systems and potential target organisms the IRG system becomes active.

The proposed model for Irgm1 as a direct effector on bacterial phagosomes stands in striking contrast to the above mentioned hypothesis. The direct effector model has gained considerable support from successive observations of Irgm1 associated with mycobacterial and listerial phagosomes in IFNγ–induced cells. Therefore, the first part of this study re-examined the subcellular localisation of Irgm1 during bacterial infection with several staining techniques. Moreover, the existence and properties of two Irgm1 isoforms was investigated.

The second part focussed on the question whether IRG proteins target protein-deficient membranes. IRG association with pure liposomes, its correlation with residual host surface proteins on *T. gondii* PVM, as well as co-localisation to artificial *Chlamydia* Inc protein-induced vesicles was examined.

In the last part, a novel role of the IRG system in resistance to the microsporidian *Encephalitozoon cuniculi* was elucidated. This intracellular parasitic fungus that is restricted by IFNγ also enters the host cell by an unusual mechanism and resides in a non-fusogenic vacuole. It was tested whether *E. cuniculi*-infected cells show similar IRG-mediated phenomena as observed upon *T. gondii* and partially also *Chlamydia* infection. This information will help to understand, whether the IRG resistance system uses a universal mechanism to exert its PVM-destructive function.

# Materials and Methods

## 2.1 Instruments

Only instruments are listed, which are not commonly used for laboratory work.

| Instrument | Company |
|---|---|
| Optima$^{TM}$ TLX Ultracentrifuge | Beckman Coulter GmbH, Krefeld, Germany |
| EmulsiFlex-C5 microfluidiser | Avestin, Ottawa, Canada |
| LiposoFast-Basic and Stabiliser (Liposome extruder) | Avestin |
| Rocky 1010 | Labortechnik Fröbel, Lindau, Germany |
| Film developing machine AGFA Curix 60 | AGFA, Mortsel, Belgium |
| Spektrophotometer Cary100 Bio UV-Visible | Spectrometer Varian, Darmstadt, Germany |
| ÄTKA fast performance liquid chromatography (FPLC) | Amersham Biosciences, Freiburg, Germany, now GE Healthcare |
| Zeiss Axioplan II fluorescence microscope/ AxioCam MRm camera | Zeiss, Oberkochen, Germany |
| Zeiss Axiovert 200 M motorized microscope | Zeiss |

## 2.2 Chemicals and other materials

All chemicals and reagents were purchased from Carl Roth GmbH + Co. KG, (Karlsruhe, Germany), Sigma-Aldrich (Saint Louis, MO, USA), Merck KGaA (Darmstadt, Germany), or Serva (Heidelberg, Germany) if not otherwise stated.

| Chemicals and other materials | Company |
|---|---|
| 4',6-Diamidino-2-phenylindol (DAPI) | Roche Diagnostics, Mannheim, Germany |
| µ-slide I chambers | Ibidi, Munich, Germany |
| Avanti 1x100Me Brain Polar Lipid Extract 141101P | Avanti Polar Lipids, Inc., Alabaster, AL, USA |
| Bisbenzimide Hoechst 33342 | Sigma-Aldrich |
| CellTiter 96 AQueous non-radioactive cell proliferation assay | Promega, Mannheim, Germany |
| cOmplete ULTRA Tablets Mini, EDTA-free | Roche Diagnostics |
| Alexa-546 labelled human Transferrin | Molecular Probes, Invitrogen |

| | |
|---|---|
| EZ-Link Sulfo-NHS-LC-LC-Biotin | Pierce, Rockford, IL, USA |
| FuGENE HD and XtremeGene 9 | Roche Diagnostics |
| Propidium iodide | Sigma-Aldrich |
| Polybead Carboxylate Microspheres 2 µm (#18327) | Polyscience, Inc., Warrington, PA, USA |
| Protran nitrocellulose membrane (0.45 µm) | Schleicher & Schüll, Dassel, Germany , now GE Healthcare |
| Nucleopore Track-Etch Membrane Filters, 100 nM | Whatman International Ltd., Maidstone, UK |
| Page Ruler Prestained Protein Ladder | Fermentas, Thermo Scientific, Schwerte, Germany |
| Protein A Sepharose 4 CL-4B | GE Healthcare, Uppsala, Sweden |
| GSTrap FF 5 ml | GE Healthcare |
| HiLoad 26/60 Superdex 75 or 200 prep grade | Amersham |
| ProLong Gold anti-fade reagent | Invitrogen Life Technology, Darmstadt, Germany |
| Puromycin | Clontech Saint-Germain-en-Laye, France |
| Recombinant mouse IFNγ | PeproTech, Rocky Hill, NJ, USA |
| Streptavidin-Cy3 conjugate # 6402 | Sigma-Aldrich |
| Super RX films | Fujifilm, Tokyo, Japan |
| Thrombin | Serva |
| Whatman paper | Macherey-Nagel GmbH & Co. KG, Düren, Germany |
| Vivaspin 20 centrifugal concentrator, 10 kDa cut-off | Vivascience, Lincoln, USA |

## 2.3 Antibodies and enzymes

Antibodies used for immunofluorescence microscopy (IF) or immunobotting (IB) are listed below.

| **Primary antibodies against IRG proteins** | | | | |
|---|---|---|---|---|
| **Name** | **recognised antigen** | **type** | **dilution** | **source and/ or reference** |
| αIGTP clone 7 | mouse Irgm3 (aa 283-423) | mouse monoclonal AB | WB 1:2000 IF 1:500 | BD Transduction Laboratories now Santa Cruz Biotechnology, Inc., Santa Cruz, CA |
| 165/3 (3rd bleed) 165/4 (4th bleed) | recombinant mouse Irga6 | rabbit polyclonal AS | WB 1:25000 IF 1:8000 | (Uthaiah et al. 2003; Martens et al. 2004) |

| | | | | |
|---|---|---|---|---|
| 10D7 | recombinant mouse Irga6 | mouse monoclonal AB | WB 1:2000<br>IF: 1:500 | J. Zerrahn, Berlin (Zerrahn et al. 2002; Martens et al. 2005; Papic et al. 2008) |
| 10E7 | recombinant mouse Irga6 | mouse monoclonal AB | WB 1:1000 | J. Zerrahn, Berlin (Zerrahn et al. 2002; Martens et al. 2005; Papic et al. 2008) |
| 2078 | mouse Irgd peptides CKTPYQHPK-YPKVIF; CDAKHLLRKI ETVNVA | rabbit polyclonal AS | WB 1:1000<br>IF 1:500 | Eurogentec (Khaminets et al. 2010) |
| L115 | mouse Irgm1 peptides QTGSSRLP-EVSRSTE, NESLKNSLGV RDDD | rabbit polyclonal AS | WB 1:2000 | Eurogentec (Khaminets et al. 2010) |
| 1B2 | mouse Irgm1 | mouse monoclonal AB | undiluted hybridoma supernatant | (Butcher et al. 2005) |
| rbMAE15 A | peptide of the N-terminus of the short mouse Irgm1 isoform MAETHYAPLS SAFPC | rabbit polyclonal AS | WB IF:<br>A.1 1:2000<br>A.2, A.3 1:4000 | Innovagen, Lund, Sweden<br>this study |
| rbMAE15 B | mouse Irgm1 (peptide MAETHYAPLS SAFPC) | rabbit polyclonal AS | IF:<br>B.1 1:2000<br>B.2, B.3 1:4000 | Innovagen<br>this study |
| chMAE15 A | mouse Irgm1 (peptide MAETHYAPLS SAFPC) | chicken polyclonal IgY | WB: 1:1000<br>IF: 1:250 | Innovagen<br>this study |
| A19 (sc-11075) and P20 (sc-11074) | mouse Irgm1 N-terminal peptide | goat polyclonal AB | WB 1:200<br>IF 1:100 | Santa Cruz Biotechnology, Inc. |
| A20 (sc-11079) | mouse Irgb6 N-terminal peptide | goat polyclonal AS | WB 1:500 | Santa Cruz Biotechnology, Inc. |
| 142/1 | mouse Irgb6 | rabbit poly-clonal AS | IF 1:2000 | Innovagen (Lilue et al. 2013) |
| H53 | mouse Irgm2 N-term. Peptide MEEAVESPEV KEFEY | rabbit polyclonal AS | WB 1:1000<br>IF 1:1000 | Eurogentec (Khaminets et al. 2010) |

| | | | | |
|---|---|---|---|---|
| ab69494 | human IRGM, mouse Irgm1, mouse Irgm2 strongly | rabbit polyclonal | IF 1:1000 o/n 4°C | Abcam plc, Cambridge, U. K. |
| ab69495 | human IRGM, mouse Irgm1, mouse Irgm3 | rabbit polyclonal | IF 1:1000 o/n 4°C | Abcam plc |
| B34 | Irgb6 | mouse monoclonal | WB 1:1000 | (Carlow et al. 1995) |
| C15A (954) | Irgb2-b1 | rabbit polyclonal | IF 1:8000 | Innovagen (Lilue et al. 2013) |
| 940/6 | Irgb10 (crossreactive) | rabbit polyclonal | WB 1:5000 IF 1:4000 | Innovagen (Howard Lab unpublished) |

The goat polyclonal antibodies M-16 and M-95 from Santa Cruz Biotechnology, Inc. directed against C-terminal peptides did not specifically detect Irgm1 (Steffi Koenen-Waisman, personal communication).

**Primary antibodies against marker proteins**

| **Name** | **recognised antigen** | **type** | **dilution** | **source** |
|---|---|---|---|---|
| α-ActA | ActA (50-126 aa) | mouse monoclonal AB | IF: 1:1000 | Pascal Cossart and Edith Gouin, Institut Pasteur, Paris, France |
| α-calnexin | C-terminal peptide of canine calnexin (aa 575-593) | rabbit polyclonal AB | WB 1:5000 IF 1:250 | Calbiochem at Merck KgaA, Darmstadt, Germany |
| α-complex II #459200 | complex II | mouse monoclonal AB | IF: 1:1000 | Molecular Probes, Invitrogen Life Technology |
| α-cytochrom C | Cytochrom C | mouse monoclonal AB | IF: 1:1000 | BD Bioscience, Heidelberg, Germany |
| a-GM130 | mouse GM130 Golgi marker | mouse monoclonal AB | IF 1:1000 | BD Bioscience, Heidelberg, Germany |
| 1D4B | LAMP1 | rat monoclonal AB, hybridoma supernatant | IF 1:2000 | Developmental Studies Hybridoma Bank, University of Iowa |
| α-GRA7 JH.3.1.2 | *T. gondii* GRA7 (GST-GRA7 aa 24-100 in rat CC2-3) | rat monoclonal, hybridoma supernatant | 1:1000 | (Fleckenstein et al. 2012) |

| | | | | |
|---|---|---|---|---|
| anti-Listeria | Listeria surface protein | rabbit polyclonal AB | IF: 1:1000 | US Biologicals, Salem, MA, USA |
| α-*M. tuberculosis* #B65601R | Mycobacteria surface protein | rabbit polyclonal AB | IF 1:8000 | Meridian, Memphis, TN, USA |
| Phalloidin Alexa Flour 546 | Actin | | IF: 1:250 | Molecular Probes, Invitrogen Life Technology |
| 6G2 | meronts of *E. cuniculi* | mouse monoclonal | IF: 1:50 WB 1:100 | (Fasshauer et al. 2005) |
| SWP1 | Spore wall protein of *E. cuniculi* | rabbit polyclonal antiserum | IF 1:2000 WB 1:2000 | (Bohne et al. 2000) |

**Secondary antibody**

| **Name** | **conjugate** | **dilution** | **source** |
|---|---|---|---|
| Donkey α-mouse IgG | Alexa Fluor 488 | IF 1:1000 | Molecular Probes, Invitrogen Life Technology |
| Donkey α-rabbit IgG | Alexa Fluor 488 | IF 1:1000 | Life Technologies |
| Donkey α-goat IgG | Alexa Fluor 488 | IF 1:1000 | Life Technologies |
| Donkey α-rat IgG | Alexa Fluor 488 | IF 1:1000 | Life Technologies |
| Donkey α-chicken IgY | Alexa Fluor 488 | IF 1:1000 | Life Technologies |
| Donkey α-mouse IgG | Alexa Fluor 555 | IF 1:1000 | Life Technologies |
| Donkey α-rabbit IgG | Alexa Fluor 555 | IF 1:1000 | Life Technologies |
| Donkey α-goat IgG | Alexa Fluor 555 | IF 1:1000 | Life Technologies |
| Donkey α-rat IgG | Alexa Fluor 555 | IF 1:1000 | Life Technologies |
| Donkey α-mouse IgG | Alexa Fluor 647 | IF 1:1000 | Life Technologies |
| Donkey α-rabbit IgG | Alexa Fluor 647 | IF 1:1000 | Life Technologies |
| Donkey α-goat IgG | Alexa Fluor 647 | IF 1:1000 | Life Technologies |
| Donkey α-rat IgG | Alexa Fluor 647 | IF 1:1000 | Life Technologies |
| Donkey-α-rabbit IgG | horse radish peroxidase (HRP) | WB 1:5000 | GE Healthcare |
| donkey anti-goat IgG | HRP | WB 1:5000 | Abcam plc |
| donkey anti-rat IgG | HRP | WB 1:5000 | Jackson ImmunoResearch Laboratories, Inc., West Grove, PA, USA |
| goat anti-mouse IgG | HRP | WB 1:5000 | Pierce, Biotechnology, Rockford, IL, USA |
| donkey anti-chicken IgY | HRP | WB 1:2000 | Pierce |

## 2.4 Buffers and media

All buffers and solutions were prepared with deionized, sterile (Seral™) or Milli-Q Synthesis (Millipore) water and autoclaved or sterilely filtered if required.

| Buffer/ media | Compounds |
|---|---|
| *Luria Bertani* (LB-) media | 1% Bacto™ Tryptone (w/v) (10 g)<br>0.5% Bacto™ Yeast Extract (w/v) (5 g)<br>0.5% NaCl (M: 58.44 g/mol, 5 g) (w/v)<br>add to 1 l $dH_2O$ and autoclave |
| LB media agar plates | 1 l LB media<br>add 15 g Bacto™ Agar and autoclave<br>cool down to 50°C<br>add antibiotics Kanamycin 1:1000 (stock 50 mg/ml, final 50 µg/ml) or<br>Ampicillin 1:1000 (stock 100 mg/ml, final 100 µg/ml)<br>pour 20 ml per petri dish and store upside down at 4°C |
| Cell culture medium for mouse fibroblasts (DMEM) | Dulbecco's modified Eagle's medium (DMEM), high glucose<br>(PAA, Pasching, Austria now sold to Invitrogen Life Technologies)<br>10% fetal calf serum (FCS, from PAA, now Biochrom, Berlin, Germany)<br>2 mM L-glutamine (PAA, now Invitrogen),<br>1 mM sodium pyruvate (PAA, now Invitrogen),<br>1x MEM non-essential amino acids (PAA, now Invitrogen),<br>100 U/ml penicillin and 100 µg/ml streptomycin (PAA, now Invitrogen), |
| Cell culture medium for Hs cells (IMDM) | Iscove´s modified Dulbecco´s medium (IMDM) (Invitrogen)<br>5% FCS<br>1x MEM non-essential amino acids,<br>100 U/ml penicillin and 100 µg/ml streptomycin. |
| Cell culture medium for 1B2 cells (IMDM) | Iscove´s modified Dulbecco´s medium (IMDM) (Invitrogen)<br>10% FCS<br>1x MEM non-essential amino acids,<br>100 U/ml penicillin and 100 µg/ml streptomycin. |
| Cell culture medium for mouse macrophages (RPMI) | Roswell Park Memorial Institute (RPMI) 1640, Invitrogen)<br>25% FCS<br>10% L929 P2 cell-conditioned medium<br>2 mM L-glutamine<br>100 U/ml penicillin and 100 µg/ml streptomycin. |
| Freeze Mix | 90% FCS<br>10% dimethylsulfoxid (DMSO) |
| 10x Trypsin | 5% Trypsin (1:250) (w/v) (5 g) (Gibeco BRL now Invitrogen)<br>17 mM EDTA (2 g or 10.8 ml of 0.5 M EDTA solution)<br>145 mM NaCl (M: 58.44 g/mol, 8,5 g) |
| 10x PBS buffer | 1.37 M NaCl (M: 58.44 g/mol, 81.8g)<br>27 mM KCl (M: 74.56 g/mol, 2g)<br>101 mM $Na_2HPO_4$ x 2 $H_2O$ (M: 177.99 g/mol, 17.97 g)<br>18 mM $KH_2PO_4$ (M: 136.09 g/mol, 2.4 g)<br>add to 1 l $dH_2O$, pH = 7.4 and autoclave |
| IF Fixing buffer | 3% Paraformaldehyde (PFA) (w/v) in PBS |

| | |
|---|---|
| IF Washing buffer | 0.1% Saponin (w/v) in PBS (1 g in 1 l PBS) |
| IF Blocking buffer | 3% bovine serum albumin (BSA) (w/v) (1.5 g in 50 ml)<br>0.1% Saponin (w/v) in PBS (1 g in 1 l PBS) |
| Cell lysis buffer | 1% Triton X-100 (v/v) (647 g/mol, prepare 10% Stock solution)<br>1 x cOmplete ULTRA Tablet Mini<br>10 ml PBS |
| 10x SDS sample buffer (Laemmli) | 0.5 M Tris-HCl, pH 6.8<br>50% Glycerol (v/v)<br>10% SDS (w/v)<br>0.025% Bromphenol blue (w/v)<br>7% β-Mercaptoethanol (v/v)<br>make 1ml aliquots and add freshly 70 µl β-mercaptoethanol before use |
| SDS-running buffer (1x) | 250 mM Tris-(hydroxymethyl)-aminomethan (M: 121.1 g/mol, 30.3 g)<br>1.92 M glycine (M: 75.07 g/mol, 144.1 g)<br>34.67 mM SDS (M: 288.38 g/mol, 10 g)<br>add to 10 l $dH_2O$ |
| SDS-PA gel (10%) separation gel | 12 ml $H_2O$ millipore<br>10 ml 30% Acrylamide solution (acryl/bisacryl)<br>7.6 ml 1.5 M Tris-HCl, pH 8.8<br>0.3 ml 10% SDS<br>100 µl 10% Ammonium peroxydisulphate (APS)<br>50 µl Tetramethylethylenediamine (TEMED) |
| SDS-PA gel (4%) stacking gel | 6.1 ml $H_2O$ millipore<br>1.3 ml 30% Acrylamide solution (acryl/bisacryl)<br>2.5 ml 0.5 M Tris-HCl, pH 6.8<br>0.1 ml 10% SDS<br>50 µl 10% APS<br>25 µl TEMED |
| 10x Electrophoresis Transfer buffer | 250 mM Tris-(hydroxymethyl)-aminomethan (M: 121.1 g/mol, 30.3 g)<br>1.92M glycine (M: 75.07 g/mol, 144.1 g)<br>Add to 1 l $dH_2O$ |
| Ponceau S solution | 0.2% Ponceau S (2 g)<br>3% acetic acid (30 g)<br>in 100 ml $dH_2O$ |
| 1x PBS/T 1 buffer | dilute 10x PBS 1:10 and add 0.1% Tween 20 (v/v) (1 ml in 1 l) |
| 1x PBS/T 2 buffer | dilute 10x PBS 1:10 and add 0.3% Tween 20 (v/v) (3 ml in 1 l) |
| Blocking buffer WB | 5% Milkpowder (2.5 g) in 50 ml PBS/T I |
| Dilution buffer WB | 1% FCS in PBS (100 µl in 10 ml) |
| Detection solution 1 | 88.5 ml $H_2O$<br>10 ml 1M Tris-HCl, pH 8.5<br>1 ml 250 mM Luminol (3-Aminophthalhydrazide) in DMSO<br>0.44 ml 90 mM p-Coumaric acid in DMSO |
| Detection solution 2 | 90 ml $H_2O$<br>10 ml 1 M Tris-HCl pH 8.5<br>60 µl 30% $H_2O_2$ |
| 10x B1 buffer | 500 mM Tris-(hydroxymethyl)-aminomethan (M: 121.1 g/mol, 60.5 g)<br>50 mM MgCl2 (M: 95.21 g/mol, 10.16 g)<br>add to 1 l $dH_2O$and adjust pH = 7.4 |

| | |
|---|---|
| DTT Stock | 1M Dithiothreitol (154.25 g/mol, 1.54 g in 10 ml $dH_2O$)<br>dilute 1:500 (add 1 ml 1M DTT for 0.5 l PBS) for final concentration of 2 mM, store 1 ml aliquods at -20°C |
| Elution buffer | 10 mM reduced L-glutathione (307.32 g/mol, 30.7 g per 100 ml)<br>in PBS/2 mM DTT |
| IPTG Stock | 1 M Isopropyl β-D-1-thiogalactopyranoside (238.30 g/mol, 2.38 g in10 ml $dH_2O$)<br>dilute 1:10.000 (200 µl per 2 l LB medium) for final concentration of 0.1 mM, store aliquods at 4°C |
| GuaHCl washing buffer | 6 M Guanidinium chloride (95.53 g/mol, 573.24 g in 1 l $dH_2O$) |
| Coomassie Staining solution | 0.1% (w/v) Coomassie Brilliant Blue R-250 (Serva)<br>40% (v/v) ethanol<br>10% (v/v) acetic acid in $H_2O$ |
| Coomassie Destain. solution | 40% (v/v) ethanol<br>10% (v/v) acetic acid in $H_2O$ |

## 2.5 Expression vectors

The following expression vectors were used in this study.

| plasmid constructs | Reference |
|---|---|
| pGEX-4T2 | bacterial protein expression vector (Amersham Biosciences, now GE Healthcare) |
| pGEX-4T2-Irgm1 | generated by Sascha Martens, (Martens et al. 2004) |
| pGEX-Irgm1-short (= Irgm1Δ1-16) | performed by Rita Lange:<br>The first 16 aa of pGEX-Irgm1-short (= Irgm1Δ1–16) were deleted using the QuikChange site-directed mutagenesis kit protocol (Stratagene, La Jolla, CA) of pGEX-Irgm1 construct with the following primer<br>5`-CCCAGGAATTCCCGGGTCGACCACCA TGGCAGAGACCCATTATGCTCCCCTGAGC-3´ |
| pGEX-4T2-Irgm2 | generated by Revathy Uthaiah, Howard lab collection |
| pGEX-4T2-Irgm3 | generated by Revathy Uthaiah, (Pawlowski et al. 2011) |
| pGEX-4T2-Irga6 | generated by Revathy Uthaiah, (Uthaiah et al. 2003) |
| pGEX-4T2-Irgb6-TevUp | generated by Nikolaus Pawlowski, (Pawlowski et al. 2011) |
| pGEX-4T2-Irgd | generated by Revathy Uthaiah, Howard lab collection |
| pGW1H | mam. expression vector (British Biotechnology, Oxford, U. K.) |
| pGW1H-Irgm1 | generated by Sascha Martens, (Martens et al. 2004) |
| pGW1H-Irgm1-short | pGW1H-Irgm1-short was generated by subcloning the Irgm1Δ1–16 fragment from pGEX-Irgm1-short into pGW1H using SalI digestion |
| pEGFP-N3/Irga6-cTag | generated by Sascha Martens, (Khaminets et al. 2010) |

| | |
|---|---|
| pPur | mammalian expression vector with Puromycin resistance (Clontech Saint-Germain-en-Laye, France) |
| pSV3-neo | mammalian expression vector with T-large antigen of SV40 virus for immortalisation of cell lines, Howard lab collection |
| pCDNA3.1-GFP-TOPO-CT229 | N-terminal fusion of GFP to CT229, generated and provided by Ted Hackstadt, (Clifton et al. 2004) |
| pmCherry-C1-IncB | generated and provided by Ted Hackstadt, (Mital et al. 2013) |

## 2.6 Unicellular Organisms

### Bacterial strains

- ***Escherichia coli* BL21:** B, F-, hsdS ($r_B$-, $m_B$-), gal, dcm, ompT
- ***Listeria monocytogenes***, strain EGD, serotype 1/2a (wildtype)
- ***Listeria monocytogenes Δhly*** (listeriolysin-deficient)
- ***Mycobacterium bovis*** bacillus Calmette-Guerin (BCG)

### Toxoplasma gondii

ME49: type II strain, avirulent, originally isolated from sheep muscle (California, USA) in 1965 (Guo et al. 1997).

### Encephalitozoon cuniculi

*E. cuniculi* spores were obtained from Wolfgang Bohne, who got them from Professor Peter Deplazes (University of Zürich, Switzerland). This *E. cuniculi* stain had the genotype I (Jingtao Li and Marialice Heider, personal communication).

## 2.7 Mammalian primary cells and cell lines

All cells were cultivate at 37°C, 7.5% $CO_2$ and 90% humidity and kept under sterile conditions.

### Primary human foreskin fibroblasts (Hs27)

Hs27 were purchased from ATCC (CRL-1634) and cultured in supplemented IMDM.

### Human Embryonic Kidney (HEK293FT) cell line

HEK293FT is an adherent cell line, kindly provided by Thomas Langer. It is a highly transfectable derivative of the HEK293 cell line, which stably express the SV40 large T-antigen. This allows amplification of transfected plasmids, which contain the SV40 origin of replication.

### Primary mouse embryonic fibroblasts

MEFs were prepared from C57BL/6 mice at day 14 post coitum (by Claudia Poschner) and cultured in supplemented DMDM until a maximum passage number of 15.

### *Irgm1*$^{-/-}$ T MEFs

Immortalised MEFs from *Irgm1*$^{-/-}$ mice (cells provided by Greg Taylor) spontaneously transformed (T) in culture conditions with supplemented DMDM and are very suitable for microscopy and transfection.

### Immortal *Irgm1*$^{-/-}$ MEFs, *Irgm3*$^{-/-}$ MEFs, *Irga6*$^{-/-}$ MEFs, *Irgd*$^{-/-}$ MEFs, *Irgm1*$^{-/-}$/*Irgm3*$^{-/-}$ MEFs and immortal wt MEFs as control line

*Irgm1*$^{-/-}$, *Irgm3*$^{-/-}$, *Irgm1/Irgm3*$^{-/-}$, *Irgd*$^{-/-}$ and wt MEFs (kindly provided by Greg Taylor ) or *Irga6*$^{-/-}$MEFs (Liesenfeld 2011) were immortalised by the simian virus 40 large T-antigen, which alters the effect of the tumour suppressor proteins pRb and p53 (Southern et al. 1982). Because the knock-out cells were already neomycin resistant, an additional plasmid carrying a puromycin resistance gene was transfected. Therefore, 5 µg pSV3-neo plasmid and 0.5 µg pPur were mixed with 10 µl FuGENE HD in 400 µl serum-free medium, incubated 20 min at RT and dropped onto 90% confluent cells in a 10 cm dish. After 24 h, cells were put under selection with 3 µg/ml puromycin.

### Mouse epithelial cell line CMT-93

CMT-93 is an epithelial cell line derived from a rectal carcinoma of a C57BL/6 mouse in 1978. It was purchased from ATCC (CCL-223), and cultured in supplemented DMDM.

### Mouse macrophage cell line RAW 269.7

RAW269.7 is a macrophage cell line transformed by Abelson murine leukemia virus in a BALB/c mouse. It was purchased from ATCC (TIB-71), and cultured in supplemented DMEM.

### Primary bone-marrow-derived macrophages (BMM)

BMMs were prepared from femurs and tibia of C57BL/6 mice (by Claudia Poschner) and cultivated in supplemented RPMI. Frozen BMMs were thawn for each experiment and seeded directly on uncoated glass slides.

### Hybridoma cells 1B2

Hybridoma cells 1B2 produce monoclonal antibodies against Irgm1 and were provided by Greg Taylor. Subclones generated by limiting dilution were selected for highest antibody

titres, pooled and cultivated in IMDM supplemented with 10% FCS in roller bottle (2 l) cultures. Antibody purification via Protein A as described in (Papic et al. 2008) or ammonium persulphate precipitation was unfortunately not successful, because the purified antibody was not functional in immunostainings anymore. To this end, only undiluted hybridoma supernatant + 0.2% sodium azide was used for immunostainings.

## 2.8 Cell-biological methods

### Freezing and thawing of mammalian cells

Mammalian cells were harvested, pelleted at 400 g for 5 min, and resuspended ($4*10^6$ cells/ml) in ice cold sterile FCS/10% DMSO (v/v). Frozen cells were stored in liquid nitrogen for long-term storage. Cells were thawn at 37°C, immediately transferred into 10 ml of medium, pelleted and plated in fresh medium in a T75 flask.

### Passaging of mammalian cells

For passaging, cells were first washed once with sterile PBS and then detached with 1x trypsin solution 1-2 min at 37°C. After addition of 8 ml medium, cells were pelleted and plated in a new flask in a dilution 1:3 (primary fibroblasts) or 1:5 to 1:10 (cell lines).

### Transient DNA transfection

Transient transfection of cells was conducted with $2*10^5$ in 6-wells plates with 1:3 or 2:5 ratio of µg DNA per µl FuGENE 6 or XtremeGene 9 according to the manufacturer's instructions. Protein overexpression was analysed 24 h later.

### Induction and stimulation of cells

Cells were stimulated with 200 U/ml of recombinant mouse IFNγ for 24 h. For IDO-inhibition, L-tryptophan (W) was added 15 min prior to infection.

### Bacterial labelling and host cell infection

performed by Michael Schramm

For bacterial infection assay, *L. monocytogenes* were grown overnight in brain-heard infusion (BHI) medium, resuspended in fresh BHI medium and harvested during mid-log phase. Before harvesting *M. bovis* BCG, suspensions were centrifuged at 25 g to remove clumps.

After washing once with PBS, concentration of the bacteria was estimated by optical density measurement. *M. bovis* BCG were incubated with 1 mM Tetramethylrhodamine isothiocyanate (TRITC) isomer R -X succinimidyl ester in 0.1 M $NaHCO_3$ in $H_2O$, pH 9 for 1 h at room temperature (RT). Unbound dye was removed by repeated washing with PBS. Heat-killed *L. monocytogenes* (HKLM) were prepared by incubating *L. monocytogenes* at 60°C for 60 min. Inactivation of HKLM was proven by plating on sheep blood agar plates before use.

The bacterial suspensions were diluted, *L. monocytogenes* was added to cells at an multiplicity of infection (MOI) of 5-10 (fibroblasts) or 0.5 (macrophages) and *M. bovis* BCG at an MOI of 5 (macrophages) in ice cold DMEM with 10% FCS. Adherence of bacteria was synchronized by centrifugation at 850 g, 4°C for 5 min. Subsequently, non-adherent *L. monocytogenes* were removed by triple washing with ice cold PBS. Infected cells were incubated in pre-warmed DMEM with 10% FCS. At specific times after infection, samples were fixed with 3% PFA in PBS for 20 min at RT followed by washing once with PBS.

### Passaging and host cell infection with *T. gondii* ME49

Tachyzoites from *T. gondii* strain ME49 were maintained by serial passage in confluent monolayers of human foreskin fibroblasts in T25 flasks with supplemented IMDM, incocculating either $2*10^6$ for harvesting after 2 days or $0.5*10^6$ parasites for 3 days. Extracellular parasites, which replicated and egressed from the lysed host cells, were harvested from the supernatant and purified from host cell debris by differential centrifugation (5 min at 100 g; 15 min at 500 g). Parasites were resuspended in fresh medium, counted using a Neubauer chamber and immediately used for infection of host cells at an MOI of 5.

### *In vitro* passaging of *E. cuniculi* and host cell infection

*E. cuniculi* spores were routinely propagated in Hs27 cells. Infected monolayers were scrapped 7-12 days post infection and the suspension was passed through a 26G needle. The differential centrifugation (10 min at 500 rpm; 20 min at 2500 rpm) first removed the host cell debris and then sedimented the spores. A stock solution with $2.5*10^7$ spores/ml PBS was stored at 4°C for max. 3 month. For infection assays, $8\text{-}12*10^4$ host cells were seeded in 6-wells 48 h prior infection, optionally stimulated, and infected with an MOI of 5 parasites per host cell unless otherwise stated. In order to obtain a synchronic infection, spores were allowed to infect the cells for 2-4 h followed by one careful washing step with PBS and addition of fresh medium. Cells were fixed or harvested at the indicated time points post infection.

## Indirect Immunofluorescense microscopy

For immunocytochemistry, cells were grown on cover slips in 6-well plates or 24-well plates. After treatments, cells were carefully rinsed once with PBS to remove the medium, fixed in 3% paraformaldehyde for 20 min at RT and then triple washed with PBS. The conventional staining included permeabilisation and blocking in blocking buffer (3% BSA and 0.1% saponin in PBS) for 1 h at RT, followed by staining with primary antibodies diluted in blocking buffer for 1 h at RT and staining with secondary antibodies diluted in blocking buffer for 30 min at RT. Between all steps cells were triple washed with 0.1% saponin in PBS.

The differential staining was extended by a first staining without permeabilisation. Exclusively extracellular bacteria were stained by blocking with 3% BSA in PBS for 1 h at RT followed by staining the unpermeabilised cells with the primary antibody against bacteria and Alexa Fluor 647-conjugated secondary antibody. Between all steps cells were triple washed with PBS. Thereafter, intra- and extracellular bacteria as well as the protein of interest (Irgm1) were stained by permeabilisation and blocking in conventional blocking buffer (3% BSA and 0.1% saponin in PBS) for 1 h at RT, followed by staining with both primary antibodies diluted in blocking buffer 2 for 1 h at RT as well as Alexa Fluor 488/555-conjugated secondary antibodies for 30 min at RT. Between all steps cells were triple washed with 0.1% saponin in PBS and then mounted on glass microscopic slides in ProLong Gold anti-fade reagent. The images were taken with an Axioplan II fluorescence microscope and AxioCam MRm camera at 630x magnification and processed by Axiovision 4.7. Confocal Images were taken with the Zeiss Meta Confocal microscope at 630x magnification and processed by Zen 2011 software (all Zeiss, Oberkochen, Germany).

## Biotin labelling of host surface proteins

To label host surface proteins, cells were incubated with 1 mg/ml EZ-Link Sulfo-NHS-LC-LC-Biotin for 20 min on ice. The NHS-activated biotin forms stable amide bonds with primary amino groups of proteins and is connected by a non-cleavable spacer arm to the charged sulfo group, which provides water solubility and membrane impermeability. Cells were then triple washed with ice cold PBS and subsequently infected with *T. gondii* ME49. Streptavidin-Cy3 diluted 1:1000 was used in the staining procedure to detect biotinylated proteins. Quenching with 100 mM glycin did not improve the staining and was therefore not performed.

## Transferrin uptake to label endosomes

Cells were first starved 1 h in FCS-free medium at 37°C, and then medium was exchanged with FCS-free medium containing 5 µg/ml Alexa-546 labelled human Transferrin. After 5 minutes of incubation, cells were fixed with ice cold fixing buffer 20 min at RT in order to label early endosomes. For recycling endosomes, the cells were incubated with FCS-free medium with diluted transferrin for 10 minutes after starvation and then triple washed with ice cold PBS. Thereafter, the full medium was added and the cells were incubated at 37°C for 30 minutes. Finally, cells were fixed with ice cold fixing buffer followed by triple washing with PBS and subjected to the immunofluorescence staining.

## Live cell imaging

For live cell imaging, 30.000 wt MEFs in a volume of 100 µl were seeded in the channel of µ-slide I chambers and the reservoirs were filled with 600 ml of medium. The next day cells were at the same time transiently transfected with pEGFP-N3-Irga6-ctag1 (1 µg DNA and 2 µl Fugen HD) and induced with 200 U/ml IFNγ. After 24 hours cells were infected with *E. cuniculi* spores at an MOI of 50, carefully washed after 2 h and kept in phenol red-free RPMI 1640. The samples at 37°C were observed at 630x magnification with a Zeiss Axiovert 200 M motorized microscope fitted with a wrap-around temperature-controlled chamber (Zeiss). The time-lapse images were obtained and processed by Axiovision 4.6 software.

## Cell viability assay

Viable cells were quantified by the CellTiter 96 AQueous non-radioactive cell proliferation assay, that is based on constitutively expressed dehydrogenase enzymes in metabolically active cells, which can reduce the membrane-permeable substrate [3-(4,5-dimethylthiazol-2-yl)-5-(3-carboxymethoxyphenyl)-2-(4-sulfophenyl)-2H-tetrazolium, inner salt] (MTS). In the presence of the electron coupling compound phenazine methosulphate (PMS), the enzymatic reduction leads to the formation of coloured formazan.

To this end, primary MEFs (5000 cells/96-well) were seeded in triplicates and stimulated with IFNγ for 24 h or left untreated. The cells were then infected with *E. cuniculi* spores at the indicated MOI for 24 h or 48 h. Infection with *T. gondii* ME49 served as positive control. The medium was carefully removed and the reaction mix of 19 µl MTS, 1 µl PMS and 100 µl medium was added to each 96-well followed by incubation at 37°C for 2 h. The absorption at 495 nm, proportional to formazan compound and thus viable cells, was measured using a Paradigm™ Detection Platform.

### Cell necrosis assay

performed by Marialice Heider

MEFs grown in 6cm-dishes were induced with IFNγ for 24 h and infected with E. cuniculi spores at an MOI of 10. At 24 h post-infection, Bisbenzimide Hoechst 33342 and Propidium iodide were added to the medium (1 µg/ml final concentration for both) and incubated at 37°C for 15 min. 10 fluorescent pictures per sample were photographed with the Zeiss Axiovert 200 M microscope with a 10x magnification. Total cell number (Hoechst-positive nuclei) and dead cells (PI-positive nuclei) were automatically enumerated using the Volocity software (PerkinElmer, Santa Clara, CA, USA). At least 500 cells were counted per sample and percentage of dead cells per total cell number was calculated. In five independent experiments, a total of 10.000 cells or more was counted per sample.

## 2.9 Protein biochemistry methods

### Transformation

1 ng of the plasmids was mixed with 50 µl *E. coli* BL21 bacteria cells and kept on ice for 20 min. A heat shock was performed for 2 minutes at 42°C to induce the uptake of the plasmid and chilled 2 min on ice. Subsequently, 400 µl LB media was added and incubated for 1 h at 37°C.The cell suspension was transferred in 20 ml LB medium supplemented with 50 µg/ml Kanamycin or 100 µg/ml Ampicillin and grown as a pre-culture over night at 37°C to select plasmid-containing bacteria.

### Protein Expression

1 l or 2 l antibiotic-supplemented LB medium were inoculated with the pre-culture and grown to an $OD_{600nm}$ of 0.8 – 0.9 at 37°C while shaking. Protein expression was induced by addition of 0.1 mM isopropyl-β-D-thiogalactoside (IPTG) (100-200 µl of 1 M stock) and let grown at 18°C overnight. Cells were harvested at 4500 g for 15 min at 4°C. Bacterial cell pellets were transferred into 50 ml falcons and frozen at -20°C.

### Bacterial cell disruption

On ice, bacterial cell pellets were resuspended and vortexed in 10 ml PBS containing 2 mM dithiothreitol (DTT), and one tablet complete mini protease inhibitors EDTA free per 1 l bacterial culture. The suspension was passed three times through the EmulsiFlex-C5 microfluidiser at 150 MPa directly on ice. Centrifugation at 50.000 g (JA 25.50 rotor), 4°C for 60 min was used to separate cell debris and undisrupted bacteria from the soluble protein.

## Protein purification via Glutathion sepharose affinity and Gel filtration columns (Irga6, Irgb6, Irgd)

Glutathione Sepharose (GST) affinity column (size: 5 ml) were pre-equilibrated with 25 ml PBS containing 2 mM DTT (PBS/DTT), loaded with the soluble protein fraction and then washed with 40 ml PBS/DTT. The GST-tag was cleaved off Irga6 and Irgd with 100 U thrombin in 5 ml PBS/DTT o/n at 4°C directly on the column. The IRG protein was then eluted from the column with 20 ml PBS/DTT and monomeric IRG protein-containing fractions were pooled. For Irgb6, GST-Irgb6 was first eluted from the column with 20 ml 10 mM Gluthation in PBS/DTT and pooled protein-containing fractions were cleaved with approximately 200 U recombinant Tev Protease (provided by Gerrit Praefcke), because Irgb6 has an internal Thrombin cleavage site. Protein precipitates were removed by ultracentrifugation at 45.000 rpm (TLA-22 rotor) for 30 min at 4°C. Soluble protein solutions were subjected to size exclusion gel filtration chromatograpy on a HiLoad 26/60 Superdex 75 (Irga6, Irgb6) or Superdex 200 (Irgd) prep grade column, which were pre-equilibrated with 600 ml PBS/DTT. 300 ml PBS/DTT ran through the column and the last 200 ml were collected in 4 ml fractions. Fractions with monomeric protein were pooled and concentrated by a centrifugal concentrator Vivaspin 20, which have a 10 kDa cut-off, at 5000 g at 4°C. Aliquots were shock-frozen in liquid nitrogen and stored at -80 °C.

Protein-containing fractions were identified and analysed by subjecting equal amounts to Sodium dodecyl sulphate polyacrylamide gel electrophoresis (SDS-PAGE, see below) and staining with Coomassie Blue. To this end, SDS-PAGE gels were incubated for about 10 min with Coomassie Staining solution at RT, rinsed with $H_2O$ and destained with Coomassie Destaining solution for at least 2 h. GST- and GeFi-columns were stored in 20% Ethanol, and GST-columns were regularly washed with 6 M GuaHCl.

## Determination of protein concentration

Protein concentrations (c) were determined using an Ultrospec 210 pro with a fixed path length (pl) of 1 cm. The absorbance at 280 nm ($A_{280}$) was measured. The extinction coefficient $\varepsilon_{280}$ ($M^{-1}$ $cm^{-1}$) for the tested proteins were: Irga6 = 35320, Irgb6 = 40230, Irgd= 33150. The dilution factor (df) was variable. The protein concentration can then be calculated with the following formula: $c = A_{280} : (E_{280} * pl) * df$.

## Cell lysis for protein analysis of post-nuclear supernatants

Cells were rinsed once with cold PBS and scraped in 1 ml PBS on ice. Cells were sedimented by a quick centrifugation step and cell pellets were lysed in cell lysis buffer (app. 100 µl per $3*10^5$ cells) by strong pipetting trough a yellow tip and incubation for 30 min at 4°C while rotating. For immunoprecipitation experiments with MEFs and L929 fibroblasts, 0.5% NP-40, 140 mM NaCl, 20 mM Tris/HCl (pH 7.6), 2 mM $MgCl_2$ supplemented with Protease Inhibitor was used as lysis buffer. For protein analysis of post-nuclear supernatants, MEFs were lysed in cell lysis buffer, which contains Triton X-100 as detergent (see above). Cells were centrifuged for 30 min at 17.000 g to remove the DNA-containing nuclei. 10% 10x Laemmli buffer was added to the post-nuclear supernatants and boiled 5 min at 95°C to denaturate proteins. 10 to 25 µl per lane were subjected to SDS-PAGE.

## Quick cell lysis for protein analysis of whole cell lysates

HEK293FT, CMT-93 and MEFs, which were used in *E. cuniculi* experiments, were rinsed once with cold PBS and directly lysed in the 6-well with 200 µl 2x Laemmli buffer. Whole cell lysates of were boiled 5 min at 95°C. 15 to 20 µl per lane were subjected to SDS-PAGE.
500 µl bacterial BL21 cell suspension with transformed with pGEX-Irgm1-long, pGEX-Irgm1-short, pGEX-Irgm2 or pGEX-Irgm3, was harvested at 5000 *g* for 15 min at 4°C. Pellets were resuspended in 500 µl 2x Laemmli buffer and boiled 5 min at 95°C. 5 to 10 µl per lane were subjected to SDS-PAGE.

## Immunoprecipitation

Irgm1 was immunoprecipitated from post-nuclear supernatants of $10^7$ L929 and C57BL/6 MEFs and incubated with 30 µl rbMAE15 antiserum ($3^{rd}$ bleed) overnight followed by 2 h incubation with 150 µl of protein A–Sepharose suspension both at 4°C. Beads were washed three times with ice cold lysis buffer without detergent and boiled in 70 µl 2xLaemmli buffer for 5 min at 95°C. All immunoprecipitated protein (70 µl) was subjected at once to 8 – 13.5% gradient SDS-PAGE

## Separation of proteins

Sodium dodecyl sulphate polyacrylamide gel electrophoresis (SDS-PAGE) was used to separate proteins of protein purifications, cell lysates as well as precipitated protein extracts.

A discontinuous gel-system concentrates polypeptides on the intersection of two gel phases before they get separated according to their molecular weight in the resolving gel (Laemmli 1970). Therefore, ¾ of the gel consist of the separating gel, which has 8 - 13.5% acrylamid and pH 8.8, and an upper ¼ of the gel consists of the stacking gel, with has 4% acrylamid and pH 6.8. Gels were casted in between two glass plates, which are separated by plastic spacers. In most of the experiments, a 10% separating gel was used; however for immunoblots with the rbMAE15 antiserum, gradient separating gels with a 13.5% (bottom) to 8% (top) gradient were mixed with a self-made gradient mixer. Additionally to equal amounts of the protein samples PageRuler™ Prestained Protein Ladder was loaded onto gels as a size marker. The SDS-PAGE was run in electrophoresis buffer at a current of 6 milliampere (mA) o/n or 20 mA for several hours for medium gels (15 cm), 1 h at 40 mA for small gels (6 cm) or over night at 30 mA for Maxi gels (45 cm).

## Transfer and immobilization of proteins (Western Blot)

For immunodetection the separated proteins were transferred from the polyacrylamide gel onto nitrocellulose membrane by wet Western Blotting. Therefore, the gel was carefully placed on top of the membrane, sandwiched between eight sheets of Whatman paper and two electrodes and placed in a blotting chamber. The chamber was filled with 1x Electrophoresis Transfer buffer and 0.5 Volts were applied, so that the negatively charged proteins were migrating towards the anode onto the membrane. After 1 h at RT the successful transfer was confirmed by unselective staining of proteins on the membrane with Ponceau S solution.

## Immunoblot staining

First the unspecific binding sites on the membrane were blocked with 5% milk powder in PBS/T 1 for about 1 h at RT. The primary antibody was diluted according to chapter 2.3 in 1% FCS in PBS an incubated with the membranes over night at 4°C or 1 h at RT. The next day, the membranes were washed three times with washing buffer PBS/T 1 for a minimum of 10 min and subsequently incubated with HRP-conjugated secondary reagents diluted in 1% FCS in PBS according to chapter 2.3. The membranes were washed again three times in washing buffer PBS/T 2. Detection buffer 1 and 2 were mixed in a ratio 1:1 and incubated with the membranes for 60 s. Membranes were dried, and chemiluminescence was visualised by exposure of Super RX films (usually 5 s, 30 s, 1 min to 5 min) and film development.

## Silver Staining

Gels from Maxi SDS-PAGE were fixed with 40% ethanol/ 10% acetic acid for 30 min. After washing in $H_2O$, the gels were sensitized with 0.2% sodium thiosulfate in 30% ethanol/6.8% sodium acetate for 30 min followed by several washes with $H_2O$ and incubated in 0.5% silver nitrate for 30 min. After several washes with $H_2O$, gels were developed with 0.0185% formaldehyde in 2.5% sodium carbonate/0.0024% sodium thiosulfate and the reaction was terminated with 0.5% glycin. All steps were performed under gentle agitation. 2-4 bands with an approximate size of 40 kDa were immediately cut out and analysed by mass spectrometry or stored at 4°C.

## Tryptic in-gel digest and Nano-LC coupled ESI mass spectrometry

performed by Tobias Lampkemeyer

After dehydration of minced bands in 100% acetonitrile (ACN), proteins were reduced 2x with 10 mM DTT in 10 mM $NH_4HCO_3$ for 45 min at 56°C and alkylated with 55 mM iodacetamide in 10 mM $NH_4HCO_3$ at RT in the dark. After dehydration in 100% ACN, gel pieces were equilibrated with 10 mM $NH_4HCO_3$ containing porcine trypsin (12.5 ng /ml) on ice for 2 h. Excess trypsin solution was removed and hydrolysis was performed for 4 h at 37°C in 10 mM $NH_4HCO_3$. Digests were acidified with 5% trifluoroacetic acid (TFA), and peptides were extracted with 0.1% TFA followed by extraction with 60% ACN/ 40% $H_2O$/ 0.1% TFA followed by a two-step treatment using 100% ACN. Extractions were combined, concentrated by vacuum centrifugation, and desalted.

## Peptide and protein identification

Sequest as implemented in the Proteome Discoverer 1.3 software (Thermo Scientific) was used for protein identification by searching the Uniprot database of *Mus musculus* using carbamidomethylation at cysteine and oxidation at methionine and phosphorylation at serine, threonine and tyrosine residues as variable modifications. Since the Mascot algorithm (version 2.2, Matrix Science) allows to set N-terminal modifications this search engine was used with acetylation at the protein N-terminus in addition to the above mentioned modifications. Mass tolerance for intact peptide masses was 10 ppm for Orbitrap data and 0.8 Da for fragment ions detected in the linear trap. Search results were filtered to contain only high confident rank 1 peptides (false discovery rate ≤1%) with a mass accuracy of ≤5 ppm, and a peptide length of ≥6 amino acid residues. In case of Sequest results peptides had to match score versus charge state criteria (2.0 for charge state 2, 2.25 for charge state 3 and

2.5 for charge state 4), in case of Mascot results the peptide score had to be at least 20 and the expectation value ≤ 0.05.

## Liposome preparation and co-sedimentation assay

Liposomes were prepared from purchased brain polar lipid extracts, termed "Folch lipids" after Jordi Folch Pi, who described quantitative extraction of tissue lipids by using a chloroform-methanol mixture and a phase partition with water, which removed of water-soluble contaminants (Folch et al. 1957). 100 µl lipid stock (25 mg/ml) were mixed with 30 µl chloroform were dried under argon while rotating the glass vial and additionally put under vacuum for at least 2 h to remove residual chloroform. The lipid film in the glass vial what then rehydrated with 1ml 1x B1 buffer, sonified first 2 min in a water bath and then with a ultra-sonicator (20 pulses, duty cycle 20, output control 2). The lipid suspension was extruded 7 times through polycarbonate membranes with a pore size of 100 nm. The liposomes were stored at -80°C for 4 weeks. For co-sedimentation assays a 50 µl reaction mix with 1 mg/ml (20 µl of 2.5 mg/ml stock solution) liposomes, 5 µM recombinant GKS protein and 1 mM nucleotide in 1x B1 buffer were incubated for 10 min at 37°C followed by ultracentrifugation for 15 min with 100.000 g at 4°C. Supernatants were transferred in new Eppis and the pellet was carefully washed once and then resuspended in 50µl B1 1x buffer. 5.5 µl 10x Laemmli buffer was added to each sample and they were boiled 5 min at 95°C. 2 µl or 10 µl were subjected to SDS-PAGE for immunoblot stainings or Coomassie stainings, respectively.

# Results

## 3. Part 1: Localisation of Irgm1 isoforms

### 3.1 Endogenous long and short isoforms of *Irgm1* can be detected on transcript and protein level

The mouse *Irgm1* gene is located on chromosome 11 composed of two introns and three exons, and two different mRNA transcripts of *Irgm1* generated through alternative splicing have been described (Bekpen et al. 2005). The mRNA of the long isoform carries the initiator codon for the first methionine at the 3'-end of the second exon and translation gives rise to a full-length Irgm1 protein of 409 amino acids. In the shorter alternative splice variant the second exon is skipped leading to usage of an initiator codon in the third exon. The first methionine of the short isoform corresponds to amino acid position 17 of the long isoform (Figure 3.1 A). Expressed sequence tags (ESTs) for both splice variants can be found abundantly in the NCBI database in different mouse strains (www.ncbi.nlm.nih.gov). A BLAST search of the *Irgm1* nucleotide sequence against the C57BL/6 mouse genome revealed 17 mRNA sequences including the second exon (encoding the long Irgm1 isoform) and 41 mRNA sequences without the second exon (encoding the short Irgm1 isoform) (Figure 3.1 B and Appendix Table I). Likewise, transcriptome sequencing of interferon-induced diaphragm-derived cells from C57BL/6 mice showed that transcripts of both splice variants are present at the same ratio (unpublished data, Benedikt Müller and Jingtao Lilue). Therefore, both splice variants of *Irgm1* are generated at the transcript level.

To answer the question whether both isoforms are also translated into proteins, endogenous Irgm1 was analysed after immunoprecipitation from IFNγ-stimulated L929 fibroblasts (C3N/An-derived cell line) or C57BL/6 mouse embryonic fibroblasts (MEFs) (Figure 3.1 C for L929 cells). Although after IFNγ-induction corresponding bands with an approximate size of 40 kDa were hardly visible in the silver stain after separation by SDS-PAGE, they were subjected to mass spectrometry (MS) (in collaboration with Tobias Lampkemeyer, Proteomics Facility, CECAD Cologne). In these bands, Irgm1 was the most abundant protein and could be recovered with a sequence coverage ranging from 43-82%. The tryptic digest of Irgm1 predicts the existence of N-terminal peptides that can discriminate long (38 aa peptide) and short Irgm1 (24 aa peptide) isoforms. Both isoform-specific N-terminal peptides were indeed detected in the MS analysis demonstrating the presence of both endogenous Irgm1 isoforms in IFNγ-stimulated fibroblasts (Figure 3.1 D, line 1 to 5). The N-terminal peptide of the short Irgm1 isoform was found repeatedly and in three different states:

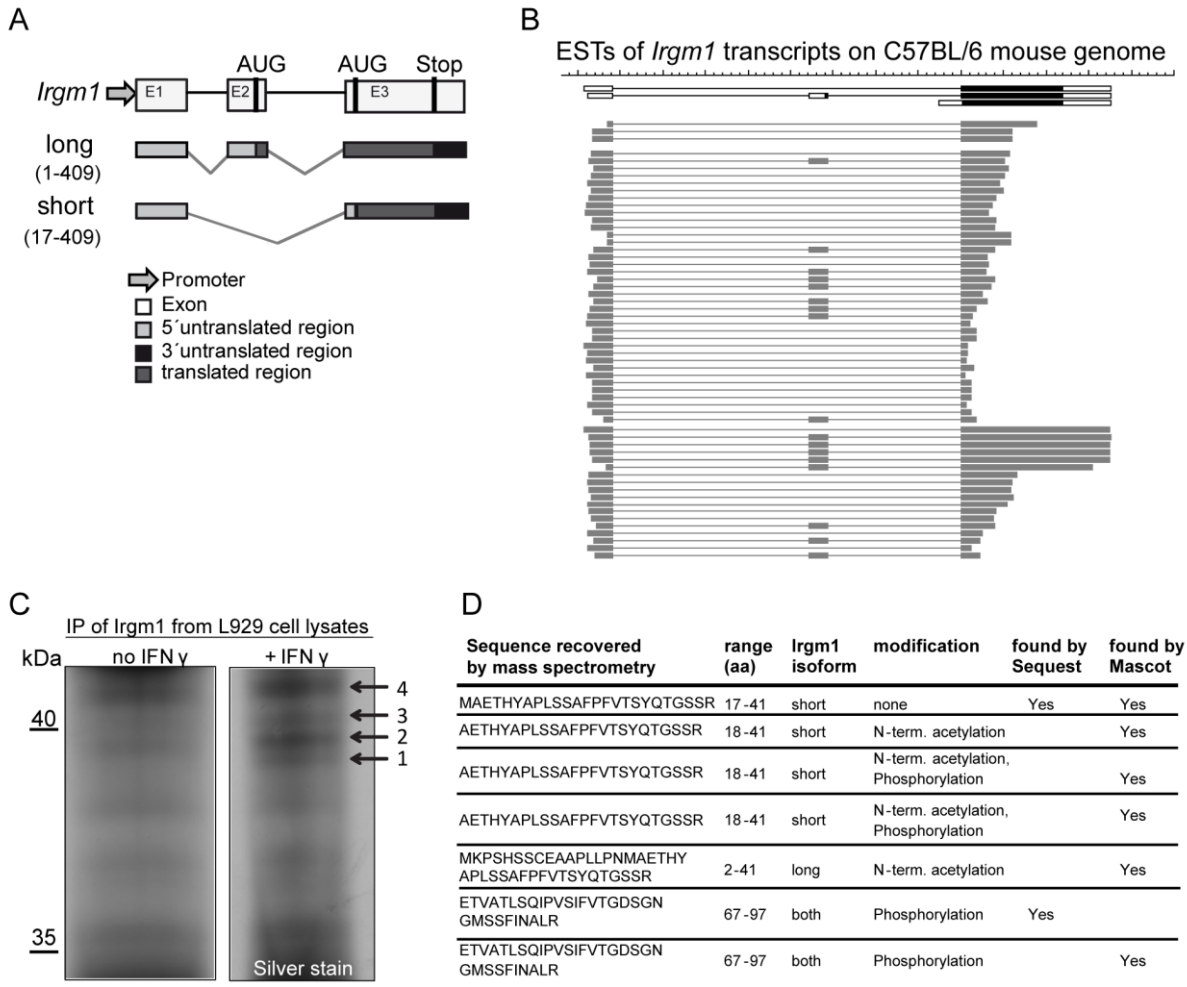


| Sequence recovered by mass spectrometry | range (aa) | Irgm1 isoform | modification | found by Sequest | found by Mascot |
|---|---|---|---|---|---|
| MAETHYAPLSSAFPFVTSYQTGSSR | 17-41 | short | none | Yes | Yes |
| AETHYAPLSSAFPFVTSYQTGSSR | 18-41 | short | N-term. acetylation | | Yes |
| AETHYAPLSSAFPFVTSYQTGSSR | 18-41 | short | N-term. acetylation, Phosphorylation | | Yes |
| AETHYAPLSSAFPFVTSYQTGSSR | 18-41 | short | N-term. acetylation, Phosphorylation | | Yes |
| MKPSHSSCEAAPLLPNMAETHY APLSSAFPFVTSYQTGSSR | 2-41 | long | N-term. acetylation | | Yes |
| ETVATLSQIPVSIFVTGDSGN GMSSFINALR | 67-97 | both | Phosphorylation | Yes | |
| ETVATLSQIPVSIFVTGDSGN GMSSFINALR | 67-97 | both | Phosphorylation | | Yes |

**Figure 3.1: Endogenous long and short Irgm1 isoforms can be detected on transcript and protein level**
**(A)** The *Irgm1* gene gives rise to a long and short isoform due to alternative splicing of the second exon. **(B)** N-terminal expressed sequence tags (ESTs in grey) spanning two or three exons of *Irgm1,* retrieved from a BLAST search of *Mus musculus Irgm1* nucleotide sequence against C57BL/6 mouse genome. Possible model mRNA of *Irgm1* gene is shown in black, the scale bar shows the region 48.871.600 bp (left) to 48.864.500 bp (right) on Chromosome 11 in 100 bp steps. **(C)** Endogenous Irgm1 from L929 cells was immunoprecipitated with the rbMAE15 antiserum, separated by SDS-PAGE and visualised by silver stain. Differential protein bands after IFNγ-induction at 40 kDa (arrows 1 to 4) were cut out for tryptic digestion and analysed by nano-LC ESI-MS/MS. **(D)** Identified N-terminal peptides specific for long and short *Irgm1* isoform as well as the posttranslational modifications such as N-terminal acetylation and phosphorylation are listed. The amino acid range of the found peptide is according to the sequence of the long *Irgm1* isoform. Sequest and Mascot algorithm was used for protein identification by searching the Uniprot database of *Mus musculus*. The MS analysis was performed in collaboration with Tobias Lampkemeyer. See complete data set of B and D in Appendix Table I and II, respectively

unmodified, N-terminally acetylated, or N-terminally acetylated and phosphorylated (Figure 3.1 D, Appendix Table II). In contrast, the N-terminal peptide of the long Irgm1 isoform was found only once as an acetylated peptide, maybe due to the large size of this peptide.

Since one phosphorylation site of Irgm1 (Ser202) has been already proposed from the analysis of phagosomes in IFNγ-stimulated RAW264.7 mouse macrophages (Trost et al. 2009),

additional phosphorylation sites of Irgm1 were investigated. Phosphorylation of Ser202 was not detected in these measurements. Besides the N-terminally acetylated and phosphorylated peptides, another phosphorylated peptide was found. PhosphoRS algorithms implemented in the Proteome Discoverer software calculated the highest probability for a phosphorylation site of this second peptide at Ser78 or Thr71 (see also Appendix Table II).

## 3.2 Irgm1 isoforms can be detected with different immunological reagents

Since several immunological reagents against Irgm1 protein have been produced up to now, a detailed overview including the respective epitopes is shown in figure 3.2 A. The mouse monoclonal antibody 1B2 was raised against the peptide CEAAPLLPNMAETHY (residues 8-22) near the N-terminus of Irgm1 (Butcher et al. 2005). This peptide crosses the differential splice site at residue 17, and only the C-terminal 6 residues (-MAETHY) of the immunising peptide are present in the short Irgm1 isoform. The 1B2 antibody is therefore expected to have a preference for the long Irgm1 isoform. The first rabbit polyclonal antiserum, which is not available anymore, was raised against the immunising peptide YNTGSSRLPEVSRSTE (residues 36-50). This epitope is shared by both isoforms (Collazo et al. 2001). The second rabbit polyclonal antiserum L115 was raised against a combination of two peptides, QTGSSRLPEVSRSTE (residues 36-50) and NESLKNSLGVRDDD (residues 284-298) of Irgm1 (Khaminets et al. 2010). These two rabbit polyclonal antisera both showed an unspecific band at about 50 kDa, perhaps due to cross-reactivity from the shared N-terminal immunogen peptide [see * in Figure 3.2 C and (Collazo et al. 2001)]. Two goat polyclonal antibodies from Santa Cruz Biotechnology, Inc., A19 and P20, were raised against peptides from N-terminal regions of Irgm1. Although the exact sequences of the immunising peptides are not available, the A19 antibody was described as having been raised and purified against a 15-25 aa peptide derived from a region between amino acids 20 and 70 of Irgm1 (Christian Gernemann, Santa Cruz Biotechnology, Inc., personal communication). Two further rabbit polyclonal antibodies from Abcam plc (ab69464 and ab69465) were produced by immunisation with a peptide from the human homologue IRGM and were described as cross-reactive on mouse IRGM proteins.

Because none of these immunological reagents was working satisfactory for both isoforms in immunofluorescence microscopy, two new reagents against the N-terminal peptide of the short isoform, MAETHYAPLSSAFPC (residues 17-31), were produced in rabbit (rbMAE15) and in chicken (chMAE15) for the present study. These antisera should

detect the short isoform but may also recognize the long isoform of Irgm1, depending on the degree of immunodominance of the free N-terminal methionine.

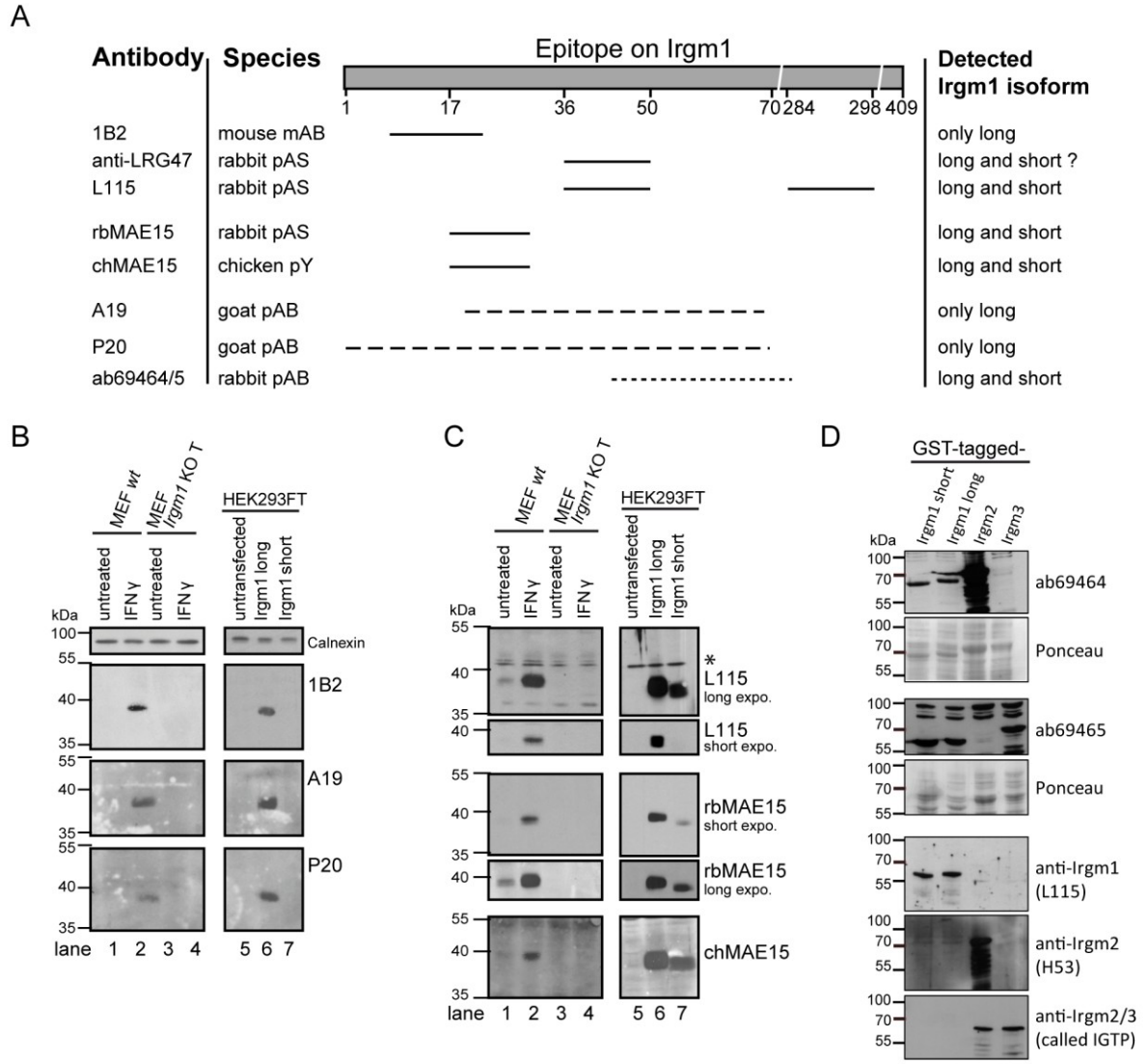


**Figure 3.2: Long and short Irgm1 isoforms are detected by various immunological reagents.**
**(A)** Immunological reagents used for the detection of Irgm1 and their epitopes on the Irgm1 protein. The immunising peptides used for the commercial goat polyclonal antibodies A19 and P20 (Santa Cruz Biotechnology, Inc.) map near the N-terminus (dashed lines). The immunising peptides of anti-human IRGM rabbit polyclonal antibodies (ab69464/5, Abcam plc) map as shown on human IRGM (dotted line). References for the immunological reagents are in Material and Methods. **(B, C)** Transformed mouse embryonic fibroblasts (MEFs) from wildtype C57BL/6 mice and *Irgm1*-deficient mice were treated with IFNγ for 24 h and lysed in 1% Triton X-100. Additionally, HEK293FT cells were transiently transfected with pGW1H-Irgm1-long or pGW1H-Irgm1-short and lysed after 24 h with 2x Laemmli buffer. Proteins were separated by SDS-PAGE and Western Blots were probed with different anti-Irgm1 antibodies (1B2, L115, rbMAE15 chMAE15, A19 and P20). Calnexin served as loading control for both panels. The asterisk marks an unspecific band; expo. abbreviates exposure time. 1B2, A19 and P20 detect only the long Irgm1 isoform whereas L115, rbMAE15 and chMAE15 detect both isoforms of Irgm1. **(D)** GST-tagged Irgm1/2/3 were bacterially expressed and whole cell lysates were subjected to SDS-PAGE. Western Blots were probed with anti-human IRGM antibodies ab69464 and ab69465 (Abcam plc). Anti-Irgm1 (L115), anti-Irgm2 (H53) antisera and anti-Irgm2/3 (anti-IGTP) antibody were used to discriminate between IRG proteins. Ponceau Red staining indicate equal loading of proteins. Anti-human IRGM ab69464 antibody cross-reacts with bacterially expressed mouse GST-Irgm1 and GST-Irgm2, whereas ab69465 detects GST-Irgm1 and GST-Irgm3.

In order to differentially detect the two isoforms of Irgm1, these antibodies were tested by Western Blot analysis. As depicted in Figure 3.2 B and C (lane 1-4), all reagents detected an IFNγ-inducible, diffuse band running at or just below 40 kDa in lysates of C57BL/6 MEFs, which was absent in MEFs from *Irgm1*-deficient mice.

Two distinct protein bands representing the two endogenous Irgm1 isoforms could not be detected. The diffuse running behaviour of endogenous Irgm1 in non-gradient SDS-PAGE seems to be characteristic, and has been observed also in earlier studies [see (Khaminets et al. 2010)]. Gradient SDS-PAGE as performed for the immunoblot with rbMAE15 antiserum did not markedly improve the resolution of distinct bands (Figure 3.2 C, lane 2). The reason for the diffuse running behaviour and low apparent molecular weight of Irgm1 in SDS-PAGE is not known, but might partially be explained by post-translational modifications, as suggested by the MS analysis (Figure 3.1 D).

In order to clarify the isoform specificity of the different immunological reagents, transient transfection of eukaryotic expression plasmids encoding the long and short Irgm1 isoforms with native N- and C-termini into HEK293FT human cells was carried out. Expression of both protein isoforms was possible (Figure 3.2 B and C, lane 5-7), although expression of the short form always appeared to be weaker. In cell lysates of *Irgm1*-deficient MEFs, however, the transfected short Irgm1 isoform could not be detected in Western Blots (data not shown). Microscopic analysis revealed lower transfection efficiency in *Irgm1*-deficient MEFs in case of the short Irgm1 isoform compared to the long Irgm1 isoform (data not shown). Thus, lower expression levels might be due to lower number of transfected cells with the short isoform in murine cells.

In the transfected HEK293FT cells, monoclonal antibody 1B2 detected indeed only the long form of Irgm1 but not the short isoform (Figure 3.2 B lane 6, 7), hence validating the specificity of 1B2 for the long Irgm1 isoform. Because 1B2 could detect a signal in IFNγ-induced MEFs (Figure 3.2 B, lane 2), it is now confirmed that the endogenous long isoform of Irgm1 is indeed expressed. The rabbit antiserum L115 detected both long and short isoforms, as expected from the locations of the immunising peptides (Figure 3.2 C lane 6, 7). However, A19 as well as P20 showed a very strong preference for the long Irgm1 isoform (Figure 3.2 B, lane 6), suggesting that the immunogenic peptides for these antibodies in fact derived from the amino acid sequence N-terminal of the splice junction. The two new antisera, rbMAE15 and chMAE15, raised against the N-terminal peptide of the short isoform, also detected both long and short Irgm1 isoforms (Figure 3.2 C, lane 6, 7). This indicates that the predominant epitopes seen by both rabbit and chicken antisera were not defined by the free N-terminus of

the short form. A conclusion from these results is that there is still no reagent available that is specific for the short isoform of Irgm1.

The commercial (Abcam plc) rabbit polyclonal antibodies ab69464 and ab69465 raised against human IRGM were used to detect specifically Irgm1 in a former study (Chang et al. 2011). The specificity of these antibodies was again investigated, since they were raised against epitopes shared by all three mouse IRGM proteins. Therefore, both isoforms of bacterially expressed GST-Irgm1, GST-Irgm2 and GST-Irgm3 were subjected to SDS-PAGE and Western Blot analysis (Figure 3.2 D). Anti-human IRGM ab69464 antibody cross-reacted with bacterially expressed mouse GST-Irgm1 and GST-Irgm2, whereas ab69465 detected GST-Irgm1 and GST-Irgm3. Thus, these reagents cannot be used to identify Irgm1 unambiguously in mouse cells.

## 3.3 The short Irgm1 isoform localises to the Golgi apparatus but does not colocalise with endolysosomal markers

Both Golgi and endolysosomal localisation of Irgm1 have been shown to depend on the amphipathic alpha helix K (αK helix) in the C-terminal domain (Martens et al. 2004; Tiwari et al. 2009; Zhao et al. 2010), but in these studies the short isoform was not investigated.

Since none of the immunological reagents detected only the short form of Irgm1 (see chapter 3.1.2), Irgm1 expression constructs encoding either the long isoform (Irgm1-long) or the short isoform (Irgm1-short) were transfected into *Irgm1*-deficient MEFs. As expected, because of the presence of the targeting αK helix in both isoforms, the short and the long Irgm1 isoforms showed a typical adnuclear Golgi signal co-localising with GM130 (Figure 3.3 A), and a widely distributed non-Golgi component. The localisation of Irgm1 outside the Golgi was shown previously to correspond in large parts with a LAMP1 positive organelle, identifying a lysosomal or late endosomal compartment [Figure 3.3 B, (Zhao et al. 2010)]. Unexpectedly, however, the non-Golgi signal of the transfected short Irgm1 isoform solidly failed to co-localise with LAMP1 (Figure 3.3 C). Without a C- or N-terminal EGFP-tag Irgm1 is only weakly associated with early or recycling endosomes which can be identified by incubation with fluorescent transferrin (Zhao et al. 2010). Whereas the long Irgm1 isoform co-localised with early endodomes (Figure 3.3 D), the transfected short Irgm1 isoform again failed to do so (Figure 3.3 E). Thus, despite the presence of the αK helix in both long and short isoforms, the short differential sequence at the N-terminus of the long isoform is required for significant targeting of Irgm1 to the endolysosomal system.

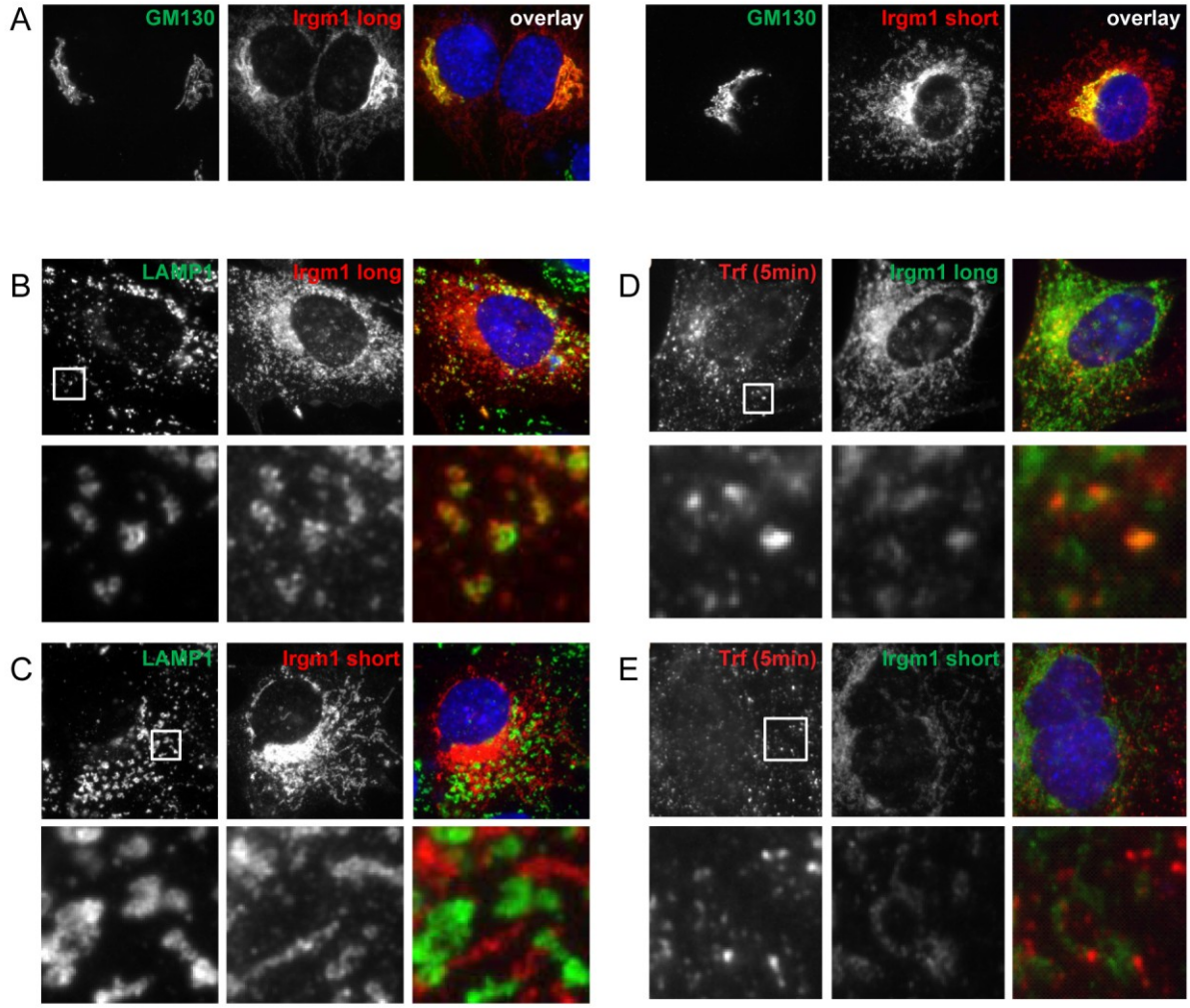


**Figure 3.3: Short Irgm1 isoform localises to Golgi, but not to endolysosomal compartment**.
Transformed *Irgm1*-deficient MEFs were transiently transfected with pGW1H-Irgm1-long or pGW1H-Irgm1-short and fixed after 24 h. Cells were stained for Irgm1 using rbMAE15 pAS. **(A)** Golgi marker protein GM130 was stained with anti-GM130 and **(B, C)** late endosomal-lysosomal marker protein LAMP1 with 1D4B antibodies. In **(D, E)** cells were incubated with Alexa-Fluor-546-labelled transferrin for 5 min prior fixation to stain early endosomes. Nuclei were labelled with DAPI. Both Irgm1 isoforms strongly co-localise with Golgi markers, but only the long Irgm1 isoform clearly overlaps with the vesicular structures of endosomes and lysosomes.

## 3.4 Both Irgm1 isoforms partially colocalise with mitochondria

Endogenous, IFNγ-induced mouse Irgm1 has been reported to be associated with mitochondria in RAW264.7 (Tiwari et al. 2009) and ML-$1_{4a}$ hepatoma cells (Chang et al. 2011), using A19 and rabbit anti-human IRGM antisera respectively to detect Irgm1, and cardiolipin or O-N-nonyl acridine orange and Tom40 respectively as mitochondrial markers. However, A19 is a relatively weak reagent in immunofluorescent microscopy, and the rabbit anti-human IRGM serum used by Chang and colleagues does not discriminate between Irgm1 and Irgm2 (see Figure 3.2 C). Therefore, the mitochondrial localisation of mouse Irgm1 in

MEFs was examined with the rbMAE15 antiserum. Confocal images show that IFNγ-induced Irgm1 as well as transfected long and short isoforms clearly co-localise partially with the mitochondrial markers complex II and cytochrome C (Figure 3.4). However, even with this powerful antiserum the staining intensity on mitochondria is weak.

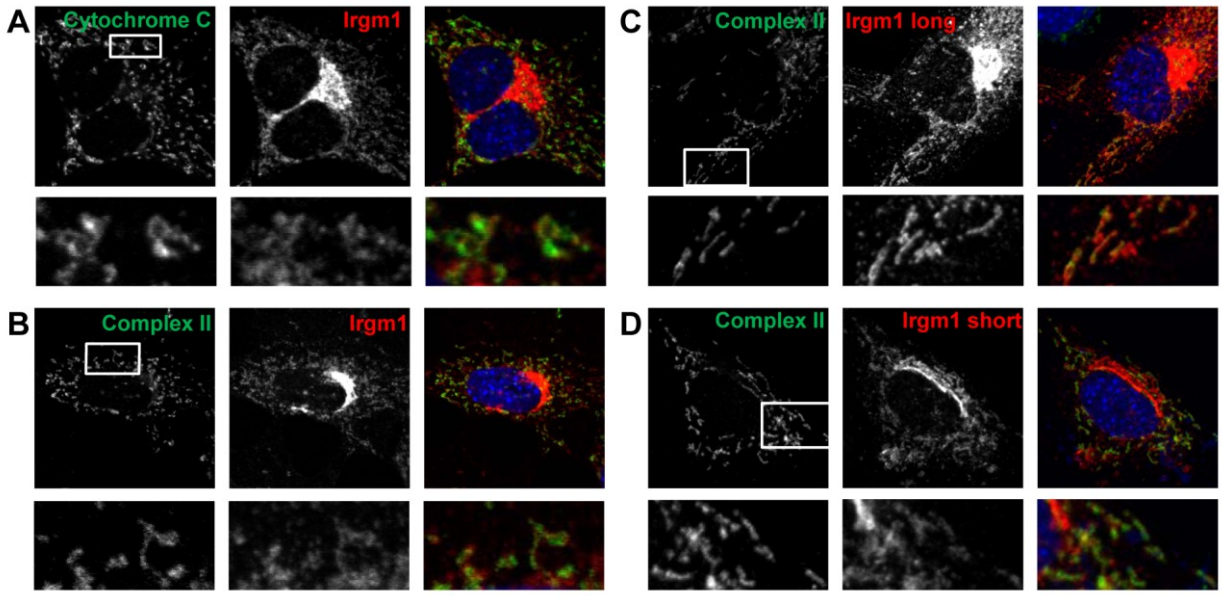


**Figure 3.4: Endogenous Irgm1 and both transfected Irgm1 isoforms partially colocalise with mitochondria.**
**(A)** MEFs from wildtype C57BL/6 mice were induced with IFNγ for 24 h. **(B)** Transformed *Irgm1*-deficient MEFs were transiently transfected with pGW1H-Irgm1-long or pGW1H-Irgm1-short for 24 h. The cells were fixed and stained for Irgm1 and mitochondrial markers using rbMAE15 pAS and anti-cytochrome C or anti-complex II antibodies. Nuclei were labelled with DAPI. Images were taken with a confocal microscope. Irgm1 can weakly be detected at mitochondria.

To sum up, the long isoform of Irgm1 can be detected with all immunological reagents (A19, 1B2, L115, rbMAE15 and chMAE15) and is associated strongly with Golgi, and weakly with mitochondrial and lysosomal membranes. In contrast, the short isoform of Irgm1 is not detected by 1B2 and A19, localises strongly to the Golgi and weakly to mitochondrial membranes but does not localise to the endolysosomal compartment.

## 3.5 Irgm1 does not localise to listerial phagosomes

An association of Irgm1 with bacterial phagosomes was first proposed in a cell-fractionations protocol in macrophages infected with *Mycobacterium tuberculosis* (MacMicking et al. 2003). Subsequently, striking co-localisation with listerial and mycobacterial phagosomes detected by immunofluorescence microscopy was reported for Irgm1 in RAW264.7 macrophages shortly after infection (Shenoy et al. 2007; Tiwari et al.

2009). These former studies had some drawbacks, because only A19 was used as the Irgm1 detection reagent and a control to discriminate between intracellular and extracellular bacteria was missing. Therefore the question whether Irgm1co-localises with bacterial phagosomes was revisited in the present study with differential staining method (see Materials and Methods) and better characterized immunological reagents. The bacterial infections were performed in collaboration with Michael Schramm (University Clinic Cologne).

A

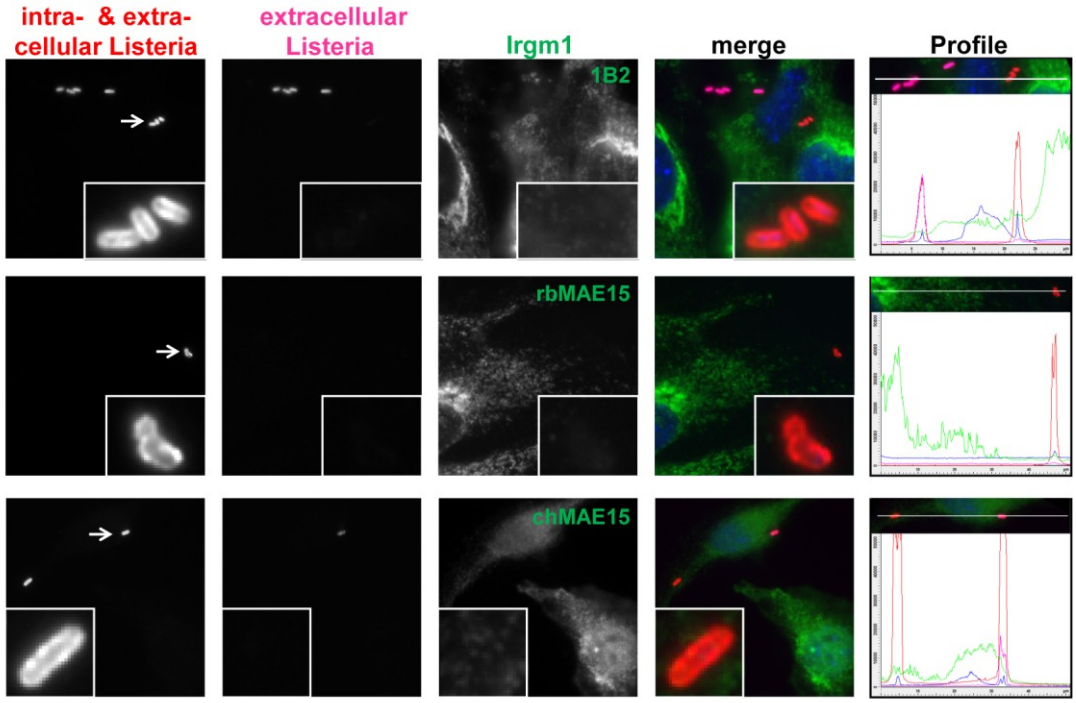


B

| Host cell | Infection | Repetitions | Intracellular Irgm1-positive Listeria |
|---|---|---|---|
| MEF wt | *L. m.* 15 min | n = 11 | 0% |
| MEF wt | *L. m.* Δ*hly* 15 min | n = 4 | 0% |
| MEF wt | *L. m.* Δ*hly* 30 min | n = 6 | 0% |
| MEF wt | *L. m.* Δ*hly* 30 min | n = 4 | 0% |
| RAW264.7 | *L. m.* 15 min | n = 2 | 0% |
| RAW264.7 | *L. m.* Δ*hly* 15 min | n = 2 | 0% |

**Figure 3.5: Endogenous Irgm1 is not detected at intracellular *Listeria monocytogenes*.**
**(A)** MEFs were induced with IFNγ for 24 h, and infected with *L. monocytogenes* for 15 min. The cells were washed, fixed and stained initially without permeabilisation against *L. monocytogenes* with Alexa Fluor 647-conjugated secondary antibody. Thereafter, cells were permeabilised (0.1% saponin) and stained for Irgm1 using mAB 1B2, pAS rbMAE15 or chMAE15 with Alexa Fluor488-conjugated secondary antibody and for *L. monocytogenes* with Alexa Fluor555-conjugated secondary antibody. Nuclei were labelled with DAPI. Transects were drawn through extracellular bacteria (far-red, shown in magenta) and intracellular bacteria (red). The profiles show the pixel intensity of the 4 different detection channels within this transect. **(B)** Quantification of (A) as well as for the infection of RAW264.7 macrophages and of later time points post infection. For the 30 min, 60 min, and 120 min p. i., cells were infected with the *L. monocytogenes* mutant Δ*hly*. 300 - 500 host cell nuclei were evaluated per sample, n indicates number of replicated samples. No local increase in the Irgm1 (green) signal is associated with intracellular *L. monocytogenes*, and no Irgm1-positive intracellular *L. monocytogenes* can be detected in all the samples.

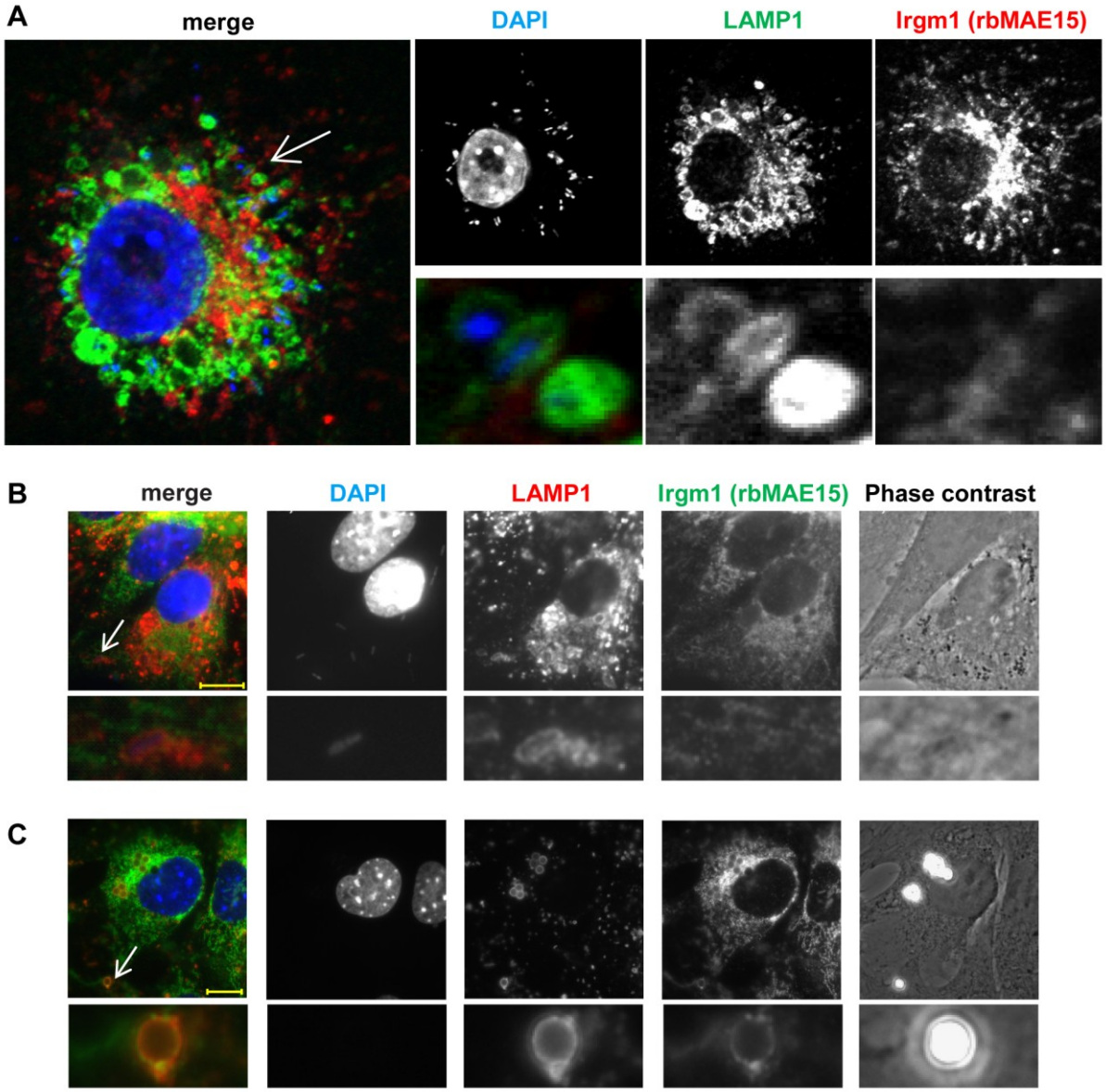


**Figure 3.6: Endogenous Irgm1 does not localise to the phagolysosome of heat-killed or living *Listeria monocytogenes*.**
**(A)** RAW264.7 cells were induced with IFNγ for 24 h, and infected with the *L. monocytogenes* mutant Δ*hly* for 2 h. **(B)** MEFs were induced with IFNγ for 24 h, and treated with heat-killed *L. monocytogenes* wt for 2 h. The cells were washed, fixed and stained for Irgm1 and LAMP1 using pAS rbMAE15 and mAB 1D4B. Nuclei were labelled with DAPI. Arrows indicated the magnified area shown below. **(C)** MEFs were induced with IFNγ for 24 h, and then 2 µm latex beads were added for 4h. Cells were stained as in B. Images were taken with a confocal laser microscope in (A) or a conventional fluorescence microscope in (B, C); scale bars: 10 µm. Irgm1 is not detected at bacterial phagolysosomes but can be detected at LAMP1-positive latex bead phagosomes.

In Figure 3.5, MEFs were treated with IFNγ, infected with *Listeria monocytogenes*, and analysed for Irgm1 localisation by immunofluorescence with the antibodies 1B2, rbMAE15, and chMAE15.Strong Golgi-like staining and weaker cytoplasmic staining with all three anti-Irgm1 reagents was consistent with positive identification of Irgm1 (Figure 3.5 A, see also Figure 3.3). Transects across cells containing intracellular bacteria were quantified for Irgm1 fluorescence intensity associated with bacteria. By these criteria, co-localisation of Irgm1 was

never detected at the phagosome of intracellular wildtype *L. monocytogenes*. The possibility that this result was due to early escape from the phagosome was excluded by applying the same techniques to IFNγ-induced cells infected with the listeriolysin O-deficient *L. monocytogenes* (Δ*hly*) which cannot escape from the phagosome (Beauregard et al. 1997). After 30 min, 60 min and 120 min of infection in MEFs, no intracellular *L. monocytogenes* Δ*hly* were found to be Irgm1-positive (Figure 3.5 B). The experiment was repeated in RAW264.7 macrophages and again no co-localisation of Irgm1 with intracellular bacteria could be detected (Figure 3.5 B).

The DNA of ingested *Listeria* in phagolysosomes can be detected with DAPI in LAMP1-positive compartments. RAW264.7 macrophages infected with *L. monocytogenes* (Δ*hly*) had ingested *Listeria* into LAMP1-positive compartments 2 h after infection (Figure 3.6 A). These bacterium-containing compartments were never found to carry Irgm1 protein. Irgm1 was also never seen on LAMP1-positive phagosomes containing heat-killed *L. monocytogenes* (Figure 3.6 B). This is surprising in view of the repeated observation of Irgm1 on latex bead phagosomes (Martens et al. 2004; Butcher et al. 2005; Zhao et al. 2010), which can also be confirmed for the new rbMAE15 antisera (Figure 3.6 C).

## 3.7 Irgm1 does not localise to the phagosome of *Mycobacterium bovis* BCG

The effector model attributing Irgm1 function to accelerate maturation of bacterial phagosomes is based partly on observations suggesting an association of Irgm1 with *M. bovis* BCG phagosomes in mouse macrophages. In a first report of this association, Irgm1 was detected by Western Blot analysis of BCG phagosomes isolated 20 minutes after infection of mouse bone marrow-derived macrophages (BMM) *in vitro* (MacMicking et al. 2003). Subsequent publications have illustrated co-localisation of anti-Irgm1 antibodies or fluorescent Irgm1 fusion constructs with BCG phagosomes (Deghmane et al. 2007; Shenoy et al. 2007; Saban et al. 2008; Tiwari et al. 2009).

In view of the contrasting results obtained with new immunological reagents against Irgm1 in the context of *L. monocytogenes* phagosome association (see Figure 3.5 - 3.6), the localisation of Irgm1 to the mycobacterial phagosome was examined with similar methods. RAW264.7 cells were infected with *M. bovis* BCG, serologically stained to discriminate intracellular and extracellular organisms and stained for Irgm1 using 1B2. Chicken MAE15 could not be used because it cross-reacted with the surface of extracellular *Mycobacteria*.

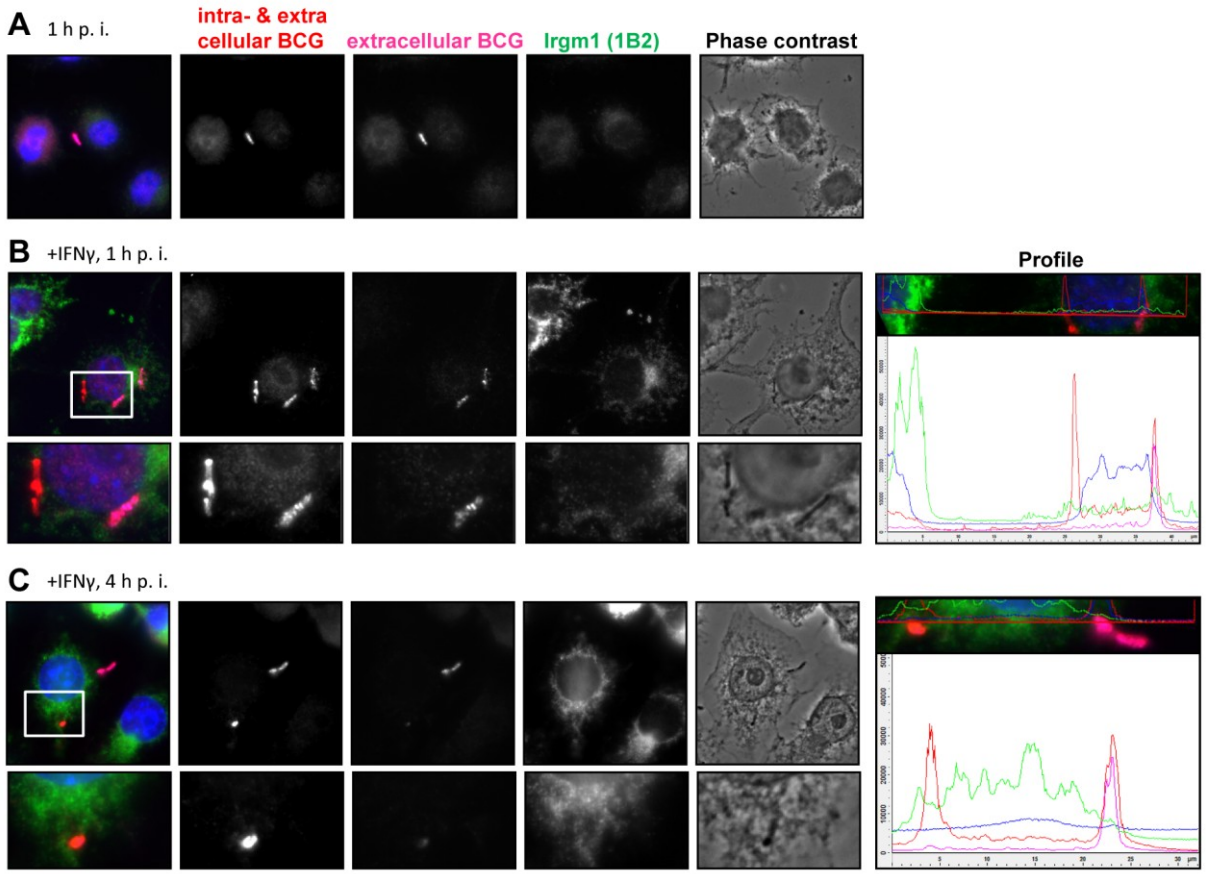


**Figure 3.7: Endogenous Irgm1 is not detected at intracellular *Mycobacterium bovis* BCG.**
RAW264.7 cells were induced with IFNγ **(B, C)** for 24 h or left untreated **(A)**, and infected with *M. bovis* BCG for 1 h **(A, B)** or 4 h **(C)**. The cells were washed, fixed, and stained initially without permeabilisation against *Mycobacteria* with Alexa Fluor647-conjugated secondary antibody. Thereafter, cells were permeabilised (0.1% saponin) and stained for Irgm1 using mAB 1B2 with Alexa Fluor488-conjugated secondary antibody, and against *Mycobacteria* with Alexa Fluor555-conjugated secondary antibody. Nuclei were labelled with DAPI. Transects were drawn through extracellular bacteria (in far-red, shown in magenta) and intracellular bacteria (red). The profiles show the pixel intensity of the different channels within this transect. No Irgm1 (green) signal is associated with intracellular *Mycobacteria*.

In contrast to published findings, Irgm1 detected by the monoclonal 1B2 antibody was absent at the mycobacterial phagosome at any time point analysed (from 15 min until 4h p. i., Figure 3.7). Rabbit MAE15 antiserum could not be used in combination with the rabbit anti-*Mycobacterium* antibody used to define intracellular organisms. As a second method macrophages were infected with TRITC-labelled *M. bovis* BCG instead. In order to validate bacterial ingestion, intracellular bacteria were visualised via co-staining with LAMP1. No Irgm1 was detected at bacterial phagolysosomes from 1 h to 4 h post infection in RAW264.7 macrophages (Figure 3.8 A and B) or BMMs (Figure 3.8 C, D).

Summarising the first part of the results, it has been unambiguously demonstrated that both Irgm1 isoforms are expressed in mouse fibroblasts upon IFNγ-induction and differentially

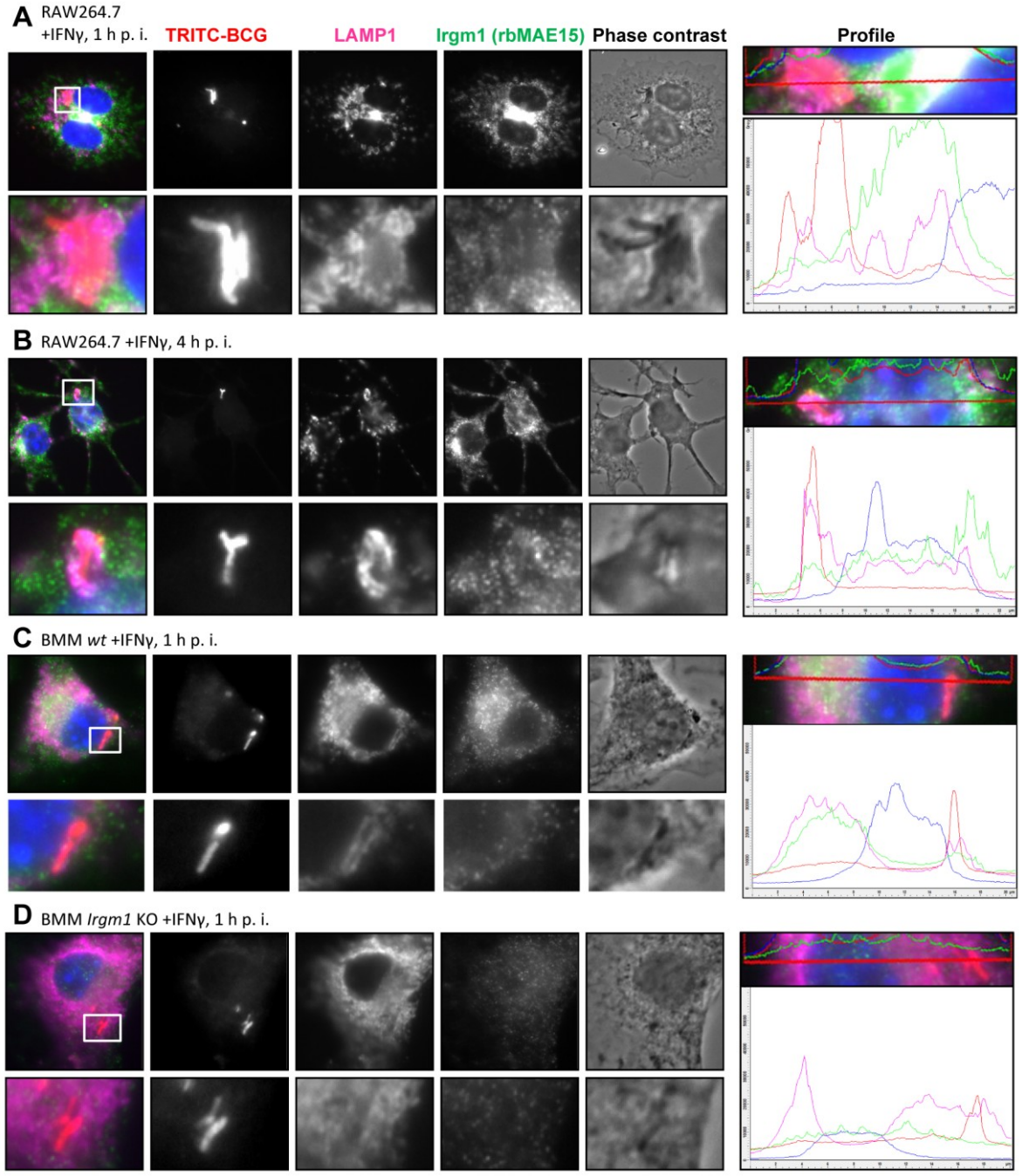


**Figure 3.8: Endogenous Irgm1 does not localise to the phagolysosome of *Mycobacterium bovis* BCG.**
**(A, B)** RAW264.7 cells or bone marrow-derived macrophages from **(C)** wildtype C57BL/6 mice or **(D)** *Irgm1*-deficient mice were treated with IFNγ for 24 h, and infected with TRITC-labelled *M. bovis* BCG for 1 h (A, C, D) or 4 h (B). The cells were washed, fixed and stained with Irgm1 and LAMP1 using pAS rbMAE15 and mAB 1D4B. Nuclei were labelled with DAPI. Transects were drawn through bacteria (in red) and LAMP1 (in far-red, shown in magenta) to demonstrate their residence in the phagolysosome, profiles show the pixel intensity of the different channels within this transect. No Irgm1 signal (green) is associated with the mycobacterial phagosomes

localise to subcellular endomembranes (both isoforms to the Golgi and partially to mitochondria but only the long isoform to the endolysosomal compartment).Moreover, in striking contrast to earlier studies, Irgm1 could never be detected at listerial or mycobacterial phagosomes.

# Results Part 2: IRG binding to protein-deficient membranes

## 3.8 GKS proteins can co-sediment with liposomes in a GTP-dependent manner

Extensive microscopical analysis demonstrated binding of GKS proteins to subcellular membranes of ER or to parasitophorous vacuoles (PV) (see chapter 1.3.5). However, the biochemical features of this membrane-binding are only poorly understood. Initial co-sedimentation experiments with phosphatidylserine or Folch liposomes suggested that Irga6 and Irgb6 but not Irgd can bind to these lipid vesicles in a GTP-dependent manner [(Martens et al. 2004) and Niko Pawlowski unpublished data].

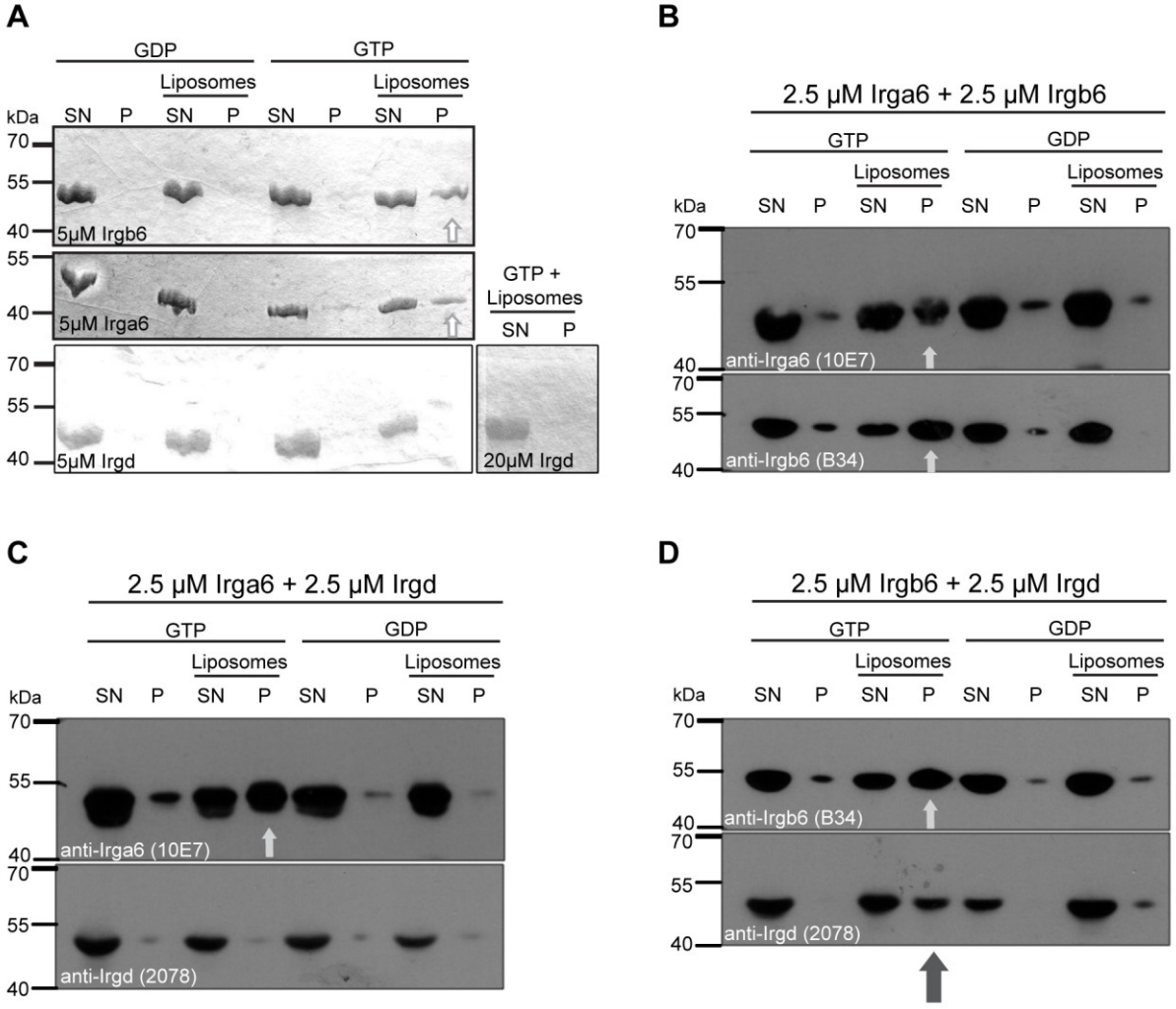


**Figure 3.9: GKS proteins can co-sediment with Folch liposomes in the presence of GTP.**
Recombinant untagged Irga6, Irgb6 or Irgd protein was incubated with Folch liposomes in the presence of GDP or GTP for 10 min at 37°C followed by ultracentrifugation. Proteins of the pellet (P) or supernatant (SN) fraction were separated by SDS-PAGE and stained with Coomassie Blue in **(A)**. In **(B-D)** equimolar amounts of two GKS proteins were mixed for the co-sedimentation assay and detected in Western Blots with specific antibodies (mAB10E7 for Irga6, mAB B34 for Irgb6 and pAS 2078 for Irgd). Irga6 and Irgb6 always bind liposomes in presence of GTP (white arrows), whereas Irgd co-sediments only in presence of Irgb6 and GTP (grey arrow).

In order to define the intrinsic membrane-binding capacities of these IRG proteins, co-sedimentation assays of bacterially-expressed Irga6, Irgb6 and Irgd with Folch liposomes were performed. Figure 3.9 shows that Irga6 as well as Irgb6 could directly associate and co-sediment with liposomes in presence of GTP. In contrast, Irgd alone was not able to co-sediment with the liposomes at the same concentration (5 μM) or at even higher concentrations (20 μM) confirming previous results (Figure 3.9 A). To examine whether GKS proteins can influence each other in membrane-binding, two recombinant proteins were mixed in equimolar amounts and the same co-sedimentation assays were performed. In these mixed preparations, Irga6 and Irgb6 associated with liposomes similar to the individual preparations (Figure 3.9 B). Interestingly, Irgd could co-sediment with liposomes in presence of GTP when it was mixed with Irgb6, but not when it was mixed with Irga6 (Figure 3.9 C, D).

## 3.9 Host cell plasma membrane proteins do not negatively correlate with GKS proteins loading on the PVM of *Toxoplasma gondii*

IRG proteins accumulate onto the parasitophorous vacuolar membrane (PVM) of avirulent *T. gondii*, but never onto all PVMs. Furthermore, there is always large variation of labelling intensity of individual vacuoles independent of a synchronous parasite entry (Khaminets et al. 2010). In the current model, IRG proteins target those PVs of *T. gondii* that efficiently excluded most of the host cell surface proteins during parasite invasion and formation of the nascent PVM (Mordue et al. 1999). This hypothesis argues that the exclusion of host cell plasma membrane proteins is sometimes inefficient and remaining host cell plasma membrane proteins can inhibit IRG loading onto the PVM. These 10-20% of IRG-negative PVs would carry remaining host cell surface proteins. As a consequence, one would expect a negative correlation of IRG proteins and host cell proteins at the PVM.

To test this hypothesis, plasma membrane proteins of MEFs were unspecifically labelled with Biotin prior infection with the avirulent *Toxoplasma* strain ME49. After 30 minutes of infection, cells were fixed and stained for GKS proteins Irga6 and Irgb6 as well as the parasite-derived GRA7 protein as marker for the PVM. Furthermore, biotinylated proteins were stained with fluorophore-conjugated Streptavidin (Figure 3.10). Independent of infection, the host cell surface of the very thin fibroblasts was mostly smoothly stained by Streptavidin-Cy3 but sometimes had an intensive spotted staining in the centre in the cell (see Figure 3.10 A, merged image, next to the blue nucleus). Therefore, those intracellular PVs were chosen for analysis that were in an area of smooth host surface staining.

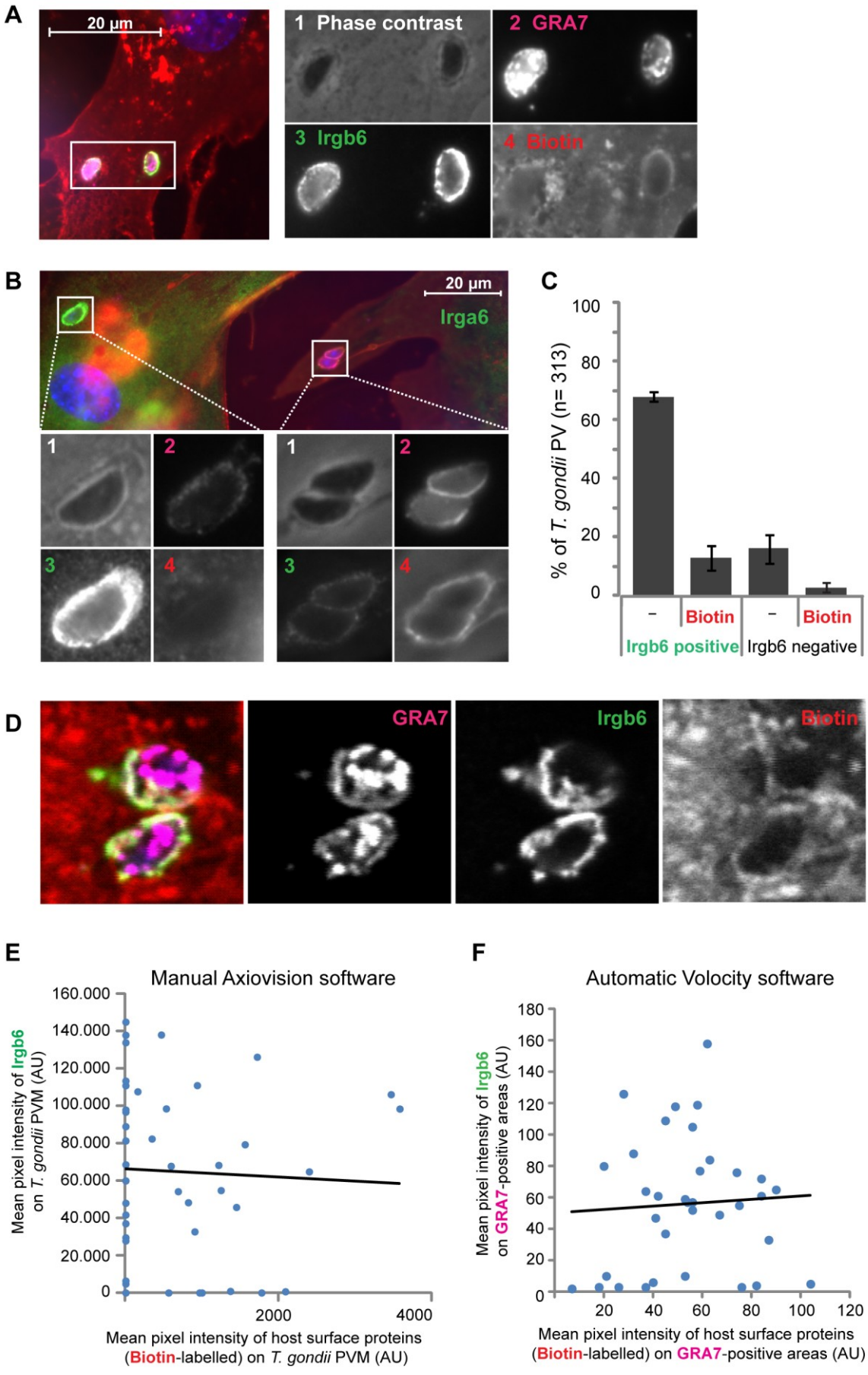


**Figure 3.10: Biotinylated host cell plasma membrane proteins do not negatively correlate with GKS protein loading at the *Toxoplasma gondii* parasitophorous vacuolar membrane.** (see next page)

(continued Figure 3.10) MEFs were induced with IFNγ for 24 h, and the host cell surface was labelled with Sulfo-NHS-LC-LC-Biotin for 20 min followed by infection with *T. gondii* ME49 for 30 min. The cells were washed, fixed, and stained for Irga6 (165/3 pAS) or Irgb6 (142/1 pAS) with Alexa Fluor488-conjugated secondary antibody (green), for biotinylated proteins with Cy3-conjugated Streptavidin (red) and for GRA7 (JH 3.1.2 mAB) with Alexa Fluor647-conjugated secondary antibody (far-red, shown in magenta). Nuclei were labelled with DAPI. **(A, B)** Images were taken with a conventional fluorescence microscope and merged images as well as magnified areas indicated by the white box in their single channels (1 phase contrast, 2 GRA7, 3 Irga6/Irgb6, 4 Biotin) are shown. **(C)** Positive or negative staining of Irgb6 and biotinylated host proteins at the PVM of *T. gondii* was evaluated from pictures as shown in B. Mean +/- SD of four individual experiments is shown, a total of 313 vacuoles was counted. In **(D)** images taken with a confocal laser microscope are shown. **(E, F)** Scattered Plot of fluorescence intensities of Irgb6 vs. fluorescence intensities of biotinylated host proteins per single PVM and a linear regression curve are shown in arbitrary units (AU). (E) Vacuoles of 42 fluorescence images were measured with the Axiovision software by averaging four data points, which were manually set on the PVM and background staining was subtracted. (F) Vacuoles of 35 confocal images were automatically evaluated with the Volocity software, which measured the entire fluorescent intensity of Irga6 or Biotin on GRA7-positive selected areas. Intensities of Biotin-labelled host cell proteins do not negatively correlate with Irga6 or Irgb6 intensities at the PVM of *T. gondii*.

A weak Biotin staining could be found at some IRG/GRA7-positive PVs (Figure 3.10 A and B right PVs) but most PVs were Biotin-negative (Figure 3.10 A and B left PVs). Quantification of four experiments revealed that almost 70% of the PVs were Irgb6-positive/Biotin-negative, but Irgb6-negative/Biotin-positive vacuoles represented the smallest fraction (2.9%) (Figure 3.10 C). However, the intensity of Biotin-labelling was always very difficult to determine due to the host surface labelling. Nevertheless, some PVs strongly stained for Irgb6 were still Biotin-positive (as seen in Figure 3.10 A, the right PV). Thus, there was no negative correlation of IRG and Biotin staining (Figure 3.10 E). To exclude that the Biotin-labelling at the PVM in Epi-fluorescence microscopy was due to the superimposed host plasma membrane, which folds around the PV, the samples were also analysed using confocal laser microscopy. Here, the Biotin-labelling was more spotted, but again no correlation of IRG loading and Biotin staining at the PV was observed (Figure 3.10 D, F). Under these staining conditions applied here, no negative correlation of the presence of host cell surface proteins versus IRG proteins could be seen.

## 3.10 Inc-induced membrane compartments are not targeted by GKS proteins

The *Chlamydia* type III effector inclusion (Inc) proteins relocalise to the inclusion membrane in order to orchestrate several host-parasite interactions (Dehoux et al. 2011). Interestingly, it has been shown recently that artificial overexpression of individual Inc proteins in HeLa cells induces *de novo* formation of membranous vesicular compartments, that do not carry any host organelle markers and are also non-fusogenic (Mital et al. 2013). Because the absence of all host cell organelle markers is also a common characteristics for PVs (see 1.6), it was tested whether IRG proteins might also target these intracellular artificial Inc-induced vesicles. To this end, fluorescently-tagged Inc proteins (either cherry-tagged IncB or GFP-tagged CT229) were transiently expressed in wt MEFs that were induced with IFNγ or left uninduced. After 24 h, cells were fixed and stained for the GKS proteins Irga6 or Irgb6. In Figure 3.11 it is shown that independent of IFNγ, transfected IncB formed big specks compared to CT229, which formed smaller specks resembling the published membranous vesicles that form upon overexpression of Incs in HeLa cells (Mital et al. 2013). Moreover, Irga6 and Irgb6 showed their typical cytosolic distribution upon IFNγ-induction. However, Irga6 and Irgb6 clearly did not co-localise with Inc proteins or accumulate near these vesicles. Thus, GKS proteins did not target these artificially Inc-induced vesicles of unknown origin. Summarising the second part of the results, it has been shown that certain GKS proteins, Irga6 and Irgb6 but not Irgd, had an intrinsic property to bind liposomes in a GTP-dependent manner. Irgd could only co-sediment with the liposomes in presence of Irgb6 suggesting formation of heterodimers. Characterisation of IRG-positive *T. gondii* PVMs revealed no negative correlation with residual host cell plasma membranes, which are mainly excluded during parasite entry. A non-fusogenic character of a vacuole was also not sufficient for IRG recognition, since Inc protein-induced membranous vesicle compartments were not targeted by IRG proteins.

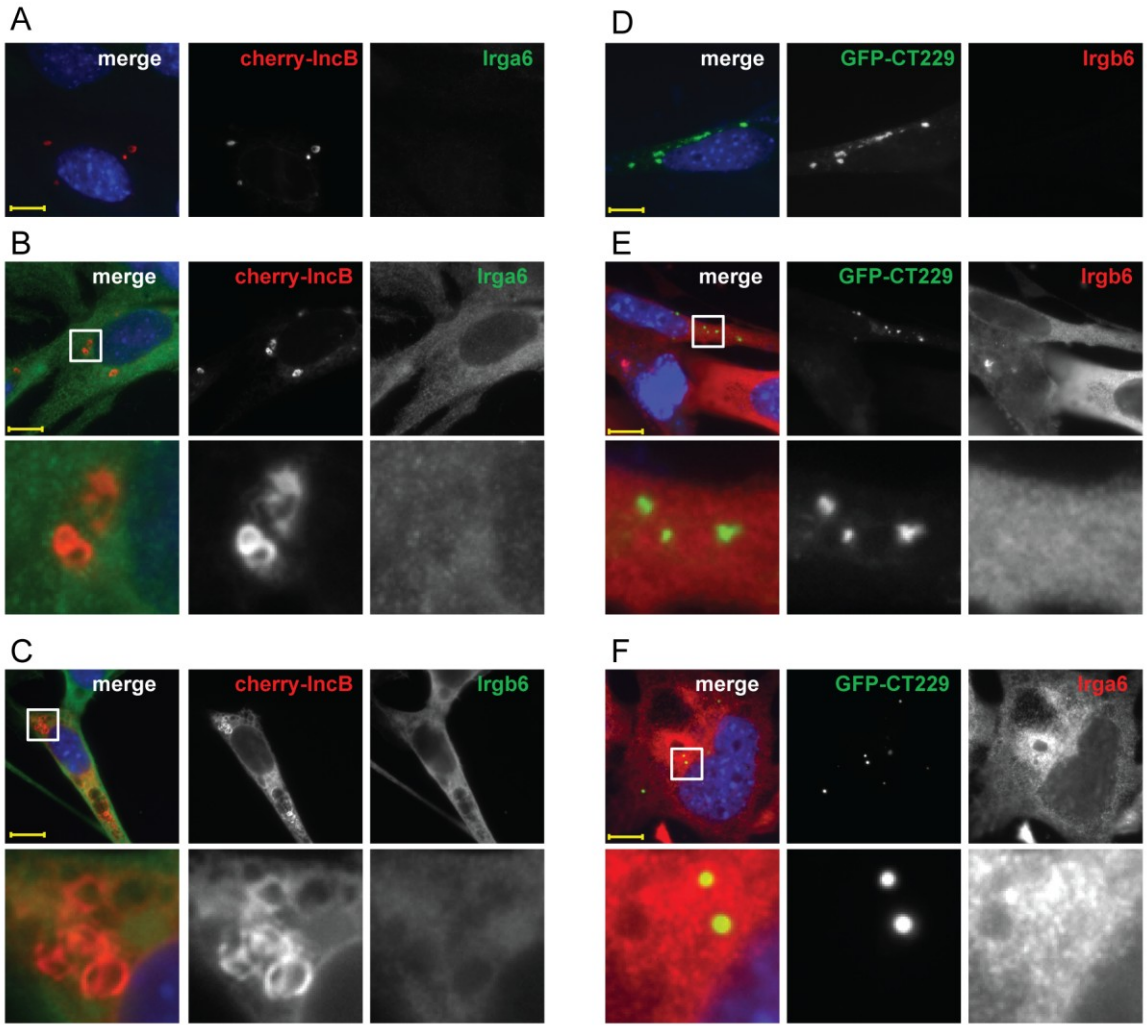


**Figure 3.11: GKS proteins do not localise to *Chlamydia* Inc protein–induced membrane compartments**
Wildtype MEFs were transiently transfected with pmCherry-IncB **(A-C)** or pGFP-TOPO-CT229 **(D-F)**. Simultaneously cells were stimulated with IFNγ for 24 h **(B, C, E, F)** or left untreated **(A, D)**. Fixed cells were stained for Irga6 (165/3 pAS) or Irgb6 (142/1 pAS). Nuclei were labelled with DAPI. White boxes indicate the magnified area shown below each panel; scale bar: 10µm. Irga6 or Irgb6 smoothly distribute in the cytosol and do not accumulate on the Inc-protein-induced vesicles.

# Results Part 3: Encephalitozoon cuniculi as novel IRG target

## 3. 11 IFNγ restricts *E. cuniculi* growth in primary mouse fibroblasts

The first evidence about microsporidial growth restriction induced by IFNγ was provided by *in vitro* studies in 1995 (Didier 1995) using *E. cuniculi* infection of murine peritoneal macrophages. Subsequent studies confirmed the suppressive effect of IFNγ on *E. cuniculi* as well as on *E. intestinalis* using murine peritoneal macrophages (Khan et al. 1999; Jelinek et al. 2007), murine enterocyte cell line CMT-93 and human enterocyte cell line Caco-2 (Choudhry et al. 2009) as well as primary human monocyte-derived macrophages (Fischer et al. 2008). Furthermore, IFNγ-deficient mice were shown to be highly susceptible to *E. cuniculi* and *E. intestinalis* infection (Khan et al. 1999; El Fakhry et al. 2001; El Fakhry et al. 2001; Salat et al. 2004).

Because it is characteristic of the IRG resistance system to also be effective in non-myeloid cells, IFNγ-dependent resistance during *E. cuniculi* infection was tested in fibroblasts. Uninduced and IFNγ-induced MEFs were infected with *E. cuniculi* spores and the replication of the parasite followed by immunofluorescence microscopy and by Western Blot analysis. The meront as earliest infectious stages of *E. cuniculi* was detected with a mouse monoclonal antibody (mAB 6G2) directed against a cytoplasmic protein of the meronts. The spore was detected with a polyclonal antiserum against a spore wall protein 1 (pAS anti-SWP1), which is synthesized later in infection (Fasshauer et al. 2005).

A time series from 30 min to 24 h post infection showed that IFNγ-mediated inhibition on *E. cuniculi* growth in MEFs increased significantly over time (determined by immunofluorescent microscopic counting of 6G2-positive meronts per host nuclei). At early time points (30 min to 2 h p. i.) the number of intracellular parasites was only slightly higher in uninduced than in IFNγ-induced host cells, showing that *E. cuniculi* invasion into the host cells was not affected by prior IFNγ treatment (Figure 3.12 A). Next, not only single meronts but also meronts, which replicated by binary fission (double meronts), were quantified and compared between uninduced and IFNγ-induced MEFs. Multiplication of meronts was largely inhibited in IFNγ-induced cells 24 h post infection (Figure 3.12 B).

In addition, Western Blot analysis of whole cell lysates from infected MEFs showed that meront development as well as the formation of new spores was blocked by IFNγ. In uninduced MEFs, *E. cuniculi* dependent protein bands were detected with the meront-specific antibody 6G2, indicative of replication; and with the spore-specific antiserum SWP1, indicative of maturation, at 2 days post infection.

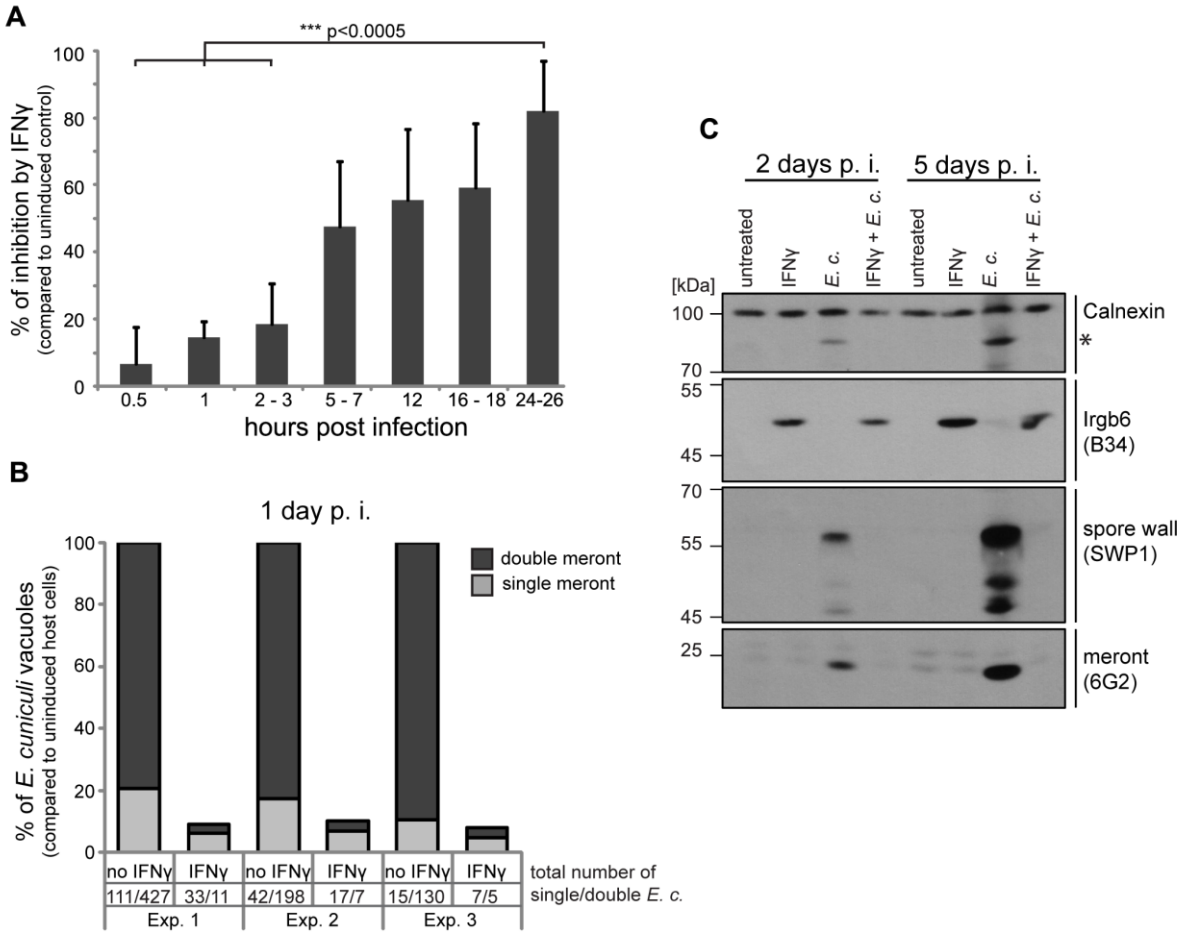


**Figure 3.12: IFNγ restricts *Encephalitozoon cuniculi* growth in mouse embryonic fibroblasts.**
**(A)** Primary wt MEFs were induced with IFNγ for 24 h or left uninduced and infected with *E. cuniculi* spores. Cells were fixed after the indicated time post infection and the number of meronts (stained with anti-meront antibody 6G2) per 500 host nuclei (stained with DAPI) was counted. The inhibition in the IFNγ-treated samples compared to the uninduced control samples (mean +/- SD) of 3-7 technical replicates per timepoint from at least 2 individual experiments is presented. Significant differences (0.5 h, 1 h and 2-3 h compared to 24-26 h) were calculated with a two tailed T-test. **(B)** MEFs were induced with IFNγ or left uninduced, infected with *E. cuniculi* spores for 24 h and stained as in A. Meronts that divided once (double meront) as well as single meronts per 500 host nuclei were counted. Percent of total vacuoles are shown, uninduced controls were set as 100% per independent experiment. Numbers in the x-axis indicate the counted number of single / double meronts per 500 host cells. **(C)** IFNγ-stimulated or unstimulated MEFs were infected with *E. cuniculi* spores for 2 or 5 days or left untreated. Whole cell lysates were separated by SDS-PAGE and Western Blots were stained using anti-meront antibody 6G2 as well as anti-spore wall protein 1 antibody SWP1. Calnexin staining served as loading control and Irgb6 staining (B34) as IFNγ-induction control. The asterisk marks an unknown *E. cuniculi*-derived protein, which is detected by calnexin antibody. IFNγ-treated samples show less *E. cuniculi* growth and development. These Western Blots emerged from one single SDS-PAGE. The 45-70 kDa region was first probed with mouse mAB B34, stripped, and then probed for rabbit pAS anti-SWP1.

The intensity of these bands further increased at 5 days post infection. In contrast, these bands could not be detected in *E. cuniculi*-infected IFNγ-induced cells, either after 2 days or after 5 days (Figure 3.12 C). Taken together, IFNγ inhibits meront replication and spore formation of *E. cuniculi* cell-autonomously in primary mouse fibroblasts.

## 3.12 IRG proteins accumulate on the *E. cuniculi* PVM

When *T. gondii* infects IFNγ-induced mouse fibroblasts, mainly the effector IRG proteins accumulate on the PVM leading to the disruption of the vacuole (Martens et al. 2005; Ling et al. 2006; Melzer et al. 2008; Zhao et al. 2009). To examine whether similar IRG-related phenomena might also apply to the microsporidian vacuole, IFNγ-induced MEFs were infected with *E. cuniculi.* The samples were co-stained for intracellular meronts and with immunological reagents against individual GKS effector proteins (Irga6, Irgb6, Irgd) as well as against the GMS regulator proteins (Irgm1 and Irgm2) 24 hours post infection (Figure 3.13). Some meronts were indeed coated with IRG proteins, but the majority of meronts was IRG-negative. Both Irga6-coated and uncoated vacuoles could be found together in multiple infected host cells as shown for 2 h post infection in panel A of Figure 3.13. In the first hours after infection, *E. cuniculi* meronts were very small and hardly visible. Therefore, 24 h post infection was chosen as a time point, in which single meronts, which have acquired more material and are therefore bigger, or double meronts could be detected. After 24 h of infection replicated meronts were found to be coated with Irga6 or Irgb6 protein (Figure 3.13 B, C). Activated GTP-bound Irga6, specifically detected with the mAB 10D7, could also be detected at the *E. cuniculi* PVM (Marialice Heider, personal communication). Irgd and Irgm2 were found at lower but consistent frequencies below 5 % (Figure 3.13 D, E), whereas Irgm1 was never found to accumulate as a clear ring around the *E. cuniculi* PVM (Figure 3.13 F).

The number of Irga6- and Irgb6-positive vacuoles at different time points post infection was examined in more detail (Figure 3.13 G). The frequency of GKS-positive vacuoles varies between experiments (1-20%), but did not significantly increase or decrease from 0.5 - 24 h post infection (Figure 3.13 G).

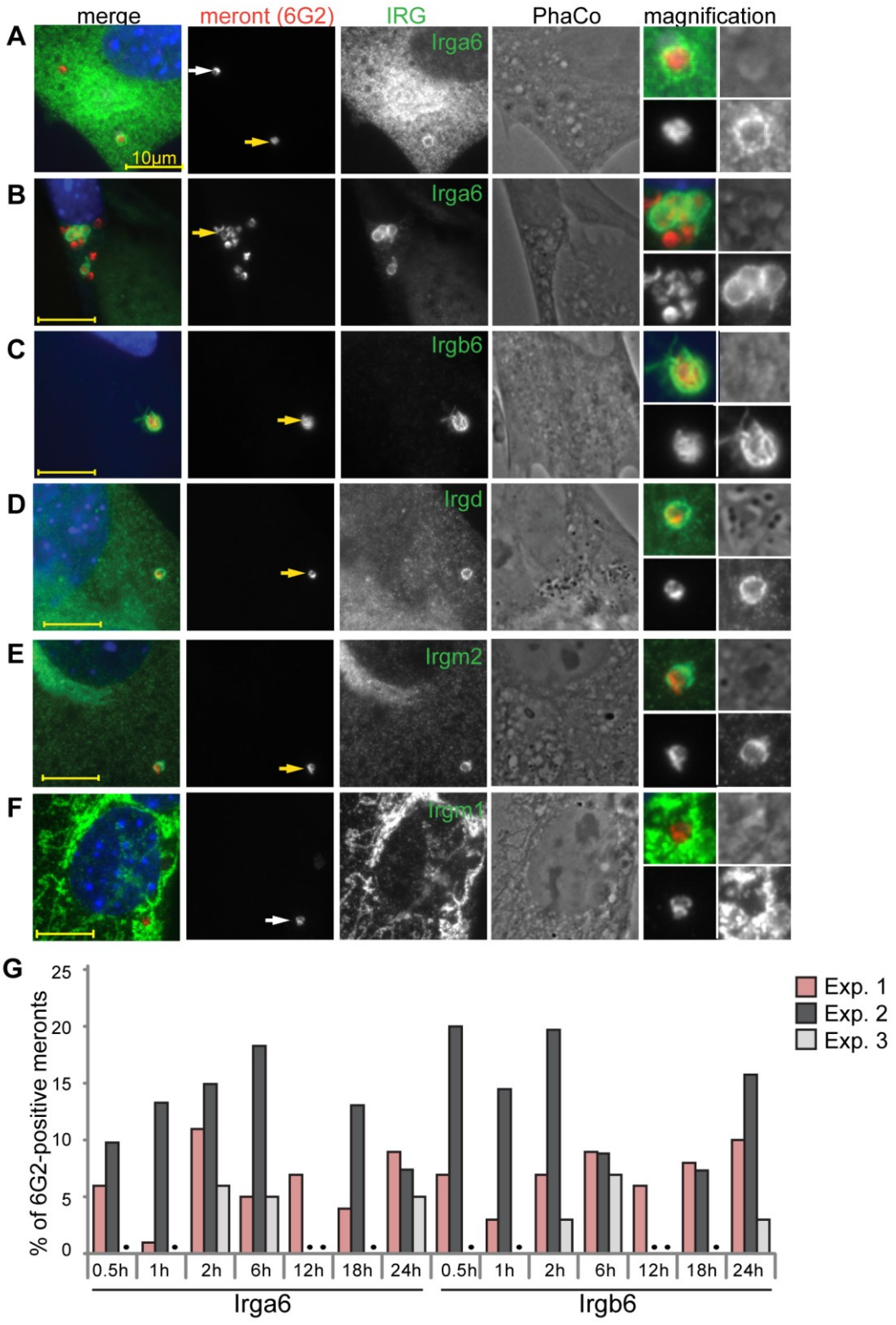


**Figure 3.13: IRG proteins accumulate at the *E. cuniculi* PVM.**
MEFs were induced with IFNγ for 24 h and then infected with *E. cuniculi* spores for 2 h in (A) or 24 h in (B-F). Fixed cells were stained with anti-meront mAB 6G2 as well as for endogenous **(A, B)** Irga6 (165/3 pAS), **(C)** Irgb6 (A20 pAB), **(D)** Irgd (2078 pAS), **(E)** Irgm2 (H53 pAS), or **(F)** Irgm1 (rbMAE15 pAS). Nuclei were labelled with DAPI. The magnified area at the end of each panel (in the order upper left: merged image, upper right: phase contrast, lower left: anti-meront, lower right anti-IRG) is indicated by yellow arrows for IRG-positive PVM (A-F) or a white arrow for IRG-negative PVM; scale bars: 10 µm. **(G)** Quantification of Irga6 and Irgb6 loading onto the *E. cuniculi* PVM at different time points post-infection. 100 vacuoles were evaluated per sample; a black dot indicates that the sample was not counted. Three independent experiments are shown. With the exception of Irgm1, IRG proteins relocalise to some vacuoles of *E. cuniculi*.

Accumulation of Irga6 or Irgb6 to vacuoles of *E. cuniculi* could thus consistently be found at every time point post infection, but it was not robust and invariable in terms of quantification and timing.

## 3.13 IRG proteins load onto the *E. cuniculi* PVM in a cooperative manner

A detailed view of IRG protein loading onto the *T. gondii* PVM has been established, demonstrating cooperative behaviour of GKS proteins as well as a hierarchical order in which IRG proteins accumulate at the PVM (Khaminets et al. 2010). In order to investigate the cooperative behaviour of IRG proteins, triple immunofluorescent stainings to identify the meront and two GKS proteins, Irga6 and Irgb6, were conducted. Individual vacuoles accumulating both IRG proteins were found at early and late time points. Representative images of a double-loaded single meront at 12 h post infection (Figure 3.14 A) as well as double-loaded replicating meronts at 24 h post infection (Figure 3.14 B, C) are shown. In many cases, Irga6 and Irgb6 co-localised (Figure 3.14 B), but not always entirely coincide on the PVM (Figure 3 C). Moreover, as observed in Figure 3.13 A, not all vacuoles within one host cell were positive for IRG proteins (Figure 3. 14 C). Notably, the number of *E. cuniculi* vacuoles accumulating both IRG proteins was higher than single-coated ones (Figure 3D). In view of the low frequencies of accumulation of individual IRG proteins, it is clear that the frequency of double-loaded vacuoles is highly non-random, suggesting cooperative behaviour, as seen on the *T. gondii* PVM.

In previous studies, live-cell video microscopy with transfected GFP-tagged Irga6 or Irgb6 impressively demonstrated how GKS proteins accumulated on *T. gondii* PVs in a time-dependent manner followed by disruption of the PVM (Zhao et al. 2009; Khaminets et al. 2010). Unfortunately, it was impossible to properly identify *E. cuniculi* meronts in phase contrast images. Moreover, infection with fluorescently-labelled *E. cuniculi* internal lipids was only partially successful due to low infection rates of labelled spores (Ronnebaumer et al. 2008). In the end, live-cell imaging performed for this study could not be established to a sufficient level that would allow to investigate the timing of IRG protein accumulation on *E. cuniculi* PVs.

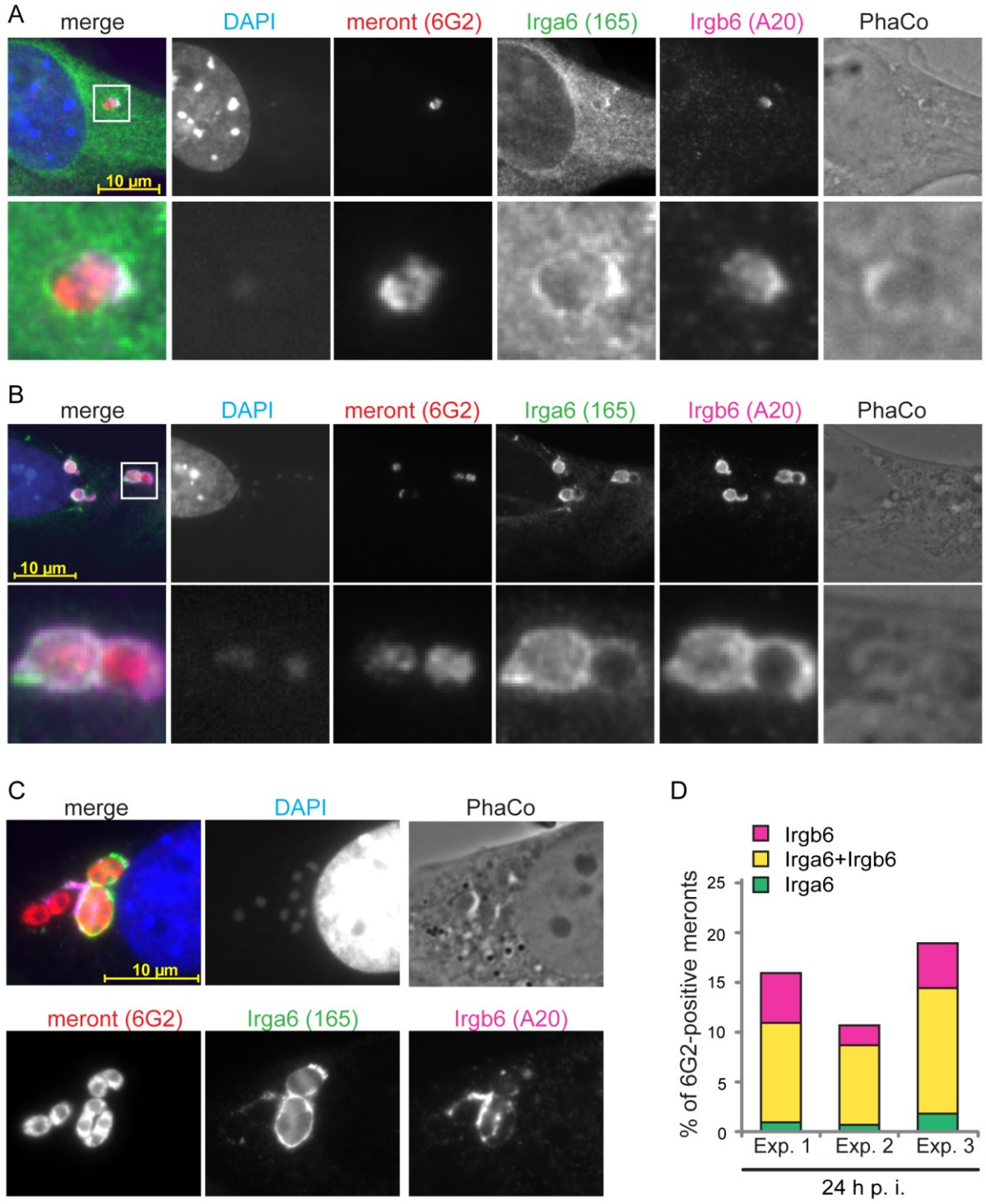


**Figure 3.14: IRG proteins load onto PVM of *E. cuniculi* in a cooperative manner.**
MEFs were induced with IFNγ for 24 h and then infected with *E. cuniculi* spores for 12 h **(A)** or 24 h **(B, C)**. Fixed cells were stained with anti-meront mAB 6G2 in red as well as for endogenous Irga6 (165/3 pAS, green) and Irgb6 (A20 pAB, far-red, shown in magenta). Nuclei were labelled with DAPI. White boxes indicate enlarged area shown below; scale bar: 10 µm. **(D)** Quantification of cooperative loading after 24 h; Irgb6-single, Irga6-single or Irgb6/Irga6-double (both) positive meronts are shown as % of total 6G2-positive meronts; 100 vacuoles were counted in each independent experiment. Most IRG-positive PVs were positive for both Irga6 and Irgb6.

## 3.14 IFNγ-mediated suppressive effect on *E. cuniculi* growth is diminished in GMS-deficient cells

(in collaboration with Marialice Heider)

To assess the importance of IRG proteins in the IFNγ-dependent restriction of *E. cuniculi*, growth and development of the parasite were analysed in cells derived from *IRG* knock-out mice. Firstly, *E. cuniculi* infection in IFNγ-induced primary MEFs derived from wildtype (wt) and *Irgm1/Irgm3*$^{-/-}$ mice was examined. The *Irgm1/Irgm3*$^{-/-}$ mice do not only lack the two regulator GMS proteins, but also express reduced levels of GKS proteins, and are exquisitely susceptible to infection with avirulent *T. gondii* (Henry et al. 2009). Moreover, *Irgm1/Irgm3*$^{-/-}$ MEFs show no IFNγ-inducible resistance to *T. gondii* (Steffi Koenen-Waisman, unpublished data). Infection of these cells with *E. cuniculi* revealed the same phenotype as seen for *T. gondii*. As described in Figure 3.12, the number of meronts in IFNγ-induced wildtype cells was drastically reduced at 24 h post infection compared with uninduced controls (Figure 3.15 A, B). In contrast, the number of meronts observed in *Irgm1/Irgm3*$^{-/-}$ MEFs 24 h post infection was the same whether the cells were induced with IFNγ or not.

Next, IFNγ-inducible resistance to *E. cuniculi* was assayed in transformed fibroblasts from mice deficient in single *IRG* genes as well as from double knock-out *Irgm1/Irgm3*$^{-/-}$ mice. In Western Blot analysis parasite growth was assessed with the anti-meront antibody, whereas the expression of Irgb6 (or Irga6) confirmed successful IFNγ-induction (Figure 3.15 C, D). In wildtype cells, IFNγ-induction resulted in complete loss of the 6G2 marker at 2 days and 5 days post infection, while in *Irgm1/Irgm3*$^{-/-}$ double knock-out cells IFNγ-induction did not affect the meront growth. Single GKS knock-outs, either *Irga6* or *Irgd*, showed no loss of resistance relative to wildtype cells. However, cells lacking one GMS proteins, *Irgm1* and *Irgm3*, both showed a clear susceptibility phenotype relative to wildtype cells. The susceptibility of the *Irgm1*-deficient cells was incomplete, while that of the *Irgm3*-deficient cells was similar to *Irgm1/Irgm3*$^{-/-}$ double-deficient cells.

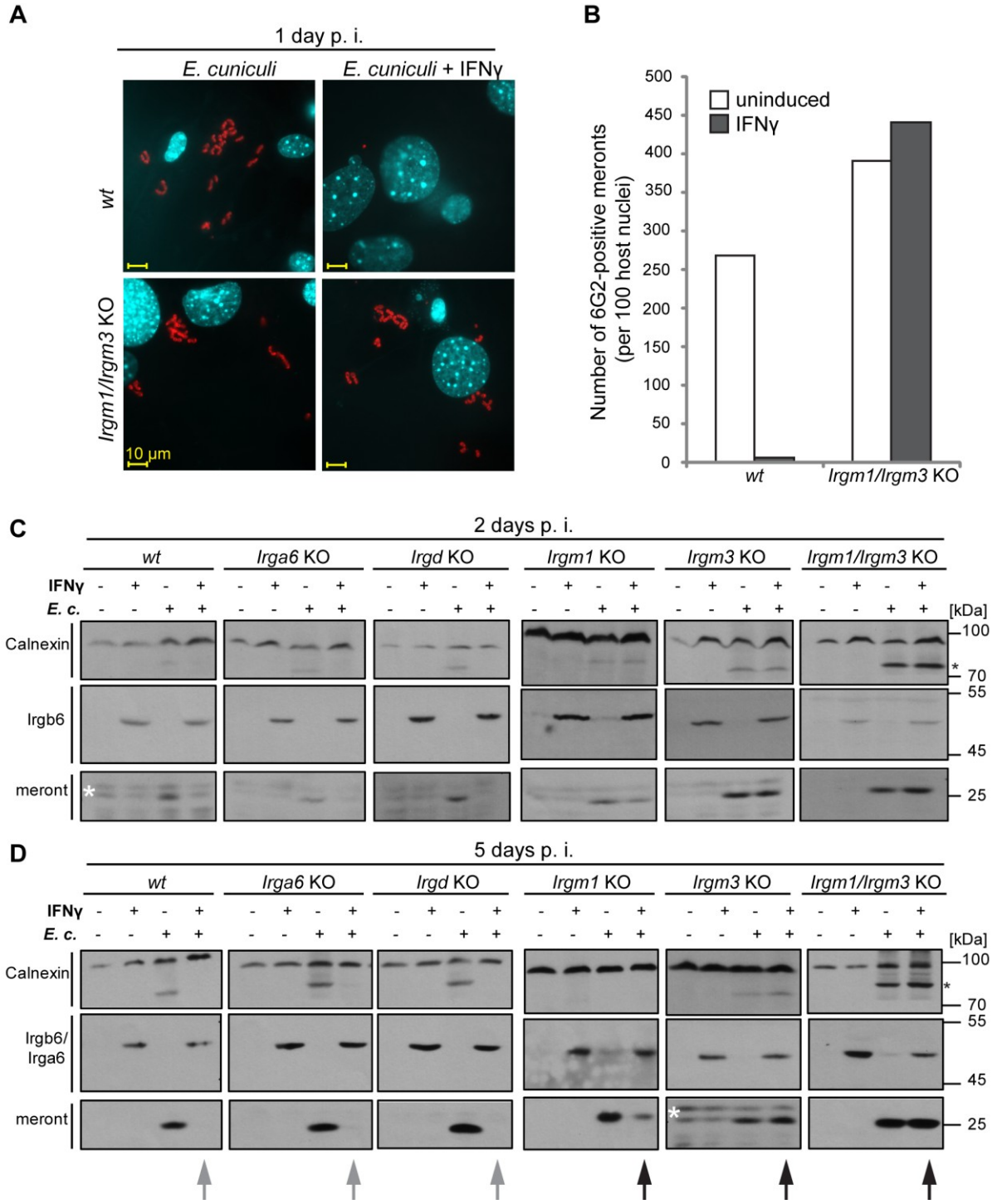


**Figure 3.15: IFNγ suppressive effect on *E. cuniculi* growth is impaired in GMS-IRG knock-out cells.**
**(A)** Wildtype or *Irgm1/Irgm3*$^{-/-}$ knock-out (KO) MEFs were induced with IFNγ for 24 h and then infected with *E. cuniculi* spores for 24 h or left untreated. The cells were fixed and stained for meronts using 6G2 mAB (red) and host nuclei with DAPI (pseudocolored in cyan). Representative fluorescence microscopic images are shown. **(B)** Quantification of A. **(C, D)** Transformed wt or transformed *IRG* KO MEFs were induced with IFNγ for 24 h and then infected with *E. cuniculi* spores or left untreated. Cells were harvested after 2 and 5 days p. i. and whole cell lysates were separated by SDS-PAGE. Western Blots were probed with anti-meront mAB 6G2, anti-calnexin pAB, which served as loading control and anti-Irgb6 (mAB B34) or anti-Irga6 (mAB 10E7 for MEF *Irgm1*KO and MEF *Irgm3*KO both at 5 days p. i.; 165/3 pAS for MEF *Irgm1/Irgm3*KO at 5 days p. i.) as IFNγ-induction control. The black arrows highlight a 6G2-positive protein band indicating *E. cuniculi* growth despite presence of IFNγ, which is normally impaired (grew arrows). The asterisk marks an unknown *E. cuniculi*-derived protein that is detected by the calnexin antibody. The white asterisks mark unspecific bands. Experiments in A and B were performed by Marialice Heider. *Irgm1/Irgm3*$^{-/-}$ and *Irgm3*$^{-/-}$ as well as partially *Irgm1*$^{-/-}$ MEFs cannot control *E. cuniculi* growth upon IFNγ-stimulation.

## 3.15 *E. cuniculi* infection triggers IFNγ-dependent host cell death

(in collaboration with Marialice Heider)

Another defining characteristic of the IRG resistance system is the disruption of the IRG protein-coated *T. gondii* PVM, followed by necrosis-like host cell death of the IFNγ-induced host cell (Martens et al. 2005; Melzer et al. 2008; Zhao et al. 2009; Zhao et al. 2009). It was therefore of interest to find out whether this endpoint of IRG protein action could also be observed in IFNγ-induced mouse cells infected with *E. cuniculi*. To this end, two different methods measuring either cell death or cell viability were applied on primary cells.

Firstly, IFNγ-induced and *E. cuniculi*-infected wt MEFs were stained and analysed under live-cell conditions with the membrane-impermeable dye Propidium iodide, which stains necrotic cells, and with the membrane–permeable dye Hoechst 33342, which stains all nuclei. In Figure 3.16 A, microscopic images show more Propidium iodide (PI)-positive nuclei in *E. cuniculi*-infected and IFNγ-treated MEFs in comparison with IFNγ only or *E. cuniculi* only treated cells. PI-positive cells also often appeard as contracted round cells in phase contrast images. Automatic quantification of these photographs revealed that treatment with both IFNγ and *E. cuniculi* results in a significant excess of membrane-permeable cells compared to untreated or single-treated control samples (Figure 3.16 B).

Secondly, a colorimetric proliferation assay was used to measure viability of wt MEFs with increasing multiplicity of infection with *E. cuniculi* spores. One day post infection, viability of infected cells was significantly reduced in dependence of IFNγ and this was even more pronounced after 2 days post infection (Figure 3.16 C). Thus, *E. cuniculi* infection seems to lead to the same consequences for the host cell in presence of IFNγ as infection with *T. gondii*, namely the death of the host cell itself. However, by which molecules this host cell death is triggered and executed remains to be elucidated.

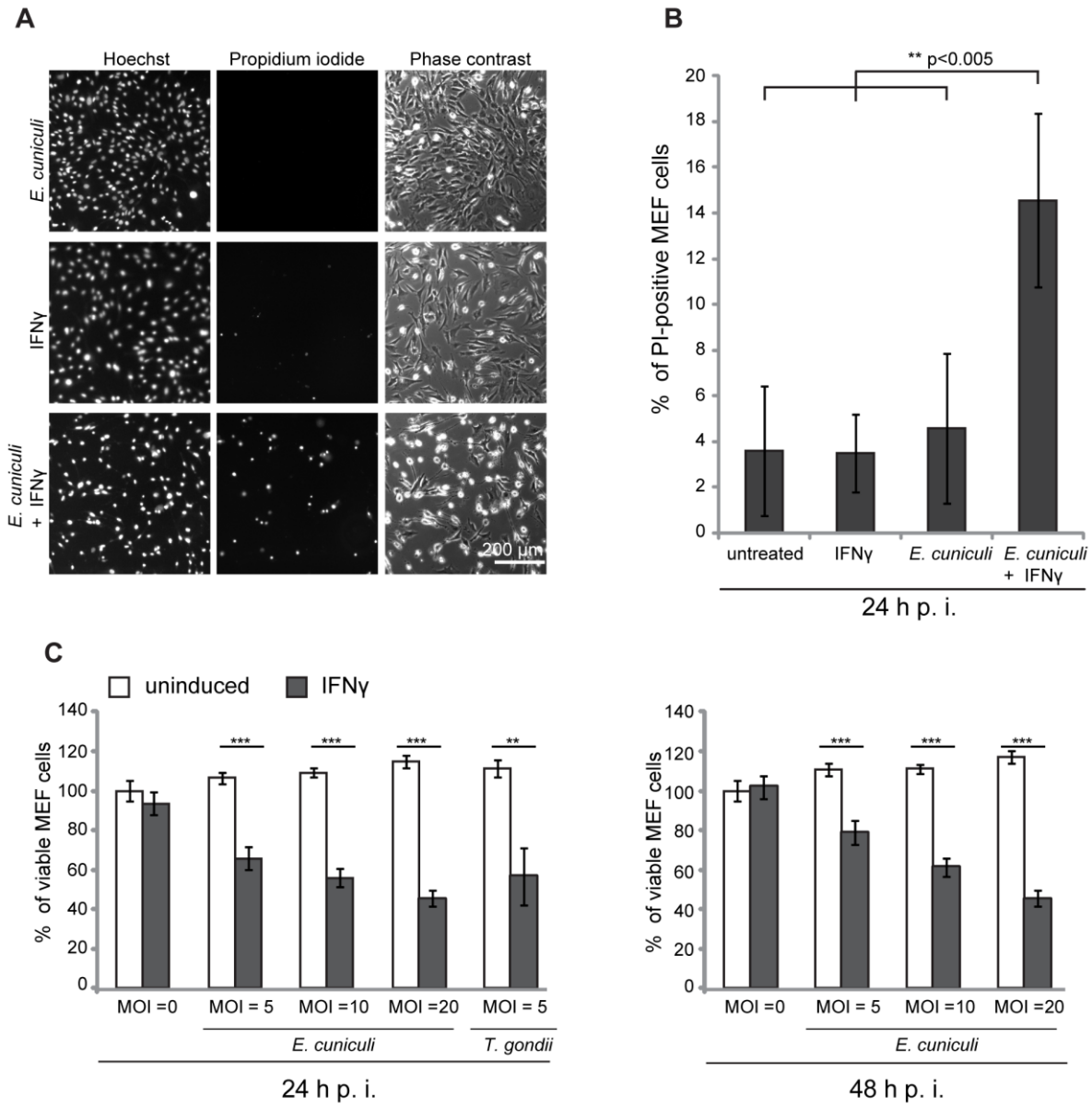


**Figure 3.16: *E. cuniculi* infection triggers IFNγ-dependent host cell death.**
**(A, B)** Wildtype MEFs were induced with IFNγ for 24 h and then infected with *E. cuniculi* spores for 24 h or left untreated. Without fixation, cells were stained with Propidium iodide and Hoechst dye, photographed under live-cell conditions, and automatically enumerated with Volocity software. 10.000 cells per sample were counted in five independent experiments together, graph represents mean values of all experiments +/- SD; scale bar in A: 200 µm. **(C)** Wt MEFs were seeded in 96-wells and induced with IFNγ for 24 h (black bars) or left untreated (white bars). Cells were infected with *E. cuniculi* spores at MOI=5-20 or with *T. gondii* ME49 tachyzoites (MOI=5) as positive control. Cell viability was assed 24 h or 48 h post-infection with a colorimetric assay and expressed as percentages of uninduced uninfected control cells. Graph represents mean value +/-SD of triplicates of one representative experiment. Significance in B and C was calculated with two-tailed T-Test: ** $p > 0.005$, *** $p > 0.0005$. Experiments in A and B were performed by Marialice Heider. IFNγ-stimulated MEFs infected with *E. cuniculi* show increased cell death as well as decreased cell viability

## 3.16 IDO is not responsible in IFNγ-mediated *E. cuniculi* restriction

Restricting nutrient acquisition is a common defence mechanism against intracellular parasites. One example is deprivation of tryptophan by the interferon-inducible indoleamine 2, 3-dioxygenase (IDO), which is widely believed to be the main inhibitor of *T. gondii* replication in IFNγ-induced human fibroblasts (reviewed in (Konen-Waisman et al. 2007, MacMicking, 2012). It is based on early reports that replication can be rescued by supplementation of the medium with tryptophan (Pfefferkorn 1984; Daubener et al. 2001). In 2009, a study by Choudhry and colleagues suggested IDO-mediated growth restriction of *E. intestinalis* in mouse enterocytic cell line CMT-93 (Choudhry et al. 2009). However, another study using *E. cuniculi* infection of activated mouse peritoneal macrophages showed that L-tryptophan supplementation failed to rescue the infection (Didier et al. 2010).

In view of these apparently inconsistent results, *E. cuniculi* growth in IFNγ-induced mouse cells was analysed by Western Blot analysis of whole cell lysates. Tryptophan supplementation would substitute the tryptophan, which has been degraded by the IDO and allow growth of an IDO-restricted parasite. In wildtype MEFs as well as in CMT-93 cells, IFNγ-mediated growth restriction on *E. cuniculi* could not be reversed by supplementation with increasing doses of excess tryptophan (Figure 3.17 A, B). Therefore, *E. cuniculi* is not restricted by the IFNγ-inducible IDO in fibroblasts. Taken together, with the complete loss of resistance caused by IRG protein deficiencies, it can be concluded that the IFNγ-mediated restriction of *E. cuniculi* in non-myeloid cells is mediated exclusively by the IRG system in mice.

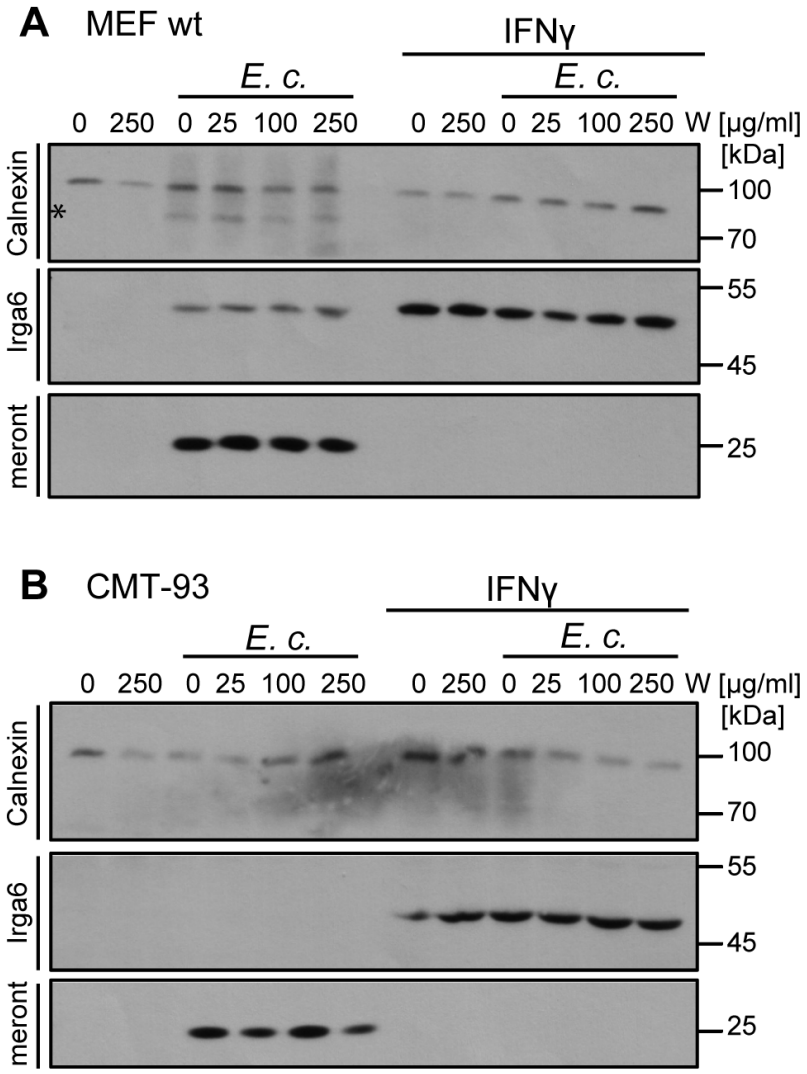


**Figure 3.17: Tryptophan supplementation cannot reverse the IFNγ-mediated *E. cuniculi* restriction.**
Wildtype MEFs **(A)** or mouse enterocytic CMT-93 cells **(B)** were treated with IFNγ for 24 h or left uninduced. 30 minutes prior to infection with *E. cuniculi* spores, indicated doses of L-Tryptophan (W) were added to the medium. Whole cell lysates were prepared 5 days post infection and separated by one SDS-PAGE. Western Blots were probed with anti-meront mAB 6G2, anti-calnexin pAB as loading control and anti-Irga6 (10E7 mAB) as IFNγ-induction control. The asterisk marks an unknown *E. cuniculi*-derived protein, which is detected by calnexin antibody. There are no meront-positive protein bands in the IFNγ-induced and tryptophan-supplemented samples.

# Discussion

The immunity-related GTPase (IRG) protein family, subdivided in GKS and GMS proteins, has been established to be the major resistance system against a particular subset of intracellular parasites in mice. Microscopic studies showed that effector GKS proteins accumulate on the parasitophorous vacuolar membrane (PVM) of *Toxoplasma gondii* (*T. gondii*), followed by disruption of these vacuoles and death of the host cell. The function of the regulatory GMS proteins is less understood. They either they only act as inhibitors of the membrane-destructive GKS proteins or they also play a direct effector role on bacterial phagosomes. The aim of this study was to clarify possible roles of the regulatory GMS protein Irgm1. Furthermore, the underlying mechanism of membrane discrimination regarding IRG accumulation was investigated. In this context the microsporidian parasite *Encephalitozoon cuniculi* (*E. cuniculi*) has been identified as a novel target of the IRG resistance system.

## 4.1 Differential subcellular localisation of Irgm1 isoforms

Several microscopic studies on endogenous and overexpressed Irgm1 in uninfected cells established a strong Golgi localisation due to an amphipathic targeting (αK) helix (Martens et al. 2004; Butcher et al. 2005; Tiwari et al. 2009; Zhao et al. 2010). It was also noted that Irgm1 shows a significant cytoplasmic punctuate staining outside the Golgi. The very first investigation did not connect this Irgm1 signal to the endolysosomal system, although the protein was seen on lysosomes enclosing recently phagocytosed latex beads (Martens 2004). Later, it was unambiguously shown that Irgm1 co-localises constitutively with LAMP1- and also weakly with transferrin-positive organelles (Zhao et al. 2010). Further co-localisation studies attributed endogenous Irgm1 to mitochondria (Tiwari et al. 2009; Chang et al. 2011).

However, subcellular localisation studies can be problematic, since tagged Irgm1 constructs have been shown to mislocalise (Zhao et al. 2010). Moreover, the specificity of immunological reagents is not always guaranteed, because the design and production of the antibody/antiserum as well as the interpretation of obtained results are not trivial. Indeed, most of the published studies used either the relatively weak commercial polyclonal antibody A19 from Santa Cruz Biotechnology, Inc. (Springer et al. 2013) or cross-reactive polyclonal antibody ab69494/5 from Abcam plc (Figure 3.2 C). In addition, the existence of two splice forms of Irgm1 has not been considered in earlier studies. To this end, the subcellular localisation of both Irgm1 isoforms was examined in this study. As previously reported, the Golgi and mitochondrial localisations of Irgm1 could be confirmed in mouse fibroblasts using

new antisera (Figure 3.3 A + 3.4). Thus, while earlier reports of individual endogenous Irgm1 localisations in uninfected, IFNγ-induced cells were certainly incomplete, there is no significant discrepancy in the results as they now stand.

It remains unclear, how membrane-binding of Irgm1 is mediated. Certainly, the amphipathic αK helix plays a key role, since this motif alone (GFP-tagged or as synthetic peptide) can target the compartments of Golgi and lysosomes (Zhao et al. 2010). Moreover, palmitoylation of Irgm1 at a cluster of cysteines near the Irgm1 αK helix strengthens membrane-binding potential, probably by adding hydrophobic character to the hydrophobic face of the amphipathic helix (Henry et al. 2014). In absence of both the amphipathic αK helix and palmitoylation, Irgm1 mainly loses its membrane-binding potential. Those Irgm1 mutants could not target the Golgi or mitochondria anymore, however the residual membrane-bound protein fraction targeted mainly the plasma membrane, similar to the truncated Irgm1 G-domain only mutant. This suggests that Irgm1 has even more membrane-binding motifs (Martens et al. 2004; Henry et al. 2014). Similar to Irgm1, Golgi targeting for IFNγ-induced hGbp1 depends also on the nucleotide binding as well as on farnesylation (Modiano et al. 2005).

Another puzzle is how Irgm1 can specifically target organelles. Recent lipid binding studies of MacMicking and colleagues using recombinant GST-tagged Irgm1 αK suggested binding to PtdIns(3,4)$P_2$, weakly to PtdIns(4,5)$P_2$, PtdIns(3,4,5)$P_3$ and cardiolipin, which are marker lipids for early endosomes, plasma membrane, forming endosomes/phagosomes and inner mitochondria, respectively. Surprisingly, however, no association with PI4P specific for Golgi, or PtdIns(3,5)$P_2$ for lysosomes could be detected (Tiwari et al. 2009; Kutateladze). Thus, Irgm1 seems not to exclusively recognize the phosphoinositide code.

Interestingly, only the long but not the short N-terminally truncated Irgm1 isoform was detected at endolysosomal organelles (Figure 3.3 B, C). This is in line with observations that Irgm1 does not co-localise with LAMP1, when it is altered by an N-terminal EGFP-tag, or furthermore when the nucleotide-binding site is mutated (S90N) (Zhao et al. 2010). Thus, a functional N-terminus and nucleotide binding site seem to be necessary for Irgm1 to target lysosomes. Even though biochemical information on Irgm1 is still missing, one can hypothesise a similar mechanism as proposed for Irga6: nucleotide binding would induce a conformational change of Irgm1 that allows lysosomal targeting; whereas without nucleotide, Irgm1 would localise to the Golgi. In such a scenario, one can now envision that either a) the N-terminus directly influences nucleotide binding or b) nucleotide binding induces a conformational change that unfolds the N-terminus to support or allow binding of the

amphipathic αK helix. In this study, two phosphorylated peptides, one short isoform-specific at the N-terminus and one derivable from both isoforms, could be detected by mass spectrometry (Figure 3.1 D and Appendix 2). Following from that, c) phosphorylation at the N-terminus of the short isoform may prevent a conformational change that is required for lysosomal targeting. Since no transfected short Irgm1 isoform was found at the lysosomes, this could mean all of the protein must have been phosphorylated by endogenous kinases. Even though the mass spectrometry data, which found also unphosphorylated short isoform of Irgm1, might argue against hypothesis c), it does not provide information about the ratio of endogenous phosphorylated vs. unphosphorylated short Irgm1 isoform. This could be further determined with specific quantitative mass spectrometry analysis (e.g. iTRAQ). In addition, future studies with mutants of the possible phosphorylation sites might resolve the importance of N-terminal phosphorylation for lysosomal targeting.

The other phosphorylation site, present in both Irgm1 isoforms, is most likely at Serine 79, which corresponds to the first β-sheet (S1) of the G-domain on the Irga6 crystal structure. Since the G-domain is responsible for nucleotide binding, this phosphorylation may also regulate the activation status of the protein. In case of Irga6, 30 amino acids further downstream just before the second β-sheet (S2), phosphorylation in the switch 1 region at threonines 102 and 108 by *T. gondii* virulence kinase ROP18 has been shown to biochemically inactivate the protein (Steinfeldt et al. 2010). Similar mechanisms are also discussed for Irgb6 (Fentress et al. 2010) but recent data indicate that Irga6 probably is the only ROP18 target within the family of IRG proteins [(Lim et al. 2013) and Tobias Steinfeldt, personal communication].

A possible functional difference for the two Irgm1 isoforms associated with their different intracellular localisation remains to be investigated. In the model of Irgm1 as negative regulator of GKS proteins and "protector of endomembranes", different functions at different organelles are actually not required so far. Future biochemical studies of the recombinant protein (and a crystal structure) will hopefully elucidate, whether Irgm1 (and other GMS proteins) can actually bind and hydrolyse nucleotides to exert their function, since they lack the conserved lysine in the G1 motif.

## 4.2 Irgm1 is not a direct effector protein on bacterial phagosomes

Functional analysis of Irgm1 has followed two "general tracks" in the past. One track describes Irgm1 as an effector of resistance at the bacterial phagosome, either by accelerating phagosome-lysosome fusion (MacMicking et al. 2003; Shenoy et al. 2007; Tiwari et al. 2009)

by the stimulation of autophagy (Gutierrez et al. 2004; Singh et al. 2006), or possibly by some other effect mediated through other organellar systems (Taylor et al. 2007). The second track stresses the role of Irgm1 as a regulator of other GKS proteins acting as a guanine nucleotide dissociation inhibitor (Hunn et al. 2008; Hunn et al. 2011) or as inhibitor of another GMS protein, Irgm3 (Henry et al. 2009; Coers et al. 2011; King et al. 2011).

In the past, several studies reported that endogenous or transfected Irgm1 co-localises with bacterial phagosomes, but data from the present study refute this claim. The first report on this topic (MacMicking et al. 2003) did not strictly show co-localisation, but rather co-purification via a procedure intended to purify phagosomes from cells infected by *Mycobacteria.* However the now known association of endogenous Irgm1 with Golgi membranes, LAMP1-positive compartments and mitochondria renders the conclusion from these experiments questionable, because these compartments were not clearly excluded from the putative phagosomal fraction (Li et al. 2010). The most direct support for a co-localisation of Irgm1 with both listerial and mycobacterial phagosomes was provided in an immunolocalisation study from Shenoy and colleagues [reprinted in Figure 1.6 for *Mycobacteria* (Shenoy et al. 2007)]. These authors showed effectively 100% co-localisation of intense immunofluorescent signals from either *M. bovis* BCG or *L. monocytogenes* and Irgm1 (detected by pAB A19) in IFNγ-induced RAW264.7 macrophages. Furthermore, another study showed a calculated overlap of 97.3% of *M. bovis* BCG and Irgm1 (stained by pAB A19) in mouse bladder urothelium (Saban et al. 2008). However, these observations raised suspicion, because one would expect Irgm1 accumulation in a ring-like pattern surrounding the bacterial phagosome instead of an entire co-localisation with the bacteria. Moreover, when two fluorescent signals exactly coincide it can also be an artefact due to cross-reactivity in the antibody staining procedure. Therefore, it was decided in the present study to reproduce the data, and indeed, cross-reaction of pAB A19 was microscopically observed on extracellular bacteria upon very long exposure times (Appendix 3). Another study attributes Irgm1 localisation to some but not all phagosomes of *Brucella abortus*, however this is not convincingly presented in the microscopic image (Ritchie et al. 2012). Furthermore, two other studies reported co-localisation of *Mycobacteria* with GFP-tagged Irgm1 and even with the GFP-tagged αK helix only (Deghmane et al. 2007; Tiwari et al. 2009). However, besides the already discussed mislocalisation of GFP-tagged Irgm1 constructs, EGFP-αK helix alone does not localise to latex bead phagosomes (Zhao et al. 2010).

The discrepancy of the data published recently and the results shown here for the same bacteria could only be explained by technical differences. The results in the present study are based on the analysis of exclusively intracellular organisms, defined by a two-stage staining protocol: only those organisms that were stained also after permeabilisation of the cells were used for analysis. Shenoy and colleagues did not distinguish between extracellular and intracellular organisms, however extracellular organisms are in the majority in such preparations (personal observations). Moreover, a new, high-titred and highly specific rabbit antiserum, rbMAE15, as well as the mouse monoclonal antibody 1B2, both detecting Irgm1, could be employed for *Listeria*-infected cells. Many different conditions were tested here – (I) time points ranging from 15 min to 4h post infection, (II) infection with wildtype *L. monocytogenes,* with the phagosome escape mutant Δ*hly,* or with *M. bovis* BCG, in (III) primary or RAW264.7 macrophages as well as mouse embryonic fibroblasts – but in no case did Irgm1 accumulate at the intracellular listerial or mycobacterial phagosome or at the LAMP1-positive vacuoles (Figures 3.5-3.8). The conclusion from these experiments is that Irgm1 is does not directly bind to bacterial phagosomes. This seriously weakens the model of Irgm1 as regulator of phagosomal maturation.

One the one hand, Irgm1 could also not be detected at phagocytosed heat-killed *Listeria* (Figure 3.6 B), conditions under which active modification on the phagosome by the parasite is excluded, or at phagosomes of opsonised or heat-killed *T. gondii* (Butcher et al. 2005). On the other hand it was repeatedly observed in our laboratory that Irgm1 localises to the phagocytic cup and around phagocytosed latex beads [Figure 3.6 C, (Martens et al. 2004; Zhao et al. 2010)]. Moreover, proteome analysis of purified latex bead-containing phagosomes from IFNγ-treated RAW264.7 macrophages also identified Irgm1 [Prof. Stefan Höning, personal communication and (Jutras et al. 2008; Trost et al. 2009)]. However, Trost and colleagues only properly excluded contamination of ER and mitochondria in their purified fraction but not Golgi. It remains an open question, why Irgm1 can be detected on the latex bead phagosome but not on the bacterial phagosomes. One explanation could be that, since a latex bead phagosome is much bigger in comparison to a bacterial phagosome, it requires also more membranous material that is then provided not only by the plasma membrane, but also by endomembranes such as Golgi. A proteomic study of latex bead-containing phagosomes report that about 1/3 of plasma membrane proteins and 2/3 of endolysosomal, ER and Golgi proteins constitute the phagosomal proteome and this ratio might also apply for the membrane composition (Campbell-Valois et al. 2012). Unfortunately, this analysis did not compare the results to bacteria-containing phagosomes, which are also

much more difficult to purify. Future microscopic analysis with Golgi and other organelle markers could also reveal, whether the membrane of latex bead-containing phagosomes versus bacteria-containing phagosomes might be derived from other organelles than the plasma membrane.

Taken together, these findings emphasize that results obtained from latex bead phagosomes should be treated with care, when they should serve as model for bacterial phagosomes. This problem is explicit in a recent proteome analysis of purified *Mycobacteria*-containing phagosomes vs. latex bead-containing phagosomes from human cells showing that only 2/3 of the identified proteins overlap (Lee et al. 2010), indicating that these phagosomal membranes are not of the same composition.

IFN-inducible guanylate binding proteins (GBP) are also discussed to be critical in immunity to bacterial infection. *Gbp1*$^{-/-}$ mice (Kim et al. 2012) and *Gbp5*$^{-/-}$ mice (Shenoy et al. 2012) are more susceptible to *Listeria monocytogenes* infection whereas *Gbp2*$^{-/-}$ mice are not (Degrandi et al. 2012). Although *Gbp*$^{chr3-/-}$ mice are lacking these genes as well (*Gbp1/2/3/5/7*$^{-/-}$), they display resistance to *L. monocytogenes* infection (Yamamoto et al. 2012). SiRNA knock-down of four of the eleven murine GBP proteins (Gbp1, Gbp6, Gbp7, and Gbp10) caused loss of IFNγ-mediated cell-autonomous resistance to *L. monocytogenes* and *Mycobacteria bovis* BCG in macrophages. Since these GBP proteins partially co-localise with bacteria-containing vacuoles and interact with several components of the NADPH oxidase and the autophagy pathway, the authors claimed that GBP proteins transport these effectors to the bacterial phagosome in order to kill the bacteria (Kim et al. 2012). Two other recent studies reported that GBP proteins are required for Caspase-11-dependent pyroptosis upon infection with intracellular bacterial pathogens (Meunier et al. 2014; Pilla et al. 2014). Gbp2 was shown to localise to the bacterial phagosomes (in a ring-like pattern) and suggested to initiate killing of the bacteria by lysis of the bacterial vacuoles. This would then expose LPS to the cytosol, which is recognised by an unknown LPS receptor triggering Caspase-11-dependent pyroptosis of the host cell. However, no significance of Irgm1 or Irgm3 could be attributed to this Caspase-11-mediated resistance to bacteria. Since the effector model of Irgm1 in phagosomal maturation can now largely be excluded, next the focus will be on the role of Irgm1 in facilitation of autophagy of *Mycobacteria.*

## 4.3 Role of Irgm1 in autophagy

The first experimental series on Irgm1 as autophagy regulator unfortunately did not test for co-localisation of Irgm1 with mycobacterial phagosomes and autophagosomes in IFNγ-induced macrophages and macrophage cell lines (Gutierrez et al. 2004; Singh et al. 2006). Instead, an Irgm1-GFP fusion construct was overexpressed and an increase in autophagic organelles, as in IFNγ-induced cells, was reported. Moreover, overexpression of Irgm1 resulted in a two-fold increase of *Mycobacteria* co-localising with lysosomes. The authors concluded that Irgm1 mediates IFNγ-induced autophagy to eliminate *Mycobacteria* (Gutierrez et al. 2004; Singh et al. 2006). The drawback of these studies is that only an artificial overexpression system was used and that no mechanistic link between Irgm1 and autophagy could be provided.

Currently, there is opposing data on IFNγ-induced autophagy in cells from *Irgm1*-deficient mice, most of which proposes Irgm1 as negative regulator of autophagy. The first insight was provided by EM images showing IFNγ-induced *Irgm1/IFNγ*$^{-/-}$ CD4$^{+}$ T-cells with more membrane-bound vacuoles (Feng et al. 2008). Secondly, haemopoietic stem cells from *Irgm1*-deficient mice that were transgenic for GFP-LC3 showed increased number of autophagosomes, which was rescued by additional knock-out of *Irgm3* or *IFNγR1* (King et al. 2011). Thirdly, staining of endogenous LC3 after 24 h of IFNγ-treatment in fibroblasts showed also increased number of autophagosomes (Traver et al. 2011). Finally, the number of LC3 punctae per LC3-positive Paneth cells from *Irgm1*-deficient mice was elevated independent of treatment. Increased co-localisation of LC3 and LAMP1 (autolysosomes) as well as more lipidated LC3II after 24 h IFNγ-stimulation could also be observed in *Irgm1*$^{-/-}$ MEFs in our laboratory (Jelena Maric, unpublished data).

When autophagy markers in IFNγ-induced *Irgm1*$^{-/-}$ cells are elevated, it is possible that either Irgm1 itself is really a direct inhibitor of autophagy or that aggregates of GKS proteins that form in the absence of Irgm1 deregulate autophagy. In addition, one has to distinguish whether elevated autophagy markers are the result of enhanced formation or impaired degradation of autophagosomes. In IFNγ-induced *Irgm1*$^{-/-}$ fibroblasts, lysosomes seem to be swollen, impaired in acidification and coated with Irga6 aggregates on the outside, which may suggest that GKS aggregates may hinder lysosomal degradation of autophagolysosomes and thus impair autophagic flux (Jelena Maric and Prof. Jonathan Howard, manuscript in preparation). Considering that selective macroautophagy is described to be a major contributor in the clearance of misfolded and aggregated protein in the cytosol in mammalian cells (Tyedmers et al. 2010), it remains to be investigated how much different

stimuli like GKS protein aggregates itself or IFNγ-stimulation contribute to the autophagy induction.

Contradictory to earlier reports, in shRNA knock-down of Irgm1 in RAW macrophages or primary macrophages derived from *Irgm1*$^{-/-}$ mice no change in autophagosome, autolysosome or LC3 turnover was observed after 4 h of IFNγ-treatment (Matsuzawa et al. 2012). These results can be explained that after 4 h of IFNγ-treatment, only the conventional signalling pathways of autophagy are induced. However, elevated autophagy as seen in *Irgm1*$^{-/-}$ cells 24 h after IFNγ-treatment, either due to blockage of autophagolysosomal breakdown or to selective clearance of GKS proteins would not have started 4 h after IFNγ-treatment, because the GKS (and other) proteins have not been fully expressed yet.

Lastly, it is also under debate whether the appearance of autophagy markers just before cell death (Feng et al. 2009) indicates that autophagy is involved in the cell death or rather that this is the last attempt of the cell to rescue itself (Deretic 2011).

In summary, it appears that two roles attributed to Irgm1 in IFNγ-induced murine cells, either being a direct effector on the phagosomal membrane or inducing autophagy to clear *Mycobacteria,* have not stood up for closer investigation.

## 4.4 The main function of Irgm1 is to regulate GKS proteins

The only property of Irgm1 that is so far robust is its role as a negative regulator of the GKS subfamily of the IRG proteins. When GKS proteins are overexpressed without GMS regulators, GKS proteins form aggregates in the cell. Moreover, Irga6 overexpression causes an enlargement of the ER lumen as observed in EM images, which is dependent on its nucleotide binding activity. GKS aggregation is abolished either by co-expression of all GMS proteins or by induction of endogenous GMS proteins (Martens et al. 2004; Hunn et al. 2008). Moreover, GKS aggregates form in IFNγ-induced cells of GMS-deficient mice (Henry et al. 2009; Traver et al. 2011) and seem to target unoccupied endomembranes. In *Irgm1*$^{-/-}$ cells they co-localise with lysosomes; in *Irgm3*$^{-/-}$ cells with ER markers and lipid droplets; and in *Irgm1/Irgm3*$^{-/-}$ cells with oleic acid-induced lipid droplets [Jelena Maric, unpublished data, (Haldar et al. 2013)]. Moreover, Gbp1 and Gbp2 also form aggregates in absence of GMS proteins, and in case of Gbp2 also accumulate on oleic acid-induced lipid droplets (Traver et al. 2011; Haldar et al. 2013).

Together with the biochemical data showing that Irgm3 binds Irga6 in presence of GDP whereas Irga6-Irgb6 interaction is GTP-dependent (Hunn et al. 2008; Pawlowski et al.

2011), these findings support the hypothesis that the main function of GMS proteins is to prevent premature activation of GKS proteins on endomembranes by forming GMS-GKS heterooligomers in the GDP-bound inactive form. A tight regulation of GKS proteins is necessary, because the deregulated GKS aggregates on endomembranes may have cytopathic effects and block of autophagosome degradation.

The severe phenotype of *Irgm1*$^{-/-}$ mice upon infection may be caused by these cytopathic GKS aggregates leading to the damage in proliferating IFNγ-induced lymphomyeloid cells (Hunn et al. 2010). Since hypothetical GKS aggregates in lymphomyeloid cells of *Irgm1*$^{-/-}$ mice have not been analysed yet, experimental data that would proof this hypothesis are still missing. First experiments with fibroblasts and bone marrow-derived macrophages deficient for *Irgm1* showed no effect on cell death upon IFNγ stimulation (Jelena Maric, unpublished data). One may argue that the hypothetical cytopathic GKS aggregates are more harmful in lymphomyeloid cells due to the smaller size of the cell. In fibroblasts, however, the cytopathic aggregates are more diluted in the cytosol. Another hypothesis is that in *Irgm1*$^{-/-}$ cells, the GKS aggregates deregulate autophagy and this limits the proliferative potential of *Irgm1*$^{-/-}$ lymphocytes upon infection rather than enhanced cell death (Jelena Maric, unpublished).

In contrast, there are less GKS aggregates in *Irgm1/Irgm3*$^{-/-}$ cells, because the protein expression levels of GKS proteins are highly reduced (Henry et al. 2009). Moreover, also no increase in LC3 specks could be observed in *Irgm1/Irgm3*$^{-/-}$ MEFs (Jelena Maric, unpublished data). In conjunction with the documented restoration of immunological competence in the *Irgm1*/*Irgm3*-deficient mouse (Henry et al. 2009), these results presented here favour the view that the loss of resistance to *Mycobacteria, Listeria* and many other organisms caused by *Irgm1*-deficiency is due to lymphomyeloid collapse and not to loss of a specific effector function of Irgm1 on the microbial phagosome.

## 4.5 GKS proteins can directly target liposomes

To gain insight which kind of membranes IRG proteins can target in general, their association with liposomes was analysed. Co-sedimentation assays indicate that Irga6 and Irgb6 but not Irgd can directly bind to Folch lipid vesicles in a GTP-dependent manner (Nikolaus Pawlowski, unpublished data and Figure 3.9 A). These data demonstrate that Irga6 and Irgb6 have an intrinsic capacity to bind lipids, independent of myristoylation, because the recombinant bacterially-expressed protein is not post-translationally lipid modified. The result that Irga6 and Irgb6 could co-sediment with the liposomes only in a GTP-dependent manner

(Figure 3.9 A) is further confirmed with the nucleotide-binding mutant Irga6-S83N, in which co-sedimentation is abolished (Nikolaus Pawlowski, unpublished data). This strongly suggests that GTP binding is essential for lipid binding, probably inducing a conformational change, which would increase the membrane avidity. Whether nucleotide binding or hydrolysis might be the driving force could be analysed by using non-hydrolysable nucleotides such as GTPγS.

Irgd alone did not co-sediment with liposomes (Figure 3.9 A). This is in line with results from membrane extraction assays, in which endogenous Irgd had the smallest membrane-bound pool of the IRG proteins tested (Martens et al. 2004). Interestingly, Irgd could associate with liposomes, when it was mixed with Irgb6 but not with Irga6 (Figure 3.9 C/D). The fact that Irgd can only co-sediment with liposomes in presence of Irgb6 can have several reasons: a) Irgb6 forms mixed oligomers with Irgd that allow association with the membrane, b) Irgb6 acts as direct adaptor protein for Irgd on the membrane, or c) Irgb6 induced a conformational change of Irgd that unfolds its membrane-binding capacity. This is again consistent with the hierarchal loading of IRG proteins on the *T. gondii* PVM, in which Irgd could only be found on Irgb6-positive but not on Irgb6-negative vacuoles (Khaminets et al. 2010). To explain why Irga6 is not able to induce co-sedimentation of Irgd, one can argue that at equimolar concentrations, Irga6 may form homooligomers with a higher affinity than heterooligomers with Irgd. Therefore, no mixed oligomers were formed that would allow Irgd to bind the liposomes. Titrating lower concentration of Irga6 to Irgd may resolve this question.

Because different sizes of liposomes (100 nm or 1 μm) behaved equally in such co-sedimentation assays (Niko Pawlowski, unpublished data), one can assume that the curvature of the vesicles does not influence GKS binding. In fact, Irga6 oligomers accumulate on the *T. gondii* PVM or on the *E. cuniculi* PVM (see chapter 4.10), two vesicle types that dramatically differ in size and curvature. However, it was not tested yet, whether GKS proteins might also bind to negatively curved membranes such as the inner cytosolic phase of the plasma membrane.

Another characteristic of the target membrane to consider is the lipid composition. In this study, the liposomes were prepared with a mixture of polar lipids obtained from a Folch extraction of porcine brain. This mixture is composed mainly of phospholipids [(33% phosphadidylethanolamine (PE), 18% phosphatidylserine (PS), 12% phosphatidylcholine (PC)] and unknown components (Homepage Avanti Polar Lipids, Inc). The parasitophorous vacuoles, which are derived from the raft and non-raft microdomains of the plasma

membrane, are expected to have a similar lipid composition as the plasma membrane. The plasma membrane of a mammalian liver cell for example is approximately composed of 24% PC, 7% PE, 4% PS, 17% cholesterol and other components (Alberts et al. 2007), and this differs to the lipid mixture tested in this study. So far, only one systematic lipid affinity screen was performed with recombinant GST-tagged proteins but without nucleotides, in which only Irgm1 bound to certain lipids but not Irgm2, Irgm3 or Irga6 [see 4.1, (Tiwari et al. 2009)]. Future analysis may reveal whether IRG proteins bind to specific lipids or lipid compositions. However, it is unlikely that IRG proteins have a certain lipid preference, because there is no evidence yet that the lipid composition differ between the PVM, which is targeted by IRG proteins, and the plasma membrane, which is not targeted by IRG proteins.

Lastly, a series of experiments by Nikolaus Pawlowski, mixing recombinant protein with thin rehydrated lipid layers, so-called membrane sheets, revealed that recombinant GKS proteins were able to crinkle and deform the membrane in a GTP-dependent manner, strongly resembling the actions of dynamins (Itoh et al. 2005). Moreover, EM studies of liposomes mixed with recombinant Irgb6 showed formation of little tubules on the vesicle surface in a GTP-dependent manner (Nikolaus Pawlowski, unpublished data). Future studies with artificial membrane systems, such as the chemically induced blebs in mammalian cells or giant unilamellar vesicles, may help to further define the characteristics of an IRG-positive membrane. Taken together, these observations suggest that similar to dynamins, energy released from GTP hydrolysis may be transduced into mechanical force that results in deformation and ultimately rupture of the vacuolar membrane (Pawlowski et al. 2011).

## 4.6 GKS proteins selectively target parasite vacuoles, but independent of residual host surface proteins

Several microscopic studies documented that GKS proteins accumulate on the parasitophorous vacuolar membrane (PVM) of *T. gondii* and *C. trachomatis*, that are both derived from the invaginated host plasma membrane and do not fuse with the endolysosomal system (see 1.4 and 1.6). However, it is still puzzling, how recognition of exactly these membranes is provided. In this study two specific aspects were investigated: the presence of residual plasma membrane proteins on the PVM as inhibitory factors of GKS protein binding and non-fusogenic compartments as a model membrane.

Firstly, biotinylation of host cell surface proteins prior *T. gondii* infection showed that the intensity of residual host plasma membrane proteins and the intensity of labelled Irga6 or Irgb6 did not negatively correlate (Figure 3.10). Since a negative correlation indicates a

competitive behaviour, the obtained results here challenge the hypothesis that residual host cell plasma membrane proteins block GKS protein accumulation on the PVM. Therefore, the wide range of fluorescence intensities observed for IRG protein loading (Khaminets et al. 2010) may not be explained with an inefficient exclusion of surface proteins, that would leave different amounts of residual proteins on the PVM. Another explanation for the different intensities of IRG proteins on the PVM may be different timing of IRG protein loading. Even though the parasites enter the host cells more or less synchronously, IRG proteins reach the PVM most likely by diffusion and this may be a stochastic event. When then once the first IRG proteins start to accumulate on the PV (and get stabilised), the IRG protein loading rises very fast (Khaminets et al. 2010). At two hours post infection, the weakly labelled vacuoles would represent those that just started to accumulate IRG proteins, whereas the strongly stained PVs started loading earlier.

The biotinylation method of host cell surface proteins has certain drawbacks. The fluorescence intensity of the Biotin-Streptavidin detection complex is just slightly above background level, and hence is difficult to measure. In addition, intracellular *T. gondii* PVs appeared in 3D images like a bulge from the otherwise flat and thin fibroblast (data not shown). Thus, in conventional Epi-fluorescence microscopy the rim around the parasite may also reflect several vertical stacks of plasma membrane. Lastly, phagocytosed latex beads should have served as positive control carrying Biotin on their phagosomal membrane. But the beads had lots of refraction light at high exposure times that outshined the Streptavidin signal (data not shown). Future studies should combine a systematic screen of host surface-derived candidates as IRG protein competitors, including marker proteins of excluded transmembrane proteins and incorporated GPI-anchored proteins (Mordue et al. 1999). Better visualisation methods such as direct antibody staining of candidate proteins as well as the choice of a bigger host cell type, in which the parasite PV is not so entangled by the host cell host plasma membrane, might improve the experimental setup.

Another approach would be to test mutant *Toxoplasma* strains that are known to be impaired in formation of the moving junction and therefore probably also impaired in selective exclusion of host plasma membrane proteins during PVM formation. Initial experiments with the AMA1-deficient *T. gondii* strain (Mital et al. 2005), which is a major component of the moving junction complex spanning the PVM, however failed to show a dramatically altered IRG protein loading (Steffi Koenen-Waisman, unpublished data and own observations). A second member of the moving junction complex, RON8, has no homologue in *Plasmodium berghei*, and is therefore of special interest because the PVM of *P. berghei* is

not targeted by IRG proteins (Liesenfeld 2011). However, the *Tg*ΔRON8 stain, as well as conditional *Tg*RON5 knock-down strain, are severely or entirely impaired in host cell invasion, respectively (Straub et al. 2011; Beck et al. 2014). This makes it difficult if not impossible to examine the invaded intracellular parasites that are relevant for IRG accumulation analysis.

The second aspect of this subject focuses on the question whether non-fusogenic vacuoles are general targets of the IRG resistance system. To this end, artificial Inc-induced membranous vesicles (Mital et al. 2013) were examined for Irga6 or Irgb6 co-localisation (Figure 3.11). Because the GKS proteins failed to accumulate on the Inc-induced vesicles, it can be concluded that the non-fusogenic character of a membrane is not enough to be recognised by IRG proteins. Thus, a membrane must carry additional features to be recognised and targeted by IRG proteins. Another possibility could be that the Inc proteins after transient overexpression occupy the vesicle surface so that IRG proteins cannot target these inclusions anymore.

## 4.7 Interplay of ATG proteins and the IRG resistance system

It remains an open question by which mechanism IRG proteins can target membranes. Two other protein families, the autophagy-related (Atg) proteins and the interferon-inducible GBP proteins (see 4.8), also play a role in resistance to *Toxoplasma, Neospora* and *Chlamydia* and are discussed to mediate the recruitment of IRG proteins.

Detailed investigation of Atg5 started with the observations that IFNγ-dependent growth restriction of avirulent *T. gondii* strains was impaired in *Atg5*$^{-/-}$ fibroblasts (Konen-Waisman et al. 2007) and in activated *Atg5*$^{-/-}$ macrophages (Zhao et al. 2008). *Atg5*-deficient mice were also susceptible to infection with *T. gondii* and *L. monocytogenes* (Zhao et al. 2008). Interestingly, *Atg5*$^{-/-}$ macrophages were impaired in accumulating Irga6 at the PVM, correlating with an inability to mediate the interferon-dependent damage and ruffling of the PVM as observed on EM level [see Figure 1.5 C, (Zhao et al. 2008)]. Failure of IRG protein accumulation onto the PVM was confirmed in *Atg5*$^{-/-}$ fibroblasts and macrophages for the GKS proteins Irga6, Irgb6, Irgd, Irgb10, as well as for Gbp1 and Gbp2 (Khaminets et al. 2010; Traver et al. 2011; Haldar et al. 2013; Selleck et al. 2013). In *C. trachomatis* infection, Meyer and colleagues described that Irga6 failed to accumulate at the inclusions in *Atg5*$^{-/-}$ fibroblasts, but Irgb10, Irgb6, Irgm2 and Irgm3 loading on inclusions was similar to wildtype host cells (Al-Zeer et al. 2009). In contrast, Coers and colleagues showed a reduced loading of all GKS proteins and Gbp2 in *Atg5*$^{-/-}$ cells (Haldar et al. 2014).

Similar to *Irgm1/Irgm3*-deficient cells, GKS protein levels are not only decreased, but also formed GTP-bound aggregates in *Atg5*-deficient cells (Zhao et al. 2008; Khaminets et al. 2010; Traver et al. 2011). Both phenomena might explain the susceptibility of *Atg5*$^{-/-}$ cells to avirulent *T. gondii* infection. When the GKS protein levels are decreased, there might not be enough protein to destroy the PVs. Moreover, because GKS aggregates, either caused by GKS protein overexpression or by IFNγ-induction in *Irgm1/Irgm3*$^{-/-}$cells, cannot accumulate on the PVM anymore (Hunn et al. 2008; Henry et al. 2009), GKS proteins may also be impaired in PVM targeting in *Atg5*-deficient cells.

Taken together, these findings suggest that Atg5 functions as a regulator of IRG proteins to prevent inappropriate GKS activation. Since no accumulation of Atg5 itself on the PVM was found, a role of Atg5 as IRG-adaptor is rather unlikely. If Atg5 acts as a regulator of IRG proteins it could either directly bind GKS proteins and keep them in an inactive state (like GMS proteins) or support GMS proteins to exert their function.

Alternatively, IRG proteins are probably always aggregate in IFNγ-stimulated cells at low levels, but are constantly degraded by autophagic or possibly non-autophagic pathways involving Atg5. In *Atg5*-deficient cells, this protein degradation (or recycling) system would be impaired resulting in GKS protein aggregation in the cell, which then exert their cytopathic effects. Thus, Atg5 itself has then no direct effect on IRG proteins, but only its absence causes deregulation of GKS aggregate degradation.

Deregulation of the IRG protein turnover as an off-target effect is strongly supported by the fact that growth inhibition of *T. gondii* is not limited to Atg5. Impaired IRG loading onto *T. gondii* PVM was also reported in fibroblasts lacking the autophagy regulators Atg3, Atg7 and Atg16L1 but not for Atg9a or Atg14 (Yamamoto et al. 2012; Haldar et al. 2014; Ohshima et al. 2014). For autophagosome elongation, Atg5 is activated by Atg7 and forms a complex with Atg12 and Atg16L1 in order to mediate lipidation of LC3. Atg9a or Atg15 play a key role in the earlier step of orchestrating the autophagosomal membrane (Maiuri et al. 2007). These findings implicate that deregulation of a certain step in autophagy, the autophagosome elongation, results in the deregulation of the IRG system acting against *T. gondii* in mice. In contrast, human ATG16L1 is not required for IFNγ-dependent inhibition of *T. gondii* growth in human cells (Ohshima et al. 2014), most likely because humans lack the IRG resistance system.

## 4.8 Interplay of GBP proteins and the IRG resistance system

Another IFN-inducible protein family that plays a role in *Toxoplasma* and *Chlamydia* resistance are the GBP proteins. *Gbp1*- and *Gbp2*-deficient mice show enhanced susceptibility to infection with avirulent *T. gondii* strains (Degrandi et al. 2012; Selleck et al. 2013). Knock-out of the GBP cluster on chromosome 3 including Gbp1, Gbp2, Gbp3, Gbp5 and Gbp7 also results in enhanced susceptibility to *T. gondii* (Yamamoto et al. 2012) as well as to *C. trachomatis* (Haldar et al. 2014). Most of the mouse GBP proteins, Gbp1, Gbp2, Gbp3, Gbp6, Gbp7 and Gbp9 but not endogenous Gbp5, accumulate on the PVM of avirulent *T. gondii* strains but not on virulent strains that express the virulence factors ROP5 or ROP18 (Degrandi et al. 2007; Virreira Winter et al. 2011; Selleck et al. 2013). Murine Gbp1 and Gbp2 but not Gbp5 also accumulate on the PVM of *Neospora caninum* (Spekker et al. 2013). Similar to IRG proteins, an intact nucleotide binding site is necessary for the PVM targeting, whereas the lipid modification (farnesylation) of mGbp1 is not necessary (Virreira Winter et al. 2011; Kravets et al. 2012). Furthermore, it was also demonstrated that PVM targeting by GBP proteins is dependent on other IFNγ-inducible factors (Virreira Winter et al. 2011). Therefore, several independent studies investigated the interplay of IRG and GBP proteins on the PVM. In macrophages of $GBP^{Chr3-/-}$ mice, Irgb6 and Irgb10 but not Irga6 loading on the PVM was impaired (Yamamoto et al. 2012). Similar results were obtained in $Gbp1^{-/-}$ macrophages (Selleck et al. 2013). Vice versa, in $Irga6^{-/-}$ fibroblasts the intensity of GBP proteins and number of positive vacuoles, detected with the pan-GBP antibody GBP1-5, was reduced on the PVM (Hermanns 2014).

Taken together, these data suggest that mainly Irga6 is prerequisite for the GBP accumulation on the PVM of *T. gondii*. GBP proteins (and Irga6) might then be prerequisite for Irgb6 and Irgb10 binding or alternatively stabilise their binding to the PVM. However, this specific order is not in line with the proposed hierarchical loading, in which Irgb6 and Irgb10 arrive as pioneers and subsequently becoming stabilized by the arrival of Irga6 and Irgd (Khaminets et al. 2010). Considering that so far widely different method were used (staining in *Irga6*-deficient cells vs. co-staining of two IRG proteins), future studies might help to understand the role of Irgb6, Irgb10 and other IRG proteins in the hierarchy of IRG protein loading.

So far, the *T. gondii* virulence factors ROP5 and ROP18 have been mainly described to act on IRG proteins (Fentress et al. 2010; Steinfeldt et al. 2010; Behnke et al. 2012; Fleckenstein et al. 2012; Niedelman et al. 2012). However, GBP proteins have not been shown to be direct targets of ROP virulence factors, only Gbp1 shows reduced loading in presence of ROP18.

(Virreira Winter et al. 2011). Supporting the model that GBP proteins might act downstream of IRG proteins, the ROP5/ROP18 complex might particularly interact with Irga6, since ROP18 seems to be Irga6 specific (Tobias Steinfeldt, Thomas Hermanns and Jonathan Howard, manuscript in preparation) Such a hierarchical loading order may be specific for the target organism, because in *GBP*$^{chr3-/-}$ cells, targeting of the *C. trachomatis* inclusion membrane is reduced for Irgb10 and Irga6 but not for Irgb6 (Haldar et al. 2014).

As already described for *Atg5*-deficiency (see chapter 4.9), impaired IRG protein loading correlates with an impaired membrane damage potential, since the PVM of *T. gondii* has no scalloped appearance on the EM level in IFNγ-treated cells of *GBP*-deficient mice (Yamamoto et al. 2012; Selleck et al. 2013).

Considering that about one third of the world population is infected with *T. gondii*, it is a serious question how the IFN-mediated resistance to *Toxoplasma* is regulated in humans. Therefore, it was of strong interest, if the GBP proteins can substitute the role of the IRG system in humans. However, hGbp1 could be detected only on extremely few vacuoles (below 1 %) of virulent or avirulent *T. gondii* strains [(Günther 2011) and Gerrit Praefcke personal communication]. In human haploid cells only 6% vacuoles were GBP1-5-positive and knock-out of the entire human GBP gene locus provided the final evidence, that hGBP proteins are not responsible for IFNγ-mediated *Toxoplasma* restriction (Ohshima et al. 2014). In contrast, *Chlamydia trachomatis* seems to be partially controlled by hGBP1 and hGBP2, which also accumulate on the inclusion membrane (Tietzel et al. 2009; Al-Zeer et al. 2012).

In summary, IRG and GBP proteins seem to clearly cooperate in mediating the IFNγ-induced resistance to *Toxoplasma* or *Chlamydia* in mice. The level of interaction is still unknown, but it is very unlikely that GBP proteins may act as adaptor proteins for IRG effectors on the target membrane.

## 4.9 Irgm2 or Irgm3 do not function as GKS adaptor proteins on the PVM

Besides GKS and GBP proteins, little amounts of Irgm2 and Irgm3 can be detected on the PVM of avirulent *T. gondii* strains (Martens et al. 2005; Khaminets et al. 2010; Haldar et al. 2013). With low amounts of GMS proteins and high amounts of GKS proteins on a PV, one may hypothesize that GMS protein loading onto a PV inhibits loading of GKS proteins. However, this can be excluded for several reasons. Firstly, it has been shown that transfected Irgm2 or Irgm3 can only target the PVM of *T. gondii* when co-expressed with other GKS proteins (Hunn et al. 2008). Secondly, co-staining of endogenous Irgm2 or Irgm3 against

Irga6 or Irgb6 showed that PVs of *T. gondii* were either positive for both proteins or for the GKS protein only but never for the GMS proteins only (Khaminets et al. 2010). Thirdly, intensity measurements of Irgm3 versus Irga6 or Irgb6 could confirm a positive correlation of fluorescent intensities, which excludes a competition of GMS and GKS proteins at the PVM (data not shown). Thus, a more reasonable explanation for the presence of GMS proteins on the PVM may be that the GMS proteins, because they have a certain cytoplasmic pool, bind secondarily to GKS proteins, which are massively abundant at the PVM. Because GMS - GKS protein interactions are GDP-dependent (Pawlowski et al. 2011), Irgm2 and Irgm3 may bind the GKS proteins when they just hydrolysed their GTP at the PVM. Whether Irgm2 and Irgm3 fulfil an important function at the PVM remains to be investigated.

## 4.10 *E. cuniculi* is a novel target of the IRG resistance system

In order to better understand mechanism how IRG protein target membranes, certain pathogens have been examined that display different modes of host cell invasion. Most of the organisms that seem to be ignored by the IRG system, such as *Salmonella, Listeria, Leishmania, Mycobacteria*, and *Rhodococcus*, are taken up by phagocytosis and reside in a more or less modified phagosomes. In contrast, the pathogens that are targeted by the IRG resistance system, *T. gondii, N. caninum* and *Chlamydia*, enter the host cell by an unusual mechanism and reside in non-fusogenic vacuoles (see introduction 1.4.2 and 1.4.3 and Figure 4.1 A). Hence, only organisms that enter cells without engaging the phagocytic mechanism may become preferential targets for IRG protein-mediated resistance, regardless of their taxonomic status. To generalise this idea, another intracellular organism with a non-phagocytic mode of host cell invasion and a wide taxonomic divergence from the other two known IRG protein targets was examined: *Encephalitozoon cuniculi.* This microsporidian parasite has already been described for IFNγ-mediated growth restriction and its peculiar entry mechanism leading to a non-fusogenic parasitophorous vacuole as intracellular niche (see introduction 1.5). The experimental design in this study was based mainly on extensive knowledge and expertise concerning the interaction of the mouse IRG resistance system and the *T. gondii* PVM. Indeed, several aspects of the obtained results closely resembled features that have been studied in detail in *T. gondii* infection and partially for *Chlamydia* and *Neospora* infection.

IFNγ mediates cell-autonomous resistance against *E. cuniculi* in fibroblasts (Figure 3.12) that is associated with accumulation of different IRG proteins onto a small proportion of *E. cuniculi* PVs (Figure 3.12). At the light microscopical level it is not possible to say

precisely where the IRG proteins are localised at early time points, but images from later time points after infection, when the vacuole is enlarged, suggest that IRG proteins are loaded onto the PVM. A decisive answer to this question will require electron microscopy. In accordance with *T. gondii* and *C. trachomatis,* all GKS proteins tested so far (Irga6, Irgb6, Irgd) accumulate at the PV of *E. cuniculi* (Figure 4.1 B). The appearance of Irgm1 next to *E. cuniculi* PVs can be explained by the observation that *E. cuniculi* is often found in the perinuclear region that also harbours the host Golgi, the main organelle for Irgm1 localisation. Moreover, the *E. cuniculi* PV has been shown to directly bind host mitochondria (Hacker et al. 2014); again organelles, which are also partially positive for Irgm1 (see Figure 3.4). However, Irgm1 does not at all load onto the *E. cuniculi* vacuoles as observed for other IRG proteins in a typical ring-like pattern. Like for vacuoles of *T. gondii* and *C. trachomatis*, Irgm1 does not load onto *E. cuniculi* PVs, while Irgm2 can be found on only a small percentage [Figure 3.13 and (Butcher et al. 2005; Martens et al. 2005; Coers et al. 2008; Al-Zeer et al. 2009; Haldar et al. 2013)]. Nevertheless, in contrast to *T. gondii*, vacuoles with multiplying *E. cuniculi* meronts also were targeted by the IRG resistance system (Figure 3.14 C).

Data from IRG proteins loading onto *T. gondii* PVMs indicates that loading of Irgb6 might be stabilised by the loading of Irga6, and is thus clearly cooperative (Khaminets et al. 2010). The frequency of *E. cuniculi* PVs loaded with IRG proteins at any time point investigated here is low, but the majority of loaded PVs accumulate both Irga6 and Irgb6 (Figure 3.14) indicative for cooperativity of IRG loading. However, loading of more than one GKS member on *E. cuniculi* PVs can also arise, if only a few vacuoles, which carry specific properties, are receptive to IRG proteins at any time. Cooperative loading of IRG protein on *Neospora* or *Chlamydia* has not been studied yet.

The hierarchical loading of the IRG members onto the PVM is well described for *T. gondii* (Khaminets et al. 2010). In this study only little information on a possible hierarchy could be obtained, because triple staining (meront marker 6G2 + two IRG proteins) could be established only for the Irga6 + Irgb6 combination. However, the importance of individual IRG proteins is not necessarily the same for the different target organisms. For example, Irgb10 and Irgm3 have been described to be the major resistance factors against *C. trachomatis* (Bernstein-Hanley et al. 2006).

Unlike the IRG loading pattern onto the vacuoles, the timing differs for different target organisms (Figure 4.1 C). In case of avirulent *T. gondii*, the number of vacuoles loaded with IRG proteins rises roughly linear to about 90% of all vacuoles within 2 h after infection

(Khaminets et al. 2010). With *E. cuniculi*, the number of vacuoles loaded ranges between 5 and 15% within 30 minutes of infection, and persists at that level for all time points investigated up to 24 h (Figure 3.13). For *C. trachomatis,* no time-course has been described yet; but two independent studies show 80% of Irga6-positive vacuoles after 3 h of infection [24 h IFNγ pre-stimulation, (Al-Zeer et al. 2009)] and 10% after 20 h [3 h IFNγ pre-stimulation, (Coers et al. 2008)]. These different IRG loading behaviours can still reflect qualitatively similar processes, if (I) the initiation of IRG protein loading onto individual *E. cuniculi* vacuoles takes on average longer than onto *T. gondii* vacuoles, and if (II) *E. cuniculi* vacuoles subsequently disintegrate and are cleared with faster kinetics than *T. gondii* vacuoles. With increasing time after infection more and more parasites are cleared from the cells, accounting for the slow but linear loading of detectable meronts (Figure 3.12).

Another difference is that in contrast to *E. cuniculi*, intracellular *T. gondii* tachyzoites have a uniform size and shape. IRG proteins that accumulate on the PVM largely reflect this regular shape. Therefore, the disruption of the PVM can relatively easy be obtained by microscopic analysis as a nick in the ring like structure of IRG proteins (see Figure 1.5 A, arrow). In case of *E. cuniculi*, however, the shapes of the vacuoles are non-uniform and the IRG proteins usually do not accumulate resembling a regular ring (see for example Figures 3.13 C, E or 3.14 A-C). Therefore, it was not possible to register clear–cut disruption of the *E. cuniculi* vacuole in live-cell imaging. Future studies with better microscopic resolution and a permanent labelling of meronts (lipids or DNA) will hopefully resolve whether the PVM of *E. cuniculi* is also disrupted as consequence of IRG protein accumulation. The disruption of the vacuole of *T. gondii* is followed by the death of the parasite and necrotic-like death of the infected cell with relatively invariant timing [chapter 1.4.2, (Zhao et al. 2009)]. Also in IFNγ-treated and *E. cuniculi*-infected fibroblasts, excess of dead host cells, presumably via necrosis, could be observed (Figure 3.16). Even though in the experiments presented in this study, technically a mixture of infected and uninfected cells was evaluated, an increase in dead cells and decrease in viable cells could be recorded in infected IFNγ-treated samples. For *T. gondii* infection, the molecules triggering this type of cell death are not known yet, since it carries some (membrane permeabilisation, HMGB1 release), but not all features (Caspase 1 cleavage) of typical necrosis (Zhao et al. 2009). IFNγ-induced death of *Chlamydia*-infected host cells has not been investigated yet.

Lastly, as for *T. gondii* resistance, the IRG system appears to be a crucial mechanism in IFNγ-induced mouse fibroblasts that is capable of restriction of *E. cuniculi*. In fibroblasts from *Irgm1/Irgm3*-deficient mice, all IFNγ-inducible resistance against the growth and

development of *E. cuniculi* was lost (Figure 3.15 C, D). A strong phenotype in the GMS-deficient cells is expected, because these deficiencies deregulate the GKS effector subfamily (Hunn et al. 2010). There is a tendency of *Irgm1*$^{-/-}$ fibroblasts being slightly impaired, *Irgm3*$^{-/-}$ being moderately impaired and the *Irgm1/Irgm3*$^{-/-}$ being fully impaired in *E. cuniculi* growth restriction (Figure 3.15). This perfectly resembles the phenotype of the different GMS-deficient fibroblasts that also cannot control *T. gondii* infection after IFNγ-stimulation (Steffi Koenen-Waisman, unpublished data). Moreover, *Irgm1/Irgm3*-deficient mice are highly susceptible to *T. gondii* infection (Henry et al. 2009). In case of *C. trachomatis* infection, *Irgm1/Irgm3*$^{-/-}$ mice also have initially higher bacterial burdens than wildtype mice, but this is then later compensated by an execrated T-cell response. Still, the IFNγ-mediated cell-autonomous response against *C. trachomatis* is entirely lost in *Irgm1/Irgm3*$^{-/-}$ fibroblasts (Coers et al. 2011).

The undetectable effects of the two GKS effector knock-outs in controlling *E. cuniculi* (Figure 3.15 C, D) are consistent with the much weaker *in vivo* phenotypes both Irga6 and Irgd deficiencies upon in *T. gondii* infection (Collazo et al. 2001; Liesenfeld 2011).

Furthermore, the IFNγ-inducible tryptophan catabolic enzyme IDO plays no role in resistance against *E. cuniculi* in mouse fibroblasts or enterocytes (Figure 3.17). Though the role of IDO in mediating the IFNγ-response to *T. gondii* in mouse cells is under debate (Konen-Waisman et al. 2007; MacMicking 2012), tryptophan deprivation also does not mediate the IFNγ-induced restriction of *Chlamydia trachomatis* in mouse fibroblasts, epithelial cells or macrophages (Nelson et al. 2005; Roshick et al. 2006).

This study provides the first evidence that IFNγ-dependent restriction of the microsporidian *Encephalitozoon cuniculi* is mediated by the IRG system. Several features of the IRG resistance system are similar in the resistance against *E. cuniculi,* the best-studied target organism *T. gondii* and partially also *C. trachomatis:* (1) the relocalisation of different IRG proteins to the cytosolic face of the PVM of *E. cuniculi*; (2) cooperativity in IRG-loading; (3) IFNγ- and infection-dependent host cell death and (4) IDO-independent IFNγ-mediated parasite growth restriction in mouse cells. Thus, the IRG resistance system seems to act in a universal manner against parasites from three kingdoms of life, protozoa, bacteria and fungi. The comparison of the three classes of target organisms of the IRG resistance system is summarised in Figure 4.1.

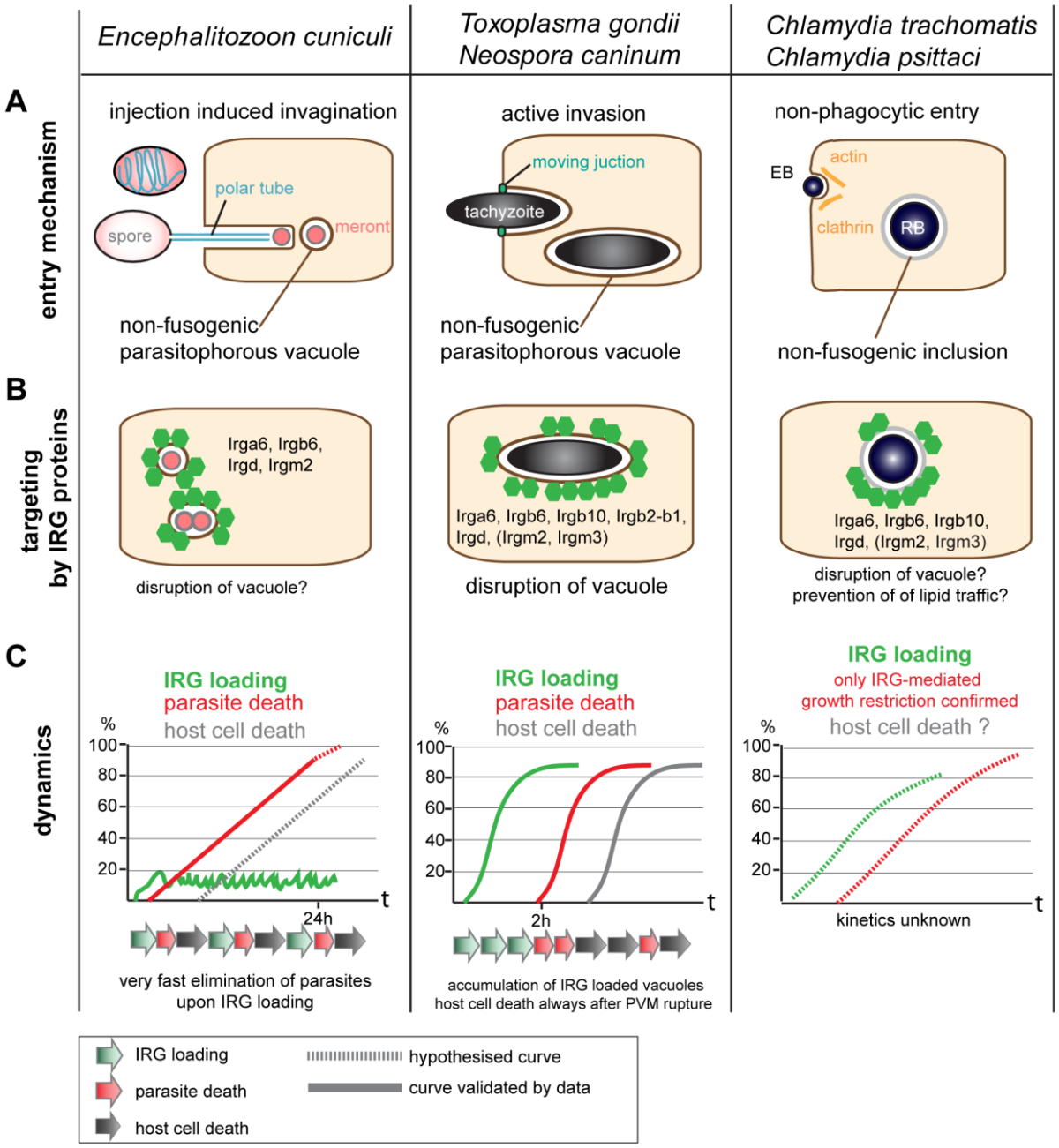


**Figure 4.1: Comparison of the three classes of organisms targeted by the IRG resistance system.**
**(A)** The microsporidian *E. cuniculi*, the protozoa *T. gondii* and *N. caninum* as well as the bacteria *C. trachomatis* and *C. psittaci* enter the host cell by an unusual entry mechanism, none of which resembles conventional phagocytosis. They form their intracellular niche in form of a parasitophorous vacuole or inclusion, which is derived from the plasma membrane, but does not fuse with the host endolysosomal system. **(B)** The same subset of IRG proteins accumulates on the vacuolar membranes of all three microorganisms. The effector mechanism of IRG proteins is likely to be the disruption of the vacuole and thereby killing of the parasite. **(C)** The dynamics of IRG loading on the vacuoles, the subsequent parasite death, as well as the death of the host cell are shown as time-dependent variables.

## 4.11 Model of the IRG resistance system

Several properties of the IRG-dependent resistance mechanism that have been analysed for *T. gondii* are also valid for resistance against *E. cuniculi,* and, as far as it has been analysed, also against *Chlamydia* (see chapter 4.10). Since effective resistance dependent on IRG proteins seems to perfectly correlate with the accumulation of IRG proteins on the PVM, the challenge is to determine the common features that enable IRG proteins to accumulate on the vacuoles of these three organisms but not on the vacuoles of other organisms. The phylogenetic range of the target organisms of the IRG resistance system - a protozoa, bacteria, and a fungus - and their vastly dissimilar biology, strongly suggests that the specificity of IRG proteins for certain PVs relates to a common feature of the host-derived vacuolar membranes rather than to a common ligand derived from the parasites themselves.

The proposed model builds on a hypothesis first formulated by Martens (Martens 2004) describing the specific targeting of IRG proteins to the *T. gondii* vacuole rather than to other cellular organelles. Martens proposed the existence of a self-derived “Factor X” present on the membranes of cellular organelles (endomembranes) that inhibits the accumulation and activation of IRG proteins on these sites, thereby protecting these organelles from GKS protein-mediated damage. In contrast, PVs lacking Factor X would be exposed to IRG accumulation and activation. This elegant "missing-self" model was confirmed later and Factor X was revealed to be the three GMS proteins, Irgm1, Irgm2 and Irgm3, which are bound to distinct subsets of endomembranes, where they act as inhibitory GDIs of the effector GKS proteins (Hunn et al. 2008).

In scheme A of Figure 4.2 it is shown that in IFNγ-induced cells, GMS proteins normally occupy endomembranes (Golgi, ER, lysosomes, mitochondria and lipid droplets are confirmed) in order to mark them as “self”. GKS proteins are kept in the GDP-bound state and shuttle between ER and cytosol. However, in the absence of one or more GMS proteins, GKS proteins form activated, GTP-bound assemblies in the cytoplasm that are associated with “unprotected” endomembranes [Figure 4.2 B, (Hunn et al. 2010; Haldar et al. 2013)]. GKS aggregates also form in cells deficient in certain regulatory autophagic proteins (see chapter 4.7), but the mechanistic link is still unknown.

However, GKS effector IRG proteins do not accumulate or activate on the plasma membrane, which is not protected by any GMS protein. Therefore, a new hypothetical inhibitor, here termed “Factor Y”, has to be introduced. This Factor Y would be associated with the plasma membrane and inhibit GKS activation at that location.

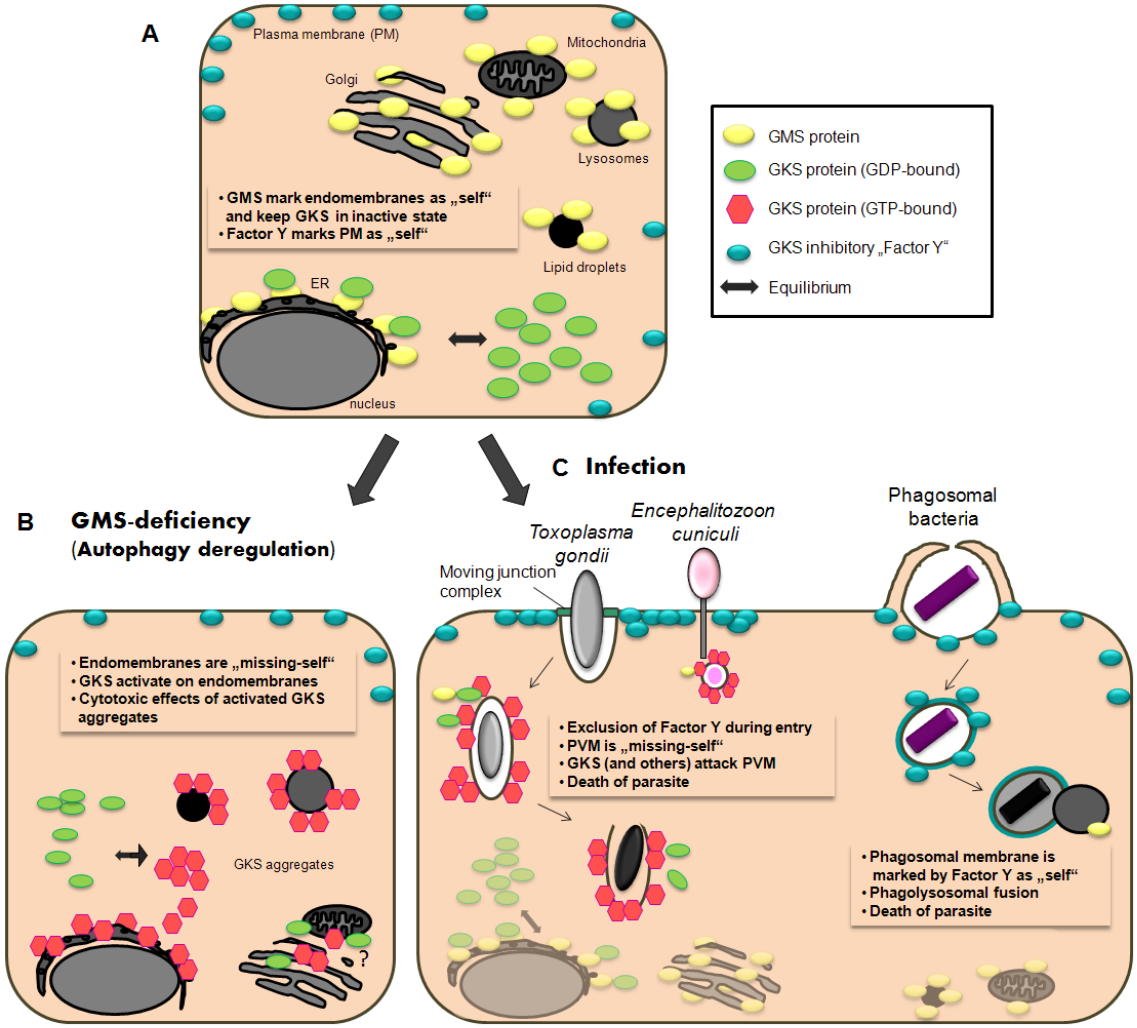


**Figure 4.2: Model of the IRG resistance system**
**(A)** In IFNγ-stimulated mouse cells GMS proteins localise mainly to endomembranes and keep GKS proteins in a GDP-bound inactive state. The plasma membrane is protected by an unknown Factor Y that inhibits GKS proteins-mediated damage. **(B)** In GMS-deficient cells, GKS proteins activate on unprotected endomembranes, thus forming cytotoxic aggregates. **(C)** During host cell infection by *T. gondii* or *E. cuniculi,* invagination of the plasma membrane creates a parasitophorous vacuole that excluded Factor Y and also does not carry GMS proteins. This "missing-self" is recognised by GKS proteins, which then activate and accumulate on the PVM leading to the PV disruption and parasite death. However, parasites entering via phagocytic mechanisms do not actively exclude Factor Y and are therefore targeted for endolysosomal degradation.

The IRG resistance system targets intracellular parasites such as *T. gondii* or *E. cuniculi* both of which reside in PV formed by invagination of the plasma membrane. The vacuoles resist fusion with the host endolysosomal system. Upon invasion of the host cell, GKS proteins reach their PV presumably by diffusion and recognise that the PVM misses "self proteins". Because the PVM is receptive to IRG loading immediately after parasite entry (Khaminets et al. 2010), the entry of the parasite and formation of the PV should entail loss of the Factor Y. For *T. gondii*, Factor Y might be excluded by the moving junction complex; for *E. cuniculi*,

the fast invagination with the very thin polar tube may lead to the exclusion of Factor Y due to physical force. GKS proteins switch to the GTP-bound active form, likely by a conformational change, and exposing the myristoylation motif, thereby enhancing the membrane-binding capacity. Oligomers of GKS proteins and GBP proteins start to accumulate on the PVM in a particular order, where they stabilise each other, ultimately leading to the deformation and destruction of the PVM (Figure 4.2 C left). In contrast, organisms that enter the cell by conventional phagocytosis are not engaged by the IRG resistance system, because Factor Y is not excluded during formation of the phagosomal membrane. The host cell can initiate lysosomal fusion to the bacterial phagosome, unless the parasite does not block this resistance mechanism (Figure 4.2 C right).

The IRG resistance system can thus recognise and distinguish intracellular parasites by missing-self motifs on vacuolar membranes that are not only deficient in regulatory GMS proteins, which usually protect endomembranes, but also have lost an inhibitory Factor Y during unusual, non-phagocytic host cell invasion processes.

# References


Abbas, A. K., A. H. Lichtman, et al. (2007). Cellular and Molecular Immunology. Philadelphia, Elsevier.

Al-Zeer, M. A., H. M. Al-Younes, et al. (2009). "IFN-gamma-inducible Irga6 mediates host resistance against Chlamydia trachomatis via autophagy." PLoS One **4**(2): e4588.

Al-Zeer, M. A., H. M. Al-Younes, et al. (2012). "Autophagy restricts Chlamydia trachomatis growth in human macrophages via IFNG-inducible guanylate binding proteins." Autophagy **9**(1): 50-62.

Alberts, B., A. Johnson, et al. (2007). Molecular Biology of the Cell.

Amani, V., A. M. Vigario, et al. (2000). "Involvement of IFN-gamma receptor-medicated signaling in pathology and anti-malarial immunity induced by Plasmodium berghei infection." Eur J Immunol **30**(6): 1646-55.

Bafica, A., C. G. Feng, et al. (2007). "The IFN-inducible GTPase LRG47 (Irgm1) negatively regulates TLR4-triggered proinflammatory cytokine production and prevents endotoxemia." J Immunol **179**(8): 5514-22.

Baldridge, M. T., K. Y. King, et al. (2010). "Quiescent haematopoietic stem cells are activated by IFN-gamma in response to chronic infection." Nature **465**(7299): 793-7.

Bancroft, G. J., R. D. Schreiber, et al. (1987). "A T cell-independent mechanism of macrophage activation by interferon-gamma." J Immunol **139**(4): 1104-7.

Barrangou, R., C. Fremaux, et al. (2007). "CRISPR provides acquired resistance against viruses in prokaryotes." Science **315**(5819): 1709-12.

Beauregard, K. E., K. D. Lee, et al. (1997). "pH-dependent perforation of macrophage phagosomes by listeriolysin O from Listeria monocytogenes." J Exp Med **186**(7): 1159-63.

Beck, J. R., A. L. Chen, et al. (2014). "RON5 Is Critical for Organization and Function of the Toxoplasma Moving Junction Complex." PLoS Pathog **10**(3): e1004025.

Behnke, M. S., S. J. Fentress, et al. (2012). "The polymorphic pseudokinase ROP5 controls virulence in Toxoplasma gondii by regulating the active kinase ROP18." PLoS Pathog **8**(11): e1002992.

Bekpen, C., J. P. Hunn, et al. (2005). "The interferon-inducible p47 (IRG) GTPases in vertebrates: loss of the cell autonomous resistance mechanism in the human lineage." Genome Biol **6**(11): R92.

Bekpen, C., T. Marques-Bonet, et al. (2009). "Death and resurrection of the human IRGM gene." PLoS Genet **5**(3): e1000403.

Bekpen, C., R. J. Xavier, et al. (2010). "Human IRGM gene "to be or not to be"." Semin Immunopathol **32**(4): 437-44.

Bernstein-Hanley, I., J. Coers, et al. (2006). "The p47 GTPases Igtp and Irgb10 map to the Chlamydia trachomatis susceptibility locus Ctrq-3 and mediate cellular resistance in mice." Proc Natl Acad Sci U S A **103**(38): 14092-7.

Betts, H. J., K. Wolf, et al. (2009). "Effector protein modulation of host cells: examples in the Chlamydia spp. arsenal." Curr Opin Microbiol **12**(1): 81-7.

Bigliardi, E. and L. Sacchi (2001). "Cell biology and invasion of the microsporidia." Microbes Infect **3**(5): 373-9.

Boehm, U., L. Guethlein, et al. (1998). "Two families of GTPases dominate the complex cellular response to IFN-gamma." J Immunol **161**(12): 6715-23.

Bogdan, C. and U. Schleicher (2006). "Production of interferon-gamma by myeloid cells--fact or fancy?" Trends Immunol **27**(6): 282-90.

Bohne, W., K. Bottcher, et al. (2011). "The parasitophorous vacuole of Encephalitozoon cuniculi: biogenesis and characteristics of the host cell-pathogen interface." Int J Med Microbiol **301**(5): 395-9.
Bohne, W., D. J. Ferguson, et al. (2000). "Developmental expression of a tandemly repeated, glycine- and serine-rich spore wall protein in the microsporidian pathogen Encephalitozoon cuniculi." Infect Immun **68**(4): 2268-75.
Borden, E. C., G. C. Sen, et al. (2007). "Interferons at age 50: past, current and future impact on biomedicine." Nat Rev Drug Discov **6**(12): 975-90.
Bougneres, L., J. Helft, et al. (2009). "A role for lipid bodies in the cross-presentation of phagocytosed antigens by MHC class I in dendritic cells." Immunity **31**(2): 232-44.
Bourne, H. R., D. A. Sanders, et al. (1991). "The GTPase superfamily: conserved structure and molecular mechanism." Nature **349**(6305): 117-27.
Butcher, B. A., R. I. Greene, et al. (2005). "p47 GTPases regulate Toxoplasma gondii survival in activated macrophages." Infect Immun **73**(6): 3278-86.
Campbell-Valois, F. X., M. Trost, et al. (2012). "Quantitative proteomics reveals that only a subset of the endoplasmic reticulum contributes to the phagosome." Mol Cell Proteomics **11**(7): M111 016378.
Canton, J., D. Neculai, et al. (2013). "Scavenger receptors in homeostasis and immunity." Nat Rev Immunol **13**(9): 621-34.
Carlow, D. A., J. Marth, et al. (1995). "Isolation of a gene encoding a developmentally regulated T cell-specific protein with a guanine nucleotide triphosphate-binding motif." J Immunol **154**(4): 1724-34.
Carlow, D. A., S. J. Teh, et al. (1998). "Specific antiviral activity demonstrated by TGTP, a member of a new family of interferon-induced GTPases." J Immunol **161**(5): 2348-55.
Carruthers, V. and J. C. Boothroyd (2007). "Pulling together: an integrated model of Toxoplasma cell invasion." Curr Opin Microbiol **10**(1): 83-9.
Chan, S. H., B. Perussia, et al. (1991). "Induction of interferon gamma production by natural killer cell stimulatory factor: characterization of the responder cells and synergy with other inducers." J Exp Med **173**(4): 869-79.
Chang, C. P., M. C. Yang, et al. (2011). "Concanavalin A/IFN-gamma triggers autophagy-related necrotic hepatocyte death through IRGM1-mediated lysosomal membrane disruption." PLoS One **6**(12): e28323.
Chang, Y. P., C. L. Chen, et al. (2011). "Autophagy facilitates an IFN-gamma response and signal transduction." Microbes Infect **13**(11): 888-94.
Charron, A. J. and L. D. Sibley (2004). "Molecular partitioning during host cell penetration by Toxoplasma gondii." Traffic **5**(11): 855-67.
Chen, G., M. H. Shaw, et al. (2009). "NOD-like receptors: role in innate immunity and inflammatory disease." Annu Rev Pathol **4**: 365-98.
Chen, X., X. Du, et al. (2010). "IFN-inducible p47 GTPases display differential responses to Schistosoma japonicum acute infection." Cell Mol Immunol **7**(1): 69-76.
Cheng, Y. S., C. E. Patterson, et al. (1991). "Interferon-induced guanylate-binding proteins lack an N(T)KXD consensus motif and bind GMP in addition to GDP and GTP." Mol Cell Biol **11**(9): 4717-25.
Choudhry, N., D. S. Korbel, et al. (2009). "Interferon-gamma-mediated activation of enterocytes in immunological control of Encephalitozoon intestinalis infection." Parasite Immunol **31**(1): 2-9.
Clifton, D. R., K. A. Fields, et al. (2004). "A chlamydial type III translocated protein is tyrosine-phosphorylated at the site of entry and associated with recruitment of actin." Proc Natl Acad Sci U S A **101**(27): 10166-71.

Coers, J., I. Bernstein-Hanley, et al. (2008). "Chlamydia muridarum evades growth restriction by the IFN-gamma-inducible host resistance factor Irgb10." J Immunol **180**(9): 6237-45.
Coers, J., D. C. Gondek, et al. (2011). "Compensatory T cell responses in IRG-deficient mice prevent sustained Chlamydia trachomatis infections." PLoS Pathog **7**(6): e1001346.
Collazo, C. M., G. S. Yap, et al. (2001). "Inactivation of LRG-47 and IRG-47 reveals a family of interferon gamma-inducible genes with essential, pathogen-specific roles in resistance to infection." J Exp Med **194**(2): 181-8.
Cooper, A. M., D. K. Dalton, et al. (1993). "Disseminated tuberculosis in interferon gamma gene-disrupted mice." J Exp Med **178**(6): 2243-7.
Cooper, M. D. and M. N. Alder (2006). "The evolution of adaptive immune systems." Cell **124**(4): 815-22.
Coppens, I., J. D. Dunn, et al. (2006). "Toxoplasma gondii sequesters lysosomes from mammalian hosts in the vacuolar space." Cell **125**(2): 261-74.
Corradi, N. and P. Keeling (2009). "Microsporidia: a journey through radical taxonomical revisions." Fungal Biology Reviews **23**(1-2): 1-8.
Cotter, T. W., K. H. Ramsey, et al. (1997). "Dissemination of Chlamydia trachomatis chronic genital tract infection in gamma interferon gene knockout mice." Infect Immun **65**(6): 2145-52.
Couzinet, S., E. Cejas, et al. (2000). "Phagocytic uptake of Encephalitozoon cuniculi by nonprofessional phagocytes." Infect Immun **68**(12): 6939-45.
Crawford, M. J., N. Thomsen-Zieger, et al. (2006). "Toxoplasma gondii scavenges host-derived lipoic acid despite its de novo synthesis in the apicoplast." Embo J **25**(13): 3214-22.
Dalton, D. K., S. Pitts-Meek, et al. (1993). "Multiple defects of immune cell function in mice with disrupted interferon-gamma genes." Science **259**(5102): 1739-42.
Daubener, W., B. Spors, et al. (2001). "Restriction of Toxoplasma gondii growth in human brain microvascular endothelial cells by activation of indoleamine 2,3-dioxygenase." Infect Immun **69**(10): 6527-31.
Dautry-Varsat, A., M. E. Balana, et al. (2004). "Chlamydia--host cell interactions: recent advances on bacterial entry and intracellular development." Traffic **5**(8): 561-70.
Dautry-Varsat, A., A. Subtil, et al. (2005). "Recent insights into the mechanisms of Chlamydia entry." Cell Microbiol **7**(12): 1714-22.
de Melo, E. J., T. U. de Carvalho, et al. (1992). "Penetration of Toxoplasma gondii into host cells induces changes in the distribution of the mitochondria and the endoplasmic reticulum." Cell Struct Funct **17**(5): 311-7.
de Souza, A. P., B. Tang, et al. (2003). "Absence of interferon-gamma-inducible gene IGTP does not significantly alter the development of chagasic cardiomyopathy in mice infected with Trypanosoma cruzi (Brazil strain)." J Parasitol **89**(6): 1237-9.
Deghmane, A. E., H. Soualhine, et al. (2007). "Lipoamide dehydrogenase mediates retention of coronin-1 on BCG vacuoles, leading to arrest in phagosome maturation." J Cell Sci **120**(Pt 16): 2796-806.
Degrandi, D., C. Konermann, et al. (2007). "Extensive characterization of IFN-induced GTPases mGBP1 to mGBP10 involved in host defense." J Immunol **179**(11): 7729-40.
Degrandi, D., E. Kravets, et al. (2012). "Murine guanylate binding protein 2 (mGBP2) controls Toxoplasma gondii replication." Proc Natl Acad Sci U S A **110**(1): 294-9.
Dehoux, P., R. Flores, et al. (2011). "Multi-genome identification and characterization of chlamydiae-specific type III secretion substrates: the Inc proteins." BMC Genomics **12**: 109.

Delorme-Walker, V., M. Abrivard, et al. (2012). "Toxofilin upregulates the host cortical actin cytoskeleton dynamics, facilitating Toxoplasma invasion." J Cell Sci **125**(Pt 18): 4333-42.

Deretic, V. (2011). "Autophagy in immunity and cell-autonomous defense against intracellular microbes." Immunol Rev **240**(1): 92-104.

Deretic, V., T. Saitoh, et al. (2013). "Autophagy in infection, inflammation and immunity." Nat Rev Immunol **13**(10): 722-37.

Didier, E. S. (1995). "Reactive nitrogen intermediates implicated in the inhibition of Encephalitozoon cuniculi (phylum microspora) replication in murine peritoneal macrophages." Parasite Immunol **17**(8): 405-12.

Didier, E. S., L. C. Bowers, et al. (2010). "Reactive nitrogen and oxygen species, and iron sequestration contribute to macrophage-mediated control of Encephalitozoon cuniculi (Phylum Microsporidia) infection in vitro and in vivo." Microbes Infect **12**(14-15): 1244-51.

Didier, E. S., C. R. Vossbrinck, et al. (1995). "Identification and characterization of three Encephalitozoon cuniculi strains." Parasitology **111 ( Pt 4)**: 411-21.

Didier, E. S. and L. M. Weiss (2011). "Microsporidiosis: not just in AIDS patients." Curr Opin Infect Dis **24**(5): 490-5.

Doherty, T. M. and A. Sher (1997). "Defects in cell-mediated immunity affect chronic, but not innate, resistance of mice to Mycobacterium avium infection." J Immunol **158**(10): 4822-31.

Du, X., J. Wu, et al. (2011). "Upregulated expression of cytotoxicity-related genes in IFN-gamma knockout mice with Schistosoma japonicum infection." J Biomed Biotechnol **2011**: 864945.

Dubremetz, J. F. and D. J. Ferguson (2009). "The role played by electron microscopy in advancing our understanding of Toxoplasma gondii and other apicomplexans." Int J Parasitol **39**(8): 883-93.

Eisenacher, K. and A. Krug (2012). "Regulation of RLR-mediated innate immune signaling--it is all about keeping the balance." Eur J Cell Biol **91**(1): 36-47.

El Fakhry, Y., A. Achbarou, et al. (2001). "Resistance to Encephalitozoon intestinalis is associated with interferon-gamma and interleukin-2 cytokines in infected mice." Parasite Immunol **23**(6): 297-303.

El Fakhry, Y., A. Achbarou, et al. (2001). "Dissemination of Encephalitozoon intestinalis, a causative agent of human microsporidiosis, in IFN-gamma receptor knockout mice." Parasite Immunol **23**(1): 19-25.

Endo, T., B. Pelster, et al. (1981). "Infection of murine peritoneal macrophages with Toxoplasma gondii exposed to ultraviolet light." Z Parasitenkd **65**(2): 121-9.

Farrar, M. A. and R. D. Schreiber (1993). "The molecular cell biology of interferon-gamma and its receptor." Annu Rev Immunol **11**: 571-611.

Fasshauer, V., U. Gross, et al. (2005). "The parasitophorous vacuole membrane of Encephalitozoon cuniculi lacks host cell membrane proteins immediately after invasion." Eukaryot Cell **4**(1): 221-4.

Feng, C. G., C. M. Collazo-Custodio, et al. (2004). "Mice deficient in LRG-47 display increased susceptibility to mycobacterial infection associated with the induction of lymphopenia." J Immunol **172**(2): 1163-8.

Feng, C. G., D. C. Weksberg, et al. (2008). "The p47 GTPase Lrg-47 (Irgm1) links host defense and hematopoietic stem cell proliferation." Cell Stem Cell **2**(1): 83-9.

Feng, C. G., L. Zheng, et al. (2008). "The immunity-related GTPase Irgm1 promotes the expansion of activated CD4+ T cell populations by preventing interferon-gamma-induced cell death." Nat Immunol **9**(11): 1279-87.

Feng, C. G., L. Zheng, et al. (2009). "Interferon-inducible immunity-related GTPase Irgm1 regulates IFN gamma-dependent host defense, lymphocyte survival and autophagy." Autophagy **5**(2): 232-4.
Fentress, S. J., M. S. Behnke, et al. (2010). "Phosphorylation of immunity-related GTPases by a Toxoplasma gondii-secreted kinase promotes macrophage survival and virulence." Cell Host Microbe **8**(6): 484-95.
Fischer, J., D. Tran, et al. (2008). "Kinetics of Encephalitozoon spp. infection of human macrophages." J Parasitol **94**(1): 169-75.
Fleckenstein, M. C. (2012). The Toxoplasma gondii pseudokinase ROP5 is crucial for inactivation of the murine IRG resistance system, University of Cologne.
Fleckenstein, M. C., M. L. Reese, et al. (2012). "A Toxoplasma gondii pseudokinase inhibits host IRG resistance proteins." PLoS Biol **10**(7): e1001358.
Flynn, J. L., J. Chan, et al. (1993). "An essential role for interferon gamma in resistance to Mycobacterium tuberculosis infection." J Exp Med **178**(6): 2249-54.
Folch, J., M. Lees, et al. (1957). "A simple method for the isolation and purification of total lipides from animal tissues." J Biol Chem **226**(1): 497-509.
Franzen, C., A. Muller, et al. (2005). "Cell invasion and intracellular fate of Encephalitozoon cuniculi (Microsporidia)." Parasitology **130**(Pt 3): 285-92.
Frucht, D. M., T. Fukao, et al. (2001). "IFN-gamma production by antigen-presenting cells: mechanisms emerge." Trends Immunol **22**(10): 556-60.
Gazzinelli, R. T., R. Mendonca-Neto, et al. (2014). "Innate Resistance against Toxoplasma gondii: An Evolutionary Tale of Mice, Cats, and Men." Cell Host Microbe **15**(2): 132-138.
Gazzinelli, R. T., M. Wysocka, et al. (1994). "Parasite-induced IL-12 stimulates early IFN-gamma synthesis and resistance during acute infection with Toxoplasma gondii." J Immunol **153**(6): 2533-43.
Ghosh, A., G. J. Praefcke, et al. (2006). "How guanylate-binding proteins achieve assembly-stimulated processive cleavage of GTP to GMP." Nature **440**(7080): 101-4.
Ghosh, A., R. Uthaiah, et al. (2004). "Crystal structure of IIGP1: a paradigm for interferon-inducible p47 resistance GTPases." Mol Cell **15**(5): 727-39.
Gilly, M., M. A. Damore, et al. (1996). "A promoter ISRE and dual 5' YY1 motifs control IFN-gamma induction of the IRG-47 G-protein gene." Gene **179**(2): 237-44.
Gilly, M. and R. Wall (1992). "The IRG-47 gene is IFN-gamma induced in B cells and encodes a protein with GTP-binding motifs." J Immunol **148**(10): 3275-81.
Goldszmid, R. S., I. Coppens, et al. (2009). "Host ER-parasitophorous vacuole interaction provides a route of entry for antigen cross-presentation in Toxoplasma gondii-infected dendritic cells." J Exp Med **206**(2): 399-410.
Gonzalez, V., A. Combe, et al. (2009). "Host cell entry by apicomplexa parasites requires actin polymerization in the host cell." Cell Host Microbe **5**(3): 259-72.
Günther, S. (2011). Membranrekrutierung von humanem Guanylat bindendem Protein 1. Cologne, University of Cologne. **Bachelor of Science**.
Guo, Z. G., U. Gross, et al. (1997). "Toxoplasma gondii virulence markers identified by random amplified polymorphic DNA polymerase chain reaction." Parasitol Res **83**(5): 458-63.
Gupta, M., P. Greer, et al. (2005). "CD8-mediated protection against Ebola virus infection is perforin dependent." J Immunol **174**(7): 4198-202.
Gustafson, P. V., H. D. Agar, et al. (1954). "An electron microscope study of Toxoplasma." Am J Trop Med Hyg **3**(6): 1008-22.
Gutierrez, M. G., S. S. Master, et al. (2004). "Autophagy is a defense mechanism inhibiting BCG and Mycobacterium tuberculosis survival in infected macrophages." Cell **119**(6): 753-66.

Hacker, C., M. Howell, et al. (2014). "Strategies for maximizing ATP supply in the microsporidian Encephalitozoon cuniculi: direct binding of mitochondria to the parasitophorous vacuole and clustering of the mitochondrial porin VDAC." Cell Microbiol **16**(4): 565-79.

Haldar, A. K., A. S. Piro, et al. (2014). "The E2-like conjugation enzyme Atg3 promotes binding of IRG and Gbp proteins to Chlamydia- and Toxoplasma-containing vacuoles and host resistance." PLoS One **9**(1): e86684.

Haldar, A. K., H. A. Saka, et al. (2013). "IRG and GBP host resistance factors target aberrant, "non-self" vacuoles characterized by the missing of "self" IRGM proteins." PLoS Pathog **9**(6): e1003414.

Haller, O., S. Stertz, et al. (2007). "The Mx GTPase family of interferon-induced antiviral proteins." Microbes Infect **9**(14-15): 1636-43.

Halonen, S. K., G. A. Taylor, et al. (2001). "Gamma interferon-induced inhibition of Toxoplasma gondii in astrocytes is mediated by IGTP." Infect Immun **69**(9): 5573-6.

Handa, K., R. Suzuki, et al. (1983). "Natural killer (NK) cells as a responder to interleukin 2 (IL 2). II. IL 2-induced interferon gamma production." J Immunol **130**(2): 988-92.

He, S., C. Wang, et al. (2012). "Immune-related GTPase M (IRGM1) regulates neuronal autophagy in a mouse model of stroke." Autophagy **8**(11): 1621-7.

Henry, S. C., X. Daniell, et al. (2007). "Impaired macrophage function underscores susceptibility to Salmonella in mice lacking Irgm1 (LRG-47)." J Immunol **179**(10): 6963-72.

Henry, S. C., X. G. Daniell, et al. (2009). "Balance of Irgm protein activities determines IFN-gamma-induced host defense." J Leukoc Biol **85**(5): 877-85.

Henry, S. C., E. A. Schmidt, et al. (2014). "Palmitoylation of the Immunity Related GTPase, Irgm1: Impact on Membrane Localization and Ability to Promote Mitochondrial Fission." PLoS One **9**(4): e95021.

Hermanns, T. (2014). Characterization of Toxoplasma gondii protein GRA7 as the first dense granule-secreted IRG-specific virulence factor. Cologne, University of Cologne. **Master of Science**.

Heuer, D., A. Rejman Lipinski, et al. (2009). "Chlamydia causes fragmentation of the Golgi compartment to ensure reproduction." Nature **457**(7230): 731-5.

Howard, J. (2008). "The IRG proteins: a function in search of a mechanism." Immunobiology **213**(3-4): 367-75.

Howard, J. C. (2007). "Introduction: cell-autonomous immunity." Microbes Infect **9**(14-15): 1633-5.

Howard, J. C., J. P. Hunn, et al. (2011). "The IRG protein-based resistance mechanism in mice and its relation to virulence in Toxoplasma gondii." Curr Opin Microbiol **14**(4): 414-21.

Hug, H., M. Costas, et al. (1988). "Organization of the murine Mx gene and characterization of its interferon- and virus-inducible promoter." Mol Cell Biol **8**(8): 3065-79.

Hunn, J. P. (2007). Evolution and Cellular Resistance Mechanisms of the Immunity-Related GTPases, University of Cologne.

Hunn, J. P., C. G. Feng, et al. (2011). "The immunity-related GTPases in mammals: a fast-evolving cell-autonomous resistance system against intracellular pathogens." Mamm Genome **22**(1-2): 43-54.

Hunn, J. P. and J. C. Howard (2010). "The mouse resistance protein Irgm1 (LRG-47): a regulator or an effector of pathogen defense?" PLoS Pathog **6**(7): e1001008.

Hunn, J. P., S. Koenen-Waisman, et al. (2008). "Regulatory interactions between IRG resistance GTPases in the cellular response to Toxoplasma gondii." Embo J **27**(19): 2495-509.

Hunter, C. A. and L. D. Sibley (2012). "Modulation of innate immunity by Toxoplasma gondii virulence effectors." Nat Rev Microbiol **10**(11): 766-78.
Hybiske, K. and R. S. Stephens (2007). "Mechanisms of Chlamydia trachomatis entry into nonphagocytic cells." Infect Immun **75**(8): 3925-34.
Inoue, S., M. Niikura, et al. (2013). "Roles of IFN-gamma and gammadelta T Cells in Protective Immunity Against Blood-Stage Malaria." Front Immunol **4**: 258.
Isaacs, A. and J. Lindenmann (1957). "Virus interference. I. The interferon." Proc R Soc Lond B Biol Sci **147**(927): 258-67.
Isaacs, A., J. Lindenmann, et al. (1957). "Virus interference. II. Some properties of interferon." Proc R Soc Lond B Biol Sci **147**(927): 268-73.
Itoh, T., K. S. Erdmann, et al. (2005). "Dynamin and the actin cytoskeleton cooperatively regulate plasma membrane invagination by BAR and F-BAR proteins." Dev Cell **9**(6): 791-804.
Janeway, C. A., Jr. (1992). "The immune system evolved to discriminate infectious nonself from noninfectious self." Immunol Today **13**(1): 11-6.
Jelinek, J., J. Salat, et al. (2007). "Effects of interferon gamma and specific polyclonal antibody on the infection of murine peritoneal macrophages and murine macrophage cell line PMJ2-R with Encephalitozoon cuniculi." Folia Parasitol (Praha) **54**(3): 172-6.
Jones, T. C. and J. G. Hirsch (1972). "The interaction between Toxoplasma gondii and mammalian cells. II. The absence of lysosomal fusion with phagocytic vacuoles containing living parasites." J Exp Med **136**(5): 1173-94.
Jutras, I., M. Houde, et al. (2008). "Modulation of the phagosome proteome by interferon-gamma." Mol Cell Proteomics **7**(4): 697-715.
Katinka, M. D., S. Duprat, et al. (2001). "Genome sequence and gene compaction of the eukaryote parasite Encephalitozoon cuniculi." Nature **414**(6862): 450-3.
Kawai, T. and S. Akira (2010). "The role of pattern-recognition receptors in innate immunity: update on Toll-like receptors." Nat Immunol **11**(5): 373-84.
Khaminets, A., J. P. Hunn, et al. (2010). "Coordinated loading of IRG resistance GTPases on to the Toxoplasma gondii parasitophorous vacuole." Cell Microbiol **12**(7): 939-61.
Khan, I. A. and M. Moretto (1999). "Role of gamma interferon in cellular immune response against murine Encephalitozoon cuniculi infection." Infect Immun **67**(4): 1887-93.
Kim, B. H., A. R. Shenoy, et al. (2012). "IFN-inducible GTPases in host cell defense." Cell Host Microbe **12**(4): 432-44.
Kim, B. H., A. R. Shenoy, et al. (2012). "A family of IFN-gamma-inducible 65-kD GTPases protects against bacterial infection." Science **332**(6030): 717-21.
King, K. Y., M. T. Baldridge, et al. (2011). "Irgm1 protects hematopoietic stem cells by negative regulation of IFN signaling." Blood **118**(6): 1525-33.
Klamp, T., U. Boehm, et al. (2003). "A giant GTPase, very large inducible GTPase-1, is inducible by IFNs." J Immunol **171**(3): 1255-65.
Kleineke, J., C. Duls, et al. (1979). "Subcellular compartmentation of guanine nucleotides and functional relationships between the adenine and guanine nucleotide systems in isolated hepatocytes." FEBS Lett **107**(1): 198-202.
Koga, R., S. Hamano, et al. (2006). "TLR-dependent induction of IFN-beta mediates host defense against Trypanosoma cruzi." J Immunol **177**(10): 7059-66.
Konen-Waisman, S. and J. C. Howard (2007). "Cell-autonomous immunity to Toxoplasma gondii in mouse and man." Microbes Infect **9**(14-15): 1652-61.
Kravets, E., D. Degrandi, et al. (2012). "The GTPase activity of murine guanylate-binding protein 2 (mGBP2) controls the intracellular localization and recruitment to the parasitophorous vacuole of Toxoplasma gondii." J Biol Chem **287**(33): 27452-66.
Kutateladze, T. G. (2010). "Translation of the phosphoinositide code by PI effectors." Nat Chem Biol **6**(7): 507-13.

Laemmli, U. K. (1970). "Cleavage of structural proteins during the assembly of the head of bacteriophage T4." Nature **227**(5259): 680-5.
Lafuse, W. P., D. Brown, et al. (1995). "Cloning and characterization of a novel cDNA that is IFN-gamma-induced in mouse peritoneal macrophages and encodes a putative GTP-binding protein." J Leukoc Biol **57**(3): 477-83.
Lapaque, N., O. Takeuchi, et al. (2006). "Differential inductions of TNF-alpha and IGTP, IIGP by structurally diverse classic and non-classic lipopolysaccharides." Cell Microbiol **8**(3): 401-13.
Lee, B. Y., D. Jethwaney, et al. (2010). "The Mycobacterium bovis bacille Calmette-Guerin phagosome proteome." Mol Cell Proteomics **9**(1): 32-53.
Leipe, D. D., Y. I. Wolf, et al. (2002). "Classification and evolution of P-loop GTPases and related ATPases." J Mol Biol **317**(1): 41-72.
Leitch, G. J., T. L. Ward, et al. (2005). "Apical spore phagocytosis is not a significant route of infection of differentiated enterocytes by Encephalitozoon intestinalis." Infect Immun **73**(11): 7697-704.
Li, G., J. Zhang, et al. (2009). "The evolutionarily dynamic IFN-inducible GTPase proteins play conserved immune functions in vertebrates and cephalochordates." Mol Biol Evol **26**(7): 1619-30.
Li, Q., C. Jagannath, et al. (2010). "Analysis of phagosomal proteomes: from latex-bead to bacterial phagosomes." Proteomics **10**(22): 4098-116.
Liesenfeld, P., Zerrahn, Han, Heinrich, Muñoz, Kaiser, Aebischer, Buch, Waisman, Reichmann, Utermöhlen, von Stebut, von Loewenich, Bogdan, Specht, Saeftel, Hoerauf, Mota, Könen-Waisman, Kaufmann, Howard (2011). "The IFN-γ-inducible GTPase, Irga6, protects mice against Toxoplasma gondii but not against Plasmodium berghei and some other intracellular pathogens." PLoS One **in press**.
Lilue, J., U. B. Muller, et al. (2013). "Reciprocal virulence and resistance polymorphism in the relationship between Toxoplasma gondii and the house mouse." Elife **2**: e01298.
Lim, D., D. A. Gold, et al. (2013). "Structure of the Toxoplasma gondii ROP18 kinase domain reveals a second ligand binding pocket required for acute virulence." J Biol Chem **288**(48): 34968-80.
Ling, Y. M., M. H. Shaw, et al. (2006). "Vacuolar and plasma membrane stripping and autophagic elimination of Toxoplasma gondii in primed effector macrophages." J Exp Med **203**(9): 2063-71.
Liu, B., A. S. Gulati, et al. (2013). "Irgm1-deficient mice exhibit Paneth cell abnormalities and increased susceptibility to acute intestinal inflammation." Am J Physiol Gastrointest Liver Physiol **305**(8): G573-84.
Liu, Z., H. M. Zhang, et al. (2008). "Focal adhesion kinase mediates the interferon-gamma-inducible GTPase-induced phosphatidylinositol 3-kinase/Akt survival pathway and further initiates a positive feedback loop of NF-kappaB activation." Cell Microbiol **10**(9): 1787-800.
Lu, X. C., Y. Tao, et al. (2014). "Association between variants of the autophagy related gene--IRGM and susceptibility to Crohn's disease and ulcerative colitis: a meta-analysis." PLoS One **8**(11): e80602.
Lubitz, F. P., D. Degrandi, et al. (2013). "In astrocytes the accumulation of the immunity-related GTPases Irga6 and Irgb6 at the vacuole of Toxoplasma gondii is dependent on the parasite virulence." ScientificWorldJournal **2013**: 480231.
MacMicking, J. D. (2004). "IFN-inducible GTPases and immunity to intracellular pathogens." Trends Immunol **25**(11): 601-9.
MacMicking, J. D. (2012). "Interferon-inducible effector mechanisms in cell-autonomous immunity." Nat Rev Immunol **12**(5): 367-82.

MacMicking, J. D., G. A. Taylor, et al. (2003). "Immune control of tuberculosis by IFN-gamma-inducible LRG-47." Science **302**(5645): 654-9.
Maiuri, M. C., E. Zalckvar, et al. (2007). "Self-eating and self-killing: crosstalk between autophagy and apoptosis." Nat Rev Mol Cell Biol **8**(9): 741-52.
Makiuchi, T. and T. Nozaki (2013). "Highly divergent mitochondrion-related organelles in anaerobic parasitic protozoa." Biochimie.
Martens, S. (2004). Cell-Biology of Interferon Inducible GTPases, University of Cologne.
Martens, S. and J. Howard (2006). "The interferon-inducible GTPases." Annu Rev Cell Dev Biol **22**: 559-89.
Martens, S., I. Parvanova, et al. (2005). "Disruption of Toxoplasma gondii parasitophorous vacuoles by the mouse p47-resistance GTPases." PLoS Pathog **1**(3): e24.
Martens, S., K. Sabel, et al. (2004). "Mechanisms regulating the positioning of mouse p47 resistance GTPases LRG-47 and IIGP1 on cellular membranes: retargeting to plasma membrane induced by phagocytosis." J Immunol **173**(4): 2594-606.
Mathews, A., A. Hotard, et al. (2009). "Innate immune responses to Encephalitozoon species infections." Microbes Infect **11**(12): 905-11.
Matsuzawa, T., B. H. Kim, et al. (2012). "IFN-gamma Elicits Macrophage Autophagy via the p38 MAPK Signaling Pathway." J Immunol **189**(2): 813-8.
Matzinger, P. (1994). "Tolerance, danger, and the extended family." Annu Rev Immunol **12**: 991-1045.
Matzinger, P. (2002). "The danger model: a renewed sense of self." Science **296**(5566): 301-5.
McCarroll, S. A., A. Huett, et al. (2008). "Deletion polymorphism upstream of IRGM associated with altered IRGM expression and Crohn's disease." Nat Genet **40**(9): 1107-12.
Medzhitov, R. (2009). "Approaching the asymptote: 20 years later." Immunity **30**(6): 766-75.
Melzer, T., A. Duffy, et al. (2008). "The gamma interferon (IFN-gamma)-inducible GTP-binding protein IGTP is necessary for toxoplasma vacuolar disruption and induces parasite egression in IFN-gamma-stimulated astrocytes." Infect Immun **76**(11): 4883-94.
Meunier, E., M. S. Dick, et al. (2014). "Caspase-11 activation requires lysis of pathogen-containing vacuoles by IFN-induced GTPases." Nature.
Michailowsky, V., N. M. Silva, et al. (2001). "Pivotal role of interleukin-12 and interferon-gamma axis in controlling tissue parasitism and inflammation in the heart and central nervous system during Trypanosoma cruzi infection." Am J Pathol **159**(5): 1723-33.
Mital, J., M. Meissner, et al. (2005). "Conditional expression of Toxoplasma gondii apical membrane antigen-1 (TgAMA1) demonstrates that TgAMA1 plays a critical role in host cell invasion." Mol Biol Cell **16**(9): 4341-9.
Mital, J., N. J. Miller, et al. (2013). "Role for chlamydial inclusion membrane proteins in inclusion membrane structure and biogenesis." PLoS One **8**(5): e63426.
Miyairi, I., V. R. Tatireddigari, et al. (2007). "The p47 GTPases Iigp2 and Irgb10 regulate innate immunity and inflammation to murine Chlamydia psittaci infection." J Immunol **179**(3): 1814-24.
Modiano, N., Y. E. Lu, et al. (2005). "Golgi targeting of human guanylate-binding protein-1 requires nucleotide binding, isoprenylation, and an IFN-gamma-inducible cofactor." Proc Natl Acad Sci U S A **102**(24): 8680-5.
Mordue, D. G., N. Desai, et al. (1999). "Invasion by Toxoplasma gondii establishes a moving junction that selectively excludes host cell plasma membrane proteins on the basis of their membrane anchoring." J Exp Med **190**(12): 1783-92.

Mordue, D. G., S. Hakansson, et al. (1999). "Toxoplasma gondii resides in a vacuole that avoids fusion with host cell endocytic and exocytic vesicular trafficking pathways." Exp Parasitol **92**(2): 87-99.

Mordue, D. G. and L. D. Sibley (1997). "Intracellular fate of vacuoles containing Toxoplasma gondii is determined at the time of formation and depends on the mechanism of entry." J Immunol **159**(9): 4452-9.

Morisaki, J. H., J. E. Heuser, et al. (1995). "Invasion of Toxoplasma gondii occurs by active penetration of the host cell." J Cell Sci **108 ( Pt 6)**: 2457-64.

Mosmann, T. R. and R. L. Coffman (1989). "TH1 and TH2 cells: different patterns of lymphokine secretion lead to different functional properties." Annu Rev Immunol **7**: 145-73.

Munder, M., M. Mallo, et al. (1998). "Murine macrophages secrete interferon gamma upon combined stimulation with interleukin (IL)-12 and IL-18: A novel pathway of autocrine macrophage activation." J Exp Med **187**(12): 2103-8.

Murphy, K. M. (2012). Janeway's Immunobiology. New York, Garland Science.

Nantais, D. E., M. Schwemmle, et al. (1996). "Prenylation of an interferon-gamma-induced GTP-binding protein: the human guanylate binding protein, huGBP1." J Leukoc Biol **60**(3): 423-31.

Nathan, C. and A. Cunningham-Bussel (2013). "Beyond oxidative stress: an immunologist's guide to reactive oxygen species." Nat Rev Immunol **13**(5): 349-61.

Nelson, D. E., D. P. Virok, et al. (2005). "Chlamydial IFN-gamma immune evasion is linked to host infection tropism." Proc Natl Acad Sci U S A **102**(30): 10658-63.

Neun, R., M. F. Richter, et al. (1996). "GTPase properties of the interferon-induced human guanylate-binding protein 2." FEBS Lett **390**(1): 69-72.

Niedelman, W., D. A. Gold, et al. (2012). "The rhoptry proteins ROP18 and ROP5 mediate Toxoplasma gondii evasion of the murine, but not the human, interferon-gamma response." PLoS Pathog **8**(6): e1002784.

Nishikawa, Y., K. Tragoolpua, et al. (2001). "In the absence of endogenous gamma interferon, mice acutely infected with Neospora caninum succumb to a lethal immune response characterized by inactivation of peritoneal macrophages." Clin Diagn Lab Immunol **8**(4): 811-6.

Ohshima, J., Y. Lee, et al. (2014). "Role of Mouse and Human Autophagy Proteins in IFN-gamma-Induced Cell-Autonomous Responses against Toxoplasma gondii." J Immunol **192**(7): 3328-35.

Ohteki, T., T. Fukao, et al. (1999). "Interleukin 12-dependent interferon gamma production by CD8alpha+ lymphoid dendritic cells." J Exp Med **189**(12): 1981-6.

Orlik, J., K. Bottcher, et al. (2010). "Germination of phagocytosed E. cuniculi spores does not significantly contribute to parasitophorous vacuole formation in J774 cells." Parasitol Res **106**(3): 753-5.

Papic, N. (2007). Biochemical Analysis of the Immunity-Related GTPase Irga6 In Vivo and In Vitro; The Role of the Myristoyl Group, University of Cologne.

Papic, N., J. P. Hunn, et al. (2008). "Inactive and active states of the interferon-inducible resistance GTPase, Irga6, in vivo." J Biol Chem **283**(46): 32143-51.

Paracer, S. and V. Ahmadjian (2000). Symbiosis : An Introduction to Biological Associations. New York, Oxford University Press.

Pawlowski, N., A. Khaminets, et al. (2011). "The activation mechanism of Irga6, an interferon-inducible GTPase contributing to mouse resistance against Toxoplasma gondii." BMC Biol **9**: 7.

Pfefferkorn, E. R. (1984). "Interferon gamma blocks the growth of Toxoplasma gondii in human fibroblasts by inducing the host cells to degrade tryptophan." Proc Natl Acad Sci U S A **81**(3): 908-12.

Pilla, D. M., J. A. Hagar, et al. (2014). "Guanylate binding proteins promote caspase-11-dependent pyroptosis in response to cytoplasmic LPS." Proc Natl Acad Sci U S A **111**(16): 6046-51.

Pomeroy, C., D. Delong, et al. (1998). "Role of interferon-gamma in murine cytomegalovirus infection." J Lab Clin Med **132**(2): 124-33.

Praefcke, G. J., M. Geyer, et al. (1999). "Nucleotide-binding characteristics of human guanylate-binding protein 1 (hGBP1) and identification of the third GTP-binding motif." J Mol Biol **292**(2): 321-32.

Praefcke, G. J. and H. T. McMahon (2004). "The dynamin superfamily: universal membrane tubulation and fission molecules?" Nat Rev Mol Cell Biol **5**(2): 133-47.

Prakash, B., G. J. Praefcke, et al. (2000). "Structure of human guanylate-binding protein 1 representing a unique class of GTP-binding proteins." Nature **403**(6769): 567-71.

Pucadyil, T. J. and S. L. Schmid (2009). "Conserved functions of membrane active GTPases in coated vesicle formation." Science **325**(5945): 1217-20.

Reid, A. J., S. J. Vermont, et al. (2012). "Comparative genomics of the apicomplexan parasites Toxoplasma gondii and Neospora caninum: Coccidia differing in host range and transmission strategy." PLoS Pathog **8**(3): e1002567.

Ritchie, J. A., A. Rupper, et al. (2012). "Host interferon-gamma inducible protein contributes to Brucella survival." Front Cell Infect Microbiol **2**: 55.

Rohde, C. (2006). Genetic and Functional Studies on the Conserved IRG (Immunity-related GTPase) Protein IRGC (CINEMA), University of Cologne.

Romano, J. D. and I. Coppens (2013). "Host Organelle Hijackers: a similar modus operandi for Toxoplasma gondii and Chlamydia trachomatis: co-infection model as a tool to investigate pathogenesis." Pathog Dis **69**(2): 72-86.

Romano, J. D., S. Sonda, et al. (2012). "Toxoplasma gondii salvages sphingolipids from the host Golgi through the rerouting of selected Rab vesicles to the parasitophorous vacuole." Mol Biol Cell **24**(12): 1974-95.

Ronnebaumer, K., U. Gross, et al. (2008). "The nascent parasitophorous vacuole membrane of Encephalitozoon cuniculi is formed by host cell lipids and contains pores which allow nutrient uptake." Eukaryot Cell **7**(6): 1001-8.

Roshick, C., H. Wood, et al. (2006). "Comparison of gamma interferon-mediated antichlamydial defense mechanisms in human and mouse cells." Infect Immun **74**(1): 225-38.

Roy, C. R. and E. S. Mocarski (2007). "Pathogen subversion of cell-intrinsic innate immunity." Nat Immunol **8**(11): 1179-87.

Rusinova, I., S. Forster, et al. (2013). "Interferome v2.0: an updated database of annotated interferon-regulated genes." Nucleic Acids Res **41**(Database issue): D1040-6.

Saban, M. R., M. A. O'Donnell, et al. (2008). "Molecular networks discriminating mouse bladder responses to intravesical bacillus Calmette-Guerin (BCG), LPS, and TNF-alpha." BMC Immunol **9**: 4.

Saka, H. A. and R. H. Valdivia (2010). "Acquisition of nutrients by Chlamydiae: unique challenges of living in an intracellular compartment." Curr Opin Microbiol **13**(1): 4-10.

Salat, J., B. Sak, et al. (2004). "Susceptibility of IFN-gamma or IL-12 knock-out and SCID mice to infection with two microsporidian species, Encephalitozoon cuniculi and E. intestinalis." Folia Parasitol (Praha) **51**(4): 275-82.

Samson, J. E., A. H. Magadan, et al. (2013). "Revenge of the phages: defeating bacterial defences." Nat Rev Microbiol **11**(10): 675-87.

Santiago, H. C., C. G. Feng, et al. (2005). "Mice deficient in LRG-47 display enhanced susceptibility to Trypanosoma cruzi infection associated with defective hemopoiesis and intracellular control of parasite growth." J Immunol **175**(12): 8165-72.

Scharton-Kersten, T., H. Nakajima, et al. (1998). "Infection of mice lacking the common cytokine receptor gamma-chain (gamma(c)) reveals an unexpected role for CD4+ T lymphocytes in early IFN-gamma-dependent resistance to Toxoplasma gondii." J Immunol **160**(6): 2565-9.

Scharton-Kersten, T. M., T. A. Wynn, et al. (1996). "In the absence of endogenous IFN-gamma, mice develop unimpaired IL-12 responses to Toxoplasma gondii while failing to control acute infection." J Immunol **157**(9): 4045-54.

Schroder, K., P. J. Hertzog, et al. (2004). "Interferon-gamma: an overview of signals, mechanisms and functions." J Leukoc Biol **75**(2): 163-89.

Schwab, J. C., C. J. Beckers, et al. (1994). "The parasitophorous vacuole membrane surrounding intracellular Toxoplasma gondii functions as a molecular sieve." Proc Natl Acad Sci U S A **91**(2): 509-13.

Schwemmle, M. and P. Staeheli (1994). "The interferon-induced 67-kDa guanylate-binding protein (hGBP1) is a GTPase that converts GTP to GMP." J Biol Chem **269**(15): 11299-305.

Scidmore, M. A. (2011). "Recent advances in Chlamydia subversion of host cytoskeletal and membrane trafficking pathways." Microbes Infect **13**(6): 527-35.

Scidmore, M. A., E. R. Fischer, et al. (2003). "Restricted fusion of Chlamydia trachomatis vesicles with endocytic compartments during the initial stages of infection." Infect Immun **71**(2): 973-84.

Selleck, E. M., S. J. Fentress, et al. (2013). "Guanylate-binding protein 1 (Gbp1) contributes to cell-autonomous immunity against Toxoplasma gondii." PLoS Pathog **9**(4): e1003320.

Selman, M., B. Sak, et al. (2013). "Extremely reduced levels of heterozygosity in the vertebrate pathogen Encephalitozoon cuniculi." Eukaryot Cell **12**(4): 496-502.

Shenoy, A. R., B. H. Kim, et al. (2007). "Emerging themes in IFN-gamma-induced macrophage immunity by the p47 and p65 GTPase families." Immunobiology **212**(9-10): 771-84.

Shenoy, A. R., D. A. Wellington, et al. (2012). "GBP5 promotes NLRP3 inflammasome assembly and immunity in mammals." Science **336**(6080): 481-5.

Sibley, L. D. (2004). "Intracellular parasite invasion strategies." Science **304**(5668): 248-53.

Sibley, L. D. (2011). "Invasion and intracellular survival by protozoan parasites." Immunol Rev **240**(1): 72-91.

Sibley, L. D., E. Weidner, et al. (1985). "Phagosome acidification blocked by intracellular Toxoplasma gondii." Nature **315**(6018): 416-9.

Sinai, A. P., P. Webster, et al. (1997). "Association of host cell endoplasmic reticulum and mitochondria with the Toxoplasma gondii parasitophorous vacuole membrane: a high affinity interaction." J Cell Sci **110 ( Pt 17)**: 2117-28.

Singh, S. B., A. S. Davis, et al. (2006). "Human IRGM induces autophagy to eliminate intracellular mycobacteria." Science **313**(5792): 1438-41.

Singh, S. B., W. Ornatowski, et al. (2010). "Human IRGM regulates autophagy and cell-autonomous immunity functions through mitochondria." Nat Cell Biol **12**(12): 1154-65.

Sorace, J. M., R. J. Johnson, et al. (1995). "Identification of an endotoxin and IFN-inducible cDNA: possible identification of a novel protein family." J Leukoc Biol **58**(4): 477-84.

Southern, P. J. and P. Berg (1982). "Transformation of mammalian cells to antibiotic resistance with a bacterial gene under control of the SV40 early region promoter." J Mol Appl Genet **1**(4): 327-41.

Spekker, K., M. Leineweber, et al. (2013). "Antimicrobial effects of murine mesenchymal stromal cells directed against Toxoplasma gondii and Neospora caninum: role of

immunity-related GTPases (IRGs) and guanylate-binding proteins (GBPs)." Med Microbiol Immunol **202**(3): 197-206.
Springer, H. M., M. Schramm, et al. (2013). "Irgm1 (LRG-47), a regulator of cell-autonomous immunity, does not localize to mycobacterial or listerial phagosomes in IFN-gamma-induced mouse cells." J Immunol **191**(4): 1765-74.
Staeheli, P., O. Haller, et al. (1986). "Mx protein: constitutive expression in 3T3 cells transformed with cloned Mx cDNA confers selective resistance to influenza virus." Cell **44**(1): 147-58.
Steinfeldt, T., S. Konen-Waisman, et al. (2010). "Phosphorylation of mouse immunity-related GTPase (IRG) resistance proteins is an evasion strategy for virulent Toxoplasma gondii." PLoS Biol **8**(12): e1000576.
Stickney, J. T. and J. E. Buss (2000). "Murine guanylate-binding protein: incomplete geranylgeranyl isoprenoid modification of an interferon-gamma-inducible guanosine triphosphate-binding protein." Mol Biol Cell **11**(7): 2191-200.
Straub, K. W., E. D. Peng, et al. (2011). "The moving junction protein RON8 facilitates firm attachment and host cell invasion in Toxoplasma gondii." PLoS Pathog **7**(3): e1002007.
Sturge, C. R., A. Benson, et al. (2013). "TLR-independent neutrophil-derived IFN-gamma is important for host resistance to intracellular pathogens." Proc Natl Acad Sci U S A **110**(26): 10711-6.
Subtil, A. (2011). "Rerouting of host lipids by bacteria: are you CERTain you need a vesicle?" PLoS Pathog **7**(9): e1002208.
Suss-Toby, E., J. Zimmerberg, et al. (1996). "Toxoplasma invasion: the parasitophorous vacuole is formed from host cell plasma membrane and pinches off via a fission pore." Proc Natl Acad Sci U S A **93**(16): 8413-8.
Suzuki, Y., M. A. Orellana, et al. (1988). "Interferon-gamma: the major mediator of resistance against Toxoplasma gondii." Science **240**(4851): 516-8.
Swihart, K., U. Fruth, et al. (1995). "Mice from a genetically resistant background lacking the interferon gamma receptor are susceptible to infection with Leishmania major but mount a polarized T helper cell 1-type CD4+ T cell response." J Exp Med **181**(3): 961-71.
Taylor, G. A., C. M. Collazo, et al. (2000). "Pathogen-specific loss of host resistance in mice lacking the IFN-gamma-inducible gene IGTP." Proc Natl Acad Sci U S A **97**(2): 751-5.
Taylor, G. A., C. G. Feng, et al. (2004). "p47 GTPases: regulators of immunity to intracellular pathogens." Nat Rev Immunol **4**(2): 100-9.
Taylor, G. A., C. G. Feng, et al. (2007). "Control of IFN-gamma-mediated host resistance to intracellular pathogens by immunity-related GTPases (p47 GTPases)." Microbes Infect **9**(14-15): 1644-51.
Taylor, G. A., M. Jeffers, et al. (1996). "Identification of a novel GTPase, the inducibly expressed GTPase, that accumulates in response to interferon gamma." J Biol Chem **271**(34): 20399-405.
Taylor, G. A., R. Stauber, et al. (1997). "The inducibly expressed GTPase localizes to the endoplasmic reticulum, independently of GTP binding." J Biol Chem **272**(16): 10639-45.
Tietzel, I., C. El-Haibi, et al. (2009). "Human guanylate binding proteins potentiate the anti-chlamydia effects of interferon-gamma." PLoS One **4**(8): e6499.
Tischler, A. D., R. L. Leistikow, et al. (2013). "Mycobacterium tuberculosis requires phosphate-responsive gene regulation to resist host immunity." Infect Immun **81**(1): 317-28.

Tiwari, S., H. P. Choi, et al. (2009). "Targeting of the GTPase Irgm1 to the phagosomal membrane via PtdIns(3,4)P(2) and PtdIns(3,4,5)P(3) promotes immunity to mycobacteria." Nat Immunol **10**(8): 907-17.
Traver, M. K., S. C. Henry, et al. (2011). "Immunity-related GTPase M (IRGM) proteins influence the localization of guanylate-binding protein 2 (GBP2) by modulating macroautophagy." J Biol Chem **286**(35): 30471-80.
Trinchieri, G. and A. Sher (2007). "Cooperation of Toll-like receptor signals in innate immune defence." Nat Rev Immunol **7**(3): 179-90.
Trost, M., L. English, et al. (2009). "The phagosomal proteome in interferon-gamma-activated macrophages." Immunity **30**(1): 143-54.
Tyedmers, J., A. Mogk, et al. (2010). "Cellular strategies for controlling protein aggregation." Nat Rev Mol Cell Biol **11**(11): 777-88.
Tyler, J. S., M. Treeck, et al. (2011). "Focus on the ringleader: the role of AMA1 in apicomplexan invasion and replication." Trends Parasitol **27**(9): 410-20.
Uthaiah, R. C., G. J. Praefcke, et al. (2003). "IIGP1, an interferon-gamma-inducible 47-kDa GTPase of the mouse, showing cooperative enzymatic activity and GTP-dependent multimerization." J Biol Chem **278**(31): 29336-43.
Valdivia, R. H. (2008). "Chlamydia effector proteins and new insights into chlamydial cellular microbiology." Curr Opin Microbiol **11**(1): 53-9.
Vestal, D. J., V. Y. Gorbacheva, et al. (2000). "Different subcellular localizations for the related interferon-induced GTPases, MuGBP-1 and MuGBP-2: implications for different functions?" J Interferon Cytokine Res **20**(11): 991-1000.
Vestal, D. J. and J. A. Jeyaratnam (2011). "The guanylate-binding proteins: emerging insights into the biochemical properties and functions of this family of large interferon-induced guanosine triphosphatase." J Interferon Cytokine Res **31**(1): 89-97.
Virreira Winter, S., W. Niedelman, et al. (2011). "Determinants of GBP recruitment to Toxoplasma gondii vacuoles and the parasitic factors that control it." PLoS One **6**(9): e24434.
von Bargen, K., J. Wohlmann, et al. (2011). "Nitric oxide-mediated intracellular growth restriction of pathogenic Rhodococcus equi can be prevented by iron." Infect Immun **79**(5): 2098-111.
von der Malsburg, A., I. Abutbul-Ionita, et al. (2011). "Stalk domain of the dynamin-like MxA GTPase protein mediates membrane binding and liposome tubulation via the unstructured L4 loop." J Biol Chem **286**(43): 37858-65.
von Wussow, P., D. Jakschies, et al. (1990). "The human intracellular Mx-homologous protein is specifically induced by type I interferons." Eur J Immunol **20**(9): 2015-9.
Wang, C., C. Wang, et al. (2012). "Immune-related GTPase Irgm1 exacerbates experimental auto-immune encephalomyelitis by promoting the disruption of blood-brain barrier and blood-cerebrospinal fluid barrier." Mol Immunol **53**(1-2): 43-51.
Weidner, E. (1975). "Interactions between Encephalitozoon cuniculi and macrophages. Parasitophorous vacuole growth and the absence of lysosomal fusion." Z Parasitenkd **47**(1): 1-9.
Weidner, E. and L. D. Sibley (1985). "Phagocytized intracellular microsporidian blocks phagosome acidification and phagosome-lysosome fusion." J Protozool **32**(2): 311-7.
Williams, B. A., R. P. Hirt, et al. (2002). "A mitochondrial remnant in the microsporidian Trachipleistophora hominis." Nature **418**(6900): 865-9.
Xia, F., R. Li, et al. (2013). "IRGM1 regulates oxidized LDL uptake by macrophage via actin-dependent receptor internalization during atherosclerosis." Sci Rep **3**: 1867.
Xu, H., Z. Y. Wu, et al. (2010). "Genetic deficiency of Irgm1 (LRG-47) suppresses induction of experimental autoimmune encephalomyelitis by promoting apoptosis of activated CD4+ T cells." Faseb J **24**(5): 1583-92.

Yamada, K., H. Akimoto, et al. (2009). "Upregulation of immunity-related GTPase (IRG) proteins by TNF-alpha in murine astrocytes." Biochem Biophys Res Commun **382**(2): 434-9.

Yamamoto, M., M. Okuyama, et al. (2012). "A cluster of interferon-gamma-inducible p65 GTPases plays a critical role in host defense against Toxoplasma gondii." Immunity **37**(2): 302-13.

Yap, G. S. and A. Sher (1999). "Effector cells of both nonhemopoietic and hemopoietic origin are required for interferon (IFN)-gamma- and tumor necrosis factor (TNF)-alpha-dependent host resistance to the intracellular pathogen, Toxoplasma gondii." J Exp Med **189**(7): 1083-92.

Yarovinsky, F. (2014). "Innate immunity to Toxoplasma gondii infection." Nat Rev Immunol **14**(2): 109-21.

Yimin, M. Kohanawa, et al. (2001). "Role of T cells in granuloma formation induced by Rhodococcus aurantiacus is independent of their interferon-gamma production." J Med Microbiol **50**(8): 688-94.

Zeng, J., I. A. Parvanova, et al. (2009). "A dedicated promoter drives constitutive expression of the cell-autonomous immune resistance GTPase, Irga6 (IIGP1) in mouse liver." PLoS One **4**(8): e6787.

Zerrahn, J., U. E. Schaible, et al. (2002). "The IFN-inducible Golgi- and endoplasmic reticulum- associated 47-kDa GTPase IIGP is transiently expressed during listeriosis." J Immunol **168**(7): 3428-36.

Zhang, H. M., J. Yuan, et al. (2003). "Overexpression of interferon-gamma-inducible GTPase inhibits coxsackievirus B3-induced apoptosis through the activation of the phosphatidylinositol 3-kinase/Akt pathway and inhibition of viral replication." J Biol Chem **278**(35): 33011-9.

Zhao, Y., D. J. Ferguson, et al. (2009). "Virulent Toxoplasma gondii evade immunity-related GTPase-mediated parasite vacuole disruption within primed macrophages." J Immunol **182**(6): 3775-81.

Zhao, Y. O., A. Khaminets, et al. (2009). "Disruption of the Toxoplasma gondii parasitophorous vacuole by IFNgamma-inducible immunity-related GTPases (IRG proteins) triggers necrotic cell death." PLoS Pathog **5**(2): e1000288.

Zhao, Y. O., S. Konen-Waisman, et al. (2010). "Localisation and mislocalisation of the interferon-inducible immunity-related GTPase, Irgm1 (LRG-47) in mouse cells." PLoS One **5**(1): e8648.

Zhao, Y. O., C. Rohde, et al. (2009). "Toxoplasma gondii and the Immunity-Related GTPase (IRG) resistance system in mice: a review." Mem Inst Oswaldo Cruz **104**(2): 234-40.

Zhao, Z., B. Fux, et al. (2008). "Autophagosome-independent essential function for the autophagy protein Atg5 in cellular immunity to intracellular pathogens." Cell Host Microbe **4**(5): 458-69.

# Appendix

**Appendix table 1:** Accession number of all ESTs retrieved from a BLAST of *Mus musculus Irgm1* nucleotide sequence against C57BL/6 mouse genome (Annotation release 103). 170 ESTs were aligned in total, but in Figure 3.1 B only the ones relevant for isoform identification are shown. Therefore, the graph retrieved from the NCBI Map Viewer was modified and color-coded with the Software Paint. *Irgm1* gene is encoded from 48865249 to 48871346 on Chromosome 11. The homepage of the NCBI (http://www.ncbi.nlm.nih.gov; BLAST Irgm1 sequence; GRCm38.p2 used as reference genome, show Mm RNA, Map Viewer) was visited 2014-03-24.

| Start | Stop | Accession number | Start | Stop | Accession number | Start | Stop | Accession number |
|---|---|---|---|---|---|---|---|---|
| 48826140 | 48874714 | AA517788.1 | 48865355 | 48865721 | BG091391.1 | 48866596 | 48871372 | DT923229.1 |
| 48847978 | 48871276 | CK019751.1 | 48865378 | 48865853 | AA266999.1 | 48866599 | 48871268 | BF164781.1 |
| 48850321 | 48871326 | CB945508.1 | 48865381 | 48865733 | BY374259.1 | 48866601 | 48871286 | BE367794.1 |
| 48861968 | 48871683 | AK083346.1 | 48865391 | 48865783 | DT908179.1 | 48866601 | 48871342 | CB945745.1 |
| 48865151 | 48871683 | BB654261.1 | 48865391 | 48865783 | DT910296.1 | 48866603 | 48867251 | BI654829.1 |
| 48865245 | 48865623 | CJ217401.1 | 48865391 | 48865783 | DT911310.1 | 48866605 | 48871314 | BI558163.1 |
| 48865245 | 48865628 | CJ218262.1 | 48865391 | 48865783 | DT920057.1 | 48866623 | 48871336 | CN677533.1 |
| 48865245 | 48865629 | CJ218257.1 | 48865391 | 48865783 | DT928637.1 | 48866630 | 48871392 | CB599188.1 |
| 48865245 | 48865662 | AA178702.1 | 48865391 | 48865783 | DT929844.1 | 48866648 | 48871306 | BI655161.1 |
| 48865245 | 48865675 | BY580975.1 | 48865391 | 48865783 | DT931518.1 | 48866674 | 48871403 | BY737226.1 |
| 48865245 | 48865746 | BI665430.1 | 48865441 | 48865806 | AA560463.1 | 48866684 | 48871354 | BU614132.1 |
| 48865245 | 48865783 | AA080447.1 | 48865461 | 48871158 | BC145957.1 | 48866690 | 48871360 | BF784652.1 |
| 48865246 | 48865638 | CJ214215.1 | 48865467 | 48865907 | AA823118.1 | 48866698 | 48871315 | BF159067.1 |
| 48865247 | 48865479 | BB323925.1 | 48865514 | 48865855 | AA199976.1 | 48866706 | 48871374 | BI659468.1 |
| 48865247 | 48865538 | BB107713.1 | 48865520 | 48866022 | AA212456.1 | 48866750 | 48871363 | BX513271.1 |
| 48865247 | 48865556 | BB520628.1 | 48865536 | 48866135 | AA711254.1 | 48866755 | 48871379 | CN681579.1 |
| 48865247 | 48865586 | BB797706.1 | 48865539 | 48866024 | AA214784.1 | 48866775 | 48871304 | CN662778.1 |
| 48865247 | 48865623 | BY687582.1 | 48865540 | 48866024 | AA212463.1 | 48866816 | 48871346 | AA107502.1 |
| 48865247 | 48865630 | BB739716.1 | 48865553 | 48866484 | BI653806.1 | 48866818 | 48871326 | BY225443.1 |
| 48865247 | 48865652 | BY482184.1 | 48865559 | 48865972 | BY157015.1 | 48866821 | 48871288 | AW227839.1 |
| 48865247 | 48871367 | AK002545.1 | 48865591 | 48865972 | BY172752.1 | 48866821 | 48871324 | BY224648.1 |
| 48865248 | 48865658 | CJ302279.1 | 48865643 | 48866460 | BF161711.1 | 48866829 | 48871187 | BB860839.1 |
| 48865249 | 48865475 | AV345311.1 | 48865682 | 48866449 | BF168437.1 | 48866845 | 48871303 | BY023068.1 |
| 48865249 | 48865518 | BB475932.1 | 48865682 | 48866467 | BG974799.1 | 48866868 | 48871374 | CF899916.1 |
| 48865249 | 48865547 | BB044267.1 | 48865841 | 48866228 | BG094936.1 | 48866877 | 48871325 | BY219280.1 |
| 48865249 | 48865855 | CO041867.1 | 48865863 | 48866725 | BI853562.1 | 48866881 | 48871326 | BY081400.1 |
| 48865249 | 48865944 | BE570459.1 | 48865872 | 48866561 | AA105762.1 | 48866884 | 48871325 | BY219925.1 |
| 48865249 | 48871346 | U19119.1 | 48865946 | 48866338 | BY161130.1 | 48866887 | 48871325 | BY219624.1 |
| 48865249 | 48871346 | NM_008326.1 | 48866052 | 48866671 | BI558790.1 | 48866888 | 48871386 | CJ165063.1 |
| 48865250 | 48865487 | AV291659.1 | 48866094 | 48866832 | BI150356.1 | 48866889 | 48871395 | BY033977.1 |
| 48865250 | 48865489 | AV001243.1 | 48866118 | 48871150 | AI326713.1 | 48866923 | 48871386 | BY231386.1 |
| 48865250 | 48865563 | BY510602.1 | 48866219 | 48866998 | BI661643.1 | 48866929 | 48871420 | BY159883.1 |
| 48865250 | 48865578 | AV014538.1 | 48866338 | 48871370 | DV046798.1 | 48866938 | 48871386 | BY100561.1 |
| 48865250 | 48865605 | BB737352.1 | 48866349 | 48866491 | DY242460.1 | 48866944 | 48871393 | BY142654.1 |
| 48865250 | 48865672 | BY391797.1 | 48866382 | 48871343 | AW045127.1 | 48866952 | 48871395 | BY037258.1 |
| 48865250 | 48865679 | BY394521.1 | 48866398 | 48871377 | AI663521.1 | 48868000 | 48871372 | CA542360.1 |
| 48865250 | 48865683 | BE285311.1 | 48866402 | 48871322 | BG973420.1 | 48868245 | 48869061 | CK021439.1 |

| | | | | | | | | |
|---|---|---|---|---|---|---|---|---|
| 48865250 | 48865689 | BY515945.1 | 48866405 | 48866796 | BY311823.1 | 48868622 | 48871366 | BY226537.1 |
| 48865250 | 48865692 | AI573450.1 | 48866406 | 48871316 | AA673803.1 | 48868651 | 48871326 | BY221932.1 |
| 48865250 | 48865703 | BI143589.1 | 48866415 | 48871362 | DV040401.1 | 48868656 | 48871326 | BY216921.1 |
| 48865250 | 48865705 | BY489498.1 | 48866419 | 48871152 | AA152951.1 | 48868660 | 48871326 | BB841139.1 |
| 48865250 | 48865723 | BB781910.1 | 48866423 | 48871150 | BF658590.1 | 48868669 | 48871320 | BY214051.1 |
| 48865250 | 48865740 | BY448752.1 | 48866435 | 48871325 | CJ083509.1 | 48868670 | 48871326 | BY219517.1 |
| 48865250 | 48865822 | AW228222.1 | 48866436 | 48871335 | BF119211.1 | 48868681 | 48871342 | BG862949.1 |
| 48865250 | 48865916 | BY757575.1 | 48866443 | 48866796 | BY308514.1 | 48868683 | 48871366 | BY150562.1 |
| 48865250 | 48871418 | AK167558.1 | 48866445 | 48871315 | BF786823.1 | 48868684 | 48871366 | BY139383.1 |
| 48865252 | 48865683 | BY565805.1 | 48866455 | 48871378 | AI789163.1 | 48870856 | 48871305 | AW227285.1 |
| 48865252 | 48865703 | BY558051.1 | 48866457 | 48871325 | CJ073108.1 | 48871093 | 48871362 | AI227277.1 |
| 48865252 | 48865705 | BY565476.1 | 48866460 | 48868741 | BI660095.1 | 48871096 | 48871205 | DY247964.1 |
| 48865252 | 48865706 | BY571806.1 | 48866462 | 48871325 | CJ086727.1 | 48871202 | 48871326 | BY154366.1 |
| 48865252 | 48865710 | BY565942.1 | 48866487 | 48871338 | BI558670.1 | 48865337 | 48865688 | BG229852.1 |
| 48865252 | 48865717 | BY562711.1 | 48866490 | 48871366 | BY703059.1 | 48865339 | 48865698 | BB809650.1 |
| 48865252 | 48865722 | BY566436.1 | 48866498 | 48871337 | BG919173.1 | 48865339 | 48865710 | BY507833.1 |
| 48865252 | 48865817 | AI265670.1 | 48866501 | 48868638 | CA579704.1 | 48865339 | 48865882 | BM246660.2 |
| 48865252 | 48871326 | AK171743.1 | 48866552 | 48871384 | CB238089.1 | 48865340 | 48865654 | BB550394.1 |
| 48865321 | 48871325 | CB951333.1 | 48866589 | 48871326 | CB601221.1 | 48865341 | 48865752 | BB733964.1 |
| 48865332 | 48865835 | BY493343.1 | 48866596 | 48871372 | AA184224.1 | | | |

**Appendix Table IIA**: N-terminal and Phospho-peptides of Irgm1 found by Sequest

Collision-induced dissociation fragmentation of phospho-serine and phosphor-threonine results in favorable and neutral loss of phosphoric acid. The MS/MS spectrum is characterized by a peak corresponding to the loss of phosphoric acid from the parent mass and fewer low intensity fragments, making it difficult to determine the exact site of phosphorylation. The phosphoRS algorithm implemented in the Proteome Discoverer software calculates only probabilities.

| Sample (band) | | Sequence | # PSMs | Modifications | XCorr | Charge | MH+ [Da] | ΔM [ppm] | pRS Site Probabilities | pRS Score |
|---|---|---|---|---|---|---|---|---|---|---|
| Exp 1 BL/6 wt MEF + IFN | 1 | ETVATLSQIPVSIFVT GDSGNGMSSFINALR | 1 | S12 (Phospho) | 2,56 | 3 | 3291,61 | 4,58 | T(2): 10.2; T(5): 10.2; S(7): 10.2; S(12): 35.6; T(16): 10.2; S(19): 10.2; S(24): 10.2; S(25): 3.2 | 30 |
| | 1 | MAETHYAPLSSAFPF VTSYQTGSSR | 1 | | 3,59 | 3 | 2735,29 | 4,42 | | |
| | 2 | ETVATLSQIPVSIFVT GDSGNGMSSFINALR | 1 | S12 (Phospho) | 2,40 | 3 | 3291,59 | -2,21 | T(2): 11.4; T(5): 11.4; S(7): 2.5; S(12): 64.8; T(16): 2.5; S(19): 2.5; S(24): 2.5; S(25): 2.5 | 25 |
| | 2 | MAETHYAPLSSAFPF VTSYQTGSSR | 1 | | 4,23 | 3 | 2735,28 | 2,21 | | |
| | 3 | MAETHYAPLSSAFPF VTSYQTGSSR | 1 | | 4,51 | 3 | 2735,29 | 3,54 | | |
| Exp 2 BL/6 wt MEF + IFN | 6 | MAETHYAPLSSAFPF VTSYQTGSSR | 1 | | 4,50 | 3 | 2735,28 | 0,60 | | |
| | 7 | MAETHYAPLSSAFPF VTSYQTGSSR | 1 | | 4,66 | 3 | 2735,28 | 0,26 | | |
| Exp 3 C3H L929 + IFN | 9 | MAETHYAPLSSAFPF VTSYQTGSSR | 1 | | 3,61 | 3 | 2735,27 | -1,14 | | |

| Sample (band) | | Sequence | # PSMs | Modifi-cations | Ion Score | Charge | MH+ [Da] | ΔM [ppm] | pRS Site Probabilities | pRS Score |
|---|---|---|---|---|---|---|---|---|---|---|
| Exp 1 BL/6 wt MEF + IFN | 1 | AETHYAPLSSAFPF VTSYQTGSSR | 5 | N-Term (Acetyl) | 54,28 | 2 | 2646,26 | 3,31 | | |
| | 2 | AETHYAPLSSAFPF VTSYQTGSSR | 3 | N-Term (Acetyl) | 53,47 | 2 | 2646,25 | 2,57 | | |
| | 2 | ETVATLSQIPVSIFV TGDSGNGMSSFINA LR | 1 | T5 (Phospho) | 29,55 | 3 | 3291,59 | -2,21 | T(2): 11.4; T(5): 11.4; S(7): 2.5; S(12): 64.8; T(16): 2.5; S(19): 2.5; S(24): 2.5; S(25): 2.5 | 18 |
| | 2 | MKPSHSSCEAAPLL PNMAETHYAPLSSA FPFVTSYQTGSSR | 1 | N-Term (Acetyl) | | 4 | 4497,11 | 2,25 | | |
| | 3 | AETHYAPLSSAFPF VTSYQTGSSR | 1 | N-Term (Acetyl) | 41,15 | 3 | 2646,26 | 3,40 | | |
| Exp 2 BL/6 wt MEF + IFN | 5 | AETHYAPLSSAFPF VTSYQTGSSR | 3 | N-Term (Acetyl); S9 (Phospho) | 37,58 | 3 | 2726,21 | -1,86 | T(3): 83.2; Y(5): 12.4; S(9): 2.0; S(10): 2.0; T(16): 0.4; S(17): 0.0; Y(18): 0.0; T(20): 0.0; S(22): 0.0; S(23): 0.0 | 58 |
| | 5 | AETHYAPLSSAFPF VTSYQTGSSR | 6 | N-Term (Acetyl) | 47,62 | 3 | 2646,25 | 2,78 | | |
| | 6 | AETHYAPLSSAFPF VTSYQTGSSR | 2 | N-Term (Acetyl); Y5 (Phospho) | 34,39 | 3 | 2726,22 | 1,16 | T(3): 11.6; Y(5): 84.9; S(9): 1.7; S(10): 1.7; T(16): 0.0; S(17): 0.0; Y(18): 0.0; T(20): 0.0; S(22): 0.0; S(23): 0.0 | 89 |
| | 6 | AETHYAPLSSAFPF VTSYQTGSSR | 5 | N-Term (Acetyl) | 82,69 | 2 | 2646,26 | 3,59 | | |
| | 6 | MAETHYAPLSSAFP FVTSYQTGSSR | 1 | | 45,95 | 3 | 2735,28 | 0,60 | | |
| | 7 | AETHYAPLSSAFPF VTSYQTGSSR | 3 | N-Term (Acetyl) | 45,44 | 3 | 2646,25 | 1,39 | | |
| | 7 | MAETHYAPLSSAFP FVTSYQTGSSR | 1 | | 61,18 | 3 | 2735,28 | 0,26 | | |
| | 8 | AETHYAPLSSAFPF VTSYQTGSSR | 2 | N-Term (Acetyl) | 36,51 | 3 | 2646,25 | 1,32 | | |
| Exp 3 C3H L929 + IFN | 9 | AETHYAPLSSAFPF VTSYQTGSSR | 4 | N-Term (Acetyl) | 50,23 | 2 | 2646,25 | 2,20 | | |
| | 10 | AETHYAPLSSAFPF VTSYQTGSSR | 3 | N-Term (Acetyl) | 43,21 | 3 | 2646,25 | 0,91 | | |

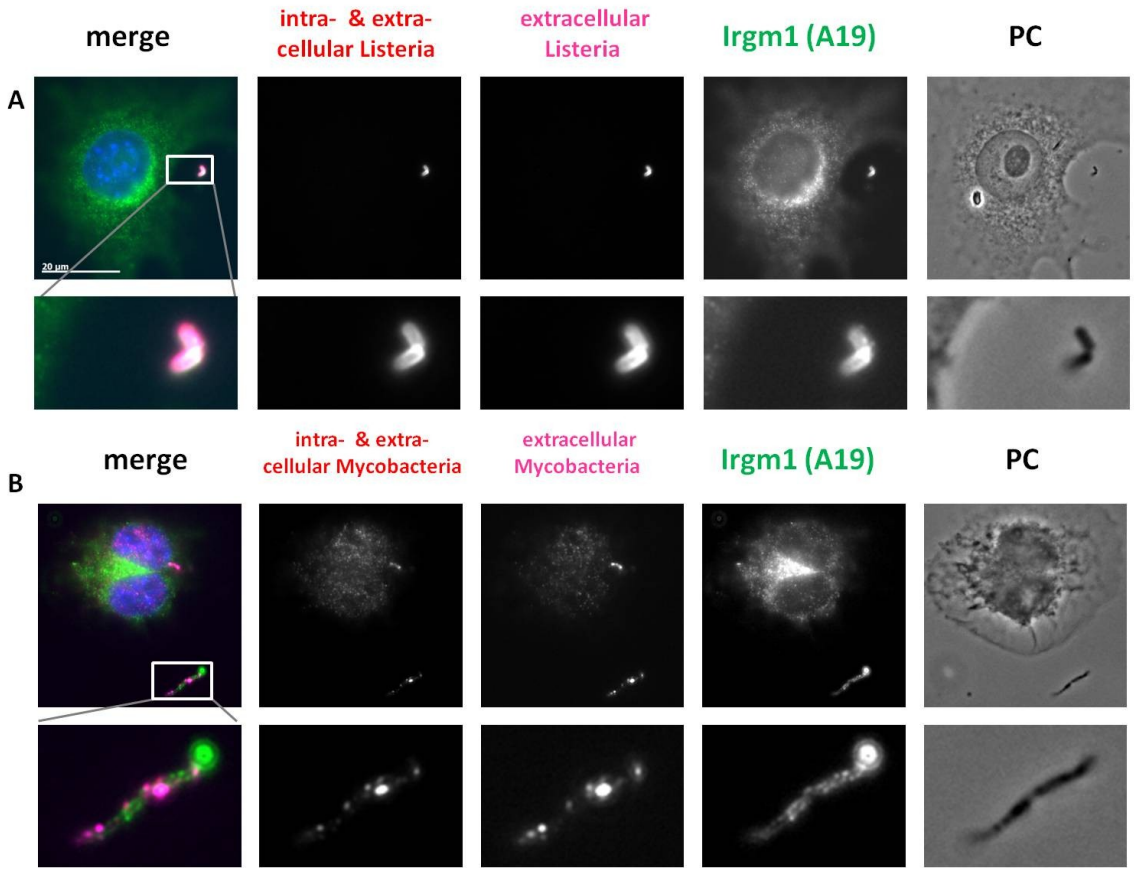


**Appendix Figure 3: Crossreactivity of A19 antibody.**
**(A)** MEFs from *Irgm1*$^{-/-}$ mice were stimulated with IFNγ for 24 h and infected with *L. monocytogenes*. **(B)** RAW 264.7 were stimulated with IFNγ for 24 h and infected with *M. bovis* BCG. Differential staining of intra-and extracellular bacteria was performed (see Materials and Methods) as well as staining for Irgm1 with goat pAB A19. The A19 antibody cross-reacts on extracellular bacteria that are identified by the differential staining and the phase contrast image, in which they are clearly next to a host cell

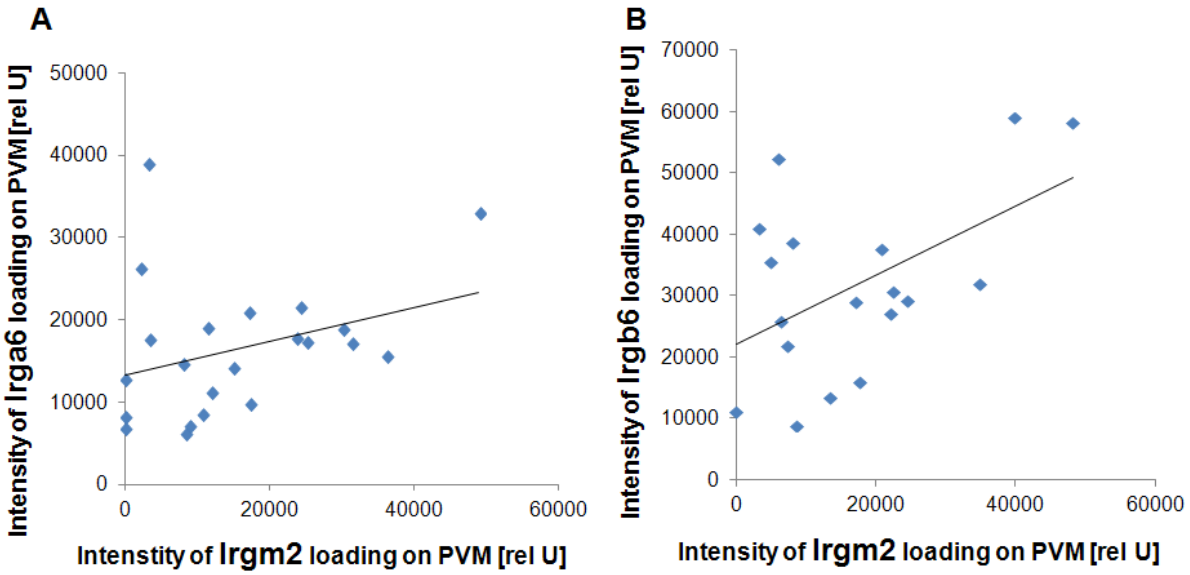


**Appendix Figure 4: Positive correlation of GKS and GMS proteins on the *T. gondii* PVM.**
MEFs were stimulated with IFNγ for 24 h and infected with T. gondii ME 49 for 2h. Fixed cells were co-stained for **(A)** Irgm2 (rabbit pAS H53) and Irga6 (mouse mAB 10D7) or **(B)** Irgm2 (rabbit pAS H53) and Irgb6 (mouse mAB B34). The intensity of IRG staining at positive vacuoles was measured with AxioVision software.

# Summary

Immunity–related GTPases (IRG) constitute a powerful resistance system against the protozoa *Toxoplasma gondii* and its close relative *Neospora caninum* as well as against two strains of the bacteria *Chlamydia* in mice. However, it remains a great mystery why all other organisms tested so far are not restricted by the IRG system. IRG-mediated restriction correlates with accumulation of effector IRG subfamily, the GKS proteins, at the parasitophorous vacuoles leading to the breakdown of the membrane barrier and death of the parasite. It is not known how GKS proteins can specifically recognise and bind to the parasitophorous vacuolar membranes (PVM), which is derived from the invaginated host plasma membrane and block fusion with the endolysosomal compartments. The second subfamily of IRG proteins, GMS proteins, prevents premature activation of GKS proteins and seems to protect endomembranes from GKS-mediated destruction. The GMS protein Irgm1 has been alternatively proposed to directly mediate acidification and destruction of bacterial phagosomes. However, this theory is incompatible with the current model that IRG resistance system acts only on non-phagosomal vacuoles.

The present study demonstrated the predicted existence of two protein isoforms of Irgm1, which localised slightly different to subcellular endomembranes. Moreover, in striking contrast to earlier studies, Irgm1 could never be detected at listerial or mycobacterial phagosomes, arguing against the alterative proposed role of Irgm1 on phagosomes. In order to understand IRG target membranes, the present study showed that certain GKS proteins have an intrinsic property to bind liposomes in a GTP-dependent manner. However, the absence of residual host cell plasma membranes on the PVM of *T. gondii* did not trigger GKS accumulation. The non-fusogenic character of a vacuole was also not sufficient for a vacuole to be recognised by GKS proteins. Lastly, this study presented a novel role of the IRG system in resistance to the microsporidian *Encephalitozoon cuniculi*. Interferon-γ stimulation, inducing IRG proteins, suppresses meront development and spore formation in mouse fibroblasts *in vitro*, and effector GKS proteins cooperatively accumulate on the PVM of *E. cuniculi*. In addition, IFNγ-induced cells infected with *E. cuniculi* died by necrosis similar to *T. gondii* infection.

Thus, the IRG resistance system provides cell-autonomous immunity to specific parasites from three kingdoms of life: protozoa, bacteria and fungi. The phylogenetic divergence of these IRG target organisms strongly suggests that the IRG system does not recognise specific parasite components. The absence of certain host components on the vacuolar membrane, such as the protective GMS proteins, might act as missing-self motifs to trigger GKS protein accumulation on parasitophorous vacuoles.

# Zusammenfassung

Die immun-verwandten GTPases (immunity-related GTPases, IRG) wirken als leistungsfähiges Resistenzsystem gegen die Protozoen *Toxoplasma gondii* und *Neospora caninum* sowie gegen zwei Stämme der Chlamydien Bakterien. Es ist bisher ein großes Rätsel, warum alle anderen bisher getesteten Organismen nicht von dem IRG System kontrolliert werden. Die IRG-vermittelte Resistenz korreliert mit der Akkumulation von IRG Effektoren der GKS Protein-Unterfamilie auf der parasitophoren Vakuole. Dies führt zur Zerstörung der Membran-Barriere und schließlich zum Tod des Parasiten. Es ist unklar, wie genau GKS Proteine die Membran der parasitophoren Vakuole (PVM) erkennen und auch daran binden. Die PVM wird aus der eingestülpten Wirtszell-Plasmamembran gebildet und fusioniert nicht mit dem Endolysosomalen Organelle. Die zweite IRG Protein-Unterfamilie sind die regulatorischen GMS Proteine. Sie verhindern die vorzeitige Aktivierung von GKS Proteinen und schützen vermutlich die Endomembranen vor Zerstörung durch GKS Proteine. Für das GMS Protein Irgm1 wurde außerdem alternativ vorgeschlagen, dass es direkt an der Ansäuerung und Zerstörung von bakteriellen Phagosomen beteiligt ist. Diese Theorie ist jedoch unvereinbar mit dem aktuellen Model, dass IRG Resistenzsystem nur auf nicht-phagosomalen Vakuolen wirkt.

In der vorliegenden Arbeit wurde die vorhergesagte Existenz der zwei Isoformen von Irgm1 nachgewiesen, welche etwas unterschiedlich an subzelluläre Endomembranen lokalisieren. Außerdem wurde im starken Gegensatz zu vorherigen publizierten Studien kein Irgm1 an Phagosomen von Listerien oder Mykobakterien detektiert. Dies spricht deutlich gegen die alternativ vorgeschlagene Effektor-Rolle von Irgm1 an Phagosomen.

Um besser zu verstehen, an welche Membranen IRG Proteine binden, wurde in der vorliegenden Arbeit gezeigt, dass bestimmte GKS Proteine eine intrinsische Eigenschaft besitzen an Liposomen in GTP-abhängiger Weise zu binden. Das Fehlen von Wirtszell-Plasmamembran Proteinen auf der PVM von *T. gondii* hat jedoch keine IRG Protein Akkumulierung ausgelöst. Auch die Eigenschaft einer Vakuole, Fusion mit dem Endolysosomalen System zu verhindern, reicht nicht aus um von IRG Proteinen erkannt zu werden.

Zuletzt wurde in der vorliegenden Arbeit eine neue Rolle des IRG Systems in der Kontrolle des Mikrosporidiums *Encephalitozoon cuniculi* präsentiert. Interferon-γ Stimulation, welches IRG Proteine induziert, supprimierte die Entwicklung von Meronten und Sporenbildung *in vitro* im murinen Fibroblasten. Die Effektor GKS Proteine akkumulieren

kooperativ auf der PVM von *E. cuniculi*. Weiterhin sterben Interferon-γ-behandelte und *E. cuniculi*- infizierte Zellen nekrotisch, ähnlich wie bei Infektion mit *T. gondii*.

Das IRG Resistenzsystem liefert somit Zell-autonome Immunität gegen spezifische Parasiten, die zu drei Reichen der Lebewesen gehören: Protozoen, Bakterien und Pilze. Das phylogenetische Spektrum dieser Organismen, die vom IRG System erkannt werden, weist darauf hin, dass das IRG System keine Parasiten-spezifische Komponente erkennt. Hingegen wird das Fehlen von bestimmen Wirtszell-Komponenten auf der Membran der fremden Vakuole erkannt, wie zum Beispiel die schützenden GMS Proteine. Dadurch wird ein "missing-self" Signal vermittelt, welches dann eine Akkumulierung von GKS Proteinen auf der PVM auslöst.

# Acknowledgement

An dieser Stelle möchte ich mich herzlichst bei Professor Dr. Jonathan Howard für die hervorragende Betreuung bedanken! Vielen Dank für die Motivation und Kreativität, in alle Richtungen zu denken, für den stetigen Ansporn zum kritischen Hinterfragen, und für die Möglichkeit, in dem so spannenden Forschungsgebiet *Host-Pathogen Interactions* ein klitzekleines Puzzleteil hinzuzufügen.

Weiterhin möchte ich Prof. Dr. Dohmen für die Übernahme der Bewertung dieser Arbeit sowie Prof. Dr. Roth als Vorsitzeder des Prüfungskomitees herzlich danken.

Ein großes Dankeschön geht auch an die Mitglieder in meinem Thesis-Komitee Dr. Gerrit Praefcke und Professor Dr. Stefan Höning für ihre wertvollen Ratschläge und Ideen zu meiner Arbeit.

Ich möchte mich bei allen Mitarbeitern und Praktikanten der Arbeitsgruppe Howard für die umfassende Unterstüzung bedanken! Vielen Dank an:
Ben (Korrekturlesen), Claudia (Zellkultur und *E. cuniculi*), Gaby (Protein-Aufreinigung), Jelena (Korrekturlesen und vieles mehr), Julia (Einführung ins Labor), Marialice (Einführung in *E. cuniculi*), Miriam (Korrekturlesen), Niko & Martin (Lipide), Rita (diverse Klonierungen), Steffi (Organisationstalent, S2), Tao (alles mit Computern), Thomas (stetige Hilfsbereitschaft), Tobi (Korrekturlesen, Immunpräzipitationen); Alba (Immortalisierung) und Dennis (GMS vs. GKS auf PVM)!

Ich bedanke mich bei den Wissenschaftlern Dr. Wolfgang Bohne, Prof. Dr. Pascal Cossart, Dr. Edith Goudin, Dr. Paul Hasselgren, Prof. Dr. Ted Hackstadt, Prof. Dr. Thomas Langer und Prof. Dr. Gregory Taylor für bereitgestellte Materialien. Ich danke Dr. Michael Schramm für die Hilfe bei den Bakterien-Infektionen, Dr. Astrid Schauss für die Einführung in die Konfokal-Mikroskopie sowie bei Dr. Tobias Lamkemeyer und Denise Ungrue für die Durchführung der Massenspektrometrie.

Ich danke auch der Graduate School for Biological Sciences, Isabelle Witt, dem SFB 670 und dem CHM Mint Programm, welche mich bei meinem Werdegang auf verschiedenen Wegen unterstützt.

Allerliebsten Dank an Lars, meine Familie, meine Freunden und die 175g Scheibe, da sie mir immer wieder zeigen, wie schön das Leben ist.

# Declaration and Publications

I hereby declare that I elaborated the entire PhD thesis on my own and that I used only the references listed.

Ich versichere, dass ich die von mir vorgelegte Dissertation selbständig angefertigt, die benutzten Quellen und Hilfsmittel vollständig angegeben und die Stellen der Arbeit − einschließlich Tabellen, Karten und Abbildungen −, die anderen Werken im Wortlaut oder dem Sinn nach entnommen sind, in jedem Einzelfall als Entlehnung kenntlich gemacht habe; dass diese Dissertation noch keiner anderen Fakultät oder Universität zur Prüfung vorgelegen hat; dass sie − abgesehen von unten angegebenen Teilpublikationen − noch nicht veröffentlicht worden ist, sowie, dass ich eine solche Veröffentlichung vor Abschluss des Promotionsverfahrens nicht vornehmen werde. Die Bestimmungen der Promotionsordnung sind mir bekannt. Die von mir vorgelegte Dissertation ist von Prof. Dr. Jonathan Howard betreut worden.

Köln, 5th of May 2014

Helen Springer-Frauenhoff

Parts of this work have been published / Teile dieser Arbeit wurden publiziert in:

Springer HM, Schramm M, Taylor GA, Howard JC. Irgm1 (LRG-47), a regulator of cell-autonomous immunity, does not localise to mycobacterial or listerial phagosomes in IFN-gamma-induced mouse cells. J Immunol 2013;191(4):1765-74.

Springer-Frauenhoff HM*, da Fonseca Ferreira-da-Silva M*, Bohne W, Howard JC. Identification of the microsporidian fungus *Encephalitozoon cuniculi* as a new target of the IFNγ-inducible IRG resistance system. PLOS Pathogens 2014 Oct 30;10(10):e1004449